LARGE-SCALE PHYSICAL MODELLING STUDY OF IMPACT MECHANISMS OF ROCKFALL AND DEBRIS FLOW ON A FLEXIBLE BARRIER

TAN DAOYUAN

PhD

The Hong Kong Polytechnic University

2019

The Hong Kong Polytechnic University

Department of Civil and Environmental Engineering

Large-Scale Physical Modelling Study of Impact Mechanisms of Rockfall and Debris Flow on a Flexible Barrier

TAN DAOYUAN

A thesis submitted in partial fulfilment of the requirements for the degree of

Doctor of Philosophy

November 2018

CERTIFICATE OF ORIGINALITY

I hereby declare that this thesis is my own work and that, to the best of my knowledge and belief, it reproduces no material previously published or written, nor material that has been accepted for the award of any other degree of diploma, except where due acknowledgement has been made in the text.

Signature:

Name: TAN Daoyuan

Abstract of thesis entitled

LARGE-SCALE PHYSICAL MODELLING STUDY OF IMPACT MECHANISMS OF ROCKFALL AND DEBRIS FLOW ON A FLEXIBLE BARRIER

Rockfalls and debris flows in mountain areas normally carry enormous kinetic energies and cause catastrophic damages to human lives, buildings, and infrastructures in the influenced areas. As a potential mitigation countermeasure, flexible barriers have been increasingly utilized to mitigate those disastrous and frequent natural geohazards. However, it is still an open question on how to design the flexible barriers economically and effectively to withstand the impact loads. The major objectives of this study are to reveal the interaction mechanisms of rockfalls and debris flows with a flexible barrier and to improve the design approach of debris flow-resistant flexible barriers based on the interaction characteristics at different impact stages. Findings of this study will help deepen the understanding of the impact mechanisms of boulders and debris flows on a flexible barrier and improve the design of flexible barriers for debris flow mitigation.

Large-scale physical modelling is adopted as the main methodology in this study considering the scale effects and the complex structures of a flexible barrier. A large-scale physical modelling facility was designed and built to perform a series of impact experiments of a single boulder, dry granular flows, and debris flows. A dynamic monitoring system was established to capture the dynamic responses of key components of a flexible barrier during impacts. Two high-speed cameras were used to trace the motions and the interactions of the impact mass with the flexible barrier. The experiment results are comprehensively presented and analysed in this thesis.

The interaction between a rockfall and a flexible barrier is investigated by two impact tests using boulders with two different diameters (400 mm and 600 mm). The impact forces on

the flexible ring net directly and transferred to the supporting structures are analyzed and compared based on measured data. From the comparison, a parameter named Impact Reduction Rate (IRR) is defined to quantify the impact force attenuated by the flexible ring net. It is found that the IRRs of two boulders with different diameters are both around 30%. A simple method is proposed to estimate the impact force from a rockfall on a flexible barrier considering the stiffness of the flexible barrier and the impact area of the boulder. This simple method is calibrated and verified by the measured impact forces in this study.

The interaction between dry granular flows and a flexible barrier is studied by two consecutive granular flow impact tests. The motions, depositions, and impact behaviours of dry granular flows were recorded during testing and are analysed in this thesis. The impact forces on the flexible ring net directly and transferred to the supporting structures were measured during testing and are analysed and compared with values calculated using several existing simple methods. It has been found that the dynamic method can properly predict the impact force on the flexible ring net, and the hydro-static method can be used to calculate the impact force on the supporting structures.

Four debris flow impact tests were conducted to investigate the interaction mechanisms of debris flows with a flexible barrier. In these tests, the man-made debris flows mixture was composed of gravel, CDG, and water. The deposition and impact behaviours of debris flows on a flexible barrier with different initial conditions are investigated from the test results of three consecutive debris flow impact tests. Another debris flow test was performed to study the interaction behaviour of a debris flow impacting, filling, and overflowing a flexible barrier in a short period (less than 1 second). Force distribution on the flexible ring net during the impact process is analysed and presented based on measured data. It is found that

the impact loading from a debris flow is not uniformly distributed on the flexible ring net, and the impact pressure on the central area is much larger than that on the side areas.

Based on the findings of the experiment results, a simple method is derived to calculate the impact force of a debris flow on a permeable flexible barrier considering the passing-through of slurry and small particles during the impact process. This method simplifies the debris flow as a two-phase flow: the debris phase that can be retained by the flexible barrier and the slurry phase that can pass through the flexible barrier. This simple method is verified by the data of the large-scale physical modelling tests and well-documented laboratory tests in the literature.

Finally, a developed design approach for flexible barriers in debris flow mitigation is proposed. Two steps are identified in this approach: firstly, the retaining capacity of a flexible barrier is determined based on the deposition characteristics and the retaining rate of potential debris flows; secondly, a new load approach is proposed and utilized to determine the impact forces on the flexible ring net and on the supporting structures separately. In the load approach, the impact process of a debris flow is divided into three stages: the first thrust, the debris filling stage, and the overflow stage. Relevant equations are derived to calculate the impact forces at different stages based on the findings in this study. With the application of this design approach, the flexible barriers in debris flow mitigation can be designed using basic parameters and active volumes of potential debris flows in the protection area.

Based on the above works, a summary of findings and conclusions are then presented. Recommendations for further studies are also suggested.

PUBLICATIONS ARISING FROM THE THESIS

Journal papers:

Tan, D. Y., Yin, J. H., Qin, J. Q., Zhu, Z. H., and Feng, W. Q. (2018). Large-scale physical modeling study on the interaction between rockfall and flexible barrier. *Landslides*, *15, 12, 2487–2497*.

Tan, D. Y., Yin, J. H., Feng, W. Q., Qin, J. Q., and Zhu, Z. H. (2018). Large-scale physical modelling study of a flexible barrier under the impact of granular flows. *Natural Hazards and Earth System Sciences, 18, 2625-2640, https://doi.org/10.5194/nhess-18-2625-2018.*

Tan, D. Y., Yin, J. H., Feng, W. Q., Zhu, Z. H., and Qin, J. Q. (2018). A New Simple Method for Calculating Impact Force on Flexible Barrier Considering Partial Debris Flow Passing-through. Submitted to *Journal of Geotechnical and Geoenvironmental Engineering.*

Tan, D. Y., Yin, J. H., Zhu, Z. H., Qin, J. Q., and Chan H.C.M. (2018). A New Fast Door-opening Method for Quick Release of a Rock Boulder or Debris in a Large-scale Physical Model. Submitted to *International Journal of Geomechanics.*

Tan, D. Y., Yin, J. H., Qin, J. Q., Zhu, Z. H., and Feng, W. Q. (2018). Experimental Study on Impact and Deposition Mechanisms of Multiple Debris Flows on a Flexible Barrier. Submitted to *Landslides*.

Conference paper:

Tan, D. Y., Yin, J. H., Qin, J. Q., and Zhu, Z. H. (2017). New Thoughts for Impact Force Estimation on Flexible Barriers. In *Workshop on World Landslide Forum* (pp. 457-463). Springer, Cham.

ACKNOWLEDGEMENTS

I would like to express my deepest gratitude to my supervisor, Chair Professor Jian-Hua Yin, for his supervision and guidance of my research. His great support and patient direction made this study possible. It is my highest privilege to own the precious opportunity of studying and working with Professor Yin. His teaching and guiding have appreciably enlightened my professional development, my perspectives, and my lifelong career.

My sincere gratitude goes to Prof. K. T. Chau for supporting me during my research project, to Prof. Jin Ooi, and to Prof. Zhong-Qi Yue. Also, financial supports from The Hong Kong Polytechnic University and a CRF project (PolyU12/CRF/13E) from Research Grants Council (RGC) of Hong Kong Special Administrative Region Government of China are gratefully acknowledged.

Many great people at the Faculty of Construction and Environment have contributed to this work in different ways. My special appreciation goes to Dr. FENG Wei-Qiang for his great support and help in my research and my daily life, who always goes the extra mile to help me without hesitation, to ZHU Zhuo-Hui and QIN Jie-Qiong for the great cooperation and memorable experience together, and to all loveable colleagues.

Finally, I would like to express my sincere thanks to my parents, my wife, my brother, my teachers, and my friends. They accompany with me, support me, and encourage me when the cloud hides the light. I will always cherish them as the treasure of the life in future.

TABLE OF CONTENTS

LIST OF FIGURES

LIST OF TABLES

CHAPTER 1: INTRODUCTION

1.1 Background of the research

It was estimated that almost 10% population in the world live in mountainous terrain (Gerrard 1990). Natural hazards in mountain areas, represented by landslides and debris flows, impose huge threat to human lives and their properties (Hewitt 2004; Takahashi 2014; Costa 1984; Su et al. 2017). According to the data from the World Bank, landslides and debris flows caused more than 18000 deaths in 1908 – 2000 (Dilley et al. 2005). In Hong Kong, over 60% of the total land area is natural terrian. High degree of urbanization and shortage of land resources have necessitated development in the vicinity of natural hillsides with increasing risks of rockfalls and debris flows (GEO 2016).

Rockfall presents a severe danger in mountainous regions and other landforms including cliffs, cuttings for transport infrastructure, and quarry faces (Spadari 2013). The lost related to a single rockfall, which has the features of high frequency and unpredictability, can be extremely high in terms of human lives, repairing or rebuilding of infrastructure, or interrupting of transportation. The damages caused by rockfall hazards were documented in the literature (Bunce et al. 1997; Badger and Lowell 1992; Chau et al. 2003; Volkwein et al. 2011a; Spadari et al. 2012). For example, a large boulder with the weight of 26 tons fell from a 30 m high rock slope, hit a van and killed the driver in 1995, Hong Kong (see Figure 1-1). Thus, appropriate mitigation systems should be established in high-risk areas to prevent the damage.

Debris flows, as one of the most disastrous natural geohazards, have caused destructive damages to human lives and their habitations in many countries such as the U.S., Japan, Swiss, and China (Nakano et al. 1974; Petley 2012; Takahashi 2014; Hungr 1995; Schuster et al. 2002; Wendeler 2008; Ishikawa et al. 2008; Su et al. 2017; Zhang 1993). In Hong Kong, a landslide in Yuen Mo Village demolished a number of houses and caused three deaths in May 1982 (see Figure 1-2). Debris flows are normally originated from shallow landslide failures, entraining loose and nearly saturated soils (Santi et al. 2011; Iverson and Vallance 2001) along complex topography (Hungr 1995), reaching the deposition area with extremely high velocity (Takahashi 2014). In mountain areas with a large amount of accumulated loose sediment, multiple debris flows may occur under intensive heavy rains (Xu et al. 2012; Yagi et al. 2009; Chen et al. 2017). Compared with rockfalls and rock avalanches, debris flows present complicated interaction mechanisms with mitigation systems. Among those countermeasures, flexible barriers can attenuate the impact forces by large deformation and by allowing partial debris flow pass through.

Flexible barriers were firstly utilized to prevent the damage from rockfalls. Recently, this countermeasure is regarded as a potential measure in the mitigation of other geohazards such as granular avalanches (Ashwood and Hungr 2016) and debris flows (Leonardi et al. 2016). Because of the light weight of a flexible barrier, it can be transported into difficult-to-access mountain regions by helicopters and installed in the triggering area to prevent the debris flows at the initial stage (Wendeler 2016, Volkwein 2014). According to Wendeler (2016), the main differences between a rockfall-resistant flexible barrier and a debris flow-resistant flexible barrier are:

- A rockfall normally imposes a concentrated impact load in a short duration between 0.2 and 0.5 s, which can lead to a large deformation of the flexible ring net from 5 - 12 m. The rockfall-resistant flexible barrier stops the motion and dissipates the kinetic energy of the falling boulder mainly by the structure strength. Flexibility of the flexible barrier can reduce the impact peak loading from the single boulder by its large deformation.

- A debris flow imposes a less dynamic distributed load on the flexible net in a longer time duration between 1 to 90 s, fills the flexible barrier gradually, and contributes to a deformation between 2 - 3 m. During the interaction process, the flexible barrier traps the first reached debris front and forms a debris deposition dam to stop the following entire debris flow. Flexibility of the flexible barrier attenuates the dynamic impact load of the debris front by its large deformation. Permeability of the flexible barrier allows water and small particles in the debris flow pass the mesh net, which can also reduce the dynamic force of the debris front and accelerate the dewatering process of the debris deposition.

Due to the unpredictability of natural hazards and the difficult-to-reach install locations of flexible barriers, few reliable field data from rockfall and debris flow events have been obtained. Moreover, the motions of rockfalls and debris flows along the natural slopes and valleys with complex topography conditions are difficult to be analysed. Therefore, physical modelling is preferred by researchers in the study on natural hazards and their mitigation because of the good controllability in testing conditions and high reliability of testing results (Paik et al. 2012; Wendeler et al. 2006; Bugnion et al. 2012). Small-scale tests are not suitable for the study on rockfall mitigation because the kinetic energy of miniaturised falling boulders and the dynamic response of the mitigation system in small-scale physical modelling facility cannot realistically replicate the real cases. Therefore, full-scale rockfall tests have been performed by researchers (Spadari 2013). For the study on debris flow and its mitigation, laboratory tests can be used to qualitatively study the interaction between a debris flow and a flexible barrier with appropriate dimensional analysis (Wendeler et al.

2018). Considerable small-scale flume tests were carried out to investigate the impact mechanisms of different debris materials and the performances of different protection measures (e.g. Scheidl et al. 2013; Wendeler and Volkwein 2015; Choi et al. 2014). However, for the quantitative study in geotechnical and geological engineering, scaling is a key parameter in the experiment design. For miniaturized debris flows generated in small-scale tests, the effects of viscous shear resistance, friction, and cohesion are over-represented, whereas the effects of excess pore-fluid pressure, which are generated by debris dilation or contraction, are under-represented (Iverson 2015). Geotechnical centrifuge facilities can reproduce the stress conditions of field-scale debris flows, but the miniaturized physical model cannot realistically replicate the dynamic responses of different components in a prototype flexible barrier and the stiffness of flexible ring nets applied in the field (Wendeler et al. 2018). Thus, centrifuge modelling is not suitable to study the dynamic interaction of a debris flow with a flexible barrier and the loading transference between different components in a flexible barrier. Large-scale physical modelling can overcome the scale effect and study the dynamic response of a prototype flexible barrier under the impacts of rockfalls and debris flows. This methodology has been widely applied by researchers to study the behaviours and mitigations of rockfalls and debris flows (Peila et al. 1998; DeNatale et al. 1999; Wendeler 2008; Paik et al. 2012; Bugnion et al. 2012; Brighenti et al. 2015). Therefore, large-scale physical modelling is selected in this study to investigate the interactions of rockfalls and debris flows with a flexible barrier.

1.2 Research gaps and objectives

Flexible barriers are efficient countermeasures to prevent the damage from rockfalls and debris flows. However, before the widespread implementation of this measure, some scientific challenges still exist:

- A comprehensive understanding of the interaction mechanisms of rockfalls and debris flows with a flexible barrier is still out of reach. How flexibility and permeability of a flexible barrier can attenuate the impact forces, and what are the impact mechanisms of multiple debris flows on a flexible barrier are still open questions.
- Accurate simple methods to calculate the impact forces from a rockfall or a debris flow on a flexible barrier are required. Reliable data from well-monitored large-scale tests are needed to calibrate and validate the proposed simple methods.
- A practical design approach for flexible barriers in debris flow mitigation is lacked.

To fulfill these research gaps, large-scale physical modelling is selected as the main methodology of this study. A large-scale physical modelling facility was designed and built in The Hong Kong Polytechnic University. A novel fast door-opening method was implemented in this facility to initiate rockfalls and debris flows without being interfered. A comprehensive dynamic measuring system was established to monitor the interaction of the impact mass with the flexible barrier and measure the impact loadings on different components of the flexible barrier. Using this facility, two boulder impact tests, two dry granular flow impact tests, and four debris flow impact tests were conducted. Basic information of those tests is listed in Table 1-1. By initiating different natural hazards and studying their interactions with the flexible barrier, the objectives of this research are as follows.

a) To identify the interaction characteristics between different impacting masses (rockfalls, granular flows and debris flows) and a flexible barrier;
b) To quantify the influence of flexibility and permeability of flexible barriers on impact force attenuation;
c) To propose reliable simple methods to determine the impact forces of a rockfall or a

debris flow on a flexible barrier;

d) To establish a practical design approach for flexible barriers in debris flow mitigation.

1.3 Structure of thesis

Including the introduction, this thesis has nine chapters, described as follows:

Chapter 2 classifies the gravitational natural hazards and reviews the research methods on rockfalls, debris flows and corresponding mitigation measures for those geohazards. Among those countermeasures, the flexible protection system, as the main research subject in this study, is comprehensively reviewed. From the review, it is concluded that large-scale experimental modelling is the most suitable research methodology for the study of natural hazards and their interactions with flexible barriers. Simple methods for impact loading calculation and design approaches for flexible barriers in debris flow mitigation are reviewed in this chapter as well.

Chapter 3 describes a developed large-scale physical modelling facility. The model setup and the instrumentation are presented in detail. There are two main developments in this large-scale model. A novel fast door-opening method was implemented to initiate rockfalls and debris flows. A dynamic monitoring system was established to measure the interaction of the impact mass with the flexible barrier. With this dynamic monitoring system, the impact force on the flexible ring net and the force transferred to the supporting structures of the flexible barrier can be directly measured using the equations derived in this chapter.

Chapter 4 presents the results of two large-scale boulder impact tests. In those tests, the boulders with different diameters (400 mm and 600 mm) were used to impact a flexible barrier. In this chapter, the motion of the boulder during impact, the impact force histories on the flexible ring net and on the supporting structures are presented and analysed. A semi-empirical method is proposed in this chapter to estimate the impact force from a single boulder on a flexible barrier. Both the impact area of the boulder and the stiffness of the flexible barrier are integrated in this method. This method is calibrated and verified by the results of the large-scale tests.

Chapter 5 presents the results of dry granular flow impact tests. In these tests, two consecutive dry granular flows were initiated to impact a flexible barrier. The motions and the deposition mechanisms of dry granular flows are plotted and analysed in this chapter. Due to the poor fluidity of dry granular flows, only the first granular flow successfully impacted on the flexible barrier. The impact and the deposition behaviour of the granular flows and the impact force on the flexible barrier are presented and analysed. The hydro-dynamic method and the hydro-static method are verified using the measured impact forces on the flexible ring net and the force on the supporting structures.

Chapter 6 presents the results of a series of debris flow impact tests. Two groups of tests were performed to study the impact mechanisms of multiple debris flows and a single debris flow on a flexible barrier. In the multiple debris flow impact tests, how the initial condition of the flexible barrier can affect the impact mechanism of a debris flow is investigated. In the single debris flow impact test, the impact force distribution on the flexible ring net during the interaction process is presented and analysed. It has been found that the impact force on the central area is larger than that on the side areas.

A new simple method for impact loading calculation is derived in Chapter 7. This method regards a debris flow as a two-phase flow which contains the debris phase that can be retained by the flexible mesh net and the fluid phase that can pass through the flexible mesh net. In this method, the total impact force on the flexible barrier is calculated from the momentum changes of both phases. The results of two large-scale physical modelling tests and the data of laboratory tests in the literature are used to verify this simple method.

A developed design approach for flexible barriers in debris flow mitigation is presented in Chapter 8. This method consists of two aspects: (a) to determine the retaining capacity of the flexible barrier and (b) to determine the design impact force on different components of the flexible barrier based on the calculation of the impact forces at different impact stages: *first thrust*, *debris filling stage* and *overflow stage*.

Finally, Chapter 9 summaries and concludes this research work. Recommendations for future studies are also provided.

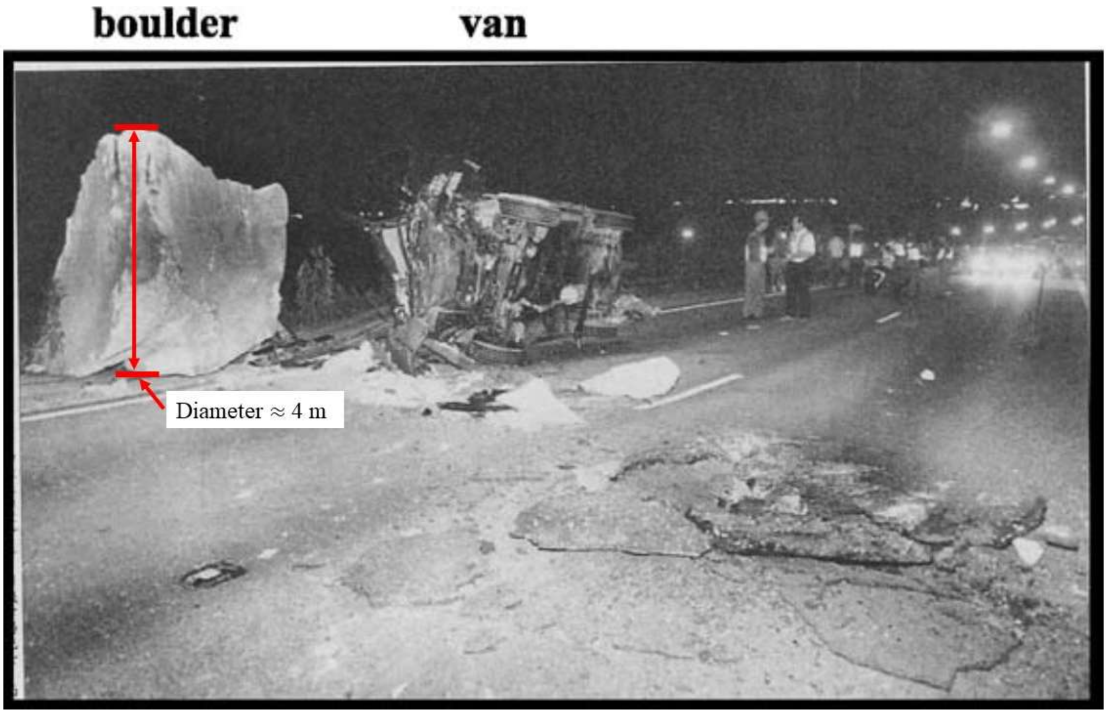

Figure 1-1. Photograph of the rockfall occurred in 1995, Hong Kong (Chau et al. 2002)

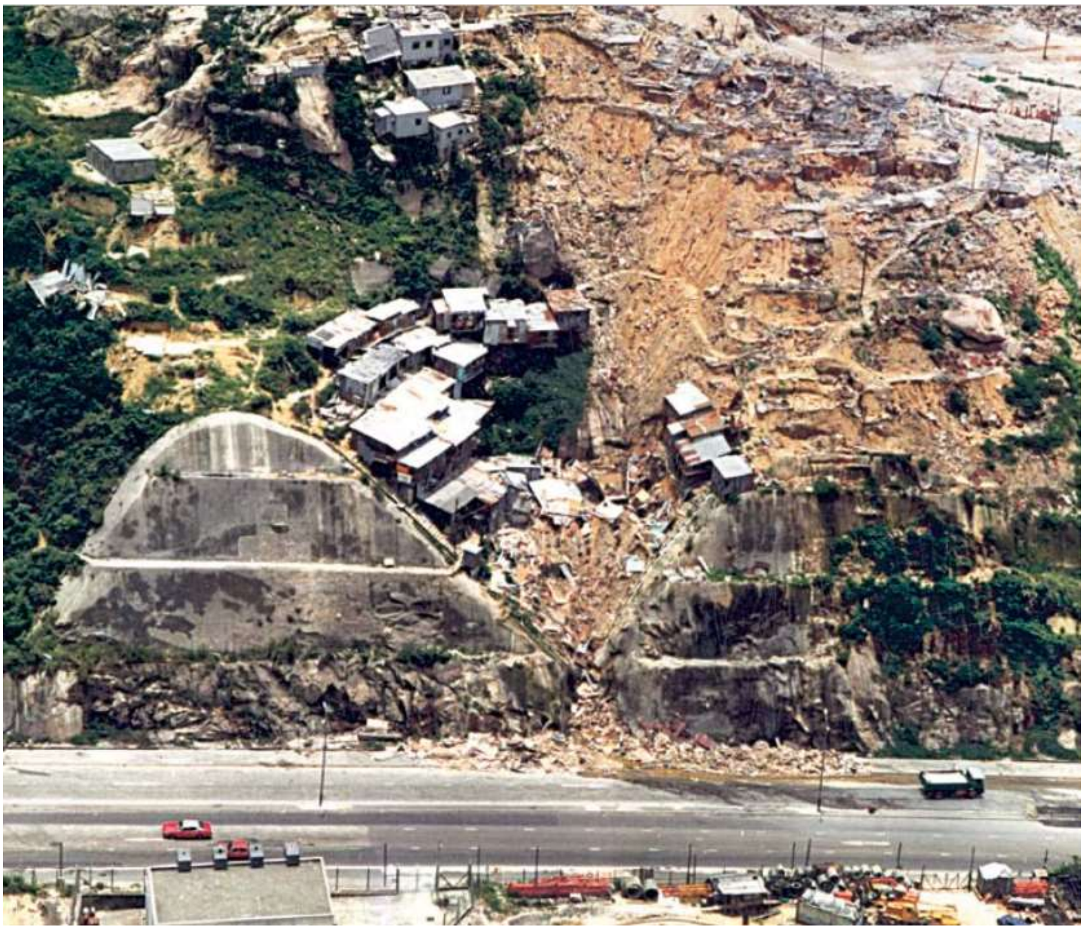

Figure 1-2. Landslide in Yuen Mo Village, Lam Tin on 29 May 1982 (CEDD 2013)

Table 1-1. List of conducted large-scale tests

Type of test	**Number of tests**	**Testing material**	**Name of test**
Boulder impacting flexible barrier	2	Boulder (400 mm, 600 mm)	Boulder Test 1 Boulder Test 2
Granular impacting flexible barrier	2	Granular (diameters between 15-30 mm)	Granular Test 1 Granular Test 2
Multiple debris flows impacting flexible barrier	3	Debris (PSD curve presented in Figure 6-1)	Debris Test 1 Debris Test 2 Debris Test 3
Single debris flow impacting flexible barrier	1	Debris (PSD curve presented in Figure 6-1)	Debris Test 4

CHAPTER 2: LITERATURE REVIEW

2.1. Rockfall

Rockfall is one of the most common natural hazards in mountainous areas with the features of high frequency and unpredictability (Labiouse et al. 1996; Matsukura 2001; Wang and Cavers, 2008; Mavrouli et al. 2017). Without suitable mitigation measures, falling boulders can cause disastrous damage to human habitats (Volkwein et al. 2011a; Spadari et al. 2012). The classification of the mass movements based on different moving processes and moving materials for engineering purpose is listed in Table 2-1 (Varnes 1958). Due to the research scope of this study, the classification focuses on the movements of soil and rock materials on natural slopes. It should be noted that the movements in the form of falling, sliding, and flowing may transform from one to another in one event.

Rockfall is the fastest type of landslide (Spadari 2013). Normally it can be divided into three categories: rockfall, rock-slide, and rock-avalanche. The classification is mainly based on the size and total volume of the travelling rock. Rockfall is an isolated rock falling suddenly and unpredictably from a rock slope or a cliff. The maximum volume of a single boulder can reach 100 m^3 (Agliardi and Crosta 2003). Rockslide is an entire block of rock with a volume from 100 to 100,000 m^3 sliding down. In comparison, rock-avalanche has a greater volume from one million to several billion cubic meters (Wendeler 2016).

This study mainly focusses on the impact of a single rockfall due to the high frequency and unpredictability. A rockfall can experience free falling, bouncing, rolling or a combination of these movements (Azzoni et al. 1992; Giani 1992; Dorren 2003). Richie (1963) suggested that the conversion between those motions depends on the slope angle: free falling occurs on slopes steeper than 70°; rolling occurs on slopes gentler than 45°; and bouncing happens on slopes with the inclination angles between 45° and 70°. Both rotational and translational motions can occur in boulders rolling from slopes inclined gentler than 70° (Chau et al. 2002).

Estimation of the maximum impact loading from the falling boulder is important for the design of protection systems (Yu et al. 2018a). Several theoretical models have been proposed to calculate the impact force on rigid barriers (Kawahara and Muro, 2006; Zhang et al. 2018). However, those models are not suitable for flexible barriers, as the behaviour of flexible barriers subjects to impact consists of both moving (sliding and rotating) and stretching of the rings (Nicot et al. 2001), which is too complicated to be predicted by theoretical models. Thus, empirical approaches were proposed to estimate the impact loading from the falling boulder (Kwan 2012; Peila et al. 1998). Basic parameters of the impact mass and empirical coefficients are integrated into those approaches.

2.2 Debris flow

2.2.1 Classification of debris flow

Hungr et al. (2001) classified landslides into 10 sub-categories based on the materials, water contents, and velocities (see Table 2-2). From the classification in Table 2-2, a debris flow is a rapid flow of saturated debris with the high water content travelling down through a channel, and a mud flow is a very rapid fine-grained debris flow with the high water content. Normally, a debris flow has a solid concentration of 30% to 70% (Wendeler 2016). Particle size distribution of debris material in a debris flow can also be used to subdivide debris flows (Wendeler 2016). If the debris material in a debris flow is mainly made up of fine material, it is referred to a slurry debris flow, which normally has a density ranging from 1600 to 1900 kg/m^3. If the debris material in a debris flow has a high content of rocks and blocks, it is normally regarded as a granular debris flow, which has a density ranging from 1900 kg/m^3 to 2300kg/m^3. The bulk density of a debris flow can obviously affect its flowing behaviour and carrying ability to large boulders (Davis 1986).

The initiation of a debris flow normally requires a steep channel ranging between 20° and 45° covered by loose sediments and fragmented rocks mixed with a large volume of water from heavy rainfall or dam-break to provide enough driving forces to the deposited debris. Sometimes, only a few tens of cubic meters of debris material will trigger a major debris flow (Jakob et al. 2005). Once the saturated debris material is mobilized, the flowing velocity can reach up to 15 m/s. During the flowing down, a debris flow can entrain loose bed material, trunks, and grow up to several hundreds of thousands cubic meters (Wartmann and Salzmann 2002; Wendeler 2016). For example, in 1990's Tsing Shan debris flow, the initial volume of 400 m^3 enlarged to tremendous 20,000 m^3 by entraining loose bed material (King 2013). The deposition of a debris flow starts when the slope angle reduces and the confinement (flowing channel) loses (Jakob et al. 2005), which can be clearly observed in the photographs of Tsing Shan debris flow plotted in Figure 2-1. A typical debris flow event may include one huge flow surge or hundreds of successive waves.

2.2.2 Simplified models for debris flow

The single-phase model was widely applied in debris flow research in the past few decades (Bagnold 1954; Chen 1988; O'Brien et al. 1993; Ancey 2007; Takahashi 2014). This model was used to deduce simple methods for impact force estimation of a debris flow (Wendeler 2008; Hungr et al. 1984; Armanini 1997; Ashwood and Hungr 2016; Song et al. 2017; Cui et al. 2015; Canelli et al. 2012; Vagnon and Segalini 2016) and establish numerical models to study the impact mechanism of a debris flow on protection structures (Sun and Law 2012; Ng et al. 2016b). Based on the grain size data of real cases, a debris flow can contain grains ranging from clay to boulders (King 2013; Iverson 1997). The boulders in debris flows is the main cause of protection structure failure (Zeng et al. 2015; Song et al. 2018b), and boulders can generate destructive impulse loads far greater than fine debris pressures (Hu et al. 2011; Song 2016). Particles with different diameters play different roles in the motion and impact of a debris flow, which is valuable to study them separately (Jeong 2014). Therefore, the two-phase flow model was proposed to describe the interaction between particles and fluid and their interactions with the mitigation structure (Hutter et al. 1995; Iverson 1997). In the two-phase model, a debris flow was divided into two-phases: the solid phase and the fluid phase. The solid phase in a debris flow had a density of ρ_s and a volume fraction of υ_s. The fluid phase in a debris flow had a density of ρ_f and a volume fraction of υ_f. By ignoring the gas entrained in the debris flow, the volume fractions of the two-phases follow:

$$\upsilon_s + \upsilon_f = 1 \tag{2-1}$$

Thus, the density of a debris flow mixture (ρ) can be calculated using:

$$\rho = \rho_s \upsilon_s + \rho_f \upsilon_f \tag{2-2}$$

Iverson (1997) suggested that the grains with the diameters smaller than 0.05 mm should also be included in the fluid phase based on the settling time of particles in fluid. Thus, the density of fluid phase (ρ_f) can be calculated with the following equation:

$$\rho_f = \rho_s \upsilon_{fines} + \rho_w \left(1 - \upsilon_{fines}\right) \tag{2-3}$$

where υ_{fines} is the volume fraction of fine grains in fluid; and ρ_w is the density of pure water.

According to Iverson (2014), mud-sized particles (diameter < 63 μm) suspended in the fluid can promote the persistence and the development of high pore-fluid pressures, which improves the debris-flow mobility by preventing the pore-pressure dissipation and reducing the energy attenuation by lubricating contacts between large particles. Considering the interaction mechanism of a debris flow with a permeable flexible barrier, the two phases of a debris flow should be classified following the impact behaviours of different phases on a permeable flexible barrier.

2.3 Flexible barriers in natural hazard mitigation

2.3.1 Introduction of mitigation measures

Protective measures are required to protect infrastructures, human lives and their properties from the threaten of natural hazards. Two types of mitigation measures are identified (Zollinger 1985): passive measures and active measures. Both types of the protection measures were classified in detail by Huebl and Fiebiger (2005) in Table 2-3 and Table 2-4. Passive measures aim to reduce the potential damage from the natural hazards. They are used to control the potential damage by hazard mapping or disaster early warning. Active measures, on the other hand, focus on mitigating the hazards directly (Huebl and Steinwendtner 2000). Their objectives are reducing the magnitude, the frequency, and the destructive power of natural hazards in the protected area, which include forestry measures, drainage control, check dams and flexible barriers. Huebl et al. (2004) proposed a strategy of protection to present the selection and design of protection measures for specific natural hazards (Figure 2-2). Following this strategy, a stepwise approach to design an appropriate protective measure for a specific objective is introduced:

Step 1: Establish the protection objectives based on risk assessment;

Step 2: Define required functions to fulfil the protection objectives;

Step 3: Select an appropriate measure to meet the specific requirements of the protection system (The selected measure should be effective in mitigating natural hazards, and they must be evaluated in the technical, economical, ecological, environmental, and political aspects);

Step 4: Establish the detailed structural design and develop a work plan of the protective project;

Step 5: Monitor and document the performance of the utilized measures to provide a better understanding of the interaction between natural hazards and mitigation measures.

2.3.2 Flexible protection systems

Flexible barriers were firstly commercially developed by Brugg in the 1970s to halt large boulders (Kane et al. 1993; Hearn et al. 1995) and suggested by Hong Kong administrative department in the report (Halcrow China Limited 2011). Detailed guidelines of rockfall-resistant flexible barrier have been published in Europe (EOTA 2013) and Swiss (Gerber 2001). Compared to conventional rigid concrete check dams, flexible barriers have a few obvious advantages: they are economical, efficient in impact energy absorption, easy to be installed, and adaptable to various terrains (Ashwood and Hungr 2016; Wendeler and Volkwein 2015). Previous studies and cases in Japan, China, U.S., and Europe have proved that the flexible protection systems can provide an efficient method of resisting dynamic loads from rockfalls and debris flows (Wendeler et al. 2008; Volkwein 2014). Therefore, as a potential countermeasure in natural hazard mitigation, flexible protection systems are valuable to be further studied. A flexible protection system normally comprises four functional components (Spadari 2013):

1) Interception structures: a flexible ring net made from stranded steel wires overlaid with a fine-meshed secondary net (see Figure 2-3) to trap huge boulders and large debris particles. The flexible ring net can attenuate the dynamic loading from the impacting mass by large deformation.
2) Connection elements: strand cables, cross tension cables (see Figure 2-4) to stretch the flexible ring net and transfer forces from the flexible ring net to the supporting structures, and energy-dissipating elements (see Figure 2-5) to dissipate kinetic energy and reduce the peak impact load.
3) Supporting structures: steel posts to increase the integral stiffness of the flexible barrier and transfer the impact forces to the foundation (see Figure 2-6). Rotatable joints connecting the post and the foundation to avoid the failure of the post at the joint (see Figure 2-7).
4) Foundations: concrete foundations to support and prevent the overturning failure of the whole protection system (see Figure 2-7).

The impact loading on a flexible barrier firstly acts on the flexible ring net, then transfers to the cross-tension outline cables, and finally distributes on the posts, cables, and supporting foundations. Generally, energy-dissipating elements are installed on the supporting cables to reduce the impact load peaks transferred to the foundations (Volkwein 2014). In Swiss and European guidelines (Buzzi et al. 2015; Volkwein et al. 2005), the maximum kinetic energy of the possible falling boulders is used to determine the retaining capacity of a flexible barrier. The kinetic energy of a boulder is obtained from the mass and the impact speed of the boulder at the location where the mitigation system is to be installed (Chau et al. 2002; Volkwein et al. 2009). However, the kinetic energy is not always a reliable criterion in the design of a flexible rockfall barrier, because, for example, the bullet effect of high-speed boulders is ignored in the kinetic energy criterion (Spadari et al. 2012; Hambleton et al. 2013; Buzzi et al. 2015; Volkwein et al. 2005; Koo et al. 2017). Thus, the impact loading of a falling boulder could be a potential alternative in the design of rockfall-resistant flexible barriers.

Recently, researchers have found that flexible barriers, which were firstly used in rockfall prevention, are effective in trapping debris flows (Canelli et al. 2012; Wendeler et al. 2007; Cui et al. 2015; Hu et al. 2006; Kwan et al. 2014). In the past years, flexible barriers have been sporadically hit by debris flows, shallow landslides or snow avalanches. From the back-analysis of those cases, flexible barriers performed well in stopping and retaining major components of debris flows and snow avalanches (Kwan and Cheung, 2012 ; Margreth and Roth, 2008). Some flexible barrier manufacturers such as Geobrugg modified the flexible rockfall barriers to improve the efficiency in debris flow mitigation. In debris flow mitigation, flexible barriers have four obvious advantages. First of all, the flexible barrier system is light in weight, which can be installed in the headstream of a risky valley with the aid of helicopters to mitigate debris flows in the early stage (Wendeler et al. 2007). Secondly, some components such as the flexible ring net and the energy dissipation elements can be replaced after being damaged, and the trapped debris can be removed by uninstalling the net (Volkwein 2014). Thirdly, the capability of large deformation and the permeability of the flexible barrier can attenuate the impact forces from debris flows and increase the capacity of trapping debris flows. Specifically, the large deformation of the flexible net can lengthen the impact period and decrease the impact loading peak, and the permeable secondary mesh net allows slurry and small particles to pass through the flexible barrier with residual velocities to reduce the impact force. In Hong Kong, brief guidelines and standards were developed by the Geotechnical Engineering Office, CEDD (Civil Engineering and Development Department) in conjunction with various academic and practicing groups (Ng. et al. 2003; GEO 2014; Kwan and Cheung 2012). Nevertheless, a comprehensive, reliable, and widely accepted design standard is necessary to be established for flexible debris-resisting barriers.

In the interaction between a flexible barrier and a debris flow, two deposition processes are identified: run-up process and pile-up process (Song et al. 2017; Wendeler et al. 2018). The run-up process was firstly defined by Wendeler (2008) from the observations of field tests, and the pile-up process was introduced by Sun and Law (2011) based on the results of numerical simulations using various initial parameters of debris flows. In the pile-up process, the debris front piles up against the barrier surface and deposits as a pile-shaped dead zone behind the barrier. The following debris flow impacts and deposits behind the previous deposition zone and can only exert pressure via the deposition zone instead on the barrier directly. In the run-up process, the debris front impacts on the flexible barrier and forms a wedge-shaped dead zone with a gentle slope surface. The following debris flow climbs up along the existing wedge and impacts the barrier directly.

2.4 Experimental study of rockfall and debris flow impact

Physical modelling has been widely used in the study of natural hazards and their interactions with barriers because of the excellent controllability in testing conditions and good reliability of testing results (Paik et al. 2012; Wendeler et al. 2006; Bugnion et al. 2012; DeNatale et al. 1999; Wendeler and Volkwein 2015).

2.4.1 Experimental study of the rockfall-barrier interaction

Flexible ring net as the key component of the flexible protection system is worthy to be tested individually. Concrete block dropping tests were performed by Grassl et al (2003) and Volkwein (2005) to study the behaviour of the net under different impacting conditions. In those tests, an accelerometer was instrumented in the dropped boulder, and load cells were used to measure reactions on the supporting ropes. Similar experiment setup was built for static loading tests (Castro-Fresno et al. 2008). This setup was used to test the failure of the net under a concentrated static load and a distributed static load. From the test results, it is found that the failure occurs first in the cables rather than the connecting points of the mesh net.

Considerable large-scale physical modelling tests have been performed to study the impact mechanism of a rockfall on a flexible protection system. Neri (1986) conducted a series of tests by using a trolley to accelerate a boulder and impact a horizontal flexible barrier. The velocities of the impacting boulders can reach up to 8.9 m/s. Peila et al. (1998) utilized an aerial ropeway to accelerate a rock block with a maximum weight of 7000 kg up to the speed of 34 m/s to impact a flexible mesh net. Using this method, the maximum kinetic energy of the boulder can reach a very high level (4000 kJ). Even though the test methods using a fixed trajectory can provide a good reproducibility, the boulders generated by those facilities can neither change the impact location nor have rotational motion. Smith and Duffy (1991) used a natural slope to accelerate the impacting blocks and built a test barrier downward the natural slope. Boulders in this type of tests can have the motion characteristics (moving with rotating) in accordance with real cases, but the reproducibility of tests is unsatisfying due to the unpredictable interaction between the block and the rough natural slope. Another option to accelerate the rockfall is free fall, which has been widely used by Gerber (2001), Gottardi and Govoni (2010), and Yu et al. (2018b). In those tests, the boulder was released from a crane at a target height to reach an expected impact velocity. Even the impact energy and the motion of the falling boulder can be quite predictable, the falling boulder cannot fully represent the realistic impact without reproducing rotation. Muraishi et al (2005) built a smooth artificial slope to accelerate a spherical block. This concept was also applied by Dhakal et al. (2011), who use cylindrical blocks as the impactor. In this way, the moving characteristics of the rockfalls can be duplicated realistically. Therefore, this method is also adopted in this study to perform rockfall impact tests.

2.4.2 Experimental study of debris flow-barrier interaction

Small-scale flume modelling

Small-scale flume tests are useful to demonstrate qualitative study on the interaction between a debris flow and a mitigation barrier with the assistance of appropriate dimensional analysis (Ishikawa et al. 2008; Wendeler et al. 2018). Small-scale tests are relatively simple to handle and easy to reproduce. This methodology allows a systematic study of the interaction of different flow types with different mitigation barriers.

Speerli et al (2010) conducted small-scale flume tests using slurry and a miniature flexible barrier to study the velocity change of a debris flow before and after passing the flexible barrier. The slurry material, with a total volume of 100 L, was a mixture of gravel, sand, silt, clay, and water. A trapezoidal flume with a basal width of 0.15 m and a side slope inclination of 45° is used in those tests. Tests were conducted using the flume with inclinations of 9° and 13° and lengths of 8 m and 6 m, respectively. Ultra-sonic measuring devices were installed to measure the flow depth and the mean velocity between two transducers. From those tests, they found that the debris flow slowed down after it overtopped the flexible barrier and accelerated again during travelling downslope. However, the determination of the flowing velocity by measuring the passing time between two known points is not accurate enough for the quantitative study of the interaction between a debris flow and a flexible barrier. To better achieve the objectives, other techniques such as high-speed video monitoring system and dynamic stress transducers shall be utilized.

Vagnon and Segalini (2016) conducted small-scale tests to analyse the impact of a debris flow on a rigid barrier and proposed a new equation to estimate the impact force. Saturated sand with the maximum diameter of 5 mm was used in the tests, which cannot represent real debris flows with a wide range of grain sizes. A steel flume with a length of 4 m, a width of 0.39 m and adjustable inclinations between 30° and 35° was used to generate debris flows. Four load cells were installed to measure normal impact forces on the barrier, ultrasonic sensors were utilized to estimate the flow velocity.

Wendeler and Volkwein (2015) utilized small-scale tests to investigate the loading characteristics of flexible barriers and investigate the relationship of the mesh size, the basal gap of the flexible barrier with the retaining rate of the debris material. Granular material was sampled from a river with the d_{90} (90% particles are smaller than this diameter) of 30 mm. The experimental facility was made up of a reservoir with the volume of 0.15 m^3 and an inclined chute with a length of 3.88 m, a width of 0.3 m and an inclination of 50°. The water content in those tests varied between 40% and 50%. A series of tests were conducted by changing the mesh size of the flexible barrier and the basal gap between the flexible barrier and the flume base. Laser devices were applied to measure the debris height and back calculate the impact velocity. High-speed cameras were used to record the filling process. Load cells were installed on the supporting posts of the flexible barrier to measure the impact loadings. In those tests, the velocities before impact varied between 3.18 m/s and 4.47 m/s. Based on the results from the small-scale tests, the authors concluded that a good retaining rate (60%) can be reached when the mesh size of the flexible barrier was smaller than d_{90} of the debris material, and the gap between the barrier bottom cable and the base surface was not larger than 2/3 of the debris flow depth.

Centrifuge modelling

Centrifuge modelling is appropriate for modelling gravity and time-dependent problems. Therefore, this technology has been widely used in natural hazard research such as earthquakes (Schofield 1981), slope failures (Timpong et al. 2007), rockfall impacts (Chikatamarla et al. 2006), and shallow landslides (Ng. et al. 2016a). The basic principle of geotechnical centrifuge modelling is creating stress conditions similar to the prototype using a model with a greatly reduced scale (Song 2016). In debris flow study, centrifuge modelling has been used to study debris entrainment (Bowman et al. 2010), debris flow initiation (Milne et al .2012), and granular flow impact and deposition (Ng. et al. 2016a; Ng. et al. 2016b).

Large-scale physical modelling

In experiment design for studying the behaviour of debris flows, scaling is a key factor because the influences of viscous shear resistance and excess pore-fluid pressure on the interaction between water and debris sediment have a close relationship with the scale of tests (Zhou et al. 2014). Iverson (2015) concluded that miniatured debris flows exhibit disproportionately large effects of viscous shear resistance and cohesion as well as disproportionately small effects of excess pore-fluid pressure, which cannot reflect the stress conditions and motion characteristics of real debris flows due to the scale effect. For the study of the interaction between debris flows and a flexible barrier, the impact energies of debris flows generated by small-scale physical models are not high enough to investigate the performance and the loading transference between different components of prototype flexible barriers. Wendeler et al. (2018) concluded based on the dimensional analysis that the flexible barriers used in the miniature tests (laboratory tests and centrifuge tests) cannot reliably replicate the stiffness and the dynamic responses of different components of a flexible barrier in the field. Neither small-scale physical modelling nor centrifuge modelling is suitable to investigate the interaction of a debris flow with particles of various diameters and a mitigation system, and the impact force distribution among different components of the protection system. Therefore, large-scale physical models have been selected by many researchers to study the behaviour of debris flows and their interaction with protection structures.

Bugnion et al. (2008) conducted full-scale experiments to study the impact and the deposition behaviours of shallow landslides. The landslide was generated by releasing 70 m^3 of debris material on slopes of 30° and 50°. Debris material used in these tests was a mixture of gravel and soil saturated with water. In the conducted tests, the velocities of the generated debris flow were between 6 m/s and 12 m/s during flowing down.

WSL (the Swiss Federal Institute for Forest Snow and Landscape Research) constructed a large-scale testing site (Figure 2-8) in Veltheim, Switzerland to investigate the interaction of multiple debris flows with a flexible barrier by conducting a series of large-scale tests (Bugnion et al. 2012). The debris flow was made up of gravel and soil mixed with abundant water. The test slope has a width of 8 m, a length of 41 m and an average inclination of 30°. At the top of the slope, a 1.8 m high tank with the capacity of 50 m^3 and a 0.8 m tall flip-down door was installed to store and release debris material (see Figure 2-8(a)). At the lower end of the slope, a prototype flexible barrier with a height of 2 m and a length of 15 m was installed to mitigate debris flows. With this facility, multiple debris flow impact tests were conducted. In the tests, multiple debris flows (between 2 and 4 releases) with the volume of 50 m^3 were released to impact the flexible barrier. Load cells, cameras, force plates, and impact pressure transducers were integrated in the instrumentation system. The front velocities of the released debris flows ranged between 2.2 m/s and 13.6 m/s. Retained volumes of debris material by the flexible barrier ranged between 15 and 40 m^3. Part of the debris material overflew the flexible barrier in the multiple debris flow tests.

The U.S. Geological Survey (USGS) in cooperation with the U.S. Forest Service built a large-scale concrete flume (Figure 2-9) with a length of 95 m, a width of 2 m, a depth of 1.2 m and an inclination of 31° in 1991 (Iverson et al. 1992). In July 1996, a series of tests were conducted using this facility to quantify the performance of flexible barrier systems under the impact of a debris flow (DeNatale et al. 1999). Four different flexible barriers with the same height of 2.4 m and the same length of 9.1 m were evaluated in the tests. A load cell, an ultrasonic depth transducer, and two piezometers were placed at the impact area to measure the flow depth, vertical stress, and pore pressure of the debris flow. Load cells were installed on the supporting cables to record the tensile forces, and an extensionmeter was attached to the net to record the barrier deformation during impact. Video cameras were used to document the impact process. In the tests, up to 10 m^3 poorly granted sand travelled through the flume with the velocities ranged between 5 m/s and 9 m/s and impacted on the flexible barrier. From the experiment results, the authors summarized that the flexible ring net overlaid with a fine-meshed secondary net have an effective performance in impact energy dissipation and debris retention.

2.5 Simple methods for impact loading estimation

Short-duration rockfall impacts can cause structural failure, and long-duration debris flow impacts can induce geotechnical instability of structures. In the design of a flexible barrier for natural hazard mitigation, the selection of the flexible net, the energy-dissipating elements, the supporting posts, and the supporting cables can be determined by design forces on those components. Once the impact load on the flexible ring net is practically and accurately obtained, the impact loads on specific components can be obtained using numerical simulations (Volkwein 2005). Thus, there is a great significance to estimate the impact load on the flexible ring net practically and accurately.

2.5.1 Boulder impact estimation

Hertz contact theory (Johnson and Johnson 1987) is normally used to calculate the impact load from boulders on a rigid structure. Modification and optimization are adjusted considering the plastic deformation (Kwan 2012) and the flexibility of protection structures. For rigid barriers, an empirical method was proposed by Kwan (2012) incorporating the material stiffnesses of the boulder and the structure, which can be given as follows:

$$F_{impact} = K_c 4000 v_0^{1.2} r^2 \tag{2-4}$$

where v_0 is the impact velocity perpendicular to the barrier in the unit of m/s, r is the radius of the boulder in the unit of m, and K_c is the reduction coefficient in the unit of $kg/(m^{2.2}s^{0.8})$. For the reduction coefficient, Kwan (2012) suggested a value of 0.1 for rigid barriers. For flexible barriers, the value of K_c should be further reduced.

Peila et al. (1998) proposed a simple method to determine the maximum design force on the flexible barrier based on the kinetic energy and the maximum displacement of the boulder during the interaction with the flexible barrier. In this model, an empirical coefficient of 2.5 was used to represent the general difference between the maximum force peak and the average force. This model is given as:

$$F_{impact} = 2.5 \cdot (0.5 m v_0^2) / d \tag{2-5}$$

where *d* is the maximum displacement during the impact process, and m is the mass of the impacting boulder. However, the above-mentioned simple methods heavily rely on the empirical coefficients determined by statistical data. Those coefficients have limited physical meanings and cannot be used to predict the cases out of the statistical range (Thakur 1991). A practical and accurate simple method considering the interaction mechanism of a falling boulder with a flexible barrier is needed to calculate the impact forces for design purpose.

2.5.2 Debris flow impact loading estimation

In the design of a protection structure for debris flow mitigation, it has a great significance to estimate the impact load accurately. Simple methods, which are preferred by engineers in the design, can feasibly predict impact forces on the mitigation structures by appropriate simplification and a few basic parameters. Several simple methods were proposed by researchers to calculate the impact force on an obstacle (Wendeler 2008; Hungr et al. 1984; Armanini 1997; Ashwood and Hungr 2016; Song et al. 2018a, Cui et al. 2015; Canelli et al. 2012; Kwan and Cheung 2012; Vagnon and Segalini 2016; Proske et al. 2011). The simple methods have also been applied in flexible barrier design guidelines in Hong Kong (Kwan and Cheung 2012) and Swiss (Volkwein 2014) to predict the impact force from a debris flow.

There are two widely accepted simple methods: the hydro-dynamic method and the hydro-static method. The hydro-dynamic method is based on momentum conservation. In this method, the impact period is taking as an ideal flow with a uniform velocity impacting the barrier and deviating along the vertical direction. The impact loading is calculated from the momentum change of the decelerated debris flow during the impact (Hungr et al. 1984; Armanini 1997). The hydro-static method, on the other hand, is calculated from the earth pressure of the deposited debris (Rankine 1856). Both methods adopt empirical coefficients to reach a good accuracy in predicting real cases.

The hydro-dynamic method was first proposed by Hungr et al. (1984) and Armanini (1997) and has been widely adopted in the flexible barrier design in Europe (Volkwein 2014) and Hong Kong (Kwan and Cheung 2012). According to this method, the impact force is calculated as:

$$F_{impact} = \alpha \rho_{bulk} v_0^2 h w \tag{2-6}$$

where ρ_{bulk} is the bulk density of the debris flow (kg/m^3); v_0 is the debris flow velocity (m/s); h and w denote the flow depth (m) and the channel width (m); and α is the dynamic coefficient. For its value, Hungr et al. (1984) firstly proposed a value of 1.5; Canelli *et. al.* (2012) recommended a range between 1.5 and 5.0; Lo (2000) suggested a value of 3.0 in the design of a rigid barrier; Kwan and Cheung (2012) suggested a reduced value of 2.0 in the design of flexible barrier considering the loading reduction due to large deformation; Wendeler (2008) preliminarily considered the passing-through of slurry in muddy debris flows with lower densities (<1900 kg/m^3) by using a reduced dynamic coefficient of 0.7 and used a higher coefficient of 2.0 for granular debris flows with higher densities based on the results of field tests.

The hydro-static method was firstly proposed by Lichtenan (1973) and further developed by Armanini (1997). According to this method, the impact force is calculated as:

$$F_{impact} = 0.5\kappa\rho_{bulk} g h_{deposit}^{2} w \tag{2-7}$$

where $h_{deposit}$ is the total deposition height of the debris flow, w denotes the channel width (m), and κ is the earth pressure coefficient. Lichtenan (1973) proposed a range of values between 2.8 and 4.4, while Scotton and Deganutti (1997) suggested a range of values between 2.5 and 7.5. Ng. et al. (2016b) back-calculated a static coefficient of 1.1 for flexible barriers based on the results from granular flow centrifuge tests. Considering the flexibility of the flexible barrier, the static coefficient of 1.0 is selected by the author in this study, which is also suggested by Kwan and Cheung (2012) and Wendeler et al. (2018).

Based on the analysis of the data from field measurements and miniaturized laboratory tests, Hübl et al. (2009) found that the hydro-dynamic method does not perform very well in predicting debris flows with low velocities and high flowing depths; while the hydro-static method cannot provide a satisfying performance in predicting debris flows with high velocities and low flowing depths. Thus, the Froude-Number (*Fr*), which indicates the kinetic energy component ratio between the horizontal and vertical directions, was introduced (Armanini 1997; Scotton and Trivellato 1995; Tiberghien et al., 2007). *Fr* is defined as:

$$Fr = \frac{v_0}{\sqrt{gh}} \tag{2-8}$$

where g is the gravitational acceleration; h is the flow height, and v_0 is the debris flow velocity.

Hübl et al. (2009) integrated Froude-Number into the simple method to eliminate the scale effect based on a correlation analysis and given as:

$$F_{impact} = 5\rho_{bulk} v_0^{0.8} \left(gh\right)^{0.6} hw \qquad (2\text{-}9)$$

Cui et al. (2015) also introduced the Froude-Number into a power method based on 155 sets of data, which is given as:

$$F_{impact} = 5.3 Fr^{-1.5} \rho_{bulk} v_0^2 hw \qquad (2\text{-}10)$$

Vagnon and Segalini (2016) proposed a simple method to estimate the impact force of a debris flow on a rigid barrier based on the data of small-scale flume tests. In this method, the impact force on the flexible barrier is considered as a combination of three force components, active earth force $\left(F_{stat}\right)$, dynamic force $\left(F_{dyn}\right)$, and drag force $\left(F_{drag}\right)$:

$$\begin{aligned} F_{peak} &= F_{stat} + F_{dyn} \pm F_{drag} = \frac{1}{2} \cdot \rho_m \cdot g \cdot K_a \cdot \left(H_{\max}^2 - h_f^2\right) \cdot B \cdot \cos\theta + \\ &\alpha \cdot \rho_m \cdot v_f^2 \cdot A \cdot \cos\beta \pm \rho_m \cdot g \cdot h_f \cdot \tan\varphi' \cdot c \cdot \frac{H_{\max} - h_f}{\sin\theta} \cdot \cos\beta \cdot B \cdot \cos\theta \end{aligned} \qquad (2\text{-}11)$$

where α is the dynamic coefficient; ρ_m, h_f and v_f are the density, the flow depth and the velocity of the debris flow; A is the impact area; B is the channel width; K_a is the active lateral earth pressure coefficient derived from Rankine theory; θ is the slope inclination; β is the included angle between the barrier and the normal direction at channel bottom; φ' is the effective stress friction angle; and H_{max} is the maximum filling height behind the barrier in m.

Impact models introduced by researchers in the past 40 years were partly collected and listed in Table 2-5. Simple methods can easily calculate the impact force on the mitigation structure with a few basic parameters and several assumptions. However, the assumptions in the simple methods may oversimplify the impact process and miss some significant interaction characteristics. Without considering those interaction characteristics of a debris flow and a flexible barrier such as the large deformation of the flexible barrier and the debris flow passing-through, the impact loading can be overestimated tremendously. Nevertheless, few of current simple methods have considered those interaction characteristics. For the design of a flexible barrier, some developments are needed considering the performance of flexible barriers and the impact mechanism of debris flows.

2.5.3 Drag force of debris flow overflowing a barrier

Debris flows can exert destructive drag forces to structures such as pipelines (Zakeri 2009; Zhu and Randolph 2009). For the overflow case of a flexible barrier, the shearing between the overflowing debris flow and the deposited debris also imposes a drag force on the flexible barrier (Kwan and Cheung 2012). Therefore, it has a great significance to select an appropriate rheological model to quantify the flow behaviour and the drag force of a debris flow (Hungr 1995). Five major types of fluids have been categorized by Locat and Demers (1988) based on their flow behaviours (see Figure 2-10), and they can be differentiated using the Herschel-Bulkley model (Herschel and Bulkley 1926; Coussot et al. 1998; Wendeler 2008; Wendeler 2016; Mullenbach 2018):

$$\tau = \tau_y + \eta \left(\frac{du}{dz} \right)^b \tag{2-12}$$

where $\frac{du}{dz}$ is the local shear velocity; τ is the shear stress; τ_y is the initial shear stress; the constant η refers to the dynamic viscosity. Different τ_y and b represents different fluid types plotted in Figure 2-10. The straight line passing through the origin represents the Newtonian fluid (Line 1), which means this type of fluid has a constant viscosity under various stress states and velocities of the flow (b=1, and τ_y=0); Curve 2 presents the shear-thickening (dilatant) fluid whose viscosity increases with shear rate (b>1, and τ_y=0); Curve 3 displays an opposite slope behaviour with curve 2, which illustrates the shear-thinning (fluidizing) fluid with a decreasing viscosity under rising shear rate (b<1, and τ_y=0); The Casson fluid (Curve 4) has the same flow behaviour as the shear-thinning fluid but with an initial yield stress (b<1, and τ_y>0); Line 5 illustrates the Bingham fluid with a constant viscosity after reaching the yield stress (b=1, and τ_y>0).

The Bingham fluid model was suggested by some researchers to calculate the shear stress of a debris flow mixture (Scotto et al. 2010; Wendeler 2008). Considering the characteristics of typical debris flows, the initial shear stress τ_y in the Herschel-Bulkley model was replaced by the critical shear stress (τ_{crit}) from the Mohr-Coulomb law to describe the solid state in the Bingham model. Therefore, this model can be regarded as a combination of a frictional term and a viscosity term:

$$\tau = \tau_{crit} + \eta_b \frac{du}{dz} = \left(\sigma - p_p\right) \cdot \mu + \eta_b \frac{du}{dz} \tag{2-13}$$

where τ is the effective shear stress; σ is the normal stress; p_p is the pore-water pressure; μ is the Coulomb friction; τ_{crit} is the critical shear stress; and η_b is the dynamic viscosity.

The Voellmy fluid model has also been widely applied to back-analyse the run distance and the velocity of a debris flow (Ayotte et al. 1999; Rickenmann et al. 2006; Naef et al. 2006; Bertolo and Wieczorek 2005; Hussin et al. 2012). The Voellmy model was firstly proposed to compute rheological properties of snow avalanches (Voellmy 1955; Yifru 2014). In the Voellmy model, the viscosity term in the Bingham model is replaced by a turbulent term to calculate the shear stress. Thus, this model is a combination of a frictional term and a turbulent term:

$$\tau = \left[\left(\sigma - p_p \right) \cdot \mu + \frac{\gamma U^2}{\xi} \right] \tag{2-14}$$

where τ is the effective shear stress; σ is the normal stress; p_p is the pore-water pressure; μ is the Coulomb friction; γ is the unit weight; U is the flow velocity; and ξ is the turbulence factor.

Bingham model and the Voellmy model have been compared to predict the debris flow behaviour with numerical simulations. Rickenmann and Koch (1997) integrated several flow methods into a numerical simulation model and compared the simulation results with the behaviours of the debris flows at the Kamikamihori field site in Japan. They found the Voellmy model has the best agreement with the observed flow behaviour. Bertolo and Wieczorek (2005) also used field data to calibrate the frictional model, the Voellmy model, and the Bingham model. From the comparisons, all the three models can accurately estimate the runout distances of debris flows, and the Voellmy model has a better performance than the Bingham model in estimating the flow velocities. Ayotte et al. (1999) used the frictional model and the Voellmy model to back-analyse the runout distances of landslides in Hong Kong. The results of case study in the literature showed that the Voellmy model can perform reasonably in modelling channelized debris flows. The Voellmy model has also been applied by Kwan and Cheung (2012) in the design suggestions of debris flow-resistant flexible barriers to estimate the drag force in the debris flow overflow stage.

2.6 Design approaches of flexible barriers

Flexible barriers for rockfall mitigation have been developed in the last few decades (Hearn et al. 1995; Gottardi and Govoni 2010; Volkwein et al. 2009; Hambleton et al. 2013). The performance of the flexible barriers in rockfall mitigation can be guaranteed by the detailed European (EOTA 2013) and Swiss guidelines (Gerber 2001). For the design of a debris flow-resistant flexible barrier, a mature guideline is still lacked. The GEO (Geotechnical Engineering Office) of Hong Kong SAR Government published Discussion Notes (Sun et al. 2005; Kwan and Cheung 2012; Sun and Law 2012) and Technical Guidance Notes (*e.g.* GEO 2014) to provide suggestions and recommendations in the design of debris flow-resistant flexible barriers. Swiss Federal Research Institute WSL (Swiss Federal Institute for Forest, Snow and Landscape Research) also published a comprehensive report (Volkwein 2014) to provide a basic guide for the assessment of flexible debris flow barriers and the requirements of specific elements.

2.6.1 Determination of impact load or energy on the flexible barrier

Two different design approaches for flexible debris resisting barriers using the impact force or the kinetic energy as the design criterion were suggested in the guide published by the Hong Kong government (Kwan and Cheung 2012). The methods calculated the maximum impact load or the total impact energy on the flexible barrier during the impact process by simple parameters of the debris flow and several assumptions. Both methods are reviewed in the following parts.

Energy Method

The energy method was firstly developed by Sun and Law (2012). This method summarized the total kinetic energy during the debris flow impact process and used the total kinetic energy, which was widely used in rockfall barrier design, as the design criterion. Before the estimation of the total kinetic energy, the deposition process of the debris flow should be known first. Sun and Law (2012) developed numerical models with the DEM code and identified two different deposition processes of the debris flows with different rheological characteristics ('viscous' and 'frictional'). The two deposition processes are plotted in Figure 2-11. The whole method was based on the energy balance theory and the lumped mass assumption. To be more specific, the total energy to be absorbed by the flexible barrier was calculated by integrating the impact force during the impact period, which depended on different deposition processes. Some assumptions were made to simplify the calculation of the kinetic energy to be absorbed by the flexible barrier based on the deposition formats. Firstly, the discharge rate (Q) and the velocity (v_0) of the debris flow were assumed to be constant during the impact process. Secondly, the flexible barrier was assumed to be able to maintain the overall stability. Thirdly, for a conservative estimation of the impact energy to be absorbed by the barrier, the internal energy dissipation of the debris flow during the impact process was ignored (*i.e.* the debris mass deposited behind the barrier was assumed to be infinitely rigid). The design energy of the flexible barrier (E) should be the maximum impact energy from the impact energies calculated with the pile-up process and the run-up process, which is expressed as:

$$E = \max\left(E_{p,} E_r\right) \tag{2-15}$$

where E_p is impact energy calculated from the pile-up deposition; and E_r is impact energy calculated from the run-up deposition.

Pile-up deposition**:** Viscous debris flows moved relatively fast and piled up against the barrier during the deposition process, which was defined as the pile-up deposition (see Figure 2-11(a)). In the deposition process, the debris front shot up against the barrier and deposited behind the flexible barrier. Following surges repeated the piling deposition process. The net resistance provided by the deposited debris behind the barrier was the basal friction subtracted by the body force vector of the debris deposition in the direction of the slope inclination behind the barrier. The residual kinetic energy of the approaching debris flow referred to the impact energy on the barrier. In the pile-up deposition, the impact force exerted on the debris deposition behind the barrier was assumed to be balanced by the basal sliding resistance of debris deposited behind the barrier and the reaction force provided by the flexible barrier. The total impact energy was calculated from the integral of the impact energy from the start of the impact to the moment when the debris impact force was fully balanced by the resistance of the debris deposition. Thus, the kinetic energy to be absorbed by the flexible barrier in the pile-up deposition process can be calculated using the following equation (Sun and Law 2012):

$$E_p = \frac{\rho_{bulk} Q \alpha_{dyn} v_0^3}{4g\left(\cos\theta \tan\phi_{friction} - \sin\theta\right)} \tag{2-16}$$

where ρ_{bulk} is the bulk density of the debris flow; Q is the discharge rate; v_0 is the impact velocity of the debris flow; α_{dyn} is the dynamic coefficient; g is the gravitational acceleration;

θ is the inclination of the slope behind the flexible barrier (see Figure 2-11(a)); and $\phi_{friction}$ is the friction angle of the debris deposition behind the barrier.

***Run-up deposition*:** Frictional debris flows moved slower and performed a layer-by-layer deposition process. In the impact period, the following debris flow climbed up *via* the previous deposition wedge, impacted on the flexible barrier, deposited behind the barrier and finally formed a sloping ramp with a gradient approximately equalled to the internal friction angle of the debris flow (Sun and Law 2012). In this deposition process, the debris flow deposited layer-by-layer behind the flexible barrier, and the deposition wedge grew up gradually (see Figure 2-11(b)). Therefore, more kinetic energy of the later coming debris flow was dissipated by the friction and transformed into gravitational potential energy. Finally, the kinetic energy of the debris surge would be fully dissipated in the climbing, which indicated the finish of the impact process. The impact energy is calculated by integrating the kinetic energy absorbed in the impact process with the following equation (Sun and Law 2012):

$$E_r = \frac{\rho_{bulk} Q v_0^5 \cos(\theta+\gamma)\sin(\theta+\gamma)}{48 g^2 h \left(\cos\gamma \tan\phi_{friction} + \sin\gamma\right)^2} \tag{2-17}$$

where γ is the sedimentation angle of the debris deposition, which is plotted in Figure 2-11(b).

Force Method

The force method was firstly proposed by Wendeler (2008) and developed by Kwan and Cheung (2012), Volkwein (2014), and Wendeler et al. (2018). In this method, the impact loading on the flexible barrier during the impact process was calculated based on the force combinations at different impact stages. Normally, the dynamic impact force from the moving debris flow and the static earth pressure from the debris deposition were regarded as two main force components on a flexible barrier during the impact. For multiple flexible barrier systems designed to mitigate large-scale debris flow disasters, the overflow situation should be considered in the design of upstream flexible barriers.

In the suggested design approach by Kwan and Cheung (2012), the dynamic loading (F_{dyn}) and the static loading (F_{sta}) were calculated by Eq.(2-3) and Eq.(2-7). Figure 2-12 shows the loading situations at different impact stages. From the figure, the loading combinations at different stages can be written as:

First thrust:

$$F_{impact,1} = F_{dyn} = \alpha v_0^2 h w \rho_{bulk} \tag{2-18}$$

Deposition stage:

$$F_{impact,2} = F_{dyn} + F_{sta} = \alpha v_0^2 h w \rho_{bulk} + 0.5\kappa \rho_{bulk} g h_{deposit}^2 w \tag{2-19}$$

where h, w, v_0, and ρ are the depth, the width, the impact velocity and the bulk density of the debris flow; α and κ are the dynamic coefficient and static coefficient; and $h_{deposit}$ is the characteristic height of the debris deposition.

In the deposition stage, the static earth pressure increased gradually with the deposition of the debris flow. Thus, the maximum loading combination in the deposition stage can be calculated using the largest deposition height in this period, which can be calculated with the following equation:

$$h_{deposit} = h_{barrier}^{'} - h \tag{2-20}$$

where $h'_{barrier}$ is the height of the flexible barrier filled by the debris deposition.

Overflow stage:

In this stage, the debris flow can no longer impact on the flexible barrier directly. Instead, the debris flow imposed a drag force on the flexible barrier when moving on the top surface of the deposition wedge. Figure 2-12(iv) presents the loading situation in this stage. Kwan and Cheung (2012) and Volkwein (2014) both used the following equation to calculate the drag force (τ) on the flexible barrier:

$$\tau = h\rho_{bulk} g \tan\phi_e \tag{2-21}$$

where $\tan\phi_e$ is the equivalent friction coefficient at the interface of the overflowing debris surge and the debris deposition. Volkwein (2014) suggested using the friction angle of the debris material to represent ϕ_e. While Kwan and Cheung (2012) considered the rheological characteristic of debris flows and used the Voellmy model to represent the equivalent friction coefficient $\tan\phi_e$:

$$\tan\phi_e = \tan\varphi + \frac{v_0^2}{h\xi} \tag{2-22}$$

where φ is the friction angle of the debris flow; and ξ is the turbulence factor.

Therefore, the loading on the flexible barrier at the overflow stage can be calculated with:

$$F_{impact} = F_{sta} + F_\tau = 0.5\kappa\rho_{bulk} g h_{deposit}{}^2 w + h\rho_{bulk} g\left(\tan\varphi + \frac{v_0^2}{h\xi}\right)\frac{wh_{deposit}}{\sin\varepsilon} \tag{2-23}$$

where ε is the deposition angle, which is the combination of the slope inclination (ε_{slope}) in the retention area and the sedimentation angle (ε_{sed}) of the debris deposition. Kwan and

Cheung (2012) suggested a maximum sedimentation angle of 10° based on the back-calculated parameter in the numerical simulation; and F_τ is the drag force from the overflowing debris flow.

Wendeler et al. (2018) proposed a simple load method based on lab tests and field data, they used a force plate to measure the shear stress τ from the debris flow in field tests and concluded that the magnitude of the shear force was too small compared with the vertical stress of the debris flow (they concluded that the shear load was only 6% of the normal force), thus it can be neglected. Based on their findings, the loading situation of the flexible barrier at the overflow stage can be abstracted to Figure 2-13, which can be presented by the following equation:

$$F_{impact} = 0.5\kappa\rho_{bulk} g\left(h_f + h_{reduced}\right)^2 w \tag{2-24}$$

where h_f is the debris flow density, and $h_{reduced}$ is the reduced height of the flexible barrier after large deformation.

Shortcomings of current simple methods for impact force calculation

The energy method is criticized because it only provides an overall design kinetic energy of the whole protection system, and the impact energy distribution on specific components of a flexible barrier such as the flexible ring net and the supporting structures are difficult to identify. Besides, the energy method cannot provide satisfactory results comparing with the field data (Volkwein 2014).

The force method is more recommended because it can provide reliable impact loads on specific components of a flexible barrier. However, the value of the dynamic coefficient α in the dynamic force calculation can be varied based on the evaluations of different researchers. Moreover, empirical methods heavily rely on the observation of experiment data, and the coefficients in the empirical methods normally have limited physical meanings (Thakur 1991). In the force method, only basic parameters such as the impact velocity and the flow depth are used in the force calculation, and the interaction characteristics between a debris flow and a flexible barrier are not considered in current methods. Apparently, other parameters, such as the flowing characteristics, the stiffness of the flexible barrier, and the passing-through of the debris material can obviously affect the impact force on the flexible barrier.

2.6.2 Design procedures of a flexible barrier

Volkwein et al. (2011) proposed a stepwise design approach for debris flow-resistant flexible barriers (see Figure 2-14). Following this design approach, the design procedures of a flexible barrier can be divided into several steps: Firstly, the maximum volume of potential debris flows in a protection area is predicted based on the raining and geological data in the protection area. This volume is regarded as the required retaining capacity of the flexible barrier. With the help of the topographic conditions in the retaining area, the dimensions of the flexible barrier (the barrier height H and the barrier width w) can be calculated by the required retaining capacity using the simple method proposed by Volkwein et al. (2011) (see Figure 2-15). In this method, the height of the flexible barrier should be the reduced height (H_0') considering the large deformation of the flexible barrier in the filling process. In this method, the sedimentation angle (θ') is regarded as 2/3 of the slope inclination (θ) based on the empirical study (Rickenmann 1999). If the retaining capacity of a single flexible barrier cannot fulfil the requirement of the retaining volume, multiple flexible barriers should be established to increase the retaining capacity of the debris flow mitigation system (Volkwein 2014). With the dimensions of the flexible barrier and the parameters of the potential debris flow, the maximum impact loading on the flexible barrier can be calculated using appropriate simple methods. Then, numerical simulations can be used to calculate the loading distribution on the specific components of the designed flexible barrier. Finally, the dimensions of the components of the designed flexible barrier can be determined.

2.6.3 Other requirements for a debris flow-resistant flexible barrier

Other requirements are listed below:

(a) Wendeler and Volkwein (2015) suggested that the opening size of the flexible barrier should be smaller than d_{90} (the diameter of 90% particles are smaller than the d_{90} diameter) to reach a high retaining rate to the debris material based on laboratory tests.

(b) For the flexible barriers allowed to be overflowed, the abrasion by the overtopping debris flow on the upper cables should be taken into consideration. Abrasion protection measures should also be adjusted to the cross-tension cables and the supporting structures (Volkwein 2014).

Figure 2-1. Overview of Tsing Shan Debris Flow in 1990 (King 2013)

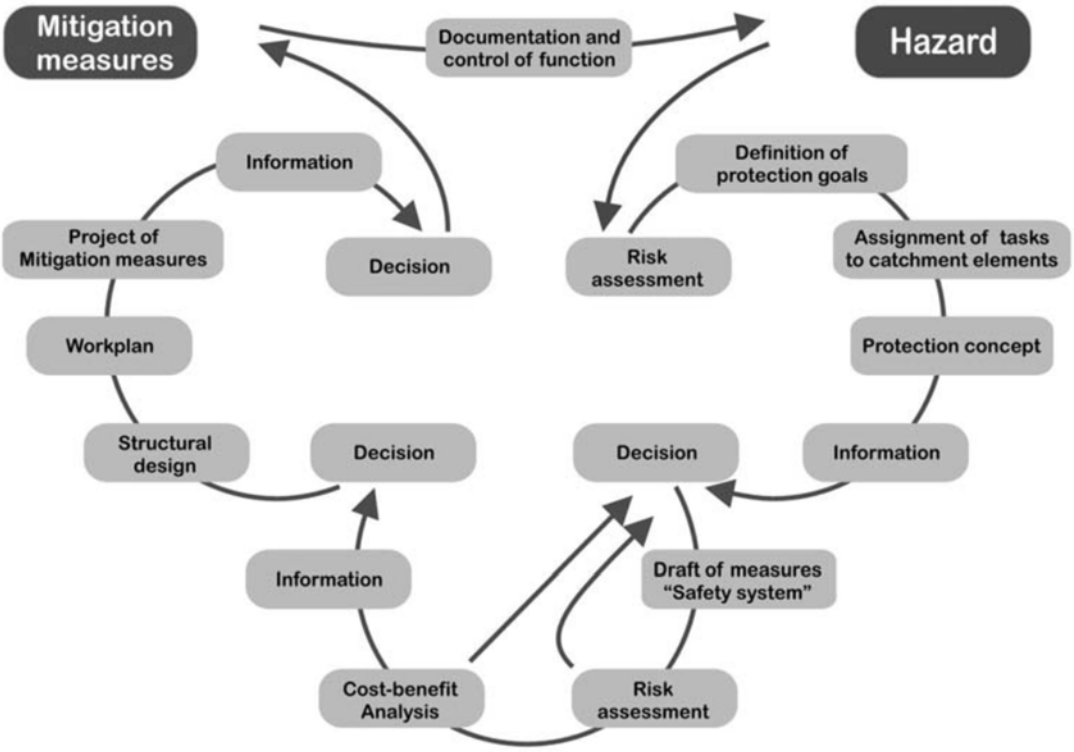

Figure 2-2. Strategy of protection (Huebl and Fiebiger 2005)

Figure 2-3. Photograph of the flexible ring net

Figure 2-4. Photograph of strand cables and cross tension cables

Figure 2-5. Photograph of energy dissipating devices

Figure 2-6. Photograph of supporting posts

Figure 2-7. Photograph of the rotatable joint and the foundation of a supporting post

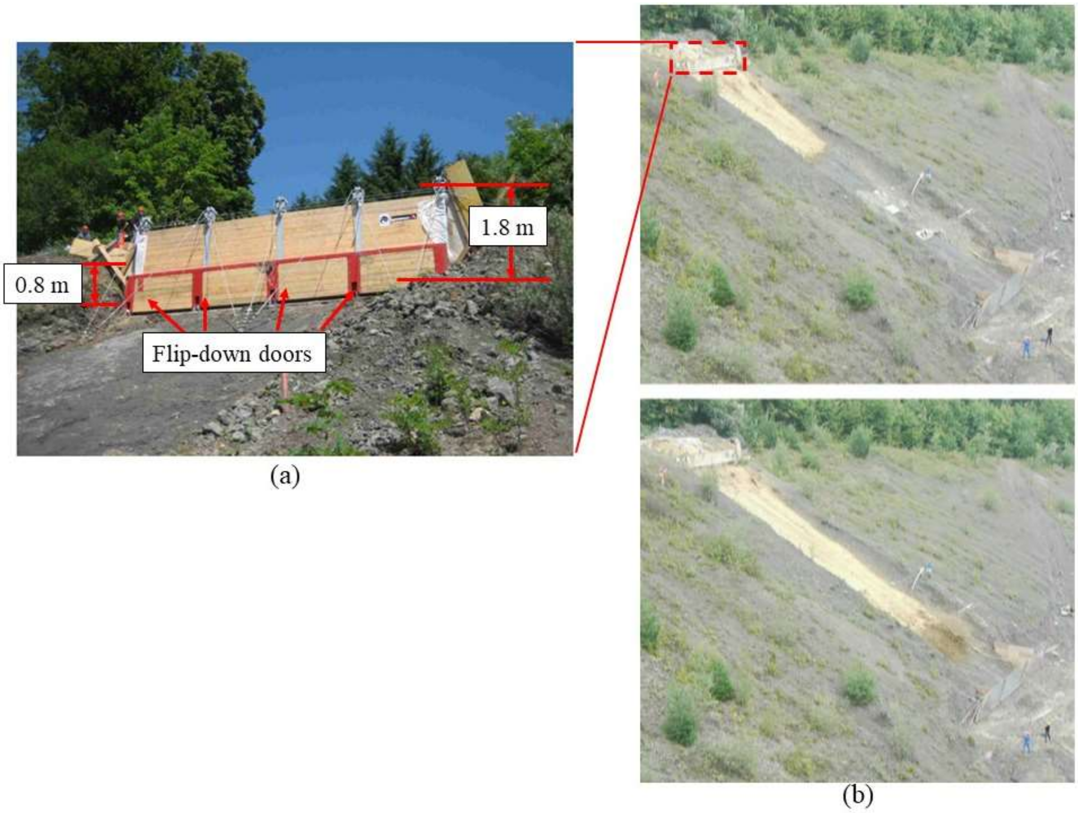

Figure 2-8. (a) Debris flow releasing apparatus and (b) lateral view of a debris flow impact test (Bugnion et al. 2012)

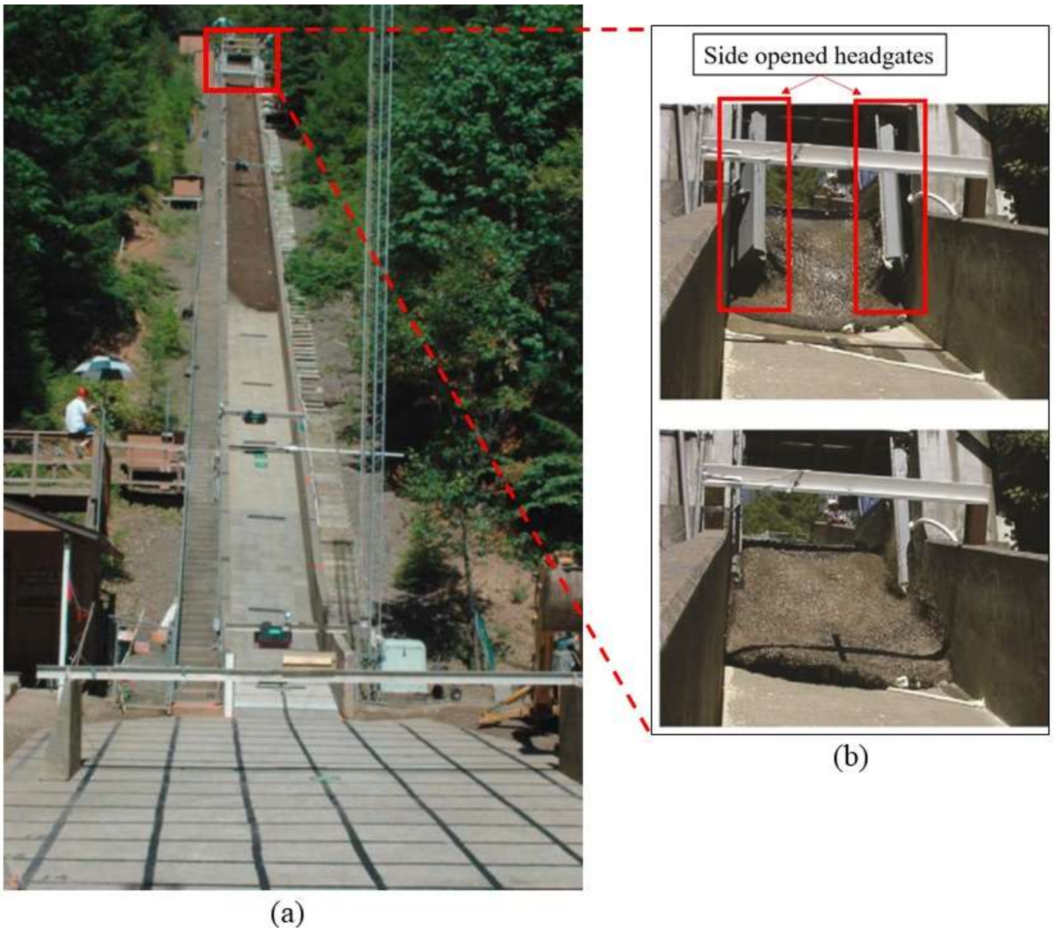

Figure 2-9. (a) Photograph of a 10 m^3 debris flow descending the USGS debris flow flume and (b) debris releasing apparatus at the H. J. Andrews Experimental Forest Test Site (Iverson et al. 2010)

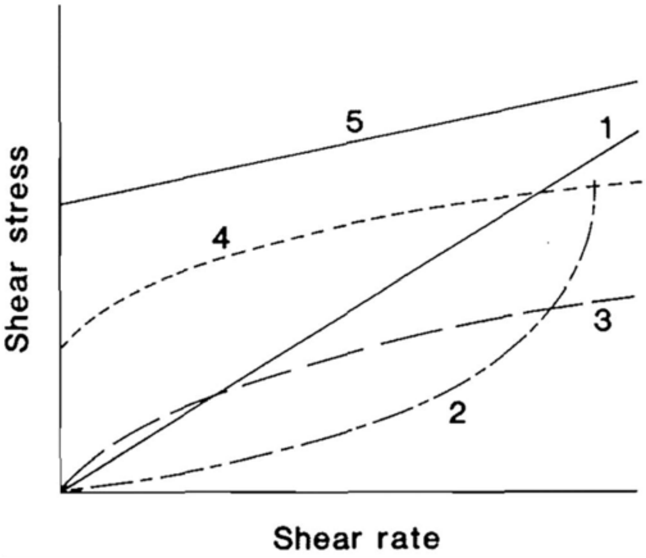

1 Newtonian fluid (b=1, and τ_y =0)

2 Shear-thickening (dilatant) fluid (b>1, and τ_y =0)

3 Shear-thinning (fluidizing) fluid (b<1, and τ_y =0)

4 Casson fluid (b<1, and τ_y >0)

5 Bingham fluid (b=1, and τ_y >0)

Figure 2-10. Relationships between shear stress and shear strain in different rheological models (Locat and Demers 1988; Yifru 2014)

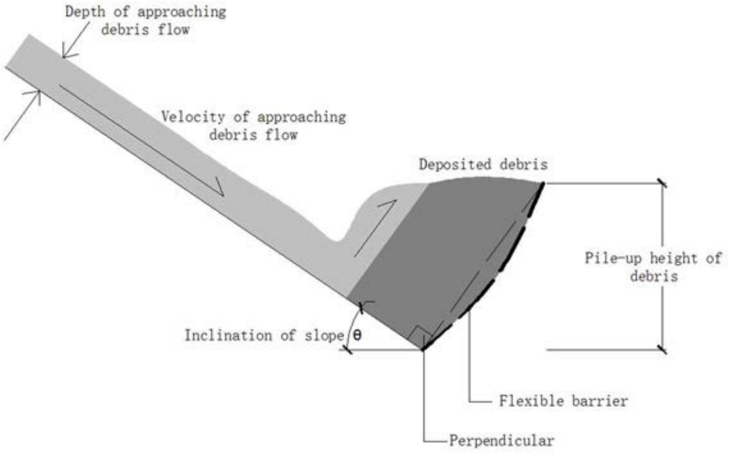

(a) Pile-up deposition process

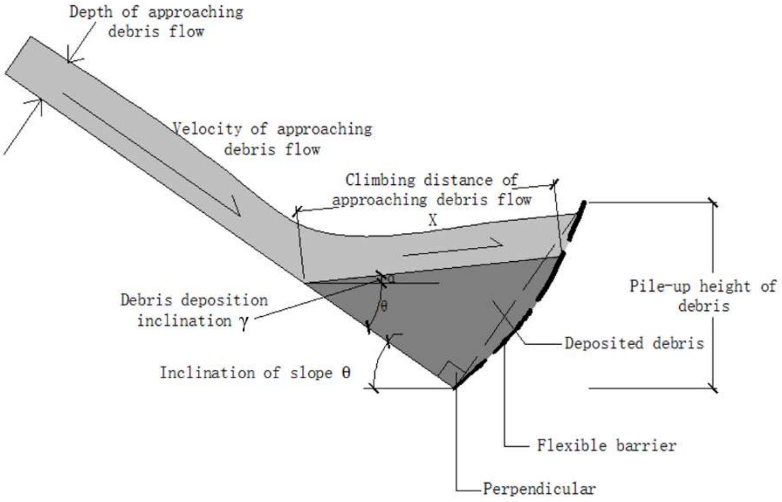

(b) Run-up deposition process

Figure 2-11. Schematic diagrams of (a) pile-up and (b) run-up deposition processes during the interaction of a debris flow with a flexible barrier

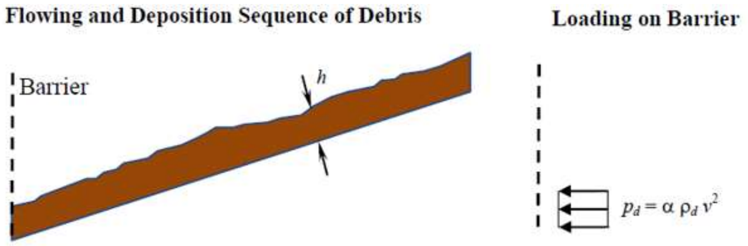

(i) Debris front reaches the barrier

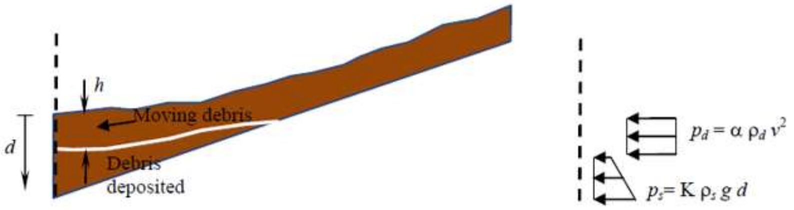

(ii) Debris starts to deposit behind the barrier

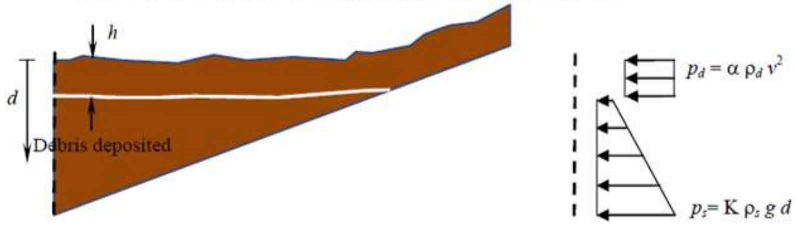

(iii) More debris deposits behind the barrier

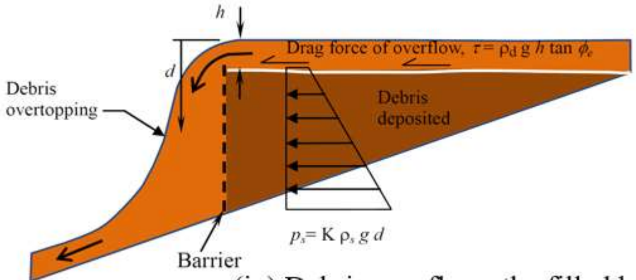

(iv) Debris overflows the filled barrier

Figure 2-12. Loading situations of the flexible barrier at different impact stages (Kwan and Cheung 2012)

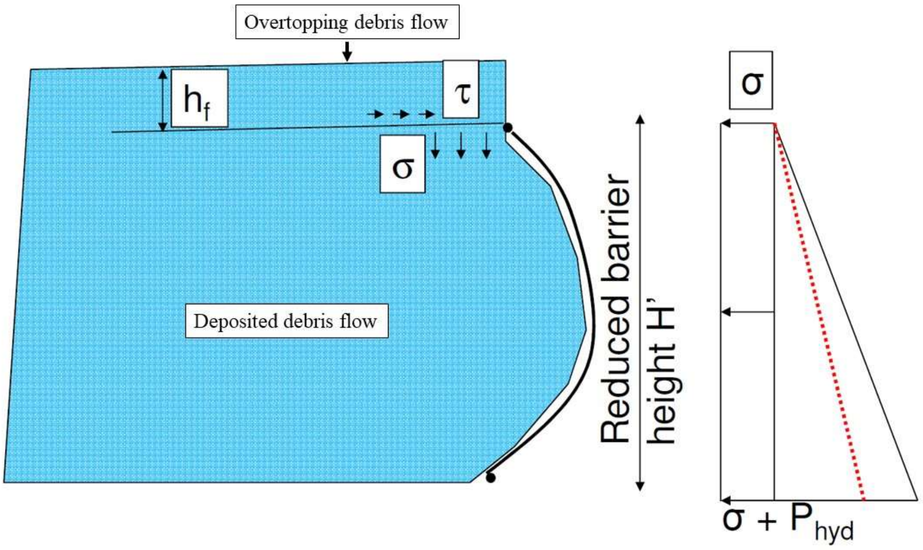

Figure 2-13. Loading situation of the flexible barrier at the overflow stage (Wendeler et al. 2018)

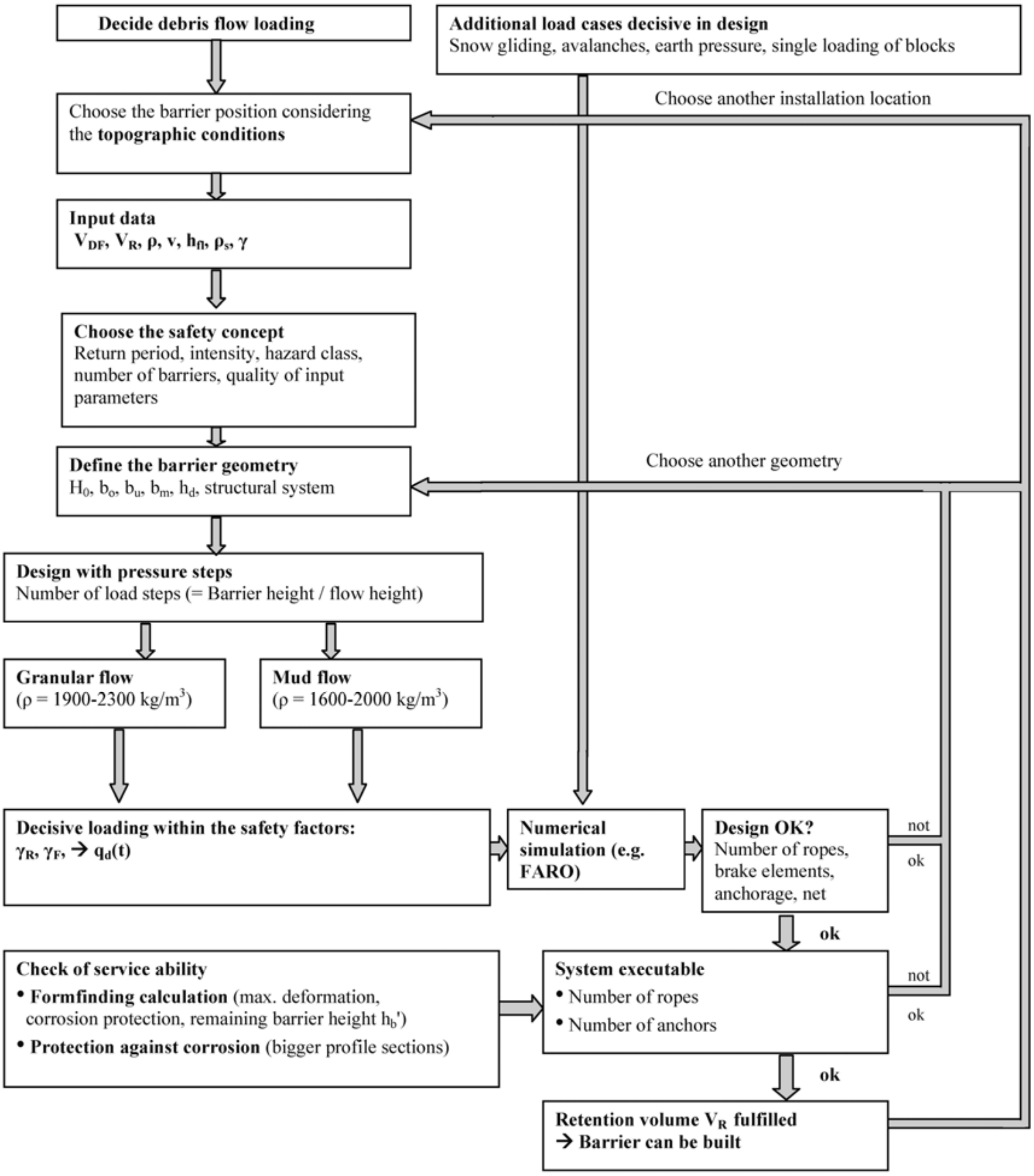

Figure 2-14. Diagram for stepwise dimensioning procedures of flexible debris flow barriers (Volkwein et al. 2011b)

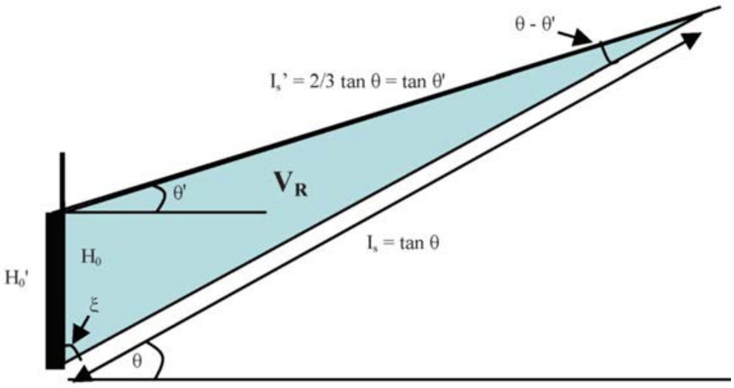

Figure 2-15. Estimation of the maximum deposition volume of a flexible barrier (Volkwein et al. 2011b)

Table 2-1. Classification of mass movements according to Varnes (1958)

Process	**Material**	
	Bedrock	Soil and sediment
Falls	Rock-/boulder fall	Soil fall
Slides	Rock-/block slide	Debris slide
Flows	Granular flow (dry)	Debris flow and mud flow (wet)

Table 2-2 Classification of flow type landslides (Hungr et al. 2001)

Material	**Water content**	**Special condition**	**Velocity**	**Name**
Silt, sand, gravel, and debris (status)	Dry, moist, or statured	No excess pore-pressure Limited volume	Various	Non-liquefied sand (silt, gravel, debris) flow
Silt, sand, debris, and weak rock	Saturated at rupture surface	Liquefiable material Constant water content	Extremely rapid	Sand (silt, debris, rock) flow slide
Sensitive clay	At or above liquid limit	Liquefaction in situ	Extremely rapid	Clay flow slide
Peat	Saturated	Excess pore-pressure	Slow to very rapid	Peat flow
Clay or earth	Near plastic limit	Slow movements Plug flow (sliding)	Less than rapid	Earth flow
Debris	Saturated	Established channel Increased water content	Extremely rapid	Debris flow
Mud	At or above liquid limit	Fine-grained debris flow	Greater than, very rapid	Mud flow
Debris	Free water present	Flood	Extremely rapid	Debris flood
Debris	Partly or fully saturated	No established channel Relatively shallow, steep source	Extremely rapid	Debris avalanche
Fragmented rock	Various, mainly dry	Intact rock at source Large volume	Extremely rapid	Rock avalanche

Table 2-3. Passive mitigation measures (Huebl and Fiebiger 2005)

Objective	Task/function	Measure
Reduction of potential loss	Local protection of an object (e.g., house, person traffic route)	● Land-use planning (local, regional) ● Information, education, and disaster management ● Specification of construction rules
Event Response	Upkeep of protective	● Closing of traffic route Information ● Warning and evacuating of hazardous areas ● Immediate technical assistance

Table 2-4. Active mitigation measures (Huebl and Fiebiger 2005)

Objective	**Task**	**Measure**
Disposition management		
Decrease runoff	Decrease peak discharge	● Forestry measures ● Watershed management ● Diversion of runoff to other catchments
Decrease erosion	Decrease surficial erosion due to overland flow	● Forestry measures and soil bioengineering ● Watershed management ● Drainage control
	Increase slope stability	● Forestry measures and soil bioengineering ● Terrain alternation (grading, scaling) ● Drainage control ● Stabilization of the toe slope (e.g., consolidation, rock buttresses)
	Decrease vertical and lateral erosion in the channel bed	● Channel enlargement ● Channel-bed stabilization ● Transverse structure (still, ramp, check dam) ● Longitudinal construction ● Groyne ● Soil bioengineering
	Decrease water discharge at high erodible channel-reach	● Diversion of runoff to other catchments ● Bypass
Event management		
Discharge control	Decrease water discharge at high erodible channel-reach	● Water storage ● Channel enlargement ● Enlargement of the cross section at channel crossings (e.g., bridges)
Debris control	Transformation process Deposition debris under controlled conditions Debris flow deflection to adjacent areas	● Debris flow breaker ● Permanent debris deposition ● Temporary debris deposition ● Deflection to area of low consequence
	Organic debris filtration	● Organic debris rake

Table 2-5 Simple models for calculating debris flow impact loading

Literature	Model	Values of coefficients	Application range
Hungr et al. (1984)	$F_{impact} = \alpha \rho_{bulk} {v_0}^2 hw$	α=1.5	Impacts of uniform debris flows on rigid barriers perpendicular to the flow direction
Kwan and Cheung (2012)	$F_{impact} = 0.5\kappa \rho_{bulk} g {h_{deposit}}^2 w$	κ=1	Static pressure of deposited debris
	$F_{impact} = \alpha \rho_{bulk} {v_0}^2 hw$	α=2	Impacts of uniform debris flows with v_0 < 12m/s on flexible barriers
Wendeler (2008)	$F_{impact} = \alpha \rho_{bulk} {v_0}^2 hw$	α=0.7	Impacts of uniform debris flows with ρ_{bulk} < 1900 kg/m^3
		α=2	Impacts of uniform debris flows with $\rho_{bulk} \geq$ 1900 kg/m^3
Ashwood and Hungr (2016)	$F_{impact} = \alpha \rho_{bulk} {v_0}^2 hw$	α=2	High-discharge tests (Fr from 4.7 to 11.5)
	$F_{impact} = 0.5\kappa \rho_{bulk} g {h_{deposit}}^2 w$	κ=1	Low-discharge tests (Fr from 1.2 to 2.7)
Lichtenan (1973)	$F_{impact} = 0.5\kappa \rho_{bulk} g {h_{deposit}}^2 w$	κ=7-11	For design the rigid structures against debris flows
Armanini (1997)	$F_{impact} = 0.5\kappa \rho_{bulk} g h^2 w$	κ=9	For flow depth h equals to the height of check dams
	$F_{impact} = \alpha \rho_{bulk} {v_0}^2 hw$	α=1	When the debris flow is deviated along the vertical direction during impact (jet-like bulge)
Zhao et al. (2018)	$F_{impact} = 0.18 \cdot F_r^{0.0052} \left(\frac{\rho_{bulk}}{\rho_{water}} \right)^{1.8142} v_0^2 hw$	N/A	Empirical equation analyzed using the data from laboratory tests
Cui et al. (2015)	$F_{impact} = 5.3 Fr^{-1.5} \rho_{bulk} v_0^2 hw$	N/A	Applicable for debris flows from miniatured scale to field scale
Hübl et al. (2009)	$F_{impact} = 5 \rho_{bulk} v_0^{0.8} \left(gh \right)^{0.6} hw$	N/A	Impacts of uniform debris flows on rigid barriers from miniatured scale to field scale
Zanuttigh and Lamberti (2006)	$F_{impact} = 0.5 C_s \left(1 + \sqrt{2} Fr \right)^2 \rho_{bulk} g h^2 w$	C_s =2-3	Impacts of debris flows with $Fr \gg 1$

CHAPTER 3: A NOVEL LARGE-SCALE PHYSICAL MODELLING FACILITY

3.1 Introduction

Research on debris flows and rockfalls and their mitigation is a very challenging topic due to the complex moving and impacting mechanisms. Large-scale physical modelling is preferred by researchers in study of debris flow and rockfall because most conditions of natural geo-hazard events can be duplicated. In this chapter, a new large-scale physical model to study the impacts of rockfalls and debris flows on a flexible barrier is described in detail. In this physical modelling facility, a novel fast door-opening method is proposed and implemented. With the application of this door-opening method, impact tests of rock boulders, dry granular flows, and debris flows were successfully performed using this facility. From the observations of different impact tests, both the unbalanced resisting force and the interference from the door were avoided. Besides, a comprehensive dynamic monitoring system is introduced in this chapter. Using this monitoring system, the interaction characteristics of the impacting masses with the flexible barrier were captured, the basic parameters of the boulders or the debris flows during the impact were obtained, and the impact force on the flexible ring net and the impact force on the supporting structures were measured.

3.2 Brief description of a large-scale physical modelling facility in Hong Kong

A large-scale testing facility is built in the Road Research Lab of The Hong Kong Polytechnic University with a length of 9.5 m, a height of 8.3 m and a width of 2 m. The view of the experiment setup is plotted in Figure 3-1. This facility can be divided into 4 main components: (i) a reservoir with the capacity of 5 m^3; (ii) a flip-up door and corresponding fast door-opening devices; (iii) a flexible barrier with supporting posts and cables; and (iv) a flume connecting the reservoir and the flexible barrier. The prototype flexible barrier with a width of 2.48 m is made up of steel rings with a diameter of 300 mm (No. ROCCO 7/3/300, Geobrugg), which are commonly used in rockfall and debris flow mitigation in Europe and Hong Kong. The ring net is covered by a flexible secondary mesh net with the mesh size of 50 mm to trap large particles in debris flows. Two parallel posts that can rotate in the plane of impact are installed to stretch and support the ring net, and each post is supported by two inclined strand cables. This flume has a channel width of 1.5 m, a length of 7 m, and an inclination of 35°. Side walls of the flume are made up of tempered glass to provide a clear observation of the generated rockfall or debris flow. Based on the parameters of the large-scale physical model built by United States Geological Survey (USGS; Iverson et al. 2010; Iverson 2015), the physical model built at The Hong Kong Polytechnic University (PolyU model) can be regarded as a large-scale physical model because it has similar dimensional parameters with respect to the USGS debris flow flume. Specifically, the capacity of testing material is 5 m^3 in the PolyU model compared to 10 m^3 in the USGS flume, and the width of the flume is 1.5 m in the PolyU model compared to 2 m in the USGS flume. Even though the length of the flume in the PolyU model is much shorter than the length of the USGS flume (7 m compared to 95 m), the flume in the PolyU model is sufficient to generate debris flows with dynamic parameters and impact energy similar to real cases. In the trial tests, the generated watery flood can reach a velocity higher than 8 m/s while flowing down.

3.3 A new fast door-opening method for quick release of a rock boulder or debris

In the design of a large-scale physical model, how to initiate or release a certain volume of debris or a giant rock boulder on a slope without being interfered is the key technical issue. In current large-scale models for debris flow research, debris material is normally released from a reservoir with a trap door located at the upper end of the flume channel. It is found that current methods for door-opening could interfere with the motions of generated debris flows. Therefore, a new fast door-opening method is proposed and implemented in the large-scale physical model to avoid the interference with the generated rockfalls or debris flows.

3.3.1 Limitations of door-opening methods in current large-scale physical models

In the design of a large-scale physical model, the release method of impacting material is very important because a poorly designed release method could seriously interfere with the motion and the impact of the debris flow. Table 3-1 lists the basic parameters and characteristics of representative large-scale physical models and their door-opening methods in detail. To better understand the interference of existing door-opening methods with generated debris flows, the representative large-scale physical facility built by USGS in 1991 is reviewed in this chapter (see Figure 2-9). This facility utilized a pair of side-opened head-gates. From the description of testing procedures and the videos of experiments (Iverson 2015), it is observed that the steel head-gates were opened by the self-weight of the debris deposit when the lock on the gates was released. The steel head-gates used in that testing facility could affect the generation of debris flows in three aspects: firstly, the kinetic energy of the generated debris flow can be dissipated obviously when pushing the heavy steel head-gates open; secondly, unbalanced frictions of the side-open doors may cause deviation of the flowing direction or asymmetrical flow velocities and depths of a generated debris flow; thirdly, the side-open doors are left in the flume as obstacles after being opened, which impedes the motion of the debris flow continuously.

To solve those problems, a developed door-opening method should have following considerations: (i) the lock of the door should be easy to operate and sturdy enough to sustain the earth pressure from the stored debris material; (ii) the door should be opened faster than the moving of the testing material to prevent the interaction with the generated rockfall or debris flow; (iii) the door should be out of the flowing path of the generated debris flow after being opened to avoid the continuous interference with the debris flow.

3.3.2 Development of a new fast door-opening method and the release system

Based on the above review, a new fast door-opening method is proposed to fulfil the requirements:

(a) A flip-up door is utilized, which can be out of the moving path after it is pulled up to avoid the continuous interference with the released boulder and debris flow.

(b) A spring set is connected to the flip-up door to lift the door up in a short period and keep the door-opening.

(c) Rotatable curve bars are utilized to lock the door, and this new type of lock can impose normal pressure on the door in the lock status by rotating up and be out of the flowing path in the unlock status by rotating beneath the flume base.

Following the above door-opening method, a new release system was designed and implemented in the large-scale facility. Beside a steel reinforced flip-up door, the release system contains 3 main components: a set of springs, a pair of rotatable steel levers, and a pair of quick release hooks (see Figure 3-2). Descriptions and functions of those components are presented in detail as follows:

The springs: in the design, 4 springs are attached to the back surface of the flip-up door. The function of the springs is lifting the flip-up door fast and keep the door open. After being stretched, the springs can provide tensile forces to flip the door up in a short time after the release of the lock and keep the door open in a large opening angle. In the facility, the designed door-opening angle is 55° to keep the door parallel to the flume. Based on the video recordings, the flip-up door can be opened in less than 0.5 s with the assistance of the spring set.

The steel levers: the levers are curved steel bars with the fulcrums installed on an I-bean underneath the flip-up door and the flume basal plate (see Figure 3-2). The levers are used to lock the door before the test and release the door to start the test. The levers can transform from the locking status to the unlocking status in a very short period (shorter than 0.5 s) by rotating up to lock the door and rotating beneath the flume to release the door and avoid interference with the initiation a rockfall or a debris flow. Rectangular openings at the basal plate of the flume provide rotation paths of the levers. Flexible rubber mats (5-mm-thick) with their upper edges fixed on the flume are used to cover those openings during the test to prevent the leakage of debris material during the test. The levers should have a high strength to resist the lateral earth pressure from debris material in the reservoir and a high stiffness to avoid a large deformation under the earth pressure. The large deformation can form a gap between the flip-up door and the reservoir, thus lead to a leakage of the debris material.

The quick release hooks: two quick release hooks are used to lock the flip-up door, which are provided by RELEASE company with the model name TGQ-5T-LS. The specially designed hook can be released fast with a small pulling force under a maximum working load of 5 t. With the application of the hooks, the door can be locked easily in the preparation stage and opened fast in the test. As shown in Figure 3-2, steel chains linking the levers and the frame base are used to restrict the rotation of the levers and lock the door when they are stretched by the quick release hooks.

3.3.3 Operating procedures of the release system using the fast door-opening method

The operation procedures of the release mechanism are plotted in Figure 3-3. The procedures can be specified into 4 steps:

(a) The door is locked by the quick release hooks via the stretched chains.

(b) Debris material is filled into the reservoir, and the springs are pre-stretched by the wire reels connected to the upper ends of the springs.

(c) At the beginning of the test, the levers are released by the quick release hooks. Then, the levers rotate beneath the flume with the assistance of dead weights connected to their tails. Meanwhile, the door is lifted in less than 0.5 second, kept open by the pre-stretched springs, and supported by energy dissipation blocks to prevent the door swinging back.

(d) After the test, the door can be closed again by releasing the springs with the wire reels.

With these simple procedures, a series of large-scale physical modelling tests with different testing materials have been successfully conducted in the large-scale testing facility using this new fast door-opening method.

3.3.4. Performance and evaluation of the new fast door-opening method

A comparison of the door-opening methods in representative large-scale debris flow physical models in the literature (Bugnion et al. 2012; Iverson et al. 2010; Paik et al. 2012) and the new door-opening method used in the present model in PolyU, Hong Kong is made in Table 3-1. Based on the comparison, the door-opening method in PolyU model is the fastest among all the representative large-scale physical models. Moreover, a series of tests have been carried with this large-scale physical model to study the interaction between different impacting masses and a flexible barrier and assess this new door-opening method. Rockfalls, dry granular flows, and debris flows have been successfully generated with the application of the fast door-opening method.

Figure 3-4 plots the performance of the door-opening method in a rockfall impact test. In the test, the flip-up door was firstly locked by the levers, and the boulder was located behind the centre of the door to make sure the boulder can hit the central area of the flexible barrier. At the beginning of the test, the flip-up door was pulled up in a short time and kept open by the pre-stretched spring set. After that, the boulder rolled down along the central axis of the flume and hit the central area of the flexible barrier. From the photographs plotted in Figure 3-4, it can be observed that the boulder was moving along the central line of the flume and impacted on the central area of the flexible barrier. Therefore, it can be speculated that the motion of the boulder was almost not impeded by the release door. The results and findings of the rockfall impact tests are analysed and presented in the literature (Tan et al. 2018b).

The performance of the door-opening method in a granular flow test is shown in Figure 3-5. In this test, around 4 m^3 aggregate was filled in the reservoir in the preparation stage, which imposed a large earth pressure on the flip-up door and the lever locks. At the beginning of the test, the door flipped up fast with the assistance of the spring set. At the same time, the levers rotated beneath the flume base, and the rubber mats covered the holes at the flume basal plate to prevent the leakage of the granular material. It can be seen from Figure 3-5 that the door opened much faster than the initiation of the granular flow. Neither the levers nor the flip-up door interfered with the granular flow. The results and findings of the granular flow impact tests are analysed and presented in the literature (Tan et al. 2018a).

The debris flow material consists of a mixture of aggregate and CDG slurry with a high water content, so the leakage of slurry should be taken into serious consideration. The leakage of slurry and water can obviously reduce the fluidity and weaken the homogeneity of the generated debris flow. To prevent the leakage problem, high compressible rubber cushions and silicone glue were filled into the gap between the door and the reservoir to provide water tightness. Besides, basket screws were attached to the ends of the chains to provide compressive stress on the door to enhance the sealing ability. It can be observed from Figure 3-5 that no leakage of slurry occurred before the test, and the generated debris front was thick and symmetrical. Therefore, it can be concluded from the tests that this new fast door-opening method applied in the large-scale physical model performed reliably, and both the unbalanced resisting force and the interference from the door were avoided.

3.4 Instrumentation of the large-scale facility and new measuring methods

3.4.1 Instrumentation

To monitor the performance of a flexible barrier under the impact, this facility is instrumented with a well-arranged high-frequency monitoring system. This monitoring system consists of numerous tension link transducers, a dynamic datalogger and two high-speed cameras. Two types of transducers are installed on the flexible protection system: mini tension link transducers and high capacity tension link transducers. The mini tension link transducers were calibrated in the soil laboratory with a maximum loading of 20 kN. The calibration process and result are plotted in Figure 3-7. Those transducers are installed on the flexible ring net to measure the impact force on the flexible ring net directly. Specifically, the central area of the flexible ring net, which consists of 5 connected rings, is separated from the main net and reconnected to the neighboring rings by 10 mini tension link transducers, (see Figure 3-8). Figure 3-9 presents the instrumentation of the large-scale physical modeling facility. From the instrumentation arrangement, four high capacity tension link transducers (Type: CFBLBH) with a certified capacity of 50 kN are installed on the supporting cables of the posts. A data-logger with the capability of sampling 48 transducers at 1000 Hz simultaneously is used to collect the data of all transducers. Two high-speed cameras capable of capturing a resolution of 1024 ×768 pixels at a sampling rate of 1000 frames per second are used to capture the motions of the granular flows and the deformation of the flexible barrier under impact. The arrangement of the high-speed cameras is plotted in Figure 3-9(b). One high-speed camera is installed at the right side of the barrier, and the other camera is set in front of the barrier.

3.4.2 Measurement of the basic parameters

The velocities of the impact boulders, granular flows, and debris flows before and after impact and the deformation of the flexible barrier in each test are measured using the photographs by the high-speed cameras, so are the flow depths and the deposition profiles of granular flows and debris flows. To increase the accuracy of the measurement, two measures are taken: firstly, the location and the shooting angle of the side-view high-speed camera are selected very carefully to make sure that the camera is perpendicular to the transparent side wall of the flume; secondly, the velocity of a debris flow is determined from the average velocities of five individual particles measured from five continuous photographs before the impact with the assistance of the reference lines attached to the flume.

3.4.3 Measurement of the impact force on the flexible ring net

As mentioned above, the central area is separated from the main ring net and reconnected to neighboring net rings by mini tension link transducers. Two assumptions are made to simplify the measurement of the impact loading on a flexible ring net. The deformation of the ring net is assumed similar to a membrane, and the deformation in the measured area is assumed cone symmetric. Based on the assumptions, the loading situation in the cross section of the measured area which contains Transducer *i* and Transducer *i+1* is analysed and shown in Figure 3-10. Thus, the impact force on the cross section can be calculated with the following equation:

$$F_{impact,i,i+1} = F_{tensile,i} \cdot \cos\frac{\theta}{2} + F_{tensile,i+1} \cdot \cos\frac{\theta}{2} \tag{3-1}$$

where $F_{tensile,i}$ and $F_{tensile,i+1}$ are the maximum tensile forces on Transducer *i* and Transducer *i+1* installed in the measured area; θ is the included angle between the opposite transducers;

and $F_{impact,i,i+1}$ is the calculated impact force on this cross section. Since the deformation in the measured area is assumed cone symmetric, θ is a constant in all cross sections formed by two opposite transducers.

Thus, the maximum impact force, $F_{measured}$, in the measured area ($A_{measured}$) with n transducers can be calculated with the following equation:

$$F_{measured} = \cos\frac{\theta}{2} \cdot \sum_{i=1}^{i=n} F_{tensile,i} \tag{3-2}$$

For the dynamic impact scenario in a rockfall or a debris flow impact event, the impact loading is originated from the dynamic impact of the fast-moving boulder or the debris front. Thus, the impact loading mainly concentrates on the central area, and A_{impact} is much smaller than $A_{measured}$. Therefore, the dynamic impact is regarded as a concentrated force in the measured area. In this case, F_{impact} equals to $F_{measured}$.

By contrast, the static impact pressure from a granular flow or a debris flow is assumed to be distributed in the cross-sectional area of the flume width multiplied by the height of the debris deposition, which covers the measured central area. Combining with Eq.(3-2), the following equation is given to estimate the distributed impact loading on a flexible ring net as:

$$F_{impact} = F_{measured} \cdot \frac{A_{impact}}{A_{measured}} = \cos\frac{\theta}{2} \cdot \sum_{i=1}^{i=n} F_{tensile,i} \cdot \frac{A_{impact}}{A_{measured}} \tag{3-3}$$

where A_{impact} and $A_{measured}$ represent the actual impact cross-sectional area and the measured central area in the test.

As a simple method with some assumptions, its measurement has two main limitations:

(1) The included angle in the moment of the largest impact force is difficult to obtain because the included angles at different cross-sections are various.

(2) The appearing time of the peak loading in the force histories of all transducers may not appear at the same time.

3.4.4 Measurement of the impact force on the supporting structures

The flexible ring net is supported by two posts that can rotate in the plane of the flow direction, and each post is supported by two inclined steel strand cables. Therefore, the impact force transferred from the flexible barrier to the supporting posts can be calculated from the tensile forces carried by the supporting cables in the direction of impact. Based on the symmetrical arrangement of the cables and the posts with respect to the flexible barrier, as plotted in Figure 3-11(a), the loading situations of the posts and the supporting cables located on both sides of the flexible barrier are also symmetrical when they are under a uniform impact pressure. Thus, the left post and its supporting cables: Cable A Left and Cable B Left are selected as the analysis objects. The force analysis of the supporting cables is divided into two steps:

Firstly, forces on Cable A Left and Cable B Left are decomposed into components in the rotation plane of the post based on the top-view sketch (seen Figure 3-11(a)):

$$F_{AL,H} = F_{AL} \cdot \cos\alpha \tag{3-4}$$

$$F_{BL,H} = F_{BL} \cdot \cos\beta \tag{3-5}$$

where F_{AL} and F_{BL} are the measured maximum tensile forces on Cable A Left and Cable B Left during the impact; $F_{AL,H}$ and $F_{BL,H}$ are the components of F_{AL} and F_{BL} decomposed in the rotation plane of the left post; and α, β are the included angles between Cable A, Cable B and the rotation plane of the post.

Secondly, based on the calculated $F_{AL,H}$ and $F_{BL,H}$, components of the tensile forces on Cable A Left and Cable B Left in the direction of impact can be calculated based on the left-side-view sketch (seen Figure 3-11(b)):

$$F_{AL,imapct} = F_{AL,H} \cdot \cos\gamma \tag{3-6}$$

$$F_{BL,imapct} = F_{BL,H} \cdot \cos\delta \tag{3-7}$$

where $F_{AL,impact}$ and $F_{BL,impact}$ are the components of tensile forces on Cable A Left and Cable B Left in the direction of impact; and γ, δ are the included angles between Cable A, Cable B and the direction of impact.

The direction of the supporting force, which is opposite to the direction of the impact force, is defined as the positive direction. Thus, the components of the tensile forces on the left cables in the direction of impact (F_L) can be calculated by substituting Eqs. (3-4) and (3-5) into Eqs. (3-6) and (3-7):

$$\begin{aligned} F_L = F_{BL,imapct} - F_{AL,imapct} &= F_{BL,H} \cdot \cos\delta - F_{AL,H} \cdot \cos\gamma \\ &= F_{BL} \cdot \cos\delta \cdot \cos\beta - F_{AL} \cdot \cos\gamma \cdot \cos\alpha \end{aligned} \tag{3-8}$$

Finally, based on the conservation of angular momentum and the symmetrical arrangement of the cables and the posts with respect to the flexible barrier, the equivalent impact force can be calculated from the tensile forces on the supporting cables with the following equation:

$$F_{Cables,equivalent} = \frac{l_{post}}{l_{impact}} \left[(F_{BL} + F_{BR}) \cdot \cos\delta \cdot \cos\beta - (F_{AL} + F_{AR}) \cdot \cos\gamma \cdot \cos\alpha \right] \tag{3-9}$$

where $F_{Cables,equivalent}$ is the equivalent impact force calculated from the tensile forces on the supporting cables; l_{post} is the distance between the rotation fulcrum of the post and the connecting point of the cables; l_{impact} is the distance between the rotation fulcrum of the post and the equivalent impact height of the granular flow; and F_{AL}, F_{AR}, F_{BL}, and F_{BR} are the measured maximum tensile forces on the supporting cables. From the arrangement of the cables plotted in Figure 3-10, Eq.(3-10) is derived:

$$F_{cables,equivalent} = \frac{l_{post}}{l_{impact}} \left(\cos 24^{\circ} \cos 60^{\circ} F_{B(sum)} - \cos 62^{\circ} \cos 76^{\circ} F_{A(sum)} \right) \tag{3-10}$$

where $F_{A(sum)}$, $F_{B(sum)}$ are the sums of the tensile forces on cable A and cable B located at both sides.

3.4.5 Calculation of Impact Reduction Rate (IRR)

It is found that the flexible net makes an obvious contribution to the reduction of the impact loading from a debris flow (Volkwein 2014; Song et al. 2017). To quantify the contribution of flexibility to impact loading reduction, the Impact Reduction Rate (IRR or β) of the flexible barrier is defined as:

$$\beta = IRR = \frac{F_{impact} - F_{Cables,equivalent}}{F_{impact}} \cdot 100\% \tag{3-11}$$

3.5 Summary

In this chapter, a large-scale physical modelling facility is described in detail. A new fast door-opening method and a systematic dynamic monitoring system are implemented in this facility. With the application of the fast door-opening method, rockfalls and debris flows can be generated without being interfered. With the application of the monitoring system, the parameters of the impacting masses, the responses of the flexible barrier under impact, and the interaction of the impact mass with the flexible barrier can be monitored in detail.

The successes of different types of tests including the impacts of single rockfalls, dry granular flows and debris flows have demonstrated that this large-scale physical modelling facility can be further applied in other experimental study of geohazards.

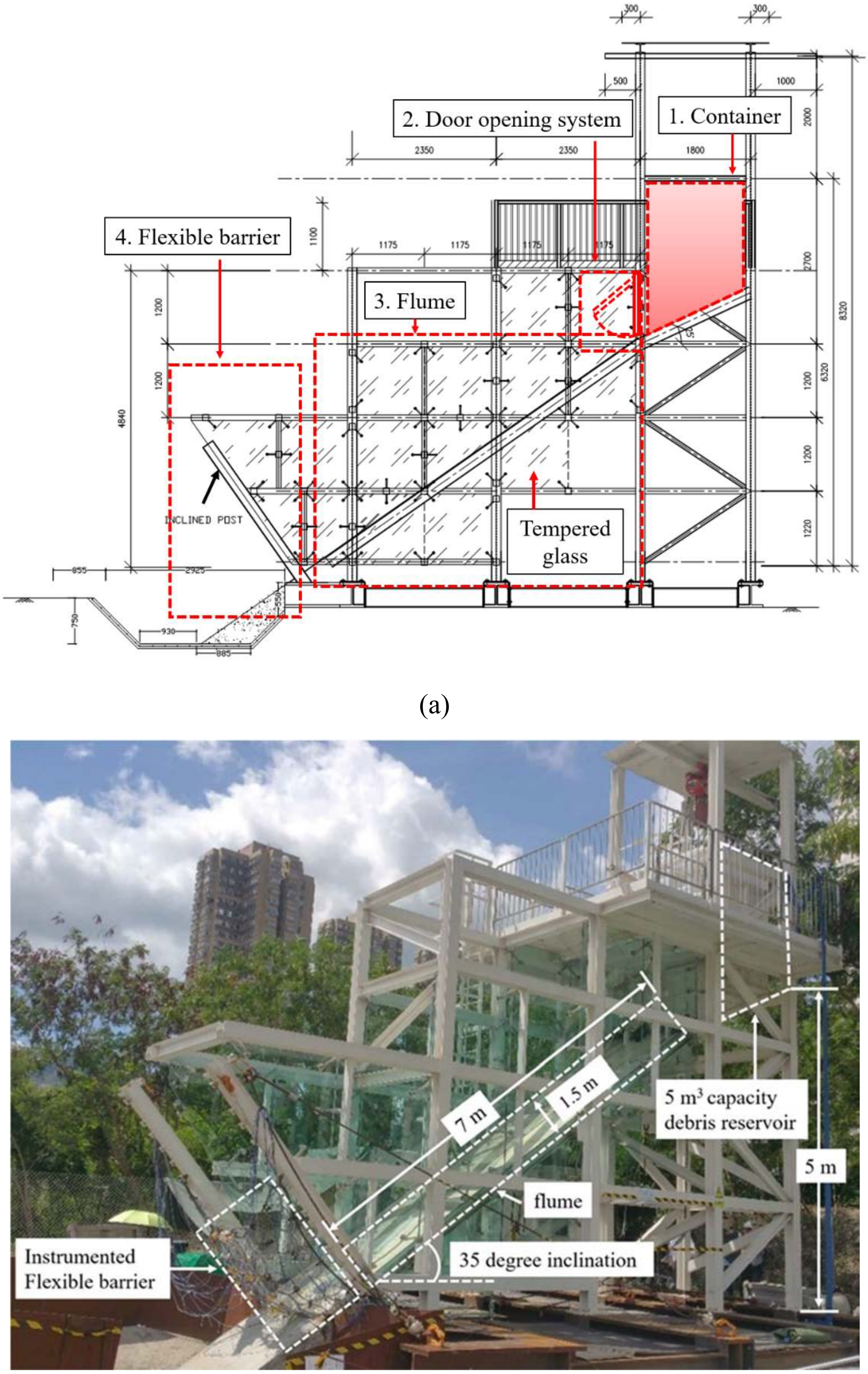

(a)

(b)

Figure 3-1. (a) Side view design sketch (unit: mm) and (b) photograph of the large-scale physical modelling facility located in a site in Hong Kong

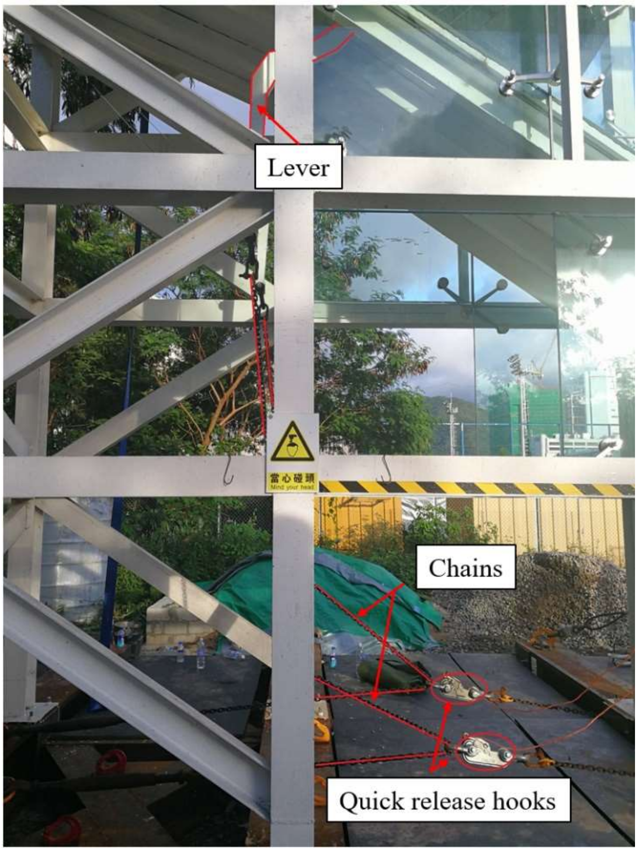

Figure 3-2. Components of the door opening system in the PolyU large-scale testing facility

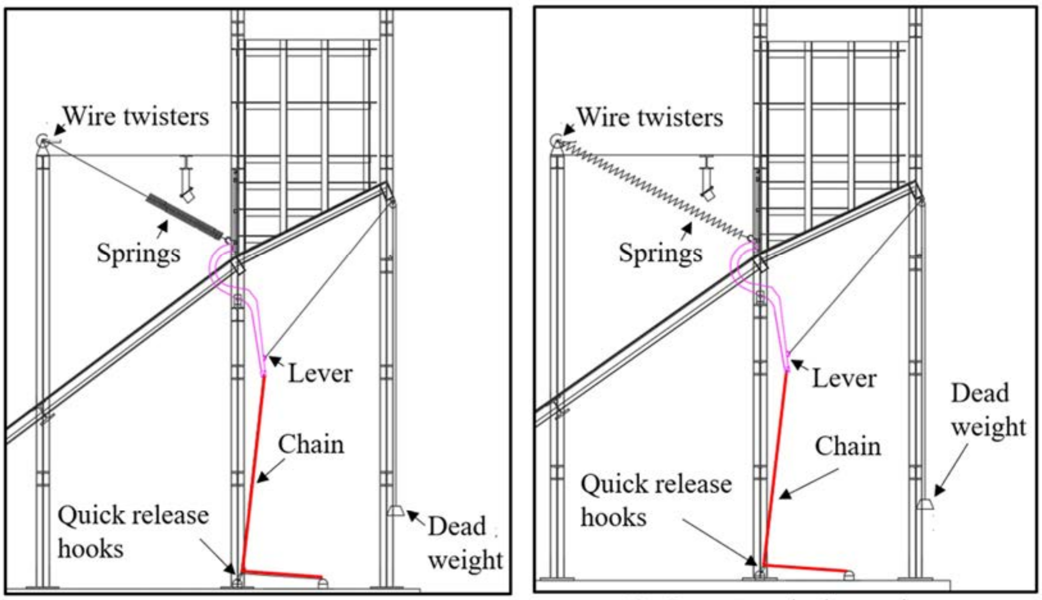

1). Close the door and lock the hook

2). Pre-stretch the springs

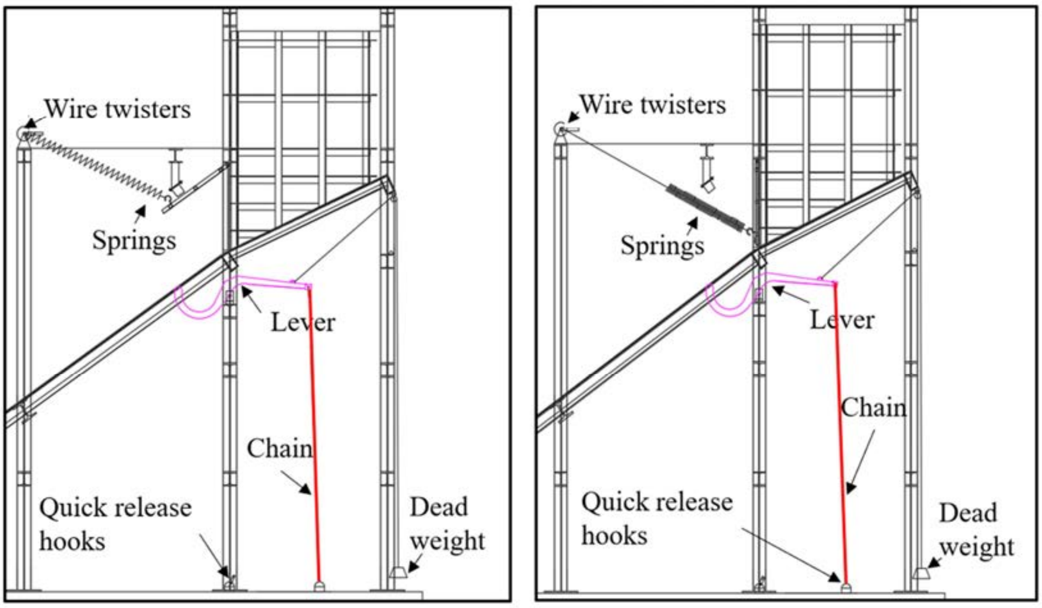

3). Release the hooks and springs bounce the door up

4). Release the springs and the door close

Figure 3-3. Operating procedures of the door opening system

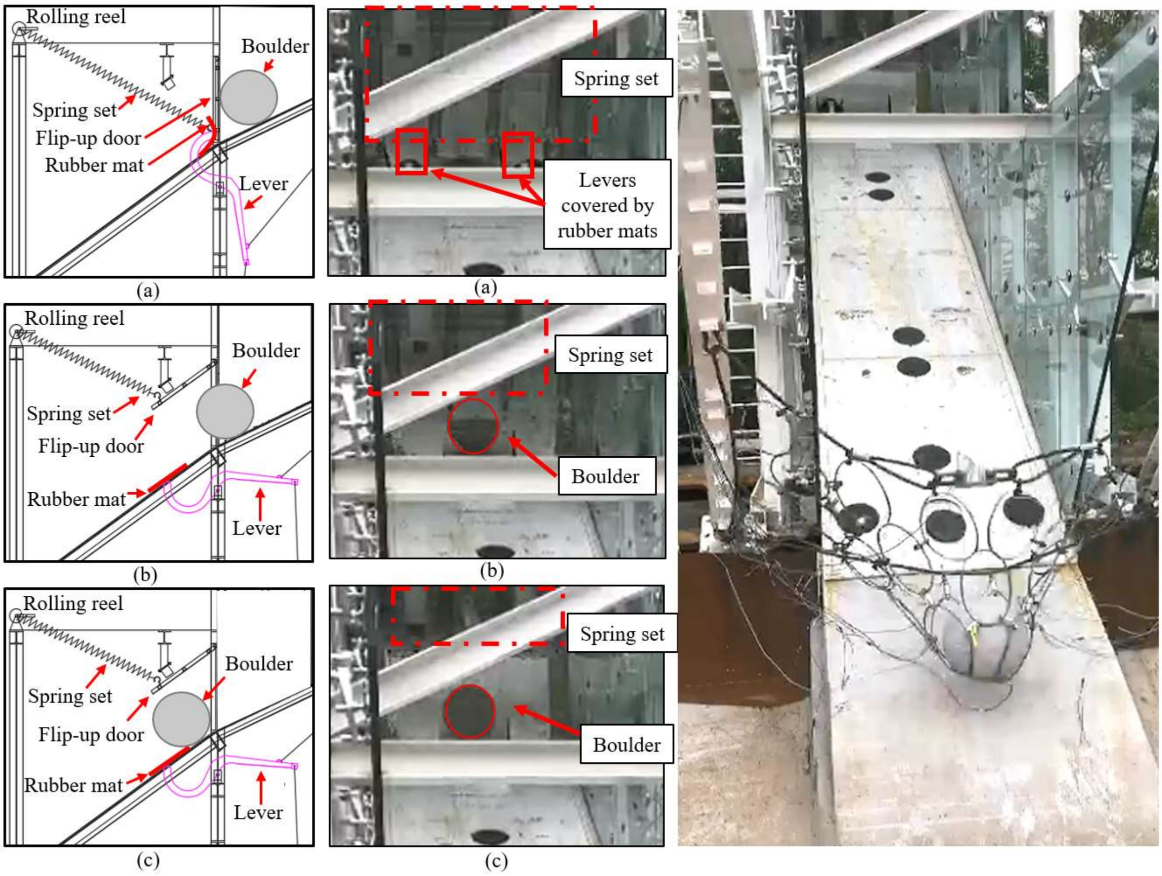

Figure 3-4. Performance of the door opening system in a rockfall impact test

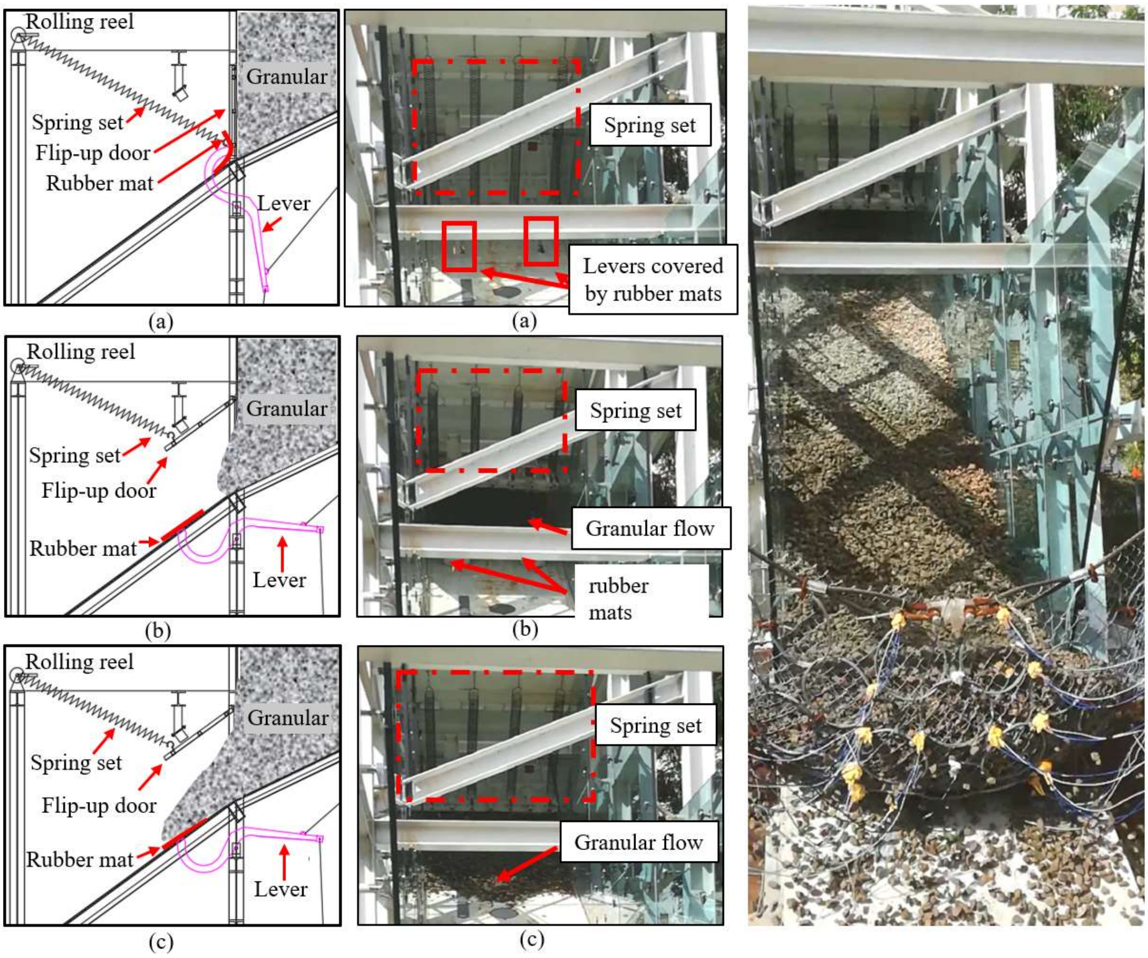

Figure 3-5. Performance of the door opening system in a granular flow impact test

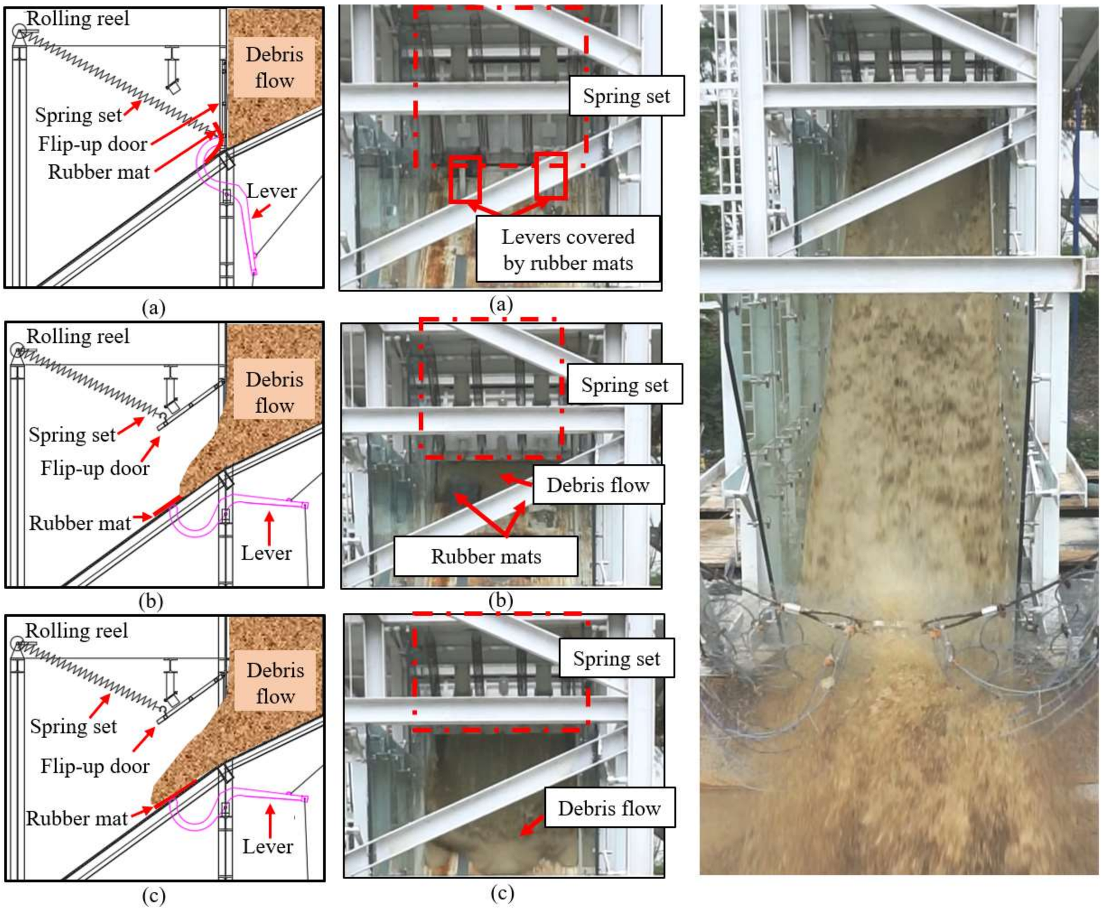

Figure 3-6. Performance of the door opening system in a debris flow impact test

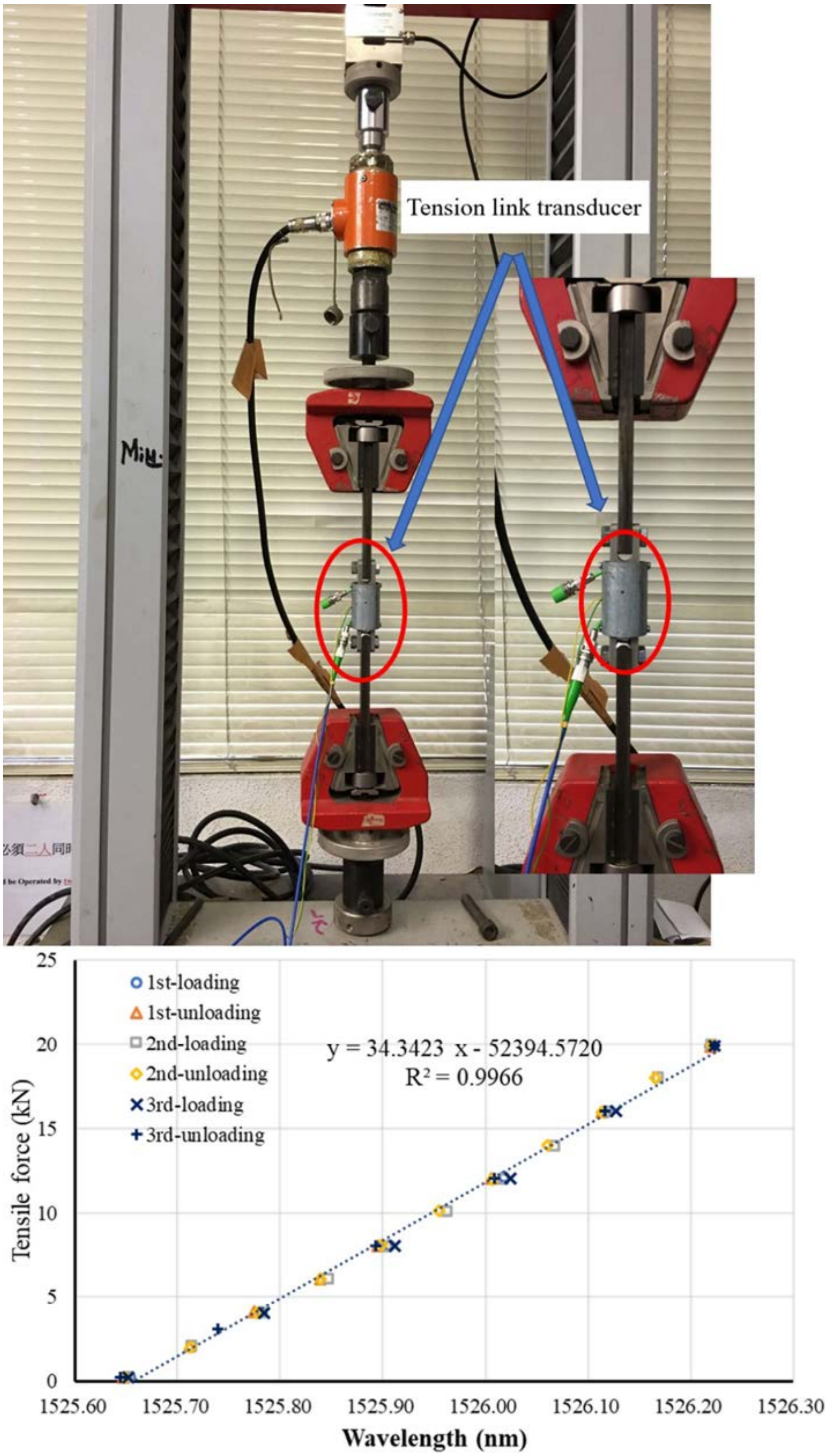

Figure 3-7. Calibration of the mini tension link transducer on the flexible ring net

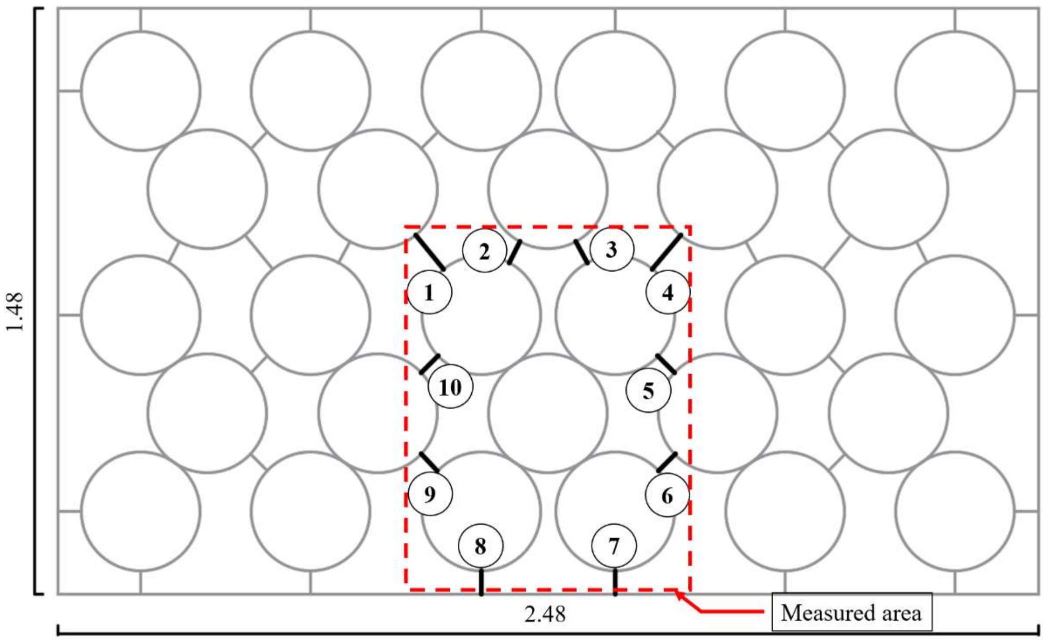

(a)

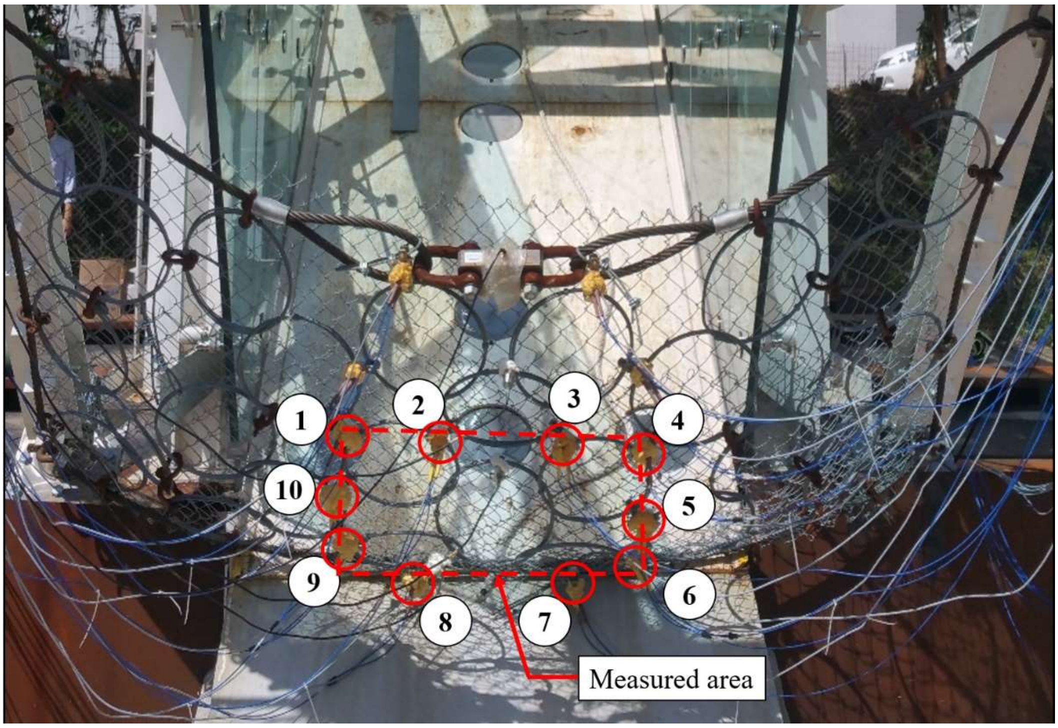

(b)

Figure 3-8. (a) Schematic sketch of a flexible ring net and (b) front view of the flexible barrier with numbered mini tension link transducers between rings (unit: m)

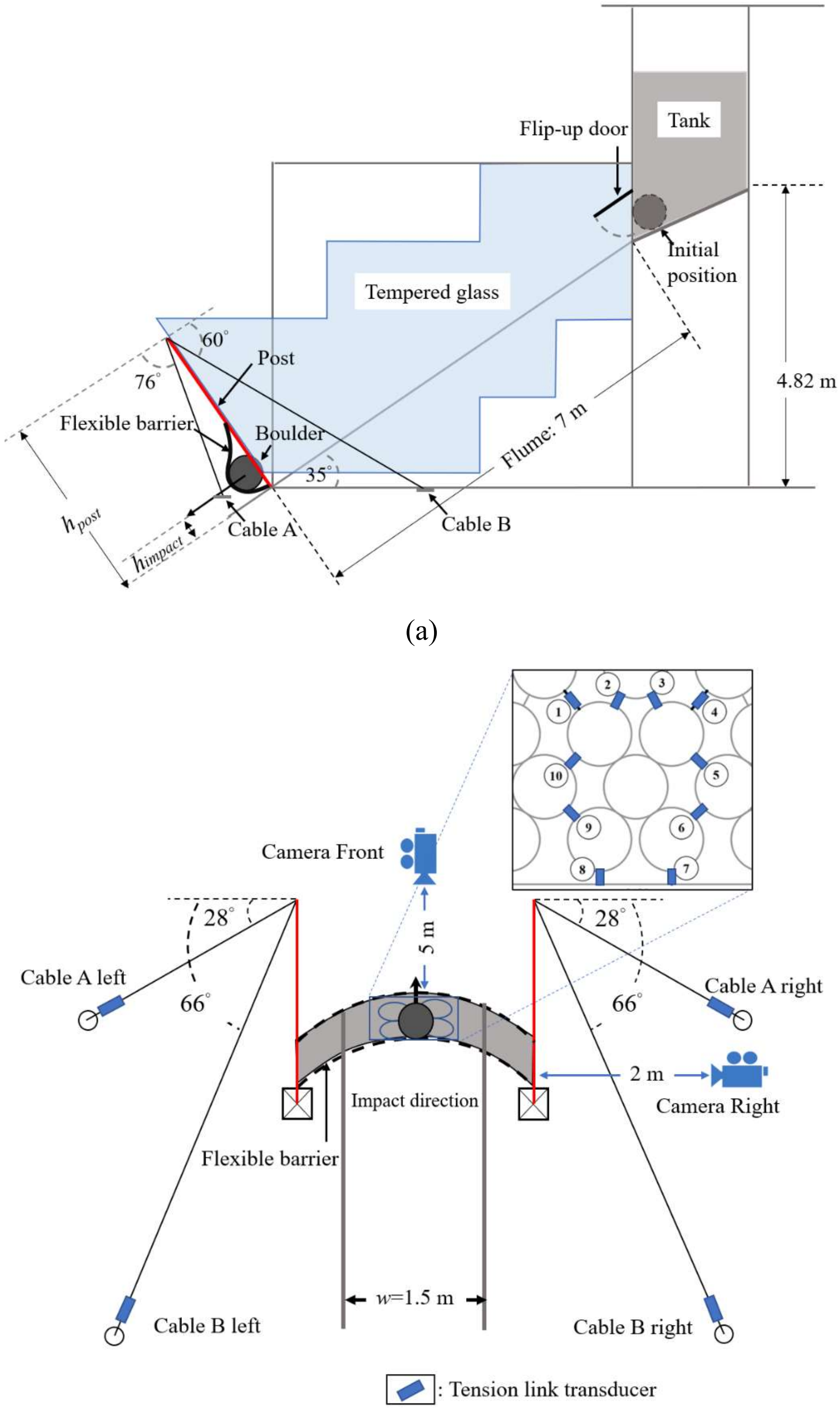

(a)

(b)

Figure 3-9. (a) Side view and (b) plain view of the instrumentation of the physical modelling facility

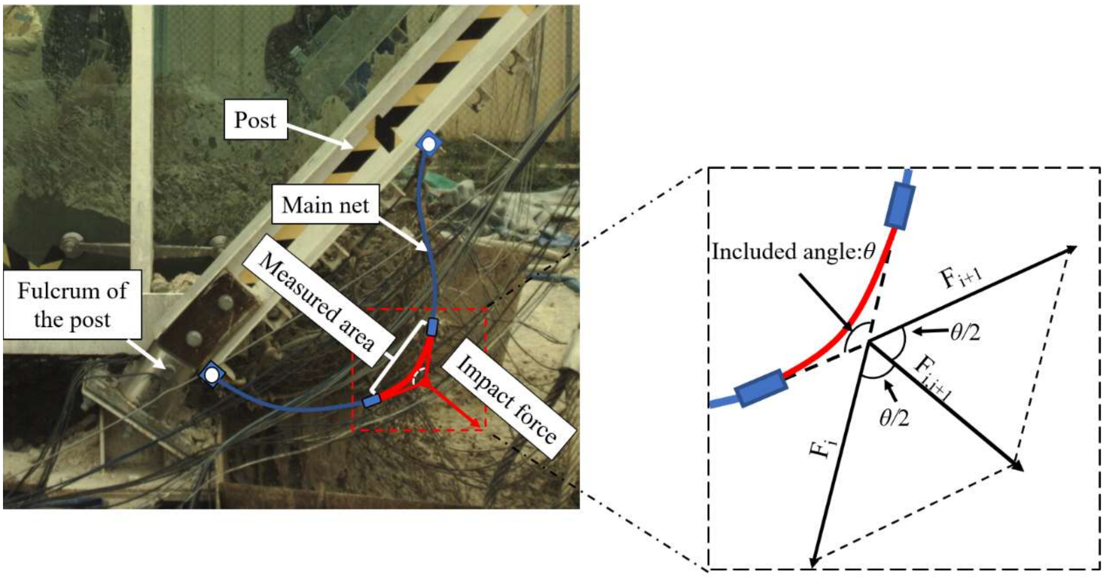

(a) (b)

Figure 3-10. (a) Sketch of a flexible barrier under impact and (b) the simplified force analysis of the measured area in the cross-section of Transducer *i* and Transducer *i+1*

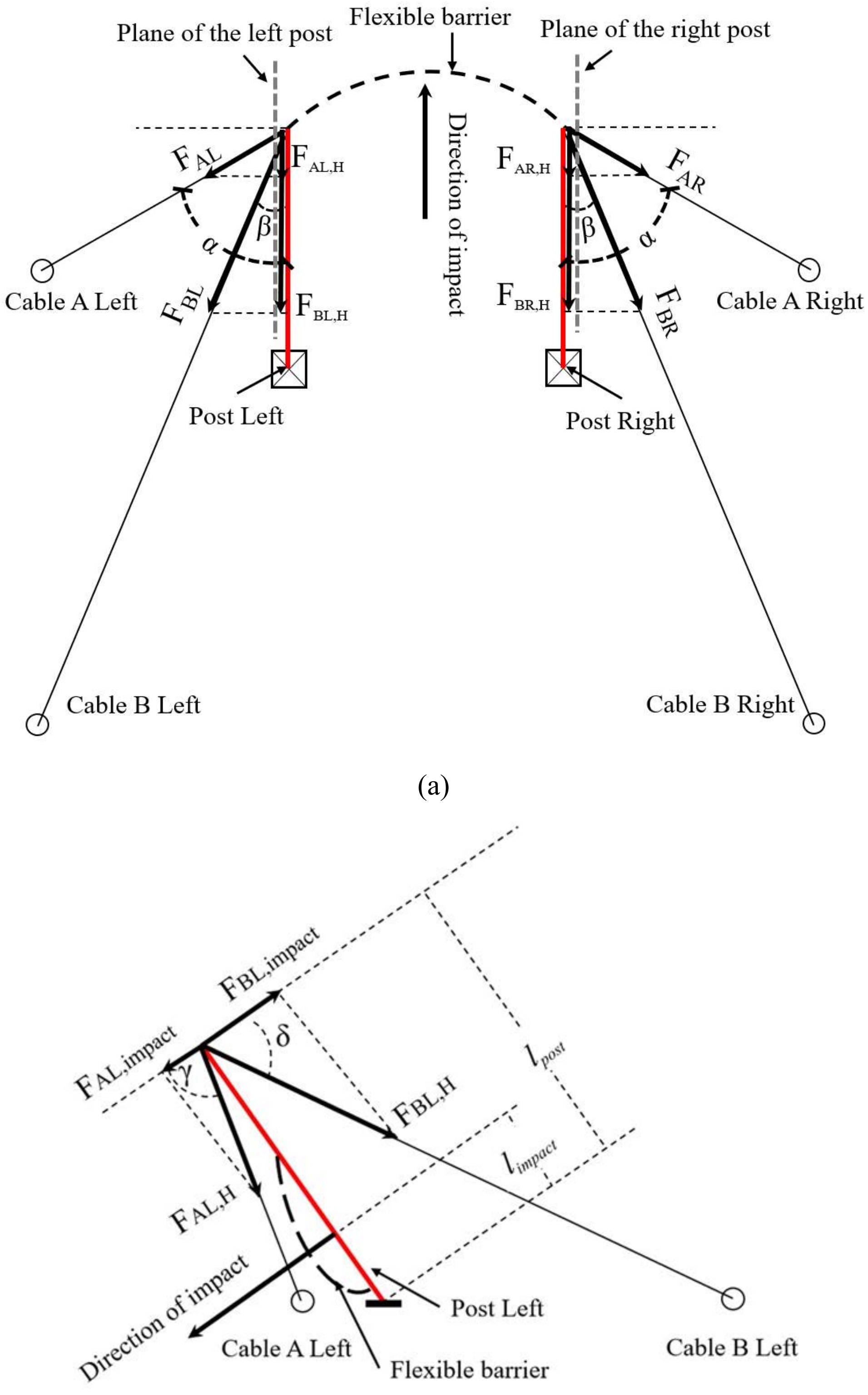

(a)

(b)

Figure 3-11. (a) Top-view and (b) left-side-view of sketches representing the force analysis of the posts and cables

Table 3-1. Comparison of large-scale physical modelling facilities in the literature with the facility built in Hong Kong Polytechnic University

Location	**Max Capacity (m3)**	**Description of door**	**Door opening mechanism**	**Open time**	**Status of door after open**	**Length (m)**	**Width (m)**	**Slope inclination (°)**	**Purpose**
Switzerland (WSL) (Bugnion et al. 2012)	50	0.8-m-high trap door hinged at the base and closed by cables	open by the earth pressure of debris material after triggered	not given	Attached to the flume bottom surface as an obstacle	41	8	30 (built on natural slope)	Study the behaviour of debris flows on a hillslope and their interaction with flexible barriers
U. S. (USGS) (Iverson et al. 2010)	20	2-m-high side-hinged two-piece headgate	Swing open horizontally by the earth pressure of debris material after triggered	about 1 s	Attached to two sides of the flume as side obstacles	95	2	31 (built on natural slope)	Study the initiation and deposition of debris flows
South Korea (Won et al. 2016, Paik et al. 2012)	600	6.8-m-high trap door hinged at the top and locked by a beam lock at the bottom edge	Swing open vertically by the earth pressure of debris material after the beam is released	not given	The door is left in front of the reservoir and interfered with the flowing out debris continuously	800	8-25	38 at the upstream 5 at the downstream (built on natural slope)	investigate the erosional and depositional patterns of debris flows
Hong Kong (Tan et al. 2018a; Tan et al. 2018b)	5	1-m-high trap door hinged at the top and locked by a pair of curved beams at the bottom	Pulled up by the pre-tensioned springs after the release of the beam locks	Less than 0.5 s	The door is pulled up until it is parallel to the flume by a set of pre-tensioned springs	7	1.5	35 (built on a steel frame)	Study the interaction of boulders, granular flows and channelized debris flows with flexible barriers

CHAPTER 4: IMPACT MECHANISM OF A SINGLE BOULDER ON A FLEXIBLE BARRIER

4.1 Introduction

Flexible barriers have been widely applied in rockfall mitigation in recent years. However, the behaviour of flexible barriers under the impact of boulders is still not fully understood. To investigate the interaction between a flexible barrier and a falling boulder, a large-scale physical modelling facility has been constructed at a site in Hong Kong. Using this facility, large-scale impact tests using boulders with different diameters were conducted. Test results are presented and analysed in this chapter. The motion of the boulder during impact is traced and analysed. The impact forces on the flexible ring net and the supporting structures are measured and compared. From the comparison, the Impact Reduction Rates (IRR) of boulders with different diameters are calculated. Moreover, a simple method for estimating the impact loading of a boulder on a flexible barrier is proposed in this study. This method is calibrated and verified using measured impact forces in the tests.

4.2 Test procedures

Two tests using spherical boulders with the diameters of 400 mm (Boulder Test 1) and 600 mm (Boulder Test 2) were conducted. In each test, the spherical boulder was released from the upper reservoir, accelerated along the flume, and finally trapped by the flexible barrier. The reservoir is 4 m higher than the bottom cable of the flexible barrier. Basic parameters of the two testing spherical boulders are listed in Table 4-1. The signals of all the transducers were recorded before the test to obtain initial values. The initiation time of the impact has been readjusted to 0 s in all plotted data and selected video frames. The negative value of time represents the moment before the impact. High-speed cameras were triggered at the instant before the impact to capture the impact process in detail.

4.3 Experiment results and analysis

4.3.1 Experiment results of Boulder Test 1 (boulder diameter of 400 mm)

Forces of all the mini tension link transducers in Boulder Test 1 are plotted in Figure 4-1(a). Two obvious impacts are observed, and the largest impact loading appears in the first impact. Compression forces occurred in some transducers (e.g. Transducers 6, 8 and 9) during and after impact. Based on the photographs taken by the high-speed cameras, the compression forces result from the swing and torsion of the ring net during and after the impact. The tensile force peaks in all transducers are plotted in Figure 4-1(b). The loading peaks range from 1.93 kN (Transducer 4) to 12.4 kN (Transducer 9). The signal of Transducer 10 combined with typical photographs at different times is plotted in Figure 4-2 to investigate the relationship between the impact process and force change on the barrier in Boulder Test 1. It can be found from the figure that the largest deformation of the barrier, as well as the largest tensile force on the transducer appears at t=0.124 s. After that, the boulder is bounced back due to the recovery of the elastic deformation of the ring net, which causes the second impact at t=1.398 s. The peak value of the second impact is only 3/5 of the first impact. The double-impact phenomenon was also observed in full-scale tests presented by Gottardi and Govoni (2010), which indicates that the large deformation of the flexible barrier can recover well after impact, and the kinetic energy of the impact boulder can partly transform into the elastic energy of the ring net. From the continuous photographs by the side view high-speed camera, the motion trail and the velocity of the boulder during the impact are plotted in Figure 4-3. It can be observed that the boulder decelerates during the impact and reaches the maximum displacement of 0.877 m. After that, it is bounced back and accelerated again by the deformation recovery of the flexible barrier. Figure 4-4(a) presents the attenuation of the kinetic energy of the boulder with the increment of the distance. The attenuation process can be divided into three stages with the assistance of the selected frames, as plotted in Figure 4-4(b). When the boulder firstly approaches, rings of the flexible barrier rotate with the profile of the boulder, and the translational kinetic energy of the boulder has no obvious loss until its moving distance reaches 0.4 m. Afterward, the rings are stretched, and the kinetic energy is dramatically dissipated until the moving distance reaches 0.92 m. At the end of the impact, the boulder swerves its moving direction with the remaining kinetic energy of 500 J. Interestingly, unlike rigid barriers or cushion layers which are designed to absorb all the impact energy of the falling boulder, the flexible barrier bounces up the boulder during the interaction, and around one-fifth of the kinetic energy remains after the first impact.

4.3.2 Experiment results of Boulder Test 2 (boulder diameter of 600 mm)

Forces on all the mini tension link transducers installed on the ring net in Boulder Test 2 are plotted in Figure 4-5(a). Compression forces occurred in some transducers in this test (e.g. Transducers 5, 6, 9 and 10). Interestingly, triple impact peaks are obviously observed in some transducers (Transducers 1, 2, 5, 10). Peak loadings of all the mini transducers are plotted in Figure 4-5(b). The signal of Transducer 10 combined with typical frames at different times is plotted in Figure 4-6 to explore the relationship between the impact process and force change on the barrier in Boulder Test 2. It can be observed that the boulder was bounced up twice by the recovery of the elastic deformation of the flexible ring net to further reduce the impact force on the flexible barrier. Three impacts occurred at the times of 0.074 s, 1.490 s, and 2.554 s, respectively. It can be concluded that the flexible barrier can decompose a large impact force into multiple smaller impacts by its large elastic deformation capacity.

4.3.3 Direct measurement of the impact force on the barrier

Due to the interlaced arrangement of the rings, Transducers 2, 3, 5, 6, 9, and 10 are not perpendicular to the edge of the measured area. From the observation of the boulder impact process (*e.g.* Figure 4-7(a)), the deformation of the flexible barrier during the impact is extremely large. Therefore, the deviation of the transducer tension with the impact direction cannot be ignored. Thus, orthogonalization is processed on the tensile forces by those transducers before they are used in the impact force calculation using the average deviation angle of 45 degrees in this study:

$$F_i' = \cos 45° \cdot F_i \tag{4-1}$$

where i=2, 3, 5, 6, 9, and 10.

Thus, Eq.(3-2) can be adjusted to:

$$F_{impact} = \cos\frac{\theta}{2} \cdot \left(\sum F_i' + \sum F_j\right) \tag{4-2}$$

where F_{impact} is the total impact force; θ is the included angle in the measured area bent by the impact mass; F_i' is the orthogonalized maximum tensile force of Transducer i (Transducers 2, 3, 5, 6, 9, and 10); and F_j is the maximum tensile force of Transducer j (Transducers 1, 4, 7, and 8). The included angle of the curved ring net is measured from the photos taken at the moment of the largest deformation (see Figure 4-7 for Boulder Test 1 and Figure 4-8 for Boulder Test 2). The measured maximum impact loadings on the flexible ring net in the two tests are listed in Table 4-1.

4.3.4 Calculation of the impact force transferred to the posts

The IRR value was defined in Chapter 3. For Boulder Test 1 and Boulder Test 2, the IRR values in the two tests are calculated and presented in Table 4-1. From the table, the flexible barrier reduces 32% and 27% of the total impact loading in Boulder Test 1 and Boulder Test 2. By applying the IRR (Impact Reduction Rate) and suitable methods for impact force calculation, the impact forces on the flexible ring net and on the supporting structures can be estimated respectively. Thus, the design of a flexible barrier for debris flow mitigation can be optimized by dimensioning and designing different components with different designed loadings, which provides a safer and more economical design approach.

4.3.5 A new simple method for maximum impact loading calculation

In this section, a simple method is proposed based on the work-energy theorem. By ignoring the transformation from kinetic energy to thermal energy during the impact, all the kinetic energy loss of the boulder equals to work done on it, and Eq.(4-3). is written as follows:

$$\int_0^s F_{estimated} \bullet ds = \frac{1}{2} m v^2 \tag{4-3}$$

where $F_{estimated}$ is the estimated impact force; s is the displacement of the boulder during the impact; m and v are the mass and the impact velocity of the boulder.

In Eq.(4-3), the kinetic energy of the impact boulder is easy to be obtained in the design. Normally, the designer firstly estimates the maximum diameter of the potential falling boulders ($d_{boulder}$) in the risky area by the geological investigation, then its mass can be estimated by:

$$m = \frac{4}{3} \pi \left(\frac{d_{boulder}}{2} \right)^3 \bullet \rho_{boulder} \tag{4-4}$$

The impact velocity (v) can be estimated by numerical simulation considering the geometric condition of the protection area. However, it is difficult to obtain ds during the impact because of the complex motion of the boulder (as shown in Figure 4-3(a)). Hence, two coefficients: *S* and *D* are introduced in this method. *S* represents the equivalent stiffness of the flexible barrier in the unit of *m*, which is a constant parameter of a type of standard flexible barriers installed with similar initial slacks. In this chapter, Boulder Test 1 is used to determine the coefficient *S* of the used flexible barrier. The other coefficient $D = {d_{boulder}}^2$ is proposed to consider the influence of the impact area. Thus, the impact force from a falling boulder on a flexible barrier can be estimated with the following equation:

$$F_{estimated} = SD^{-1}\frac{1}{2}\left[\frac{4}{3}\pi\left(\frac{d_{boulder}}{2}\right)^3 \bullet \rho_{boulder}\right]v^2 = \frac{1}{12}\pi S\rho_{boulder}d_{boulder}v^2 \tag{4-5}$$

From back analysis using the data in Boulder Test 1, *S*=2.76 m.

Data for Boulder Test 2 is used to verify this method. By applying Eq.(4-5), the calculated impact force is 67.7 kN, which fits well with the measured maximum impact force on the flexible ring net (72.4 kN, see Table 4-1) with a small relative error of 6.5%. Thus, this simple method can be preliminarily proved feasible. By applying this simple method, the designed impact loading of rockfalls can be easily estimated using basic parameters of possible falling boulders and the selected barrier. The stiffness parameter *S* of a standard flexible barrier can be determined by conducting a calibration test on each type of standardized flexible barriers.

4.4. Summary

In this chapter, large-scale physical modeling tests were conducted using spherical granite boulders with different diameters to impact a flexible barrier. Spherical granite boulders with the diameter of 400 mm (Boulder Test 1) and the diameter of 600 mm (Boulder Test 2) were used in the impact tests to study the performance of a flexible barrier subjected to falling boulders with different diameters. The interactions between the boulders and the flexible barrier have been clearly presented and analysed in this study. From the experiment results and their analysis, the following findings and conclusions are summarized and presented:

(a) Multiple impacts were observed in Boulder Test 1 and Boulder Test 2. This phenomenon indicates that the large deformation of the flexible barrier can recover well after the first impact, and the kinetic energy of the falling boulder can be dissipated during the multiple interactions.

(b) The impact loadings on the flexible barrier and the loadings transferred to the supporting structures in the two tests were calculated and compared. It is found that the flexible barrier reduces around 30% of the total impact loadings in both Boulder Test 1 and Boulder Test 2. The design loading for the supporting structures can be accurately estimated with the help of IRR value instead of using the impact forces on the flexible ring net.

(c) A simple method for impact loading estimation is proposed in this study. The coefficient S is proposed to represent the equivalent stiffness of flexible barriers, and the coefficient D is identified to represent the impact area of the single boulder. The data of Boulder Test 1 are used to calibrate the stiffness coefficient S, and the data of Boulder Test 2 are used to verify this simple method. The calculated result using the simple method is consistent well with the measured values.

In the future, numerical simulations using different impact velocities, testing materials, and diameters of boulders will be conducted to further verify and optimize the IRR values and the proposed simple method.

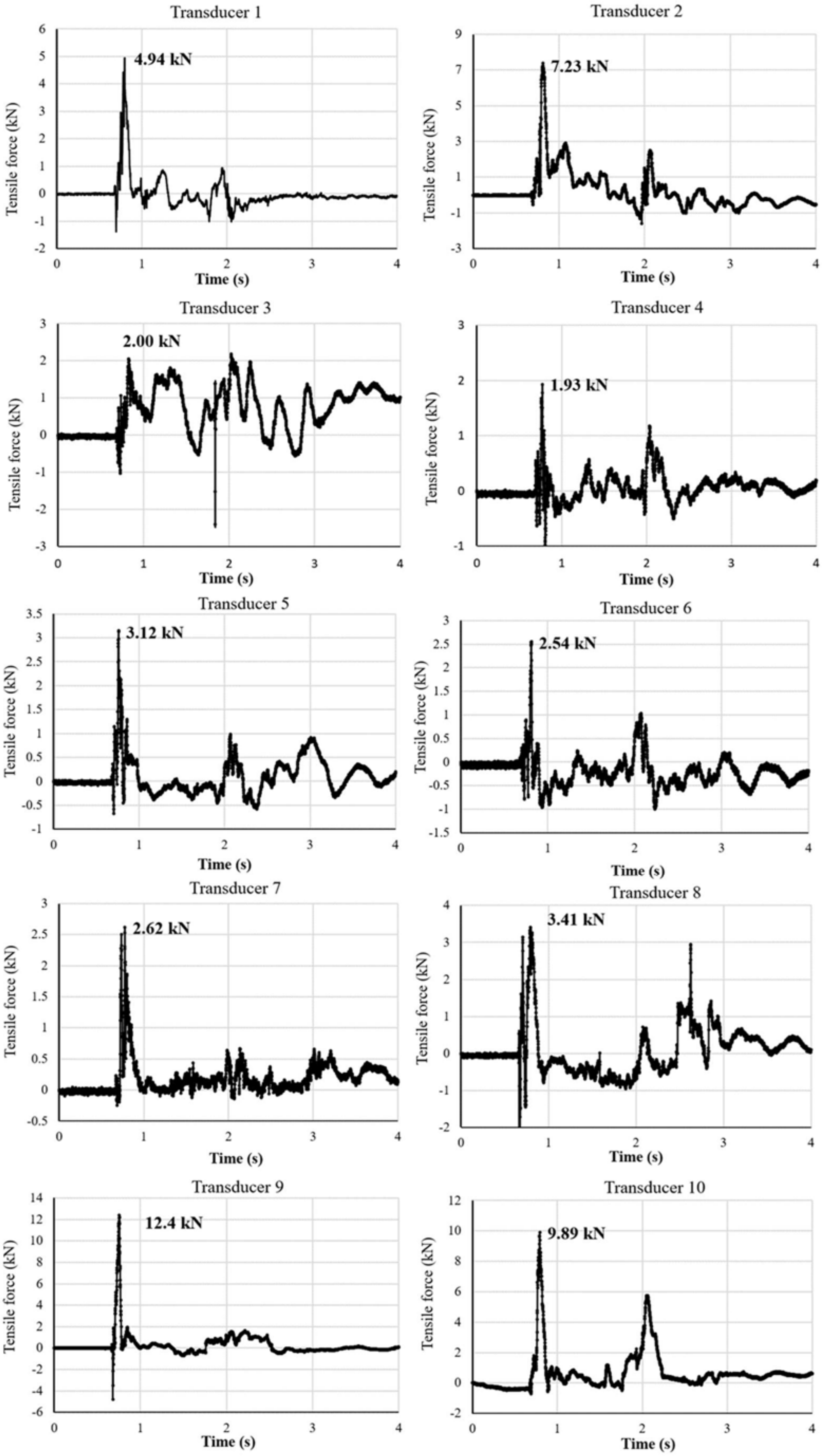
Transducer 1
4.94 kN
Transducer 2
7.23 kN
Transducer 3
2.00 kN
Transducer 4
1.93 kN
Transducer 5
3.12 kN
Transducer 6
2.54 kN
Transducer 7
2.62 kN
Transducer 8
3.41 kN
Transducer 9
12.4 kN
Transducer 10
9.89 kN
Tensile force (kN)
Time (s)
0
1
2
3
4

(a)

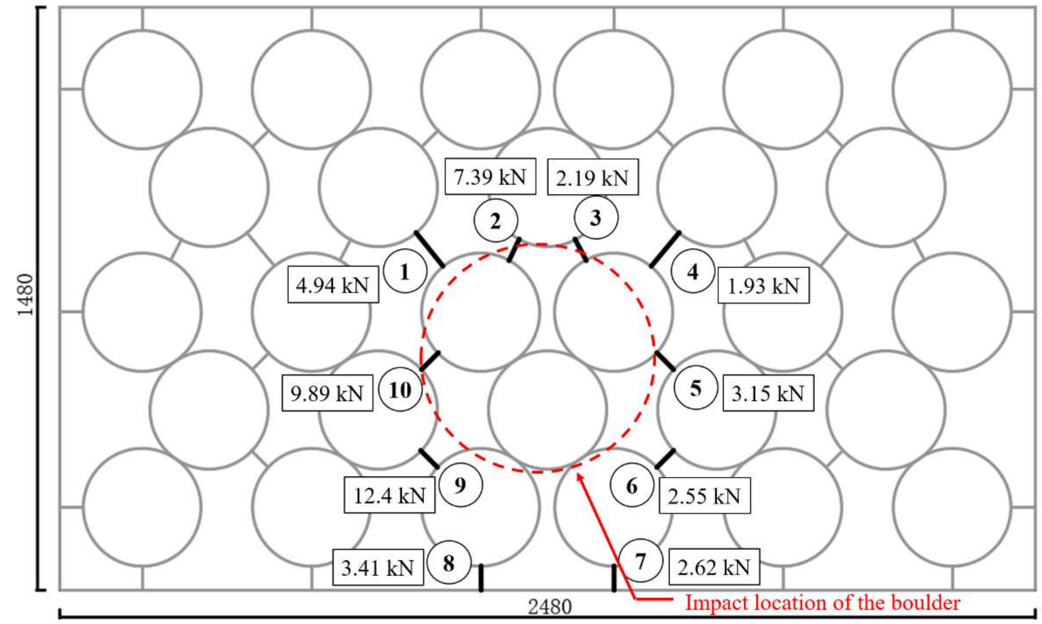

(b)

Figure 4-1. (a) Forces v.s. time and (b) the peak tensile forces on the mini tension link transducers between rings in Boulder Test 1

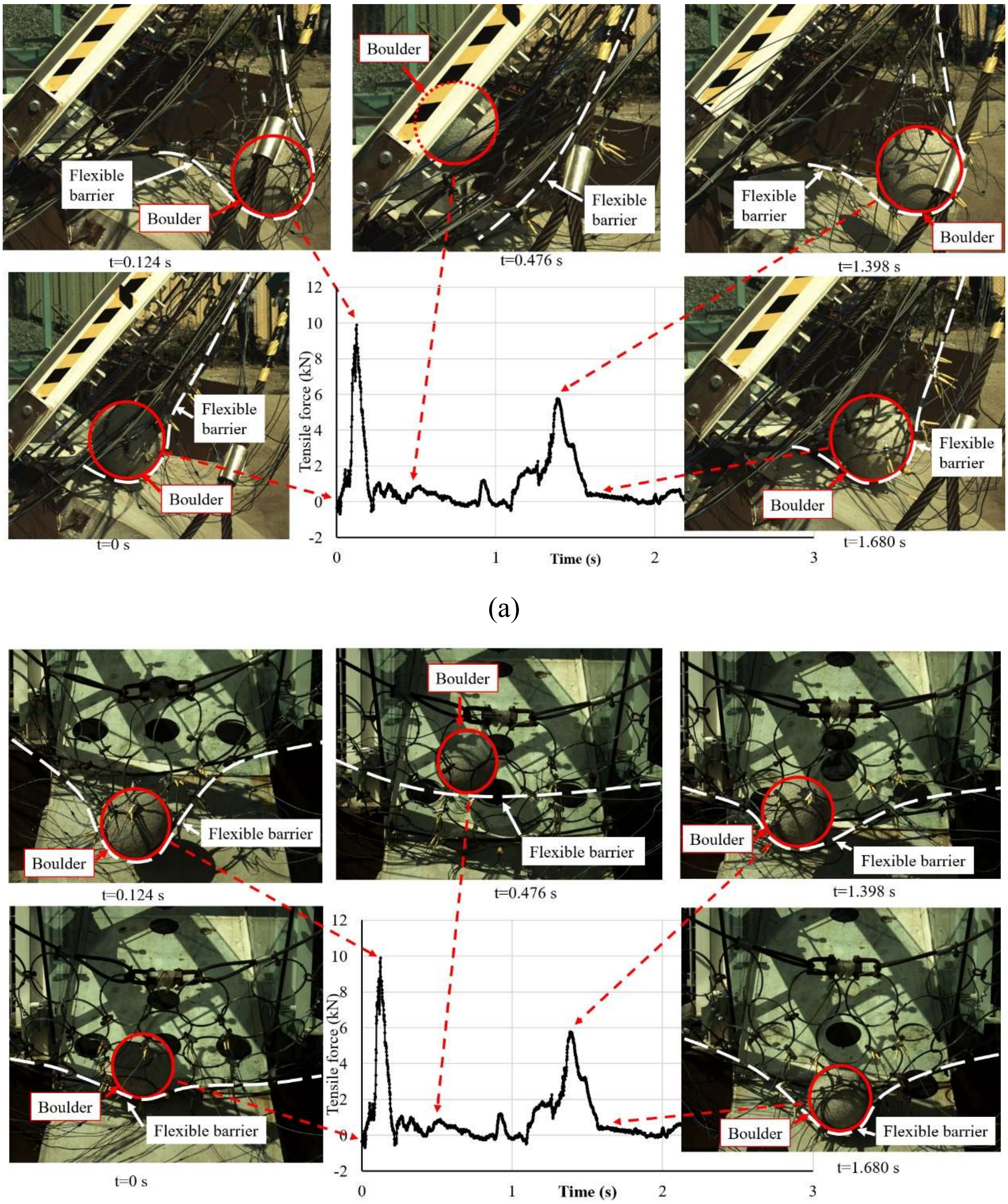

(a)

(b)

Figure 4-2. Interpretation of the typical video frames recorded by (a) the side-view camera and (b) the front-view camera combined with the tensile force on Transducer 10 in Boulder Test 1

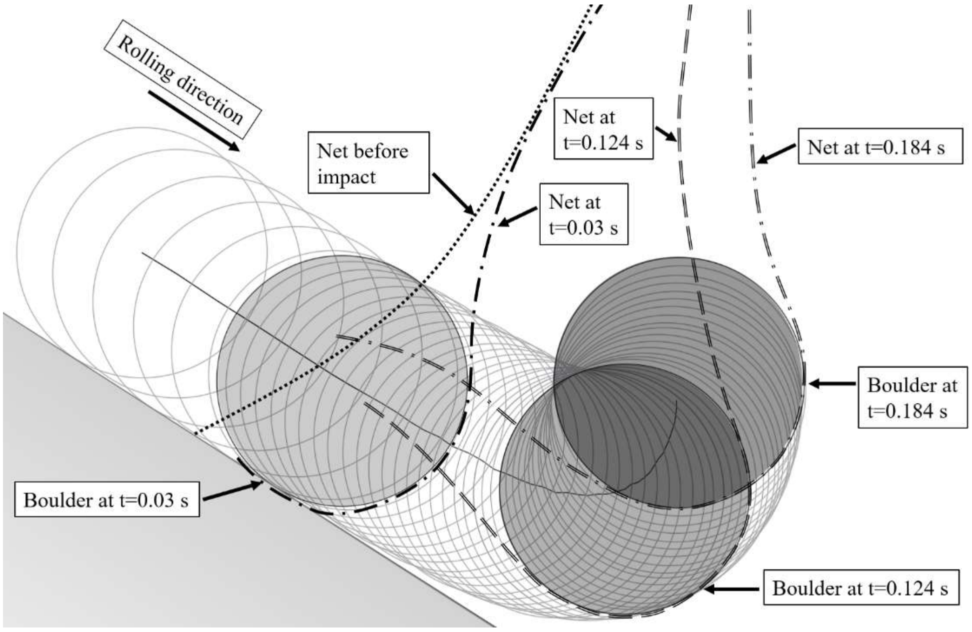

(a)

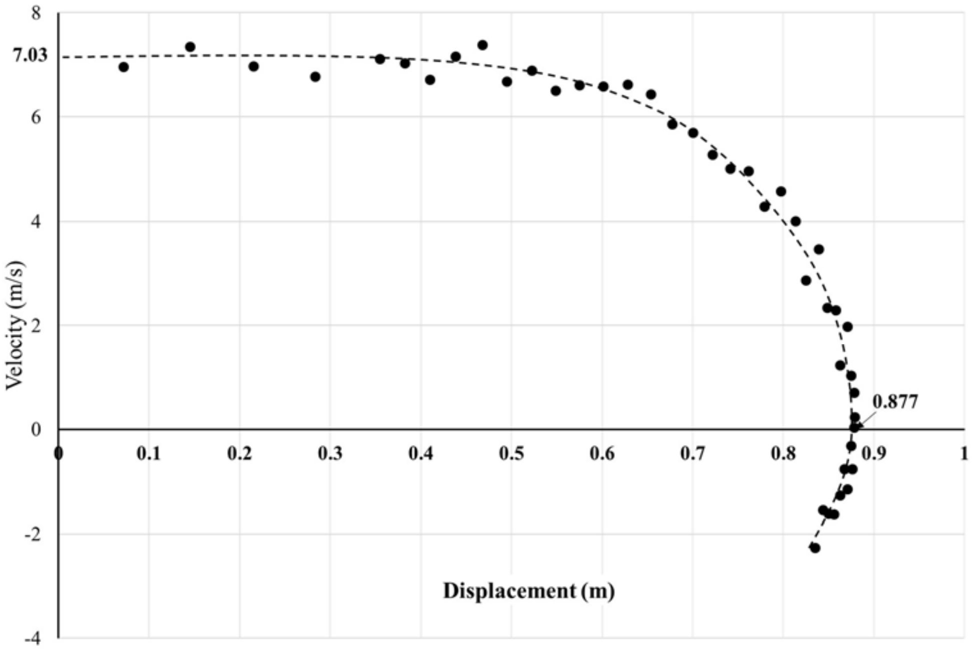

(b)

Figure 4-3. (a) Motion trail of the boulder during the impact process and (b) the relationship between velocity and displacement in the direction of the impact in Boulder Test 1

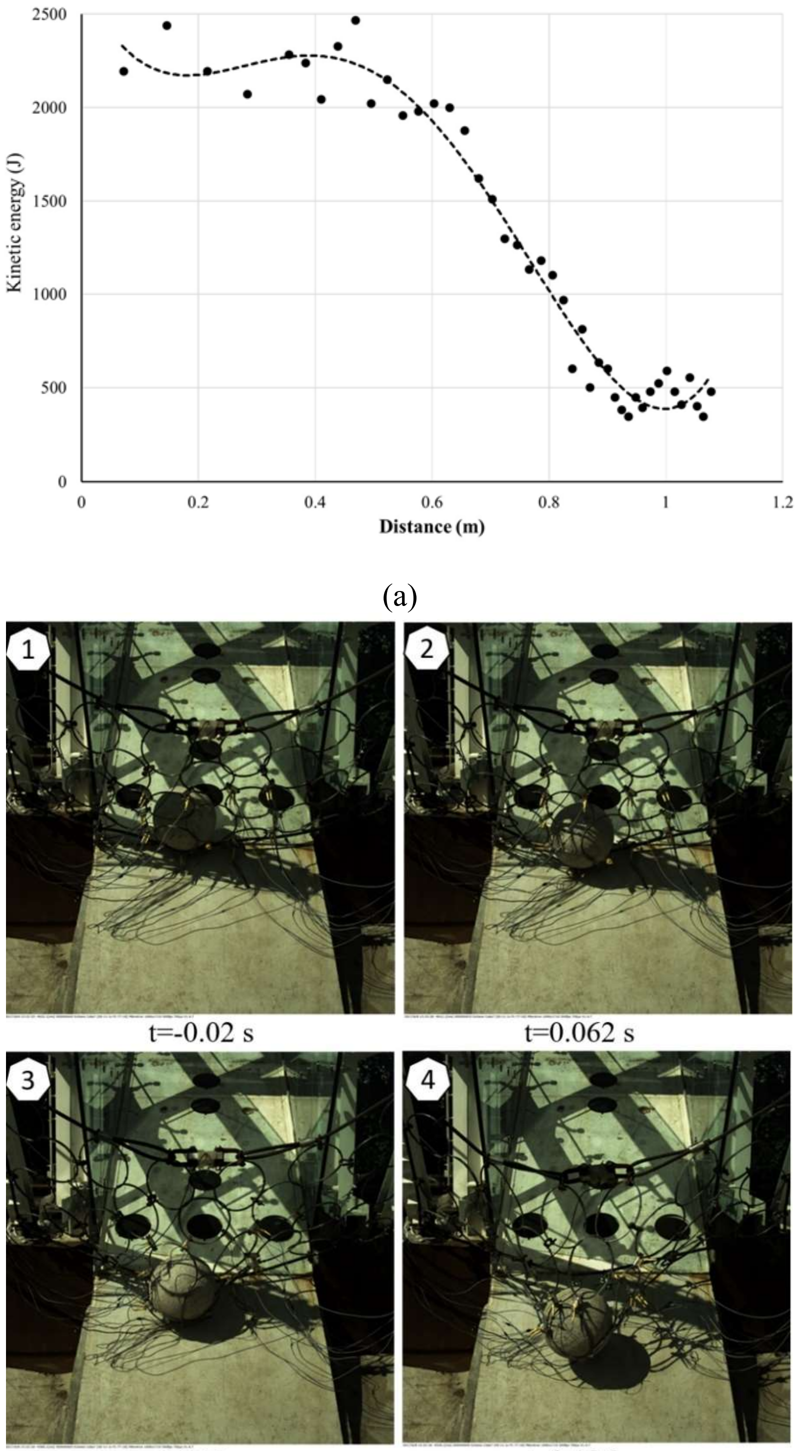

(a)

(b)

Figure 4-4. (a) Kinetic energy dissipation of the boulder with the moving distance and (b) movement of the boulder during the first impact in Boulder Test 1

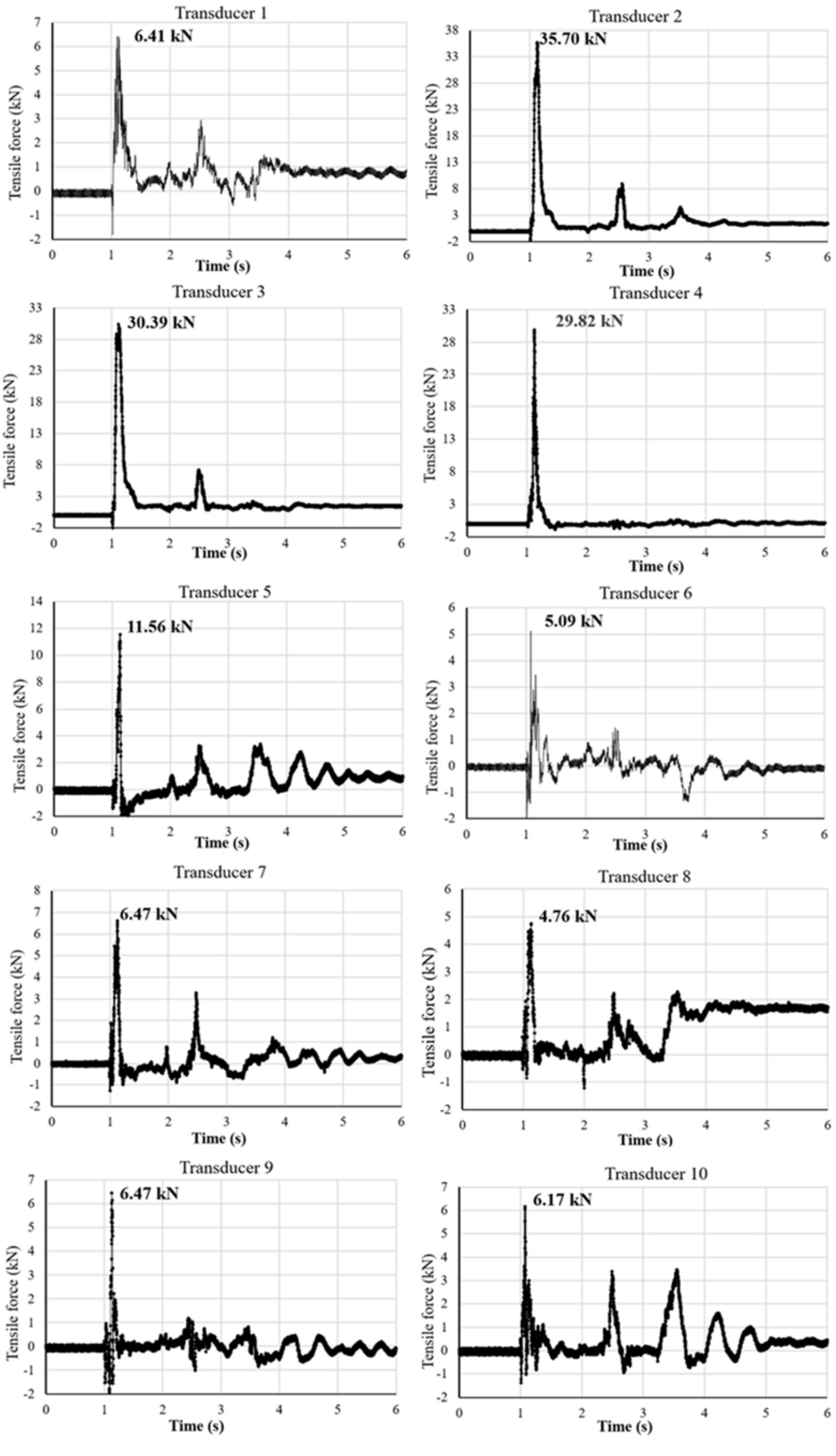
Transducer 1
6.41 kN
Transducer 2
35.70 kN
Transducer 3
30.39 kN
Transducer 4
29.82 kN
Transducer 5
11.56 kN
Transducer 6
5.09 kN
Transducer 7
6.47 kN
Transducer 8
4.76 kN
Transducer 9
6.47 kN
Transducer 10
6.17 kN
Tensile force (kN)
Time (s)
0
1
2
3
4
5
6

(a)

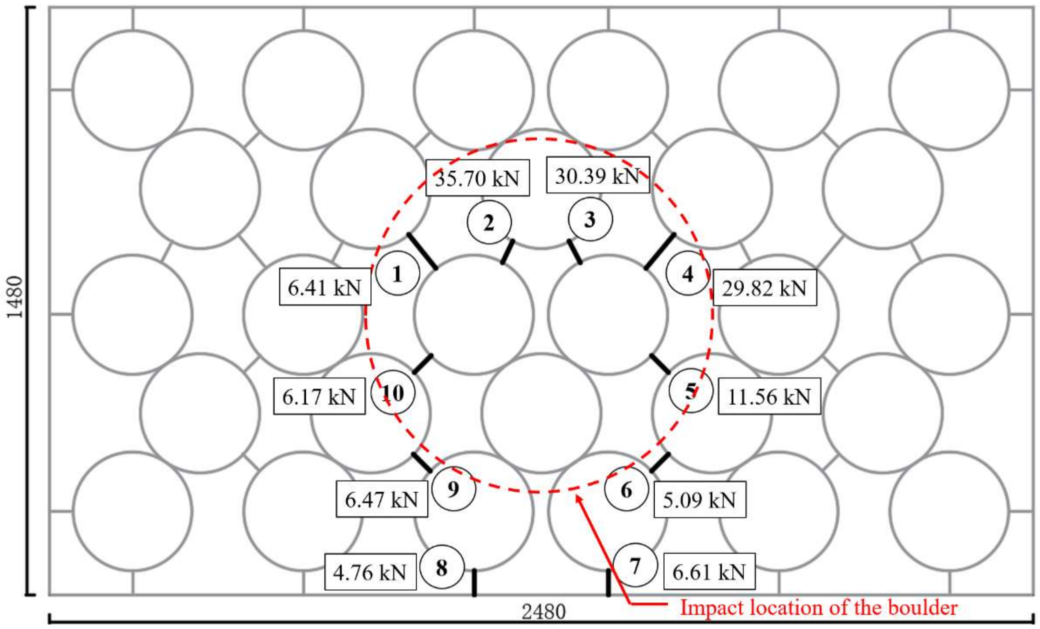

(b)

Figure 4-5. (a) Forces v.s. time and (b) peak tensile forces on the mini tension link transducers between rings in Boulder Test 2 (in *mm*)

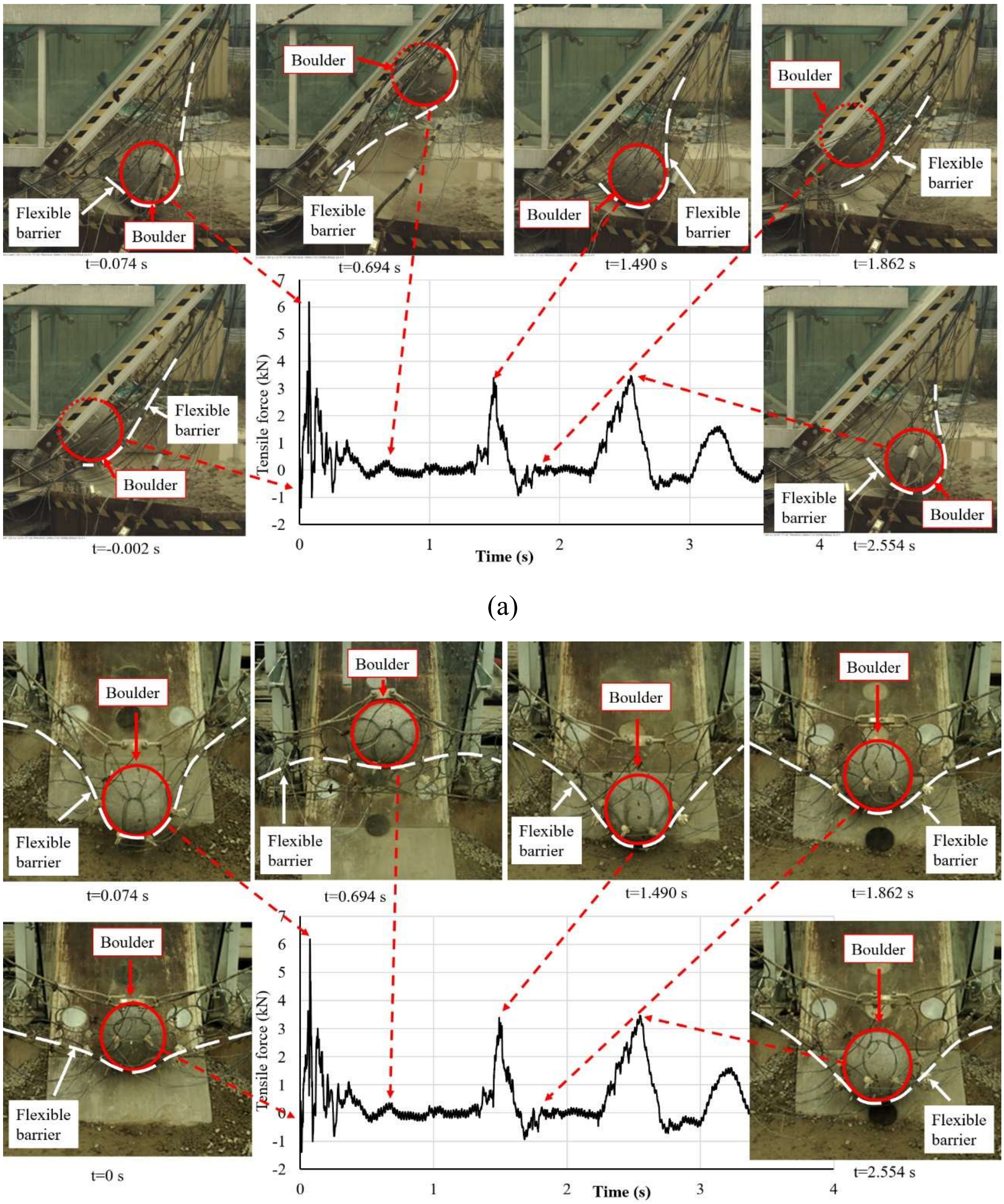

(a)

(b)

Figure 4-6. Interpretation of the typical video frames recorded by (a) the side-view camera and (b) the front-view camera combined with the tensile force on Transducer 10 in Boulder Test 2

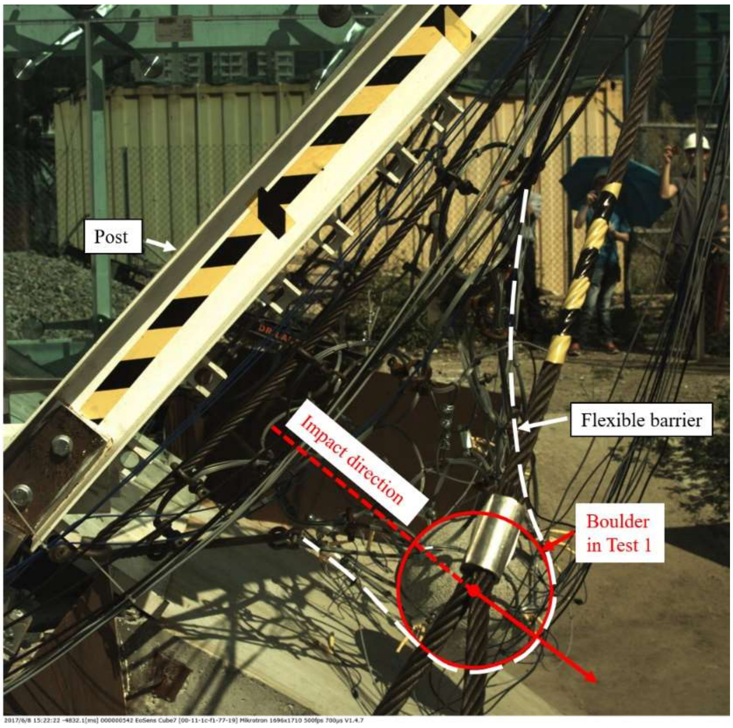
Post
Flexible barrier
Impact direction
Boulder in Test 1
2017/6/8 15:22:22 -4832.1[ms] 000000542 EoSens Cube7 [00-11-1c-f1-77-19] Mikrotron 1696x1710 500fps 700μs V1.4.7

(a)

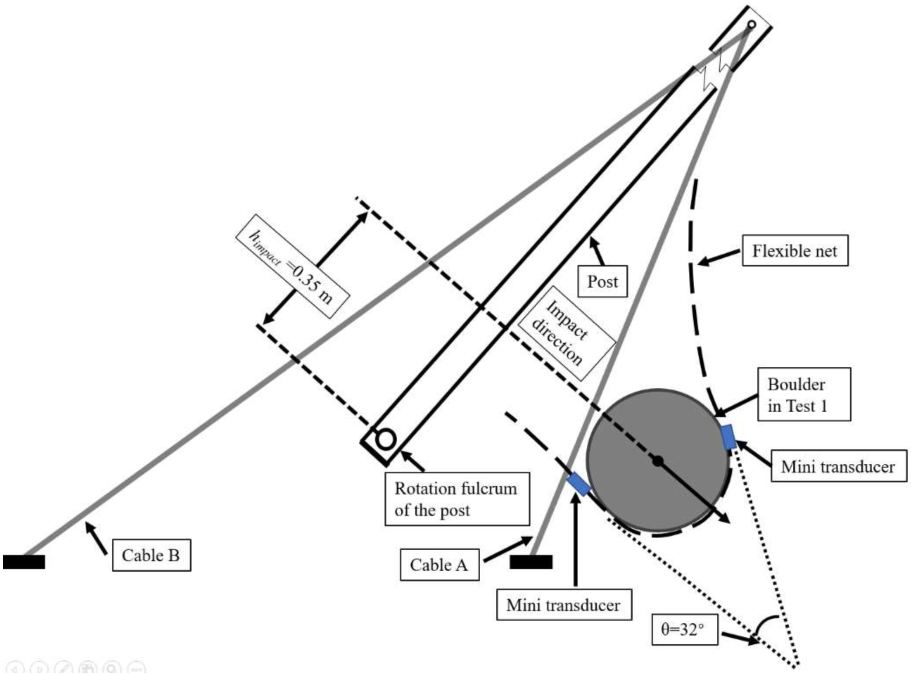
h_{impact} =0.35 m
Post
Flexible net
Impact direction
Boulder in Test 1
Mini transducer
Rotation fulcrum of the post
Cable B
Cable A
Mini transducer
θ=32°

(b)

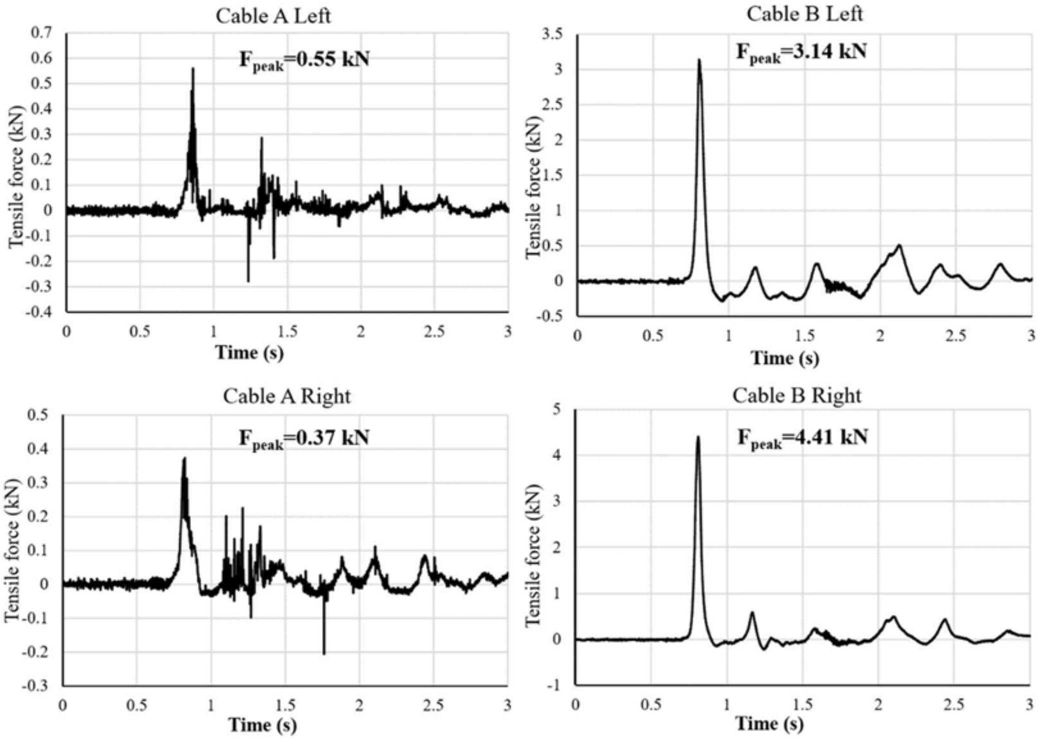

(c)

Figure 4-7. (a) Photograph at the moment of the largest deformation (side view), (b) the parallel schematic view, and (c) the tensile forces on the supporting cables in Boulder Test 1

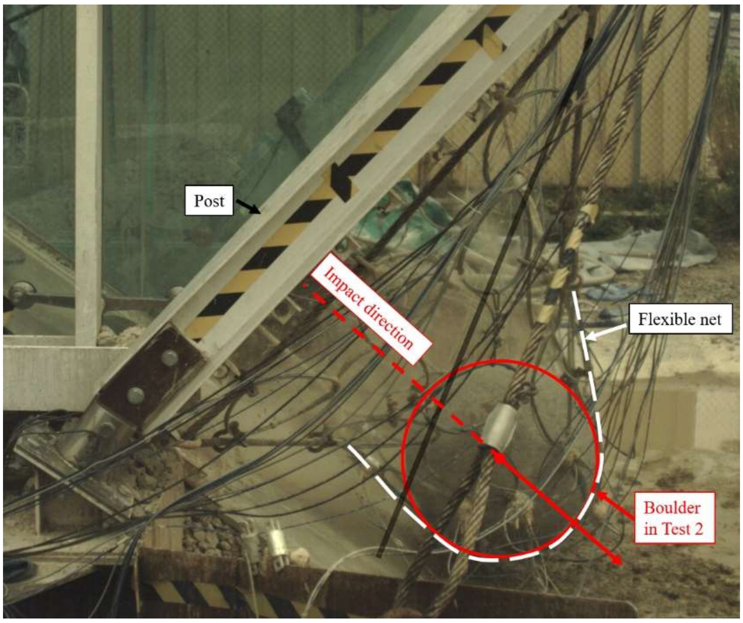
Post
Impact direction
Flexible net
Boulder in Test 2

(a)

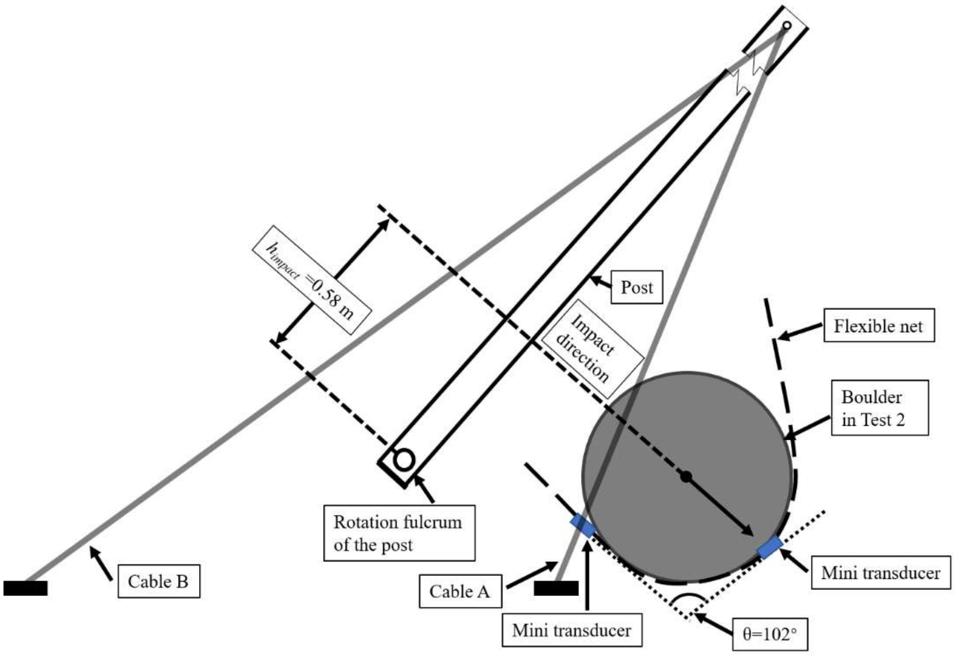
h_{impact} =0.58 m
Post
Impact direction
Flexible net
Boulder in Test 2
Rotation fulcrum of the post
Cable B
Cable A
Mini transducer
Mini transducer
θ=102°

(b)

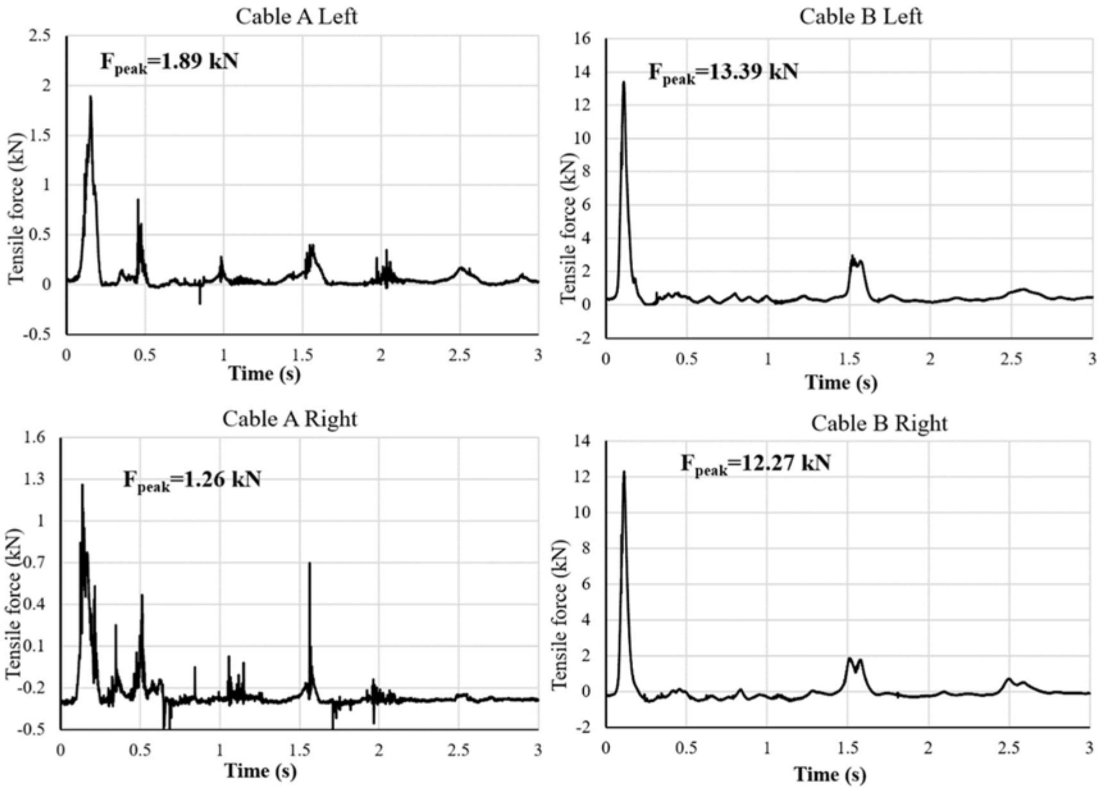

(c)

Figure 4-8. (a) Photograph at the moment of the largest deformation (side view), (b) the parallel schematic view, and (c) the tensile forces on the supporting cables in Boulder Test 2

Table 4-1. Parameters and the measured impact forces in Boulder Test 1 and Boulder Test 2

Test name	**Boulder Test 1 (400 mm diameter)**	**Boulder Test 2 (600 mm diameter)**
h_{post} (m)	*2.7*	
Boulder diameter (mm)	400	600
Boulder density (kg/m^3)	2650	2650
Mass (kg)	90.5	305.4
Impact velocity (m/s)	7.03	7.67
h_{impact} (m)	0.35	0.58
Included angle θ (°)	32	102
$\sum F_i' + \sum F_j$ **(kN)**	39.46	115.04
$F_{A(sum)}$ **(kN)**	*0.92*	*3.15*
$F_{B(sum)}$ **(kN)**	7.55	25.66
$F_{residual}$ (kN)	*25.8*	*52.9*
F_{impact} (kN)	37.9	72.4
IRR (%) (Impact Reduction Rate)	*32*	*27*
Calculated impact force (kN)		***67.7***
Relative Error (%)		***6.5***

CHAPTER 5: IMPACT AND DEPOSITION MECHANISMS OF DRY GRANULAR FLOWS ON A FLEXIBLE BARRIER

5.1 Introduction

Flexible barriers are being increasingly applied to mitigate the danger of debris flows. However, how barriers can be better designed to withstand the impact loads of debris flows is still an open question in natural hazard engineering. The results of two consecutive large-scale granular flow tests are reported to study how flexible barriers react under the impact of granular flows. In the chapter, the impact force directly on the flexible barrier and the impact force transferred to the supporting structures are measured, calculated and compared. Based on the comparison, the impact loading attenuated by the flexible barrier is quantified. The hydro-dynamic methods with different dynamic coefficients and the hydro-static method are validated using the measured impact forces.

5.2 Experiment material and procedures

The sample of material used in the tests is plotted in Figure 5-1, and their properties are listed in Table 5-1. The bulk density of the granite aggregate is determined from the loose dry bulk density according to ASTM C29/C29M-17a (ASTM, 2017) before the tests. The internal friction angle of the aggregate, which is regarded having the same value with the angle of repose, is measured by the pouring tests introduced by Miura et al. (1997) and Zhou et al. (2014). The interface friction angle is determined by the tilting plane method introduced by Hutter and Koch (1991) and Zhou et al. (2014). Two consecutive tests, named Granular Test 1 and Granular Test 2 were conducted using the same granular material. In Granular Test 1, the granular flow travelled on the steel plate of the flume and impacted on an empty flexible barrier, while in Granular Test 2 the granular flow moved on the upper surface of the deposition in Granular Test 1 to simulate the second surge in multiple flows. At the beginning of the tests, the door was flipped up in less than 0.5 s with the help of a fast door-opening system to generate a uniform granular flow. The data logger started to obtain data several seconds before the triggering of the granular flow to obtain initial values of all the transducers. Simultaneously, the high-speed cameras started to capture the motion of the granular flow and its interaction with the flexible barrier during the impact.

5.3 Test results

5.3.1 Motion and impact of granular flow in Granular Test 1

In Granular Test 1, the initial time of the impact was readjusted to 0 s in all plotted data and selected video frames, and the negative value of time represents the moment before the interaction. By tracking the motion of the granular flow with high-speed cameras, the average speed of the granular flow was 5 m/s, which was relatively low compared with the measured velocities from 2 m/s to 12 m/s in the literature (Arattano and Marchi 2005; Prochaska et al. 2008; Berti et al. 1999). The motion of the granular flow in Granular Test 1 is plotted in Figure 5-2. From this figure, it can be observed that the granular flow firstly travelled down and impacted on the flexible barrier, which caused a large deformation of the lower part. Afterward, the following debris front moved on the top surface of the previous deposition layer and deposited behind the barrier as a pile, which indicates that frictional flow can perform a pile-up deposition behaviour. Finally, the flexible barrier was almost filled by the granular flow, and the later reaching granular flow deposited behind the deposition pile instead of climbing on the previous deposition wedge due to its poor fluidity. The deposition height of the granular flow and the maximum horizontal deformation of the flexible barrier at different times are measured from the profiles of the granular flow in photographs taken by the side-view high-speed camera during the impact period in Figure 5-3. It can be observed that the front portion of the granular flow shot up, impacted on the barrier directly, and was deposited as a wedge-shaped dead zone at the bottom of the flexible barrier from 0 s to 1.0 s. The following granular flow was deposited behind the barrier layer by layer. The measured deposition height, the maximum horizontal deformation and the tensile force history of Transducer 1's change over time are plotted in Figure 5-4. It can be seen that the deposition height of the trapped aggregate rises almost linearly with time and reaches 0.82 m at the time of 1.0 s, and the horizontal deformation of the barrier increases from an initial value of 0.26 m to 0.48 m at the time of 1.0 s. It is worth noting that the tensile force on the net keeps increasing even as the deposition height of the granular flow reaches the maximum value. This phenomenon indicates that the granular flow can continuously exert impact pressure on the flexible barrier via the deposition wedge.

5.3.2 Impact loading analysis in Granular Test 1

Tensile forces recorded by the mini tension link transducers between rings are plotted in Figure 5-5. Signals of the transducers have some noise due to the intensive impacts from thousands of particles during the impact period. Thus, trend lines are added to those figures to clarify the changes of tensile forces. A gradual rise of static load and two dynamic impact peaks are observed in the signals of most transducers. The first impact peak occurred at the beginning of the impact, and the second impact peak appeared at the end of the impact. These two peaks are much smaller than the accumulated static load. It is indicated that the dynamic load and the static load co-existed in the impact process, and the static load was dominant. The loading situations of the flexible barrier in the study fit well with the observations of the field tests by Wendeler et al. (2018) that the impact loadings on the supporting ropes increase gradually over time during the impact process. Since the dynamic loading due to the oncoming debris fronts is nearly constant, they concluded that the increase of the impact loading is mainly attributable to the incremented debris deposition. Besides, transducers connected to the bottom cross-tension cable (Transducer 7 and Transducer 8) show negative values, which indicates that they were compressed in the impact process. The peak impact loading of all the transducers installed on the net, the impact area and the measured area in Granular Test 1 are plotted in Figure 5-6. Figure 5-7 presents typical frames recorded by the side-view camera and the front-view camera combined with the signal from Transducer 1. From this figure, it can be seen that the first dynamic loading came from the direct impact of the first debris front on the flexible barrier, and the gradual increase of the static load was caused by the deposition of the aggregate. With the growth of the deposition zone, the impact loading of the following granular flow was finally fully resisted by the deposition cushion. Afterward, only the static earth pressure of the deposition acted on the flexible barrier. The included angle of the net during the impact and the force history of transducers installed on the supporting posts are plotted Figure 5-8. With the deformation and the loading situation of the flexible protection system, the measured impact forces on the flexible barrier directly and on the supporting posts are calculated using Eq.(3-3) and Eq.(3-10). All the parameters and calculated results are listed in Table 5-2. Thus, IRR in the granular flow tests is calculated and presented in Table 5-2. It is found that around 26 % of the impact loading from the dry granular flow in Granular Test 1 was attenuated by the flexible barrier.

5.3.3 Motion of granular flow in Granular Test 2

The second granular flow was triggered after Granular Test 1 to simulate the second flow in a multiple-debris-flow event. In Granular Test 2, the granular flow travelled on the top surface of the deposition in Granular Test 1 and came to rest without reaching the net. The motion of the granular flow in Granular Test 2 is plotted in Figure 5-9. In that figure, since the granular did not impose any measurable impact loading on the flexible barrier, the initiated time of the granular flow is defined as 0 s. It can be found that the granular flow had a thick front when it was first triggered, and then the thickness kept decreasing during movement. Based on the recording of the side-view camera, the side view of depositions in the two tests and the velocity change with the flowing distance of the granular flow in Granular Test 2 are plotted in Figure 5-10. Thickness and velocity of the front reduced dramatically with the increase of the moving distance and finally stopped 0.7 m before the flexible barrier. Correspondingly, neither impact force nor deformation increment of the flexible barrier was recorded by the transducers or the high-speed cameras. The reason for the flow stopping before the flexible barrier is the large basal friction from the rough interface between the moving granular flow and the deposition and the low fluidity of the dry granular flow. The multi-flow tests show that the impact from the latter arrived debris flows can be attenuated or eliminated by the resistance from the deposition of the previous debris flow in a multiple-debris-flow event.

5.3.4 Comparison of simple methods with measured impact forces

Two widely accepted simple methods for impact force estimation: hydro-dynamic method and hydro-static method (Kwan and Cheung 2012; Volkwein 2014; Song et al. 2017; Ashwood and Hungr 2016; Wendeler 2008; Wendeler et al. 2018) are compared in this section to validate their applications in the design of flexible barriers. To quantify the accuracies of the simple methods, Relative Error (RE) is usually defined as:

$$RE = \left| \frac{F_{calculated} - F_{measured}}{F_{measured}} \right| \times 100\% \tag{5-1}$$

where $F_{calculated}$ represent the calculated impact force of the simple methods, which are obtained by substituting the parameters listed in Table 5-1 and Table 5-2 into the simple methods listed in Table 5-3; and $F_{measured}$ is the measured impact force on different components of the flexible barrier. In the table, two dynamic coefficients suggested by Wendeler (2008): 0.7 for mud flow, 2.0 for granular flow, and a static coefficient of 1.0- are utilized.

The calculated results are validated using the measured impact forces on the flexible ring net and on the supporting structures. The validation results are quantified with the value of Relative Error. The results of the calculation and the validation are listed in Table 5-3. Compared with the measured impact force on the flexible ring net directly, the hydro-dynamic method with the dynamic coefficient of 2.0 has the best performance in estimating the impact force on the flexible ring net with a small deviation of 3.5 %, which verifies the dynamic coefficient suggested by Wendeler (2008) for granular flows. The reduced dynamic coefficient of 0.7 for debris flows with lower densities (lower than 1900 kg/m^3), on the other hand, obviously underestimated the loading on the flexible ring net by 50%. The reduction of the dynamic coefficient takes account of the dewatering and passing-through of small particles during the impact based on lab tests and field observations (Wendeler 2008; Wendeler and Volkwein 2015; Wendeler et al. 2018). Therefore, the underestimation of the impact loading could be attributed to the all trapped granular material by the secondary mesh net in the dry-granular-flow impact tests based on the observations of the impact process with the high-speed cameras. In contrast, the hydro-static method with the static coefficient of 1.0 fits quite well with the measured impact force on the supporting structures. This is reasonable since part of the dynamic impact from the granular flow can be attenuated by the flexible ring net, and the static loading can be fully transferred to the supporting structures. This phenomenon is also proved by the gradually increased tensile forces on Cable B Left and Cable B Right shown in Figure 5-8(b). Thus, in the design of a flexible barrier for debris flow mitigation, the hydro-dynamic method and the hydro-static method can be used in the design and the selection of the flexible ring net and the supporting structures, respectively. Even though the dynamic coefficients and the static coefficient are verified by the data of large-scale tests in this study, more tests are required to further verify and select suitable coefficients before they can be used in the design.

5.4 Summary

In this chapter, two tests were performed to study the behaviour of a flexible barrier subjected to the impacts of granular flows. From the experimental data and their analysis, key findings and conclusions are summarized and presented as below:

(a) In Granular Test 1, the front of the granular flow impacted on the flexible ring net directly, deposited behind the barrier, and formed a deposition wedge in the first second. After 1.0 s, the following granular flow deposited behind the deposition wedge.

(b) The static loading and the dynamic loading co-existed in the impact process, and the static loading was dominant. The static loading attributed to the gradual deposition of aggregate, and the dynamic loading was caused by the impact of the debris front. The latter arrived granular front applied impact loading on the flexible barrier via the deposition wedge. With the deposition of aggregate, the stationary debris formed a cushion behind the barrier and attenuated all the impact loading from the following granular front.

(c) In Granular Test 2, the second granular flow in a multiple-flow event was performed. The velocity and the flow depth of the granular flow decreased during movement, and the front stopped before it could reach the flexible barrier due to the large basal friction between the moving granular flow and the granular deposition and the poor fluidity of the dry granular flow.

(d) The impact loading on a flexible ring net was directly measured from the tensile forces in the central area of the flexible ring net. In Granular Test 1, the measured impact force on the flexible ring net is 10.69 kN.

(e) The contribution of flexibility to impact loading reduction is quantified by introducing the Impact Reduction Rate (IRR). By calculating the impact loading transferred to the supporting structures, it can be concluded that almost 26 % of the impact loading from the granular flow was attenuated by the flexible ring net in Granular Test 1.

(f) From the comparisons of the hydro-dynamic method and the hydro-static method with the measured impact forces on different components, it is found that the hydro-dynamic method with the dynamic coefficient of 2.0 fits well with the measured impact force on the flexible ring net, and the hydro-static method with the static coefficient of 1.0 has a good performance in estimating the impact force on the supporting structures.

With the conclusions drawn from the large-scale tests in this chapter, it can be found that the impact force on the flexible ring net and the impact force on the supporting structures are different due to the large deformation of the flexible ring net, thus the loadings on them should be estimated separately. By applying the IRR and suitable impact loading estimation methods (see the verification results plotted in Table 5-3), the impact forces on the flexible ring net and on the supporting structures can be estimated separately. Thus, the design of a flexible barrier for debris flow mitigation can be optimized by dimensioning and designing different components with different design loadings, which provides a safer and more economical design approach.

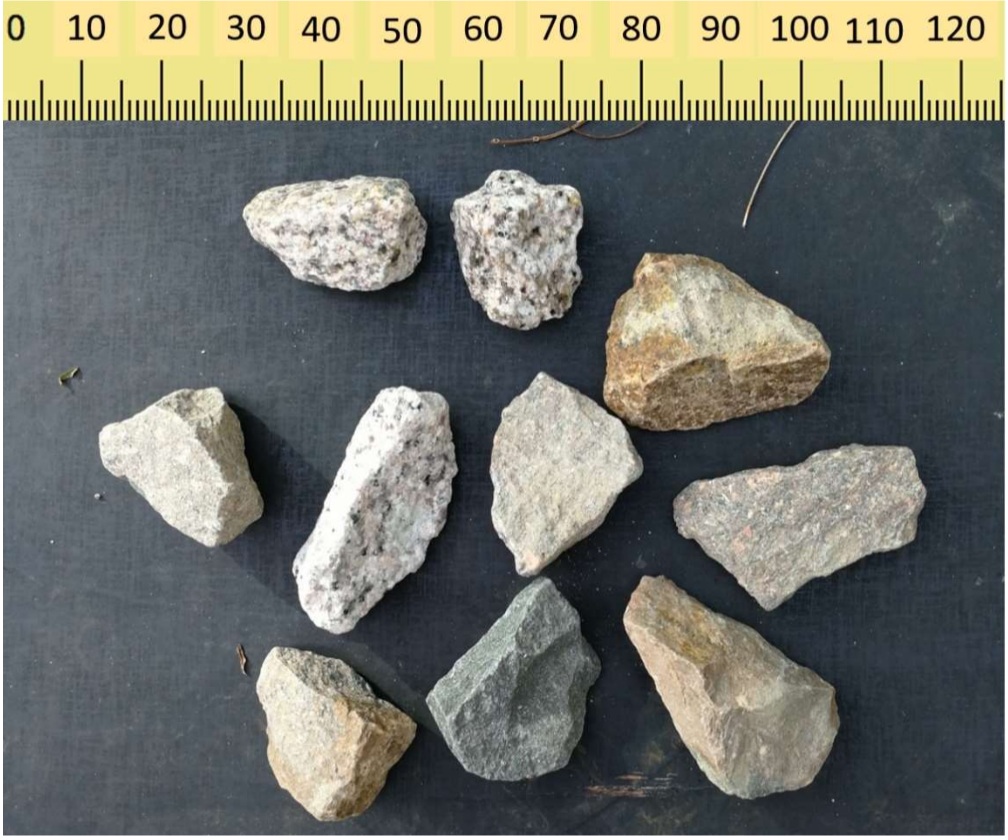

Figure 5-1. Aggregate samples in the granular flow impact tests (unit: mm)

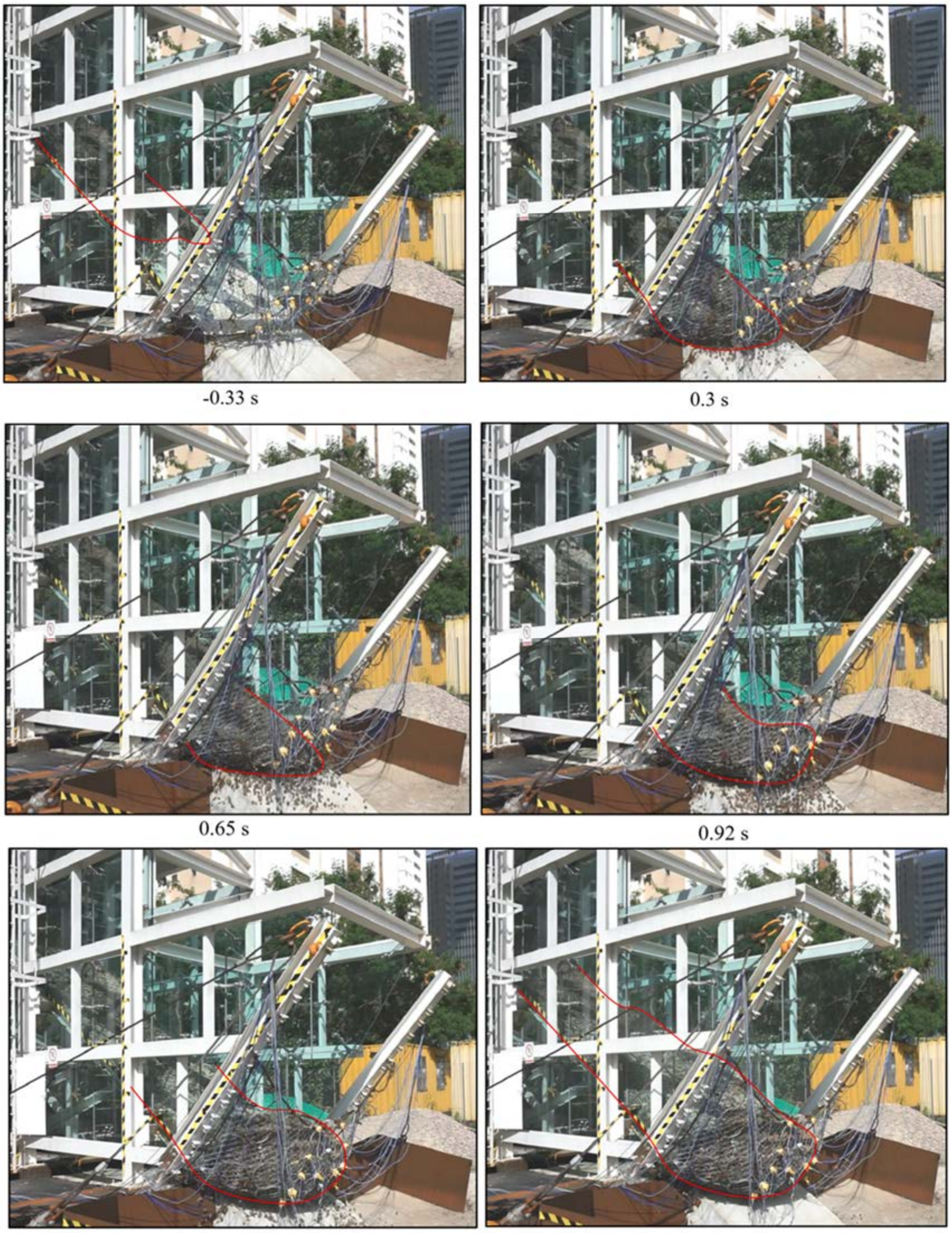

-0.33 s

0.3 s

0.65 s

0.92 s

1.39 s

2.61 s

Figure 5-2. Motion of the granular flow in Granular Test 1

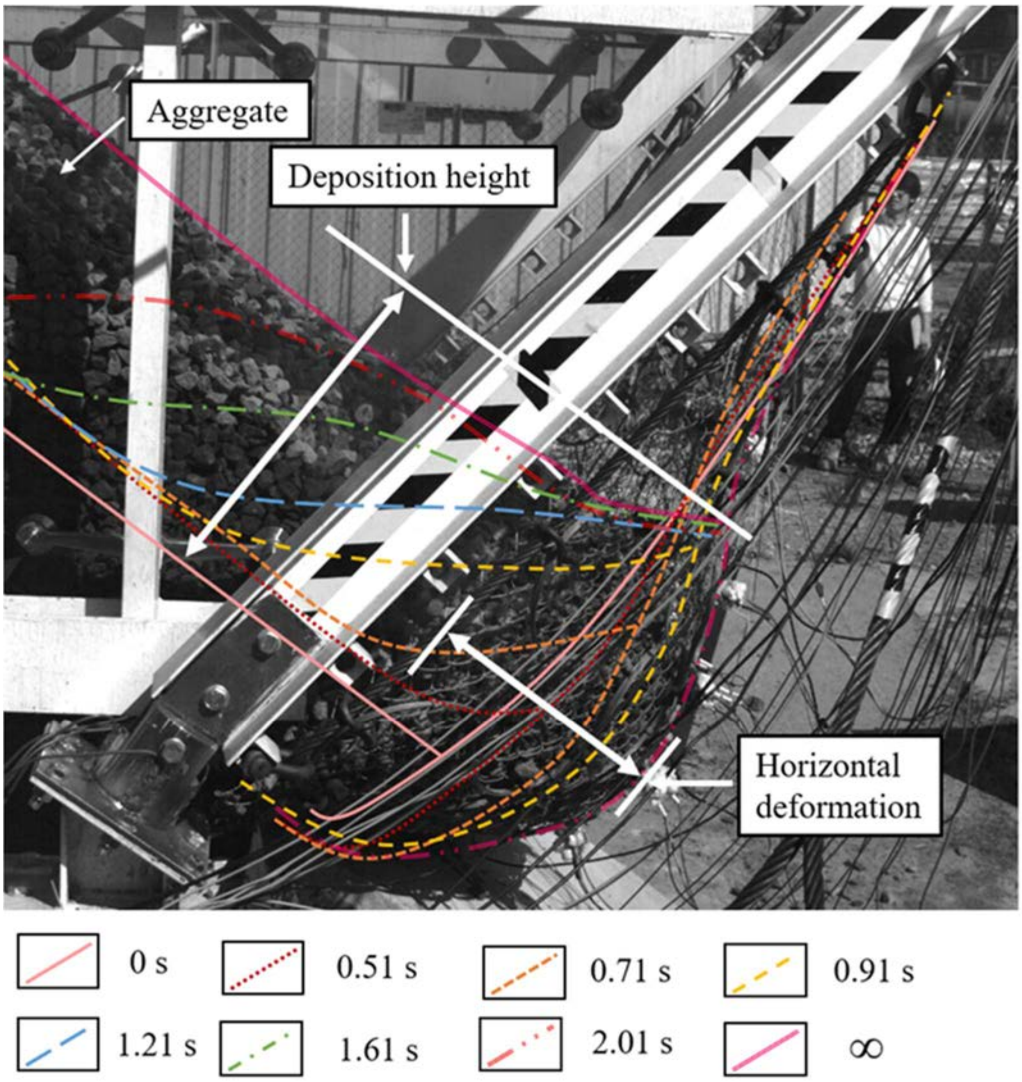

Figure 5-3. Side profiles of the deposited granular flow at different times in Granular Test 1

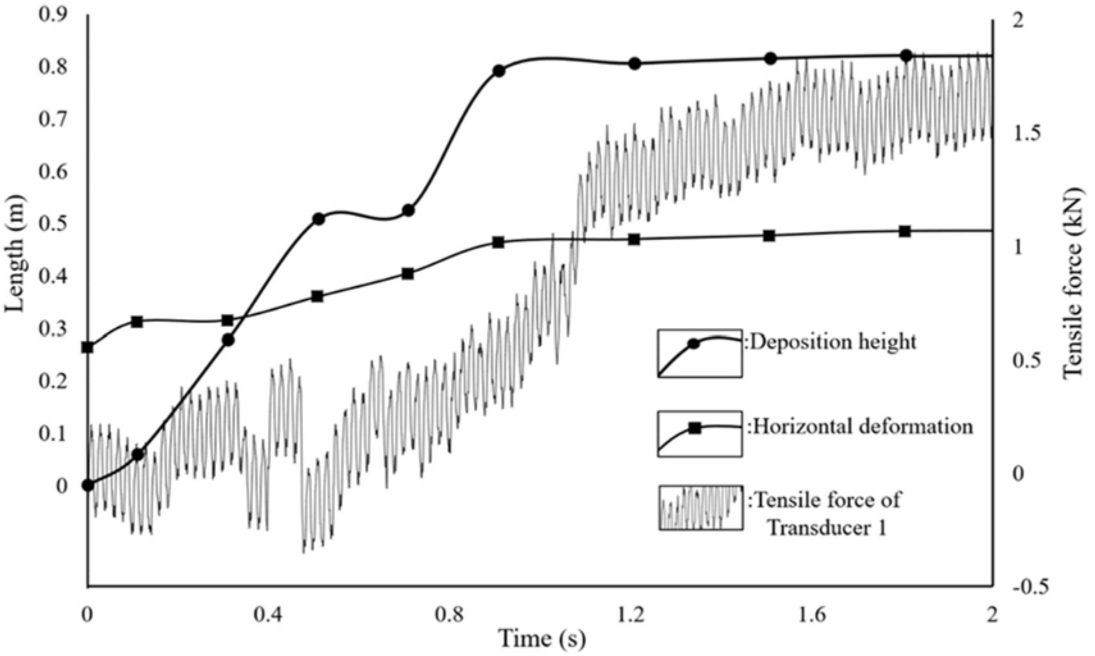

Figure 5-4. Deposition height of the granular flow, the horizontal deformation of the flexible barrier, and the tensile force of Transducer 1 *v.s.* time in Granular Test 1

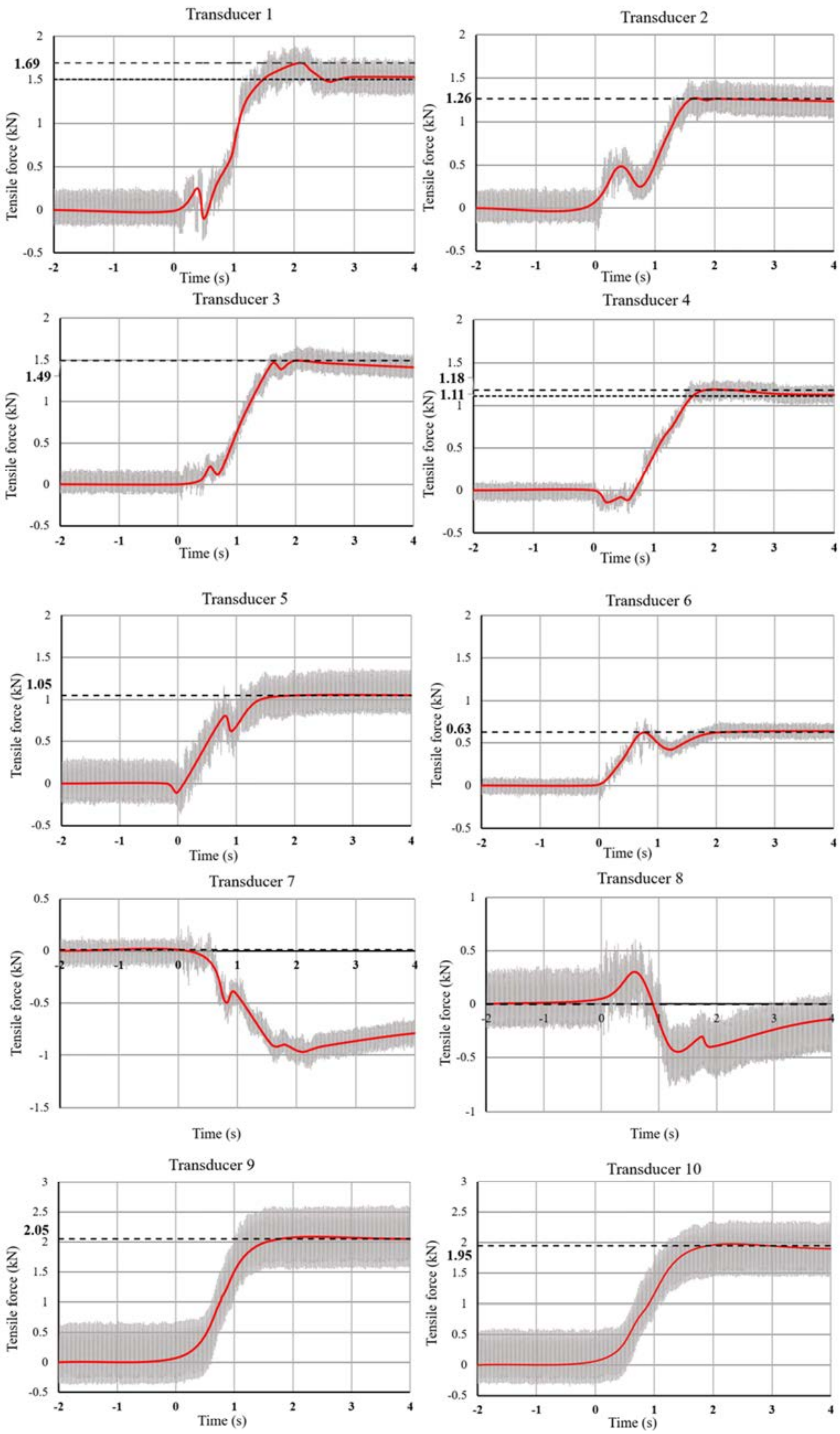

Figure 5-5. Recorded forces with time by the mini tension link transducers between rings in Granular Test 1

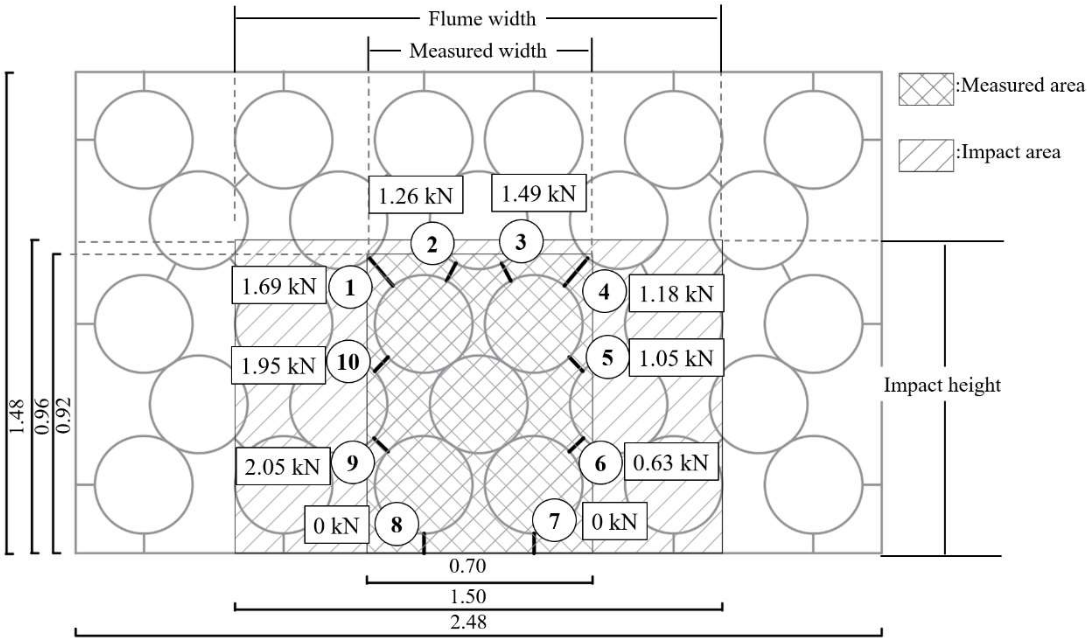

Figure 5-6. Sketch of the impact and measured area in Granular Test 1 and the maximum tensile forces measured from 10 mini tension link transducers under the impact of the granular flow (unit: m)

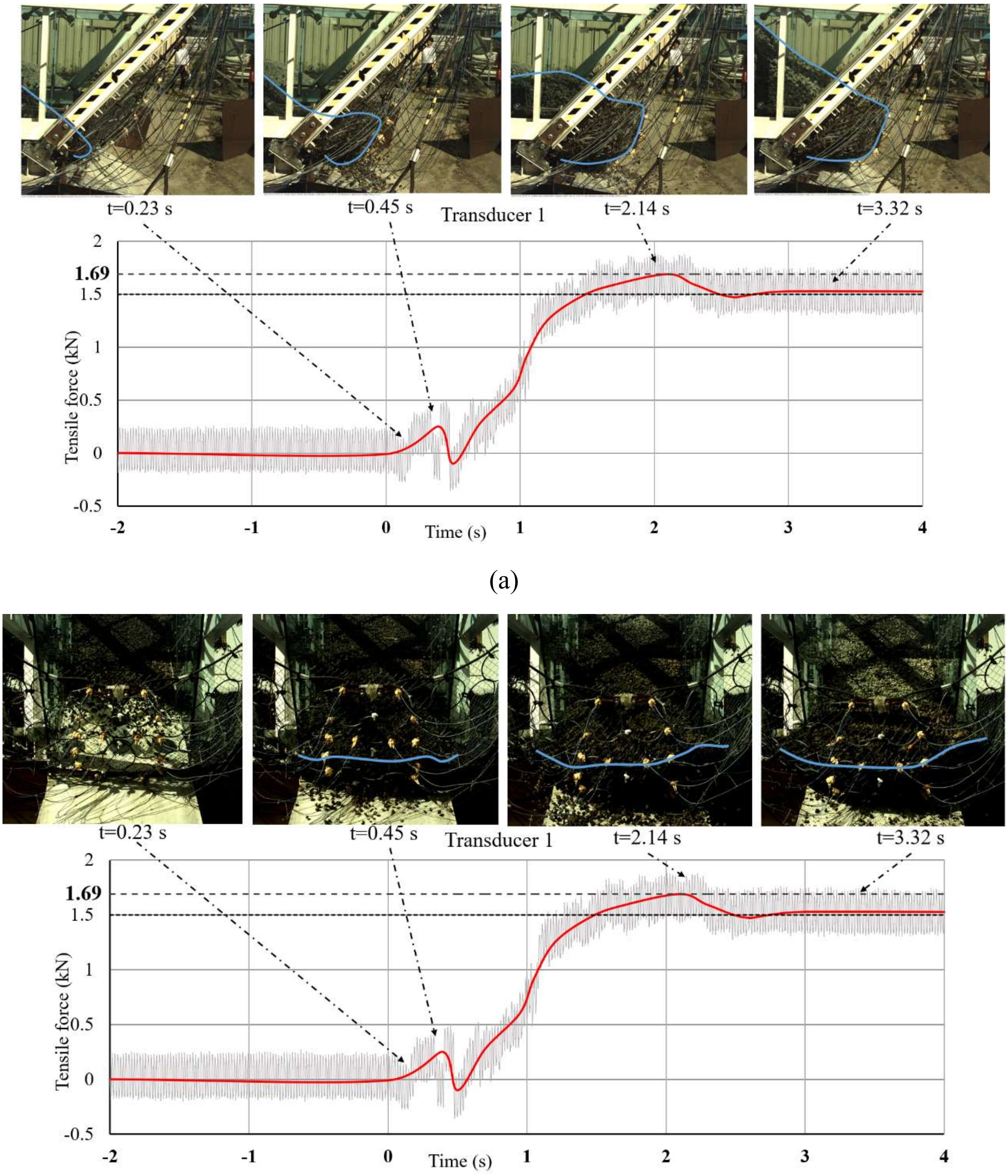

(a)

(b)

Figure 5-7. Interpretation of the typical video frames in Granular Test 1 recorded by (a) the side-view camera and (b) the front-view camera with the tensile force from Transducer 1

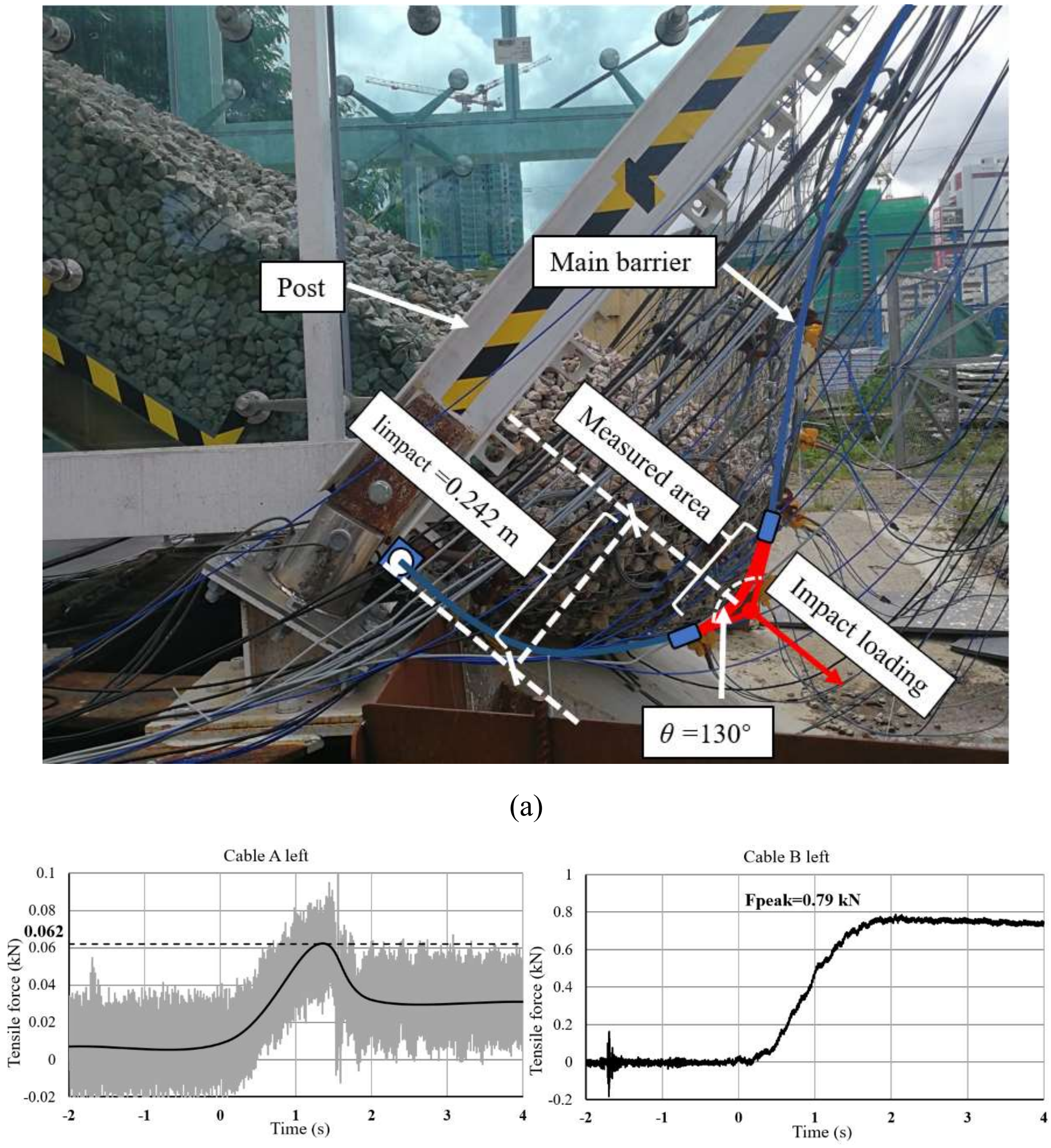

(a)

(b)

Figure 5-8. (a) Photograph at the instant of the largest deformation (side view) and (b) the tensile forces on the supporting cables in Granular Test 1

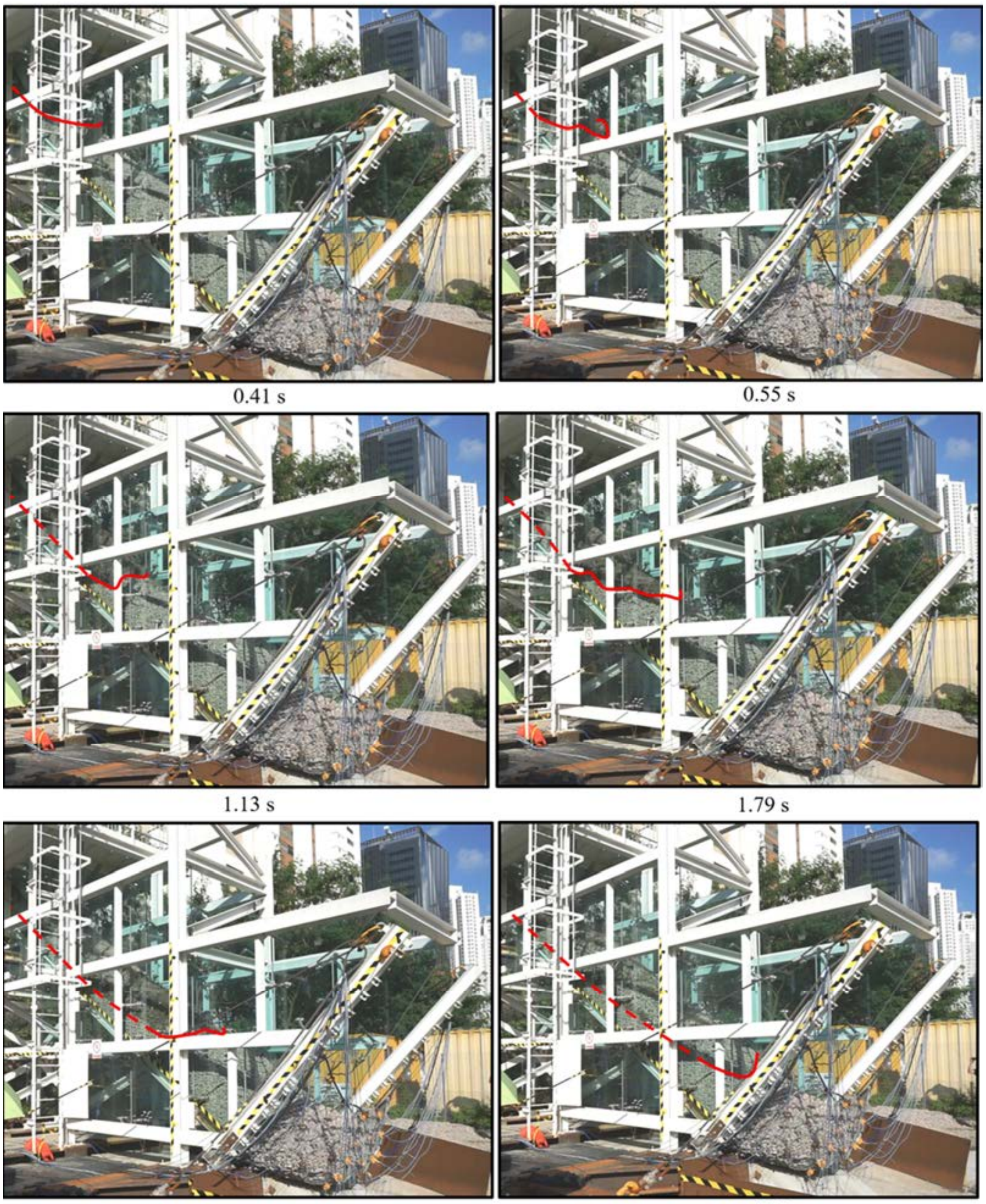

0.41 s

0.55 s

1.13 s

1.79 s

2.32 s

5.30 s

Figure 5-9. Motion of the granular flow in Granular Test 2

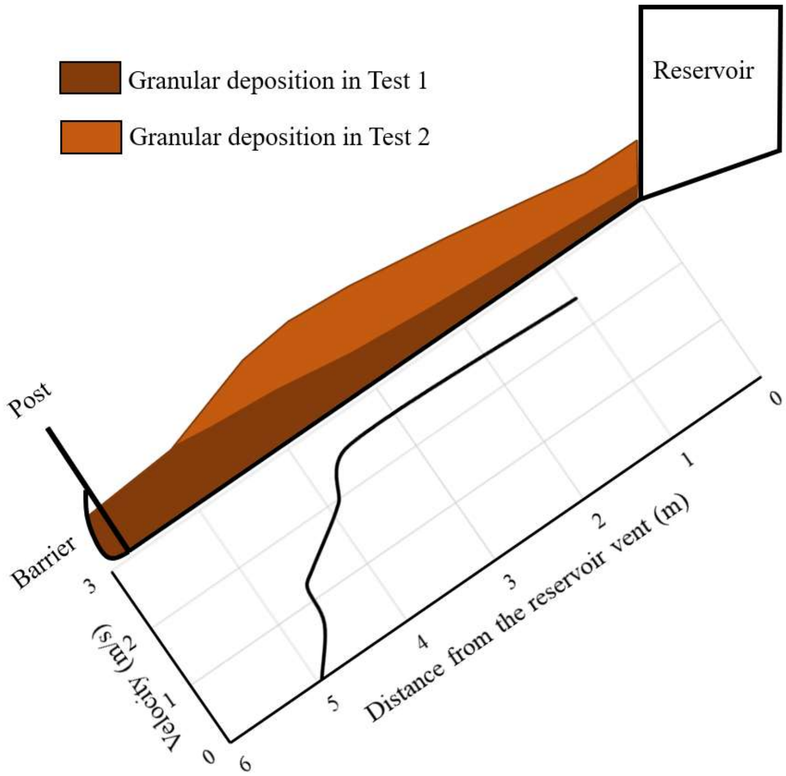

Figure 5-10. Side-view sketch of the depositions in Granular Test 1 and Granular Test 2 and the velocity decay of the granular flow in Granular Test 2 with the moving distance

Table 5-1. Main properties of aggregate used in Granular Test 1 and Granular Test 2

Main properties	**Values**
The total volume of aggregate in Granular Test 1 and 2 (m^3)	4
Particle diameters (mm)	15 - 30
Internal friction angle (°)	36
Interface friction angle (°) **(between aggregate and painted steel plate)**	28
Bulk density (kg/m^3)	1600

Table 5-2. Values of measured parameters and calculated results in Granular Test 1

Parameters and results	Values
Moving speed (m/s)	5
Included angle θ (°)	130
$A_{measured}$ (m^2)	0.644
A_{impact} (m^2)	1.44
$\sum_{i=1}^{i=n} F_{tensile,i}$ **(kN)**	11.30
$F_{measured}$ (kN)	4.9
l_{impact} (m)	0.242
l_{post} (m)	2.7
h_{debirs} (m)	0.086
$h_{deposit}$ (m)	0.82
F_{AL} (kN)	0.062
F_{AR} (kN)	0.062
F_{BL} (kN)	0.79
F_{BR} (kN)	0.79
$F_{Cables,equivalent}$ (kN)	7.89
F_{impact} (kN)	10.69
Impact Reduction Rate (IRR) (%)	26.19

Table 5-3. Comparisons of the calculated impact forces using simple approaches with the measured impact forces on different components of a flexible barrier in Granular Test 1

Simple approaches for impact force estimation	**Calculated impact force (kN)**	**RE with impact force on the flexible net (%)**	**RE with impact force on the supporting structures (%)**
		F_{impact}=10.69 kN	$F_{Cables,equivalent}$ =7.89 kN
$F_{calculated} = \alpha\rho_{bulk}v_0^2hw$ **(hydro-dynamic approach with α=0.7) (for muddy debris flows with lower densities)** **(Wendeler 2008)**	3.61	66.2	54.3
$F_{calculated} = \alpha\rho_{bulk}v_0^2hw$ **(hydro-dynamic approach with α=2)** **(for granular flows)** **(Wendeler 2008)**	10.32	**3.5**	30
$F_{calculated} = 0.5K\rho_{bulk}gh_{deposit}^2w$ **(hydro-static approach with K=1)** **(Kwan and Cheung 2012)**	7.92	25.9	**0.38**

CHAPTER 6: IMPACT AND DEPOSITION MECHANISMS OF DEBRIS FLOWS ON A FLEXIBLE BARRIER

6.1 Introduction

Overflow should be taken into account in the design of multiple-flexible-barrier systems to provide a larger retaining capacity to channelized debris flows. To investigate the response of a flexible barrier impacted and overflowed by multiple debris flows and by a single debris flow, a series of three continuous debris flow impact tests (Debris Test 1, Debris Test 2 and Debris Test 3) and a single debris flow impact test (Debris Test 4) were conducted. For the multiple debris flow impact tests, a parameter named Initial Block Rate (IBR) is defined to describe the initial condition of the flexible barrier before each test. This parameter represents the blocking rate of the flexible mesh net by the debris deposition in the previous debris flow impact test. In this study, the influence of the Initial Block Rate (IBR) on the debris-barrier interaction is investigated, especially in the aspect of the impact and deposition mechanisms. For the single debris flow impact test, a shorter flexible barrier was utilized to replicate the impact process including dynamic impact, debris deposition and overflow in a short period (in 1 second). The impact characteristics and the impact loading distribution on the flexible ring net are revealed.

A mixture of Completely Decomposed Granite (CDG), aggregate and water is used in this study to simulate debris flows. The basic parameters of the debris flows in Debris Test 1, Debris Test 2, Debris Test 3 and Debris Test 4 are plotted in Table 6-1. The PSD (Particle Size Distribution) curves of the testing materials in these tests are plotted in Figure 6-1. Three successive tests (Debris Test 1, Debris Test 2 and Debris Test 3) were conducted continuously with the time interval of one week to study a flexible barrier impacted and filled by multiple debris flows. While in Debris Test 4, a shorter flexible barrier was impacted by a single debris flow to simulate the situation that the retaining capacity of the flexible barrier was smaller than the total volume of the debris flow. The depth of the approaching debris front and the velocities of the debris flow before and after the interaction in each test are measured from the continuous photographs taken by the side-view high-speed camera, which are listed in Table 6-1.

6.2 Multiple debris flow impact tests with overflow (Debris Test 1-3)

In this section, the results of three continuous debris flow impact tests are presented and analysed with the help of the high-speed photographs and the force histories during the impact process. How the initial condition of the flexible barrier affects the impact and deposition mechanism of a debris flow is briefly studied. The blocked area of the flexible barrier by the deposited debris from the previous test is regarded as the initial condition of the next test.

6.2.1 Initial conditions of the flexible barrier in multiple debris flow tests

The initial conditions of the flexible barrier before Debris Test 1, 2 and 3 are plotted by photographs in Figure 6-2. Based on those photographs, the flexible barrier was empty before Debris Test 1, and the initial block areas in Debris Test 2 and 3 were measured before each test as A_{block}. The initial condition of the flexible barrier in each test is abstracted to a defined parameter named Initial Block Ratio (IBR):

$$IBR = \frac{A_{block}}{A_{impact}} \tag{6-1}$$

where A_{impact} is the effective impact area of the debris flow, which equals to the cross-sectional area with the flume width multiplied by the flexible barrier height. The initial

Block Rates of Debris Test 1, Debris Test 2 and Debris Test 3 are 0, 0.44 and 0.78 as presented in Figure 6-3.

6.2.2 Impact force estimation and analysis

The maximum impact force and the impact force history on the supporting structures in Debris Test 1, 2 and 3 are calculated from the tensile forces on the strand cables using Eq.(3-10). The accumulated impact forces on the supporting structures in the three tests are combined in Figure 6-4. From the force history, it can be found that the impact forces in the three tests have different impact characteristics. To be more specific, a dynamic impact peak occurred at the beginning of the impact in Debris Test 1, followed by a stable static loading. Both the dynamic impact loading and the static earth pressure were relatively low compared to the other two tests. In Debris Test 2, the impact loading increased gradually during the impact and kept stable afterward, which indicates that the static earth pressure due to the accumulation of the debris deposition was dominant in the test. In Debris Test 3, an instant impact peak, a consecutive impact loading lasting 1.5 s and a stable static earth pressure coexisted during the impact. The magnitude of the impact force in Debris Test 3 is the largest among the series of tests.

6.2.3 Test results of multiple debris flow tests with different initial IBRs

Results of Debris Test 1 with IBR of 0

To clarify the impact process revealed by photographs, the starting time of impact in each test is set to 0 second, while the negative values indicate the times before impact. The flexible barrier before Debris Test 1 is empty. Thus, the IBR value in this test is 0. The impact process of Debris Test 1 is plotted in Figure 6-5 (side-view) and Figure 6-6 (front-view) with photographs by high-speed cameras. It can be observed that a certain percentage of small particles and slurry passed through the flexible barrier with a residual velocity. In fact, only 10% of the debris material was trapped by the flexible barrier in this test. The low trapping rate may be attributed to the high water content (89.4%) of the debris flow in Debris Test 1 compared to the debris flow in Debris Test 4 (61.1%) and the large difference between the diameter of the mesh net (50mm) and the d_{90} of the debris material (25mm) (Wendeler and Volkwein 2015).

Results of Debris Test 2 with IBR of 0.44

From Figure 6-2(b), the mesh net before Debris Test 2 was partially blocked by the trapped debris material in Debris Test 1 with the Initial Block Rate (IBR) value of 0.44. The impact process in Debris Test 2 is plotted in Figure 6-7 by the high-speed photographs (due to the delayed triggering of the high-speed cameras in this test, the beginning of the impact was not recorded, thus the recording time of the high-speed cameras started at the time of 0.78 s). It can be observed that a certain percentage of the debris material was trapped by the flexible barrier during the interaction. At the end of the test, the deposited debris material filled the flexible barrier as a wedge with the deposition height nearly equaling to the height of the deformed flexible barrier. From the measurement of the retained debris material volume after the test, 45% of the debris material was trapped by the flexible barrier with 44% of the mesh opening blocked. Interestingly, the impact force history in Debris Test 2 (see Figure 6-4) is similar to the impact force history in Granular Test 1 (Figure 5-8). In analogy with the impact mechanism in Granular Test 1, it is deduced that the impact force in Debris Test 2 mainly came from the static earth pressure of the gradually incremented debris flow deposition. The maximum impact loading in Debris Test 2 is much larger than that in Debris Test 1 even both tests have similar total volumes of the testing materials and the impact velocities. Therefore, it can be concluded that the IBR value of the flexible barrier can affect the impact and deposition mechanisms of debris flows.

Results of Debris Test 3 with IBR of 0.78

It can be observed from Figure 6-2(c) that the flexible barrier was almost filled by the debris deposition wedge in Debris Test 2, and the mesh net in the impact area was almost fully blocked. In Debris Test 3, the debris flow shot up via the top surface of the deposition wedge and overflew the flexible barrier at the beginning of the impact instead of passing through the net (Debris Test 1) or being trapped by the net (Debris Test 2). From the force history in Debris Test 3 (see Figure 6-4), three force components are identified in the overflow process: an instant impact loading, an impact thrust lasting almost 1.5 s, and a long-term static loading. It should be noted that the instant impact loading is observed at the beginning of the impact, which is the largest impact loading among the three tests. Some researchers regarded the loading situation in the overflow scenario as a combination of the drag force from the overflowing debris flow and the static earth pressure of the debris deposition (Kwan and Cheung 2012; Volkwein 2014). Wendeler et al. (2018) neglected the drag force and added the earth pressure from the overflowing debris flow into the loading combination. From the photographs plotted in Figs.6-8 and 6-9, it can be observed that the moving direction of the debris flow was changed during the shooting up, which can lead to a dynamic impact on the flexible barrier. Thus, it is deduced that the instant impact loading comes from the direction change of the debris flow, the impact thrust lasting 1.5 s is originated from the drag force between the overflowing debris flow and the debris deposition, and the static loading is attributed to the earth pressure of the debris deposition.

6.2.4 The influence of initial conditions on impact and deposition mechanism

A series of three continuous tests were conducted to investigate the interaction mechanism between a flexible barrier and multiple debris flows. For the initial condition of Debris Test 1, the flexible barrier before impact is empty and permeable (IBR=0). Under this initial condition, obvious passing-through of debris flow and a large deformation of the flexible barrier were observed during the impact process. In fact, only 10% of the debris material was trapped by the flexible barrier, which obviously reduced the dynamic impact loading and the static earth pressure from the debris flow. Due to undamaged flexibility and permeability of the flexible barrier with IBR=0, the dynamic impact loading and the static earth pressure on the flexible barrier were relatively low. For the initial condition of Debris Test 2 (IBR=0.44), nearly half of the mesh net in the impact area was blocked by the trapped debris in Debris Test 1. Therefore, no obvious passing-through of the debris flow was observed in Debris Test 2, and 44% of the debris material was deposited behind the flexible barrier. The difference of debris trapping rates in Debris Test 1 (10%) and Debris Test 2 (44%) indicates that the initial block rate of a flexible barrier can obviously affect the deposition mechanism of a debris flow. The flexible barrier before Debris Test 3 was almost filled by the deposition of the debris flows in Debris Test 1 and Debris Test 2 with IBR=0.78. Under this initial condition, the debris flow in Debris Test 3 climbed up the deposition wedge and overflew the flexible barrier. From the impact force history of the flexible barrier in the three continuous tests (see Figure 6-4), it can be observed that the maximum impact loading in Debris Test 3 is the largest among 3 tests because the flexibility and the permeability of the flexible barrier were seriously jeopardized by the previous debris flows.

6.3 Single debris flow impact test with overflow (Debris Test 4)

In Debris Test 4, a debris flow with similar debris material and a similar volume to the debris flows in the previous tests was initiated. A shorter flexible barrier with a lower retaining capacity was utilized in the test to make sure it can be overflowed by a single debris flow in a short period. The impact process in Debris Test 4 is plotted in Figure 6-10 (side-view) and Figure 6-11 (front-view) by the photographs of high-speed cameras. From those photographs, the debris flow firstly escaped from the bottom gap between the flexible barrier and the flume base due to the thin flow depth. Afterward, a thick debris front impacted on and blocked the flexible barrier. Because of the blockage, the flexible barrier was filled by the following debris flow in less than 0.2 s. Afterward, the debris flow overflowed the flexible barrier via the top surface of the debris deposition wedge.

To better understand the impact loading distribution on the flexible ring net, thirteen mini tension link transducers were installed on the shorter flexible barrier. The arrangement of the transducers is plotted in Figure 6-12(a). Transducers 1 to 8 were used to measure the impact loading on the central area of the flexible ring net. Transducers 9 to 12 were installed on the right side of the flexible barrier to measure the impact loading on the side area of the flexible ring net. Transducer 13 was installed on the cross-tension cable of the flexible ring net to measure the tensile force on it. The cross-tension cable was used to stretch the ring net and transfer the impact loading on the ring net to the supporting structures. The equivalent impact force on the supporting structures was calculated from the tensile forces on the supporting strand cables using Eq.(3-10).

The tensile force histories of all mini tension link transducers in Debris Test 4 are presented in Figure 6-12(b). Dynamic impact forces are observed in the signals of Transducers 1 to 8 with the peak loadings ranging from 2.4 kN to 3.64 kN. As a contrast, the tensile forces on Transducers 9 to 12 are much smaller than the forces on the transducers installed in the central area. For the force history of Transducer 13, which represents the tensile force on the cross-tension cable, two dynamic impacts with similar peak values around 6 kN are observed. The static loading after impact is similar to the dynamic impact loading with the value of 5.5 kN. The peak loadings of all the mini tension link transducers are plotted in Figure 6-12(c). From the figure, it can be observed that the maximum impact force on the central area is much larger than the value on the side area instead of uniform distribution on the flexible ring net, which fits well with the back-calculation by Wendeler et al. (2018). Based on the force histories of the mini tension link transducers, the tensile force distribution on the flexible barrier at typical times are plotted by the contours in Figure 6-13(a). The selection of the time points is based on the force history of Transducer 13 (see Figure 6-13(b)). From those contours, it can be observed that the debris flow firstly impacted on the bottom central area of the flexible barrier at the time of 0.255 s. After that, the dynamic impact on the flexible barrier moved up with the accumulation of the debris deposition. Finally, the second impact and the static loading of the debris deposition mainly acted on the upper central area of the flexible barrier. The impact force history on the supporting structures in Debris Test 4 is plotted in Figure 6-14. Two dynamic impacts are observed in the force history. The first impact peak occurs at 0.30 s with the value of 7.07 kN. After two dynamic impacts, around 4 kN of the static loading from the debris deposition acts on the flexible barrier.

6.4 Summary

Four large-scale debris flow impact tests were performed to study the interactions of multiple debris flows with a flexible barrier (Debris Test 1, 2 and 3) and the interaction of a single debris flow with a shorter flexible barrier (Debris Test 4). Based on the presented test results, the impact and deposition mechanisms of the debris flows in those tests are investigated in this chapter.

Since the debris materials, the debris volumes, and the flowing path of the debris flows in Debris Tests 1, 2 and 3 are similar (see Table 6-1 and Figure 6-1), the influence of the initial conditions of the flexible barrier on the impact mechanisms is preliminarily investigated. A value named IBR (Initial Block Rate) is identified to represent the proportion of the blocked area in the total impact area. The tensile forces on the supporting structures and the deposition processes of the debris flows are presented and compared. For the flexible barriers with different IBRs, the impact and deposition mechanisms of the debris flows are totally different. In Debris Test 4, thirteen mini tension link transducers were installed on the flexible barrier to investigate the impact force distribution on the flexible ring net in the impact process. From the experimental data and their analysis, key findings and conclusions are summarized and presented as below:

(a) With the increase of the Initial Block Rate, the retaining rate of the debris material increased correspondingly. In this study, the retaining rate increased from 10% in Debris Test 1 (IBR=0) to 44% in Debris Test 2 (IBR=0.44).

(b) Before Debris Test 1, the flexible barrier was empty. The dynamic impact force acting on the flexible barrier was much smaller than the dynamic impacts in Debris Test 2 and 3 due to passing-through of the debris material.

(c) Before Debris Test 2, the flexible barrier was partially blocked by the debris deposition in Debris Test 1. The permeability of the flexible barrier was jeopardized. Therefore, a large percentage of debris material was deposited behind the flexible barrier in Debris Test 2. The impact force in this test gradually increased with the increment of the debris deposition.

(d) Before Debris Test 3, the flexible barrier was almost filled by the debris deposition in the previous tests. Thus, most of the debris material overflowed the flexible barrier *via* the top surface of the deposition wedge during the interaction. The drag force from the overflowing debris flow, the impact force from the debris flow direction change, and the static earth pressure from the debris deposition are three force components during the overflow process.

(e) In Debris Test 4, a debris flow impacted, filled and overflowed a flexible barrier in less than 1 s. The impact force distribution on the flexible ring net during the impact process is presented by visualized contours. From those contours, the impact force on the central area of the flexible barrier was much larger than the force on the side area. Moreover, the debris flow firstly impacted on the central bottom area of the flexible barrier, then the major impact area rose up with the deposition of the debris material.

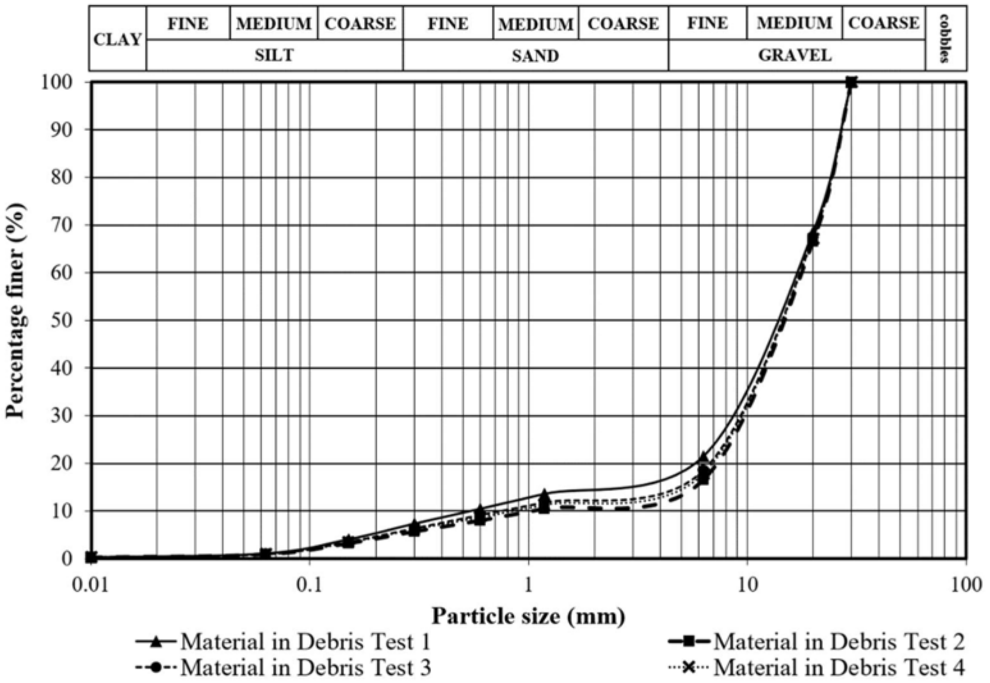

Figure 6-1. PSD curves of Materials in Debris Tests 1, 2, 3, and 4

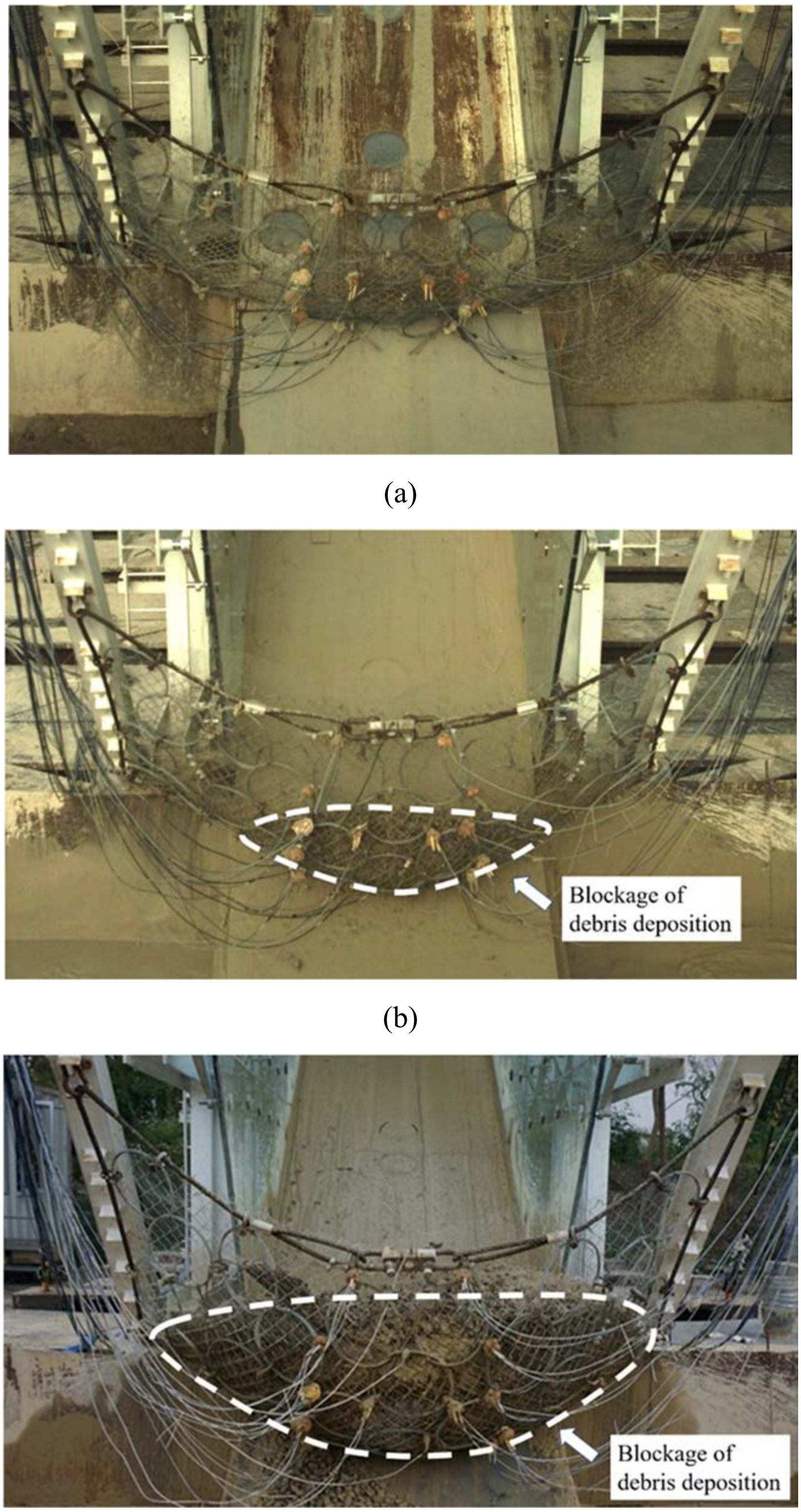

(a)

(b)

(c)

Figure 6-2. Initial conditions of the flexible barrier in (a) Debris Test 1, (b) Debris Test 2, and (c) Debris Test 3

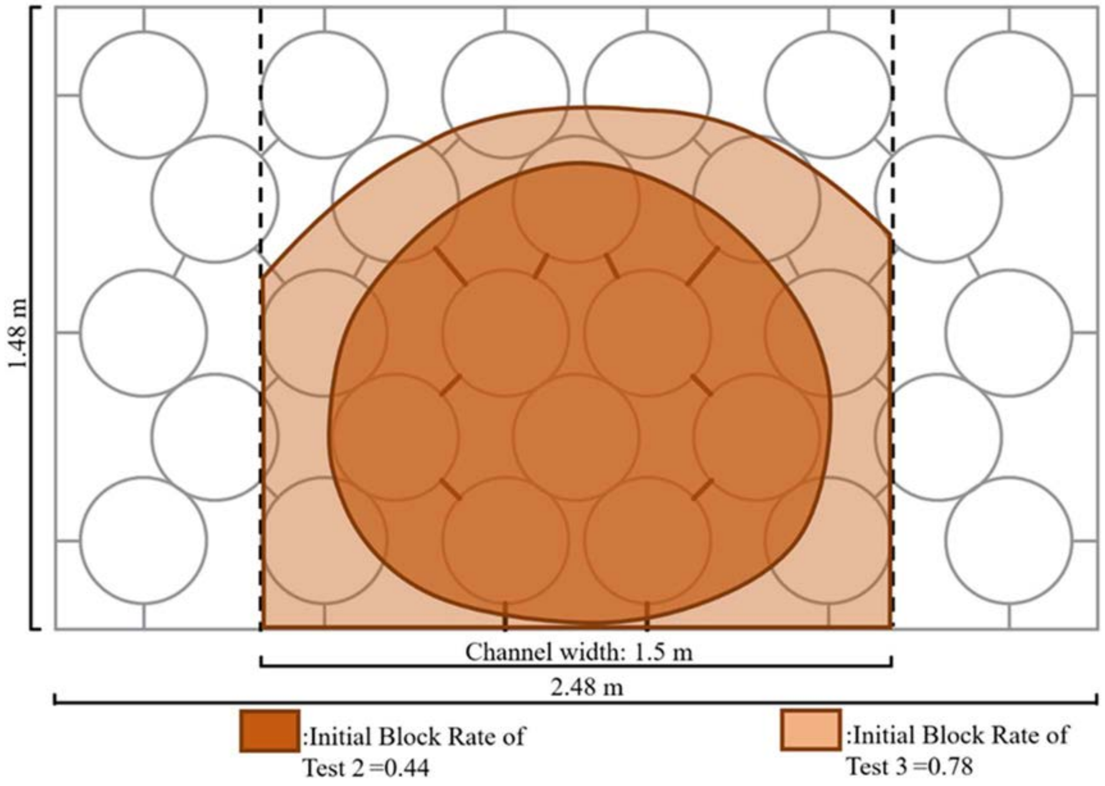

Figure 6-3. Initial blocked areas and the IBRs of Debris Test 2 and Debris Test 3

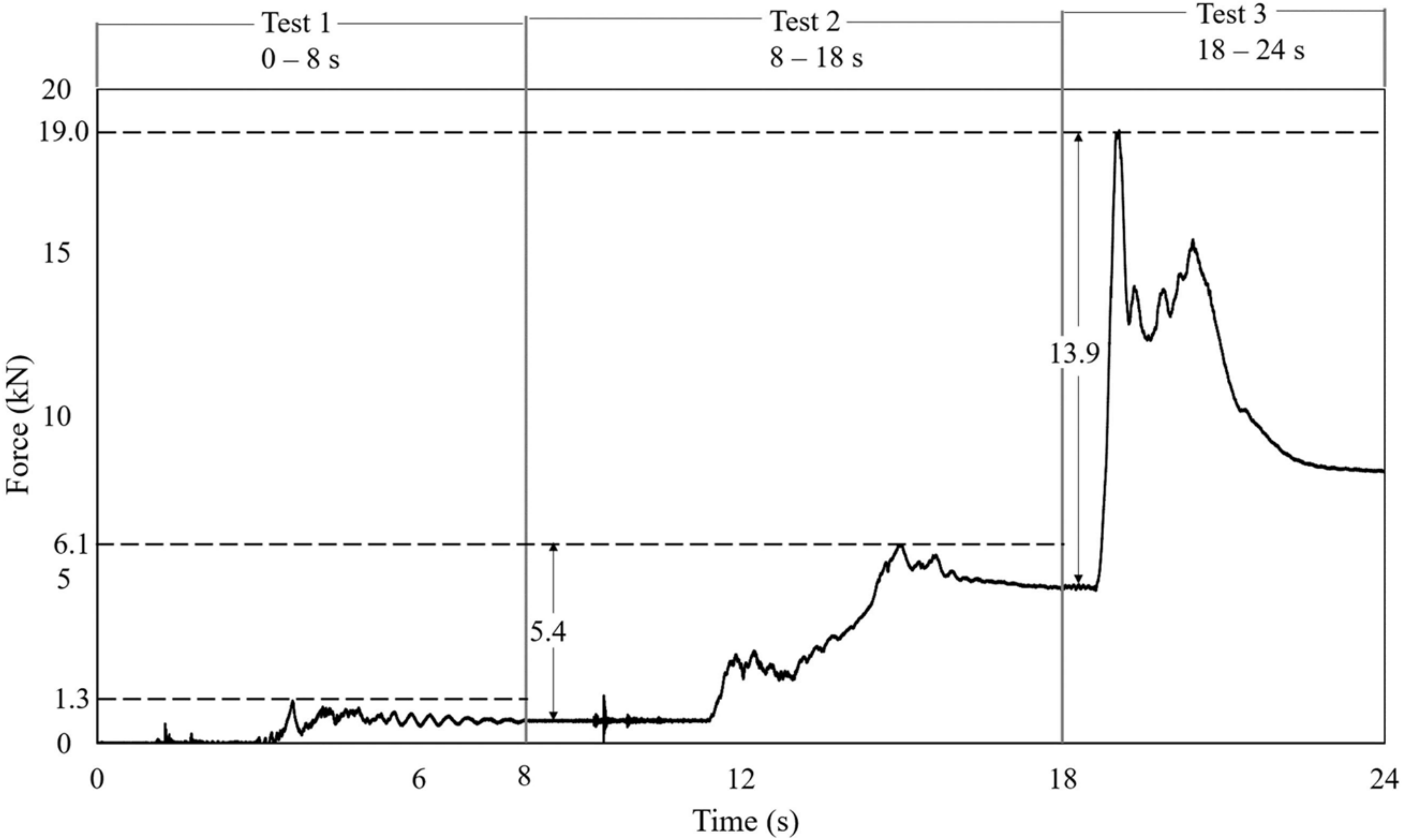

Figure 6-4. Combined impact force history on the supporting structures in Debris Test 1, 2, and 3

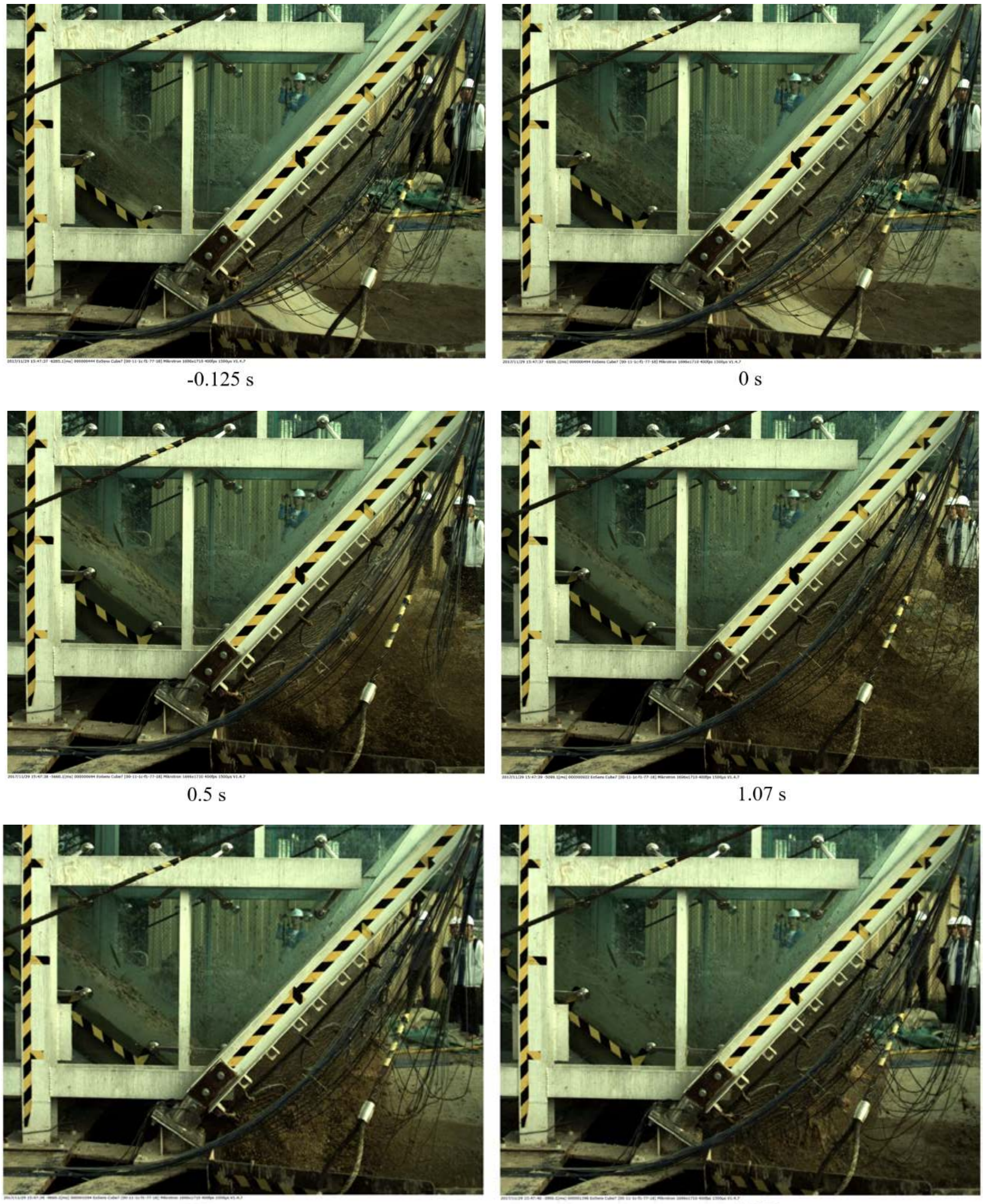

-0.125 s

0 s

0.5 s

1.07 s

1.5 s

2.26 s

Figure 6-5. Side-view photographs of the impact process in Debris Test 1 with IBR=0

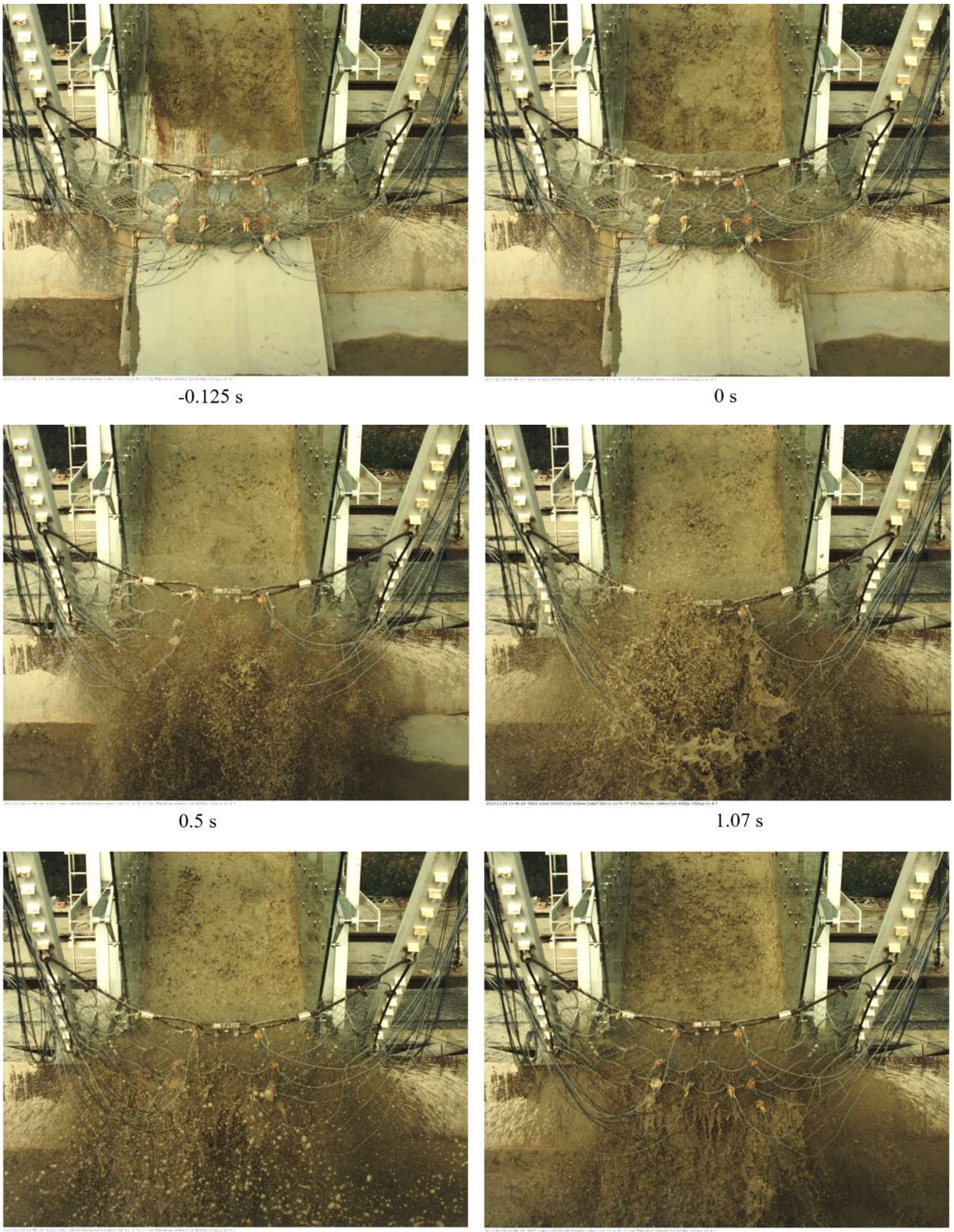

-0.125 s

0 s

0.5 s

1.07 s

1.5 s

2.26 s

Figure 6-6. Front-view photographs of the impact process in Debris Test 1 with IBR=0

0.78 s 1.78 s

(a)

0.78 s 1.78 s

(b)

Figure 6-7. (a) Side-view and (b) front view photographs of the impact process in Debris Test 2 with IBR=0.44

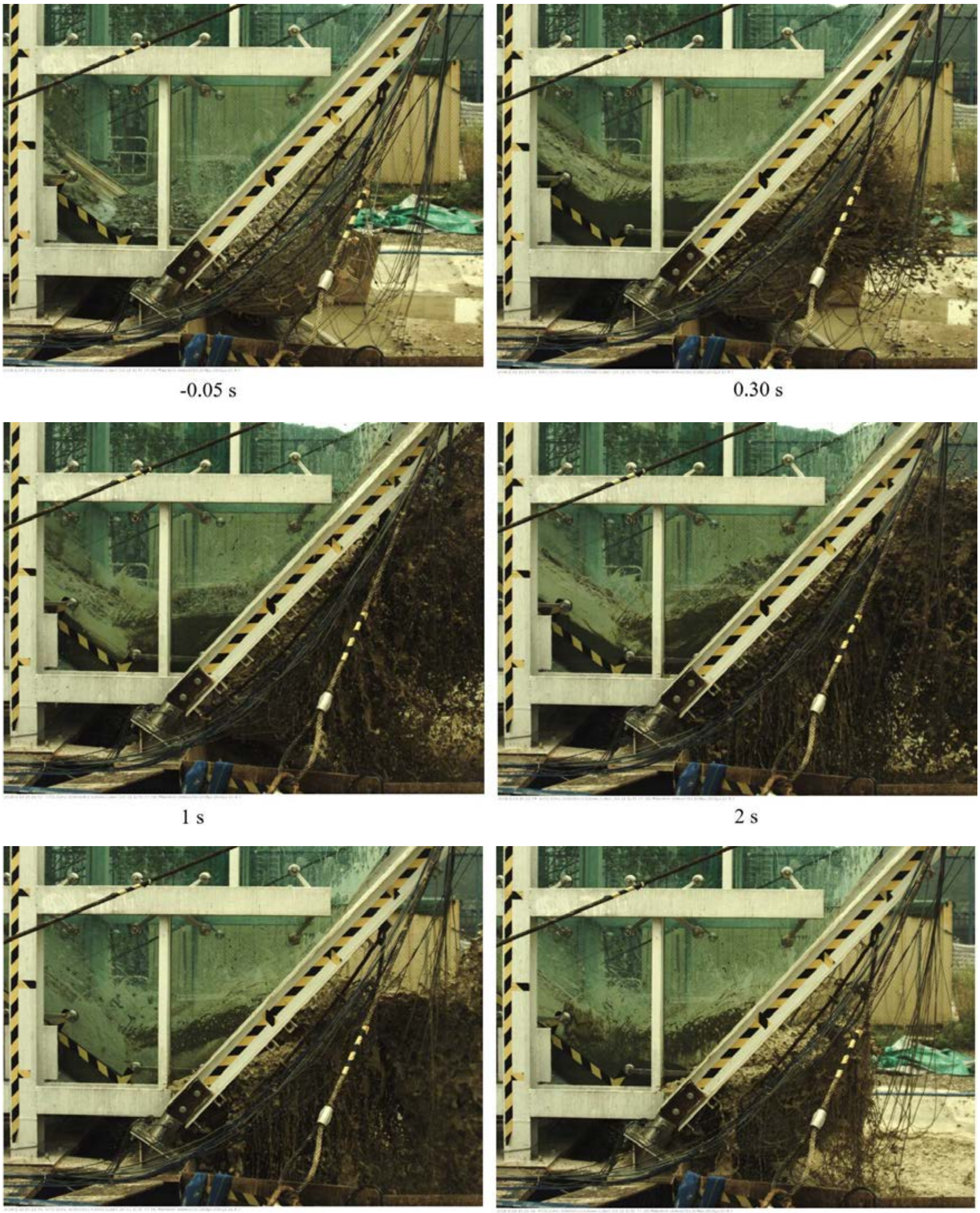

-0.05 s

0.30 s

1 s

2 s

3 s

4 s

Figure 6-8. Side-view photographs of the impact process in Debris Test 3 with IBR=0.78

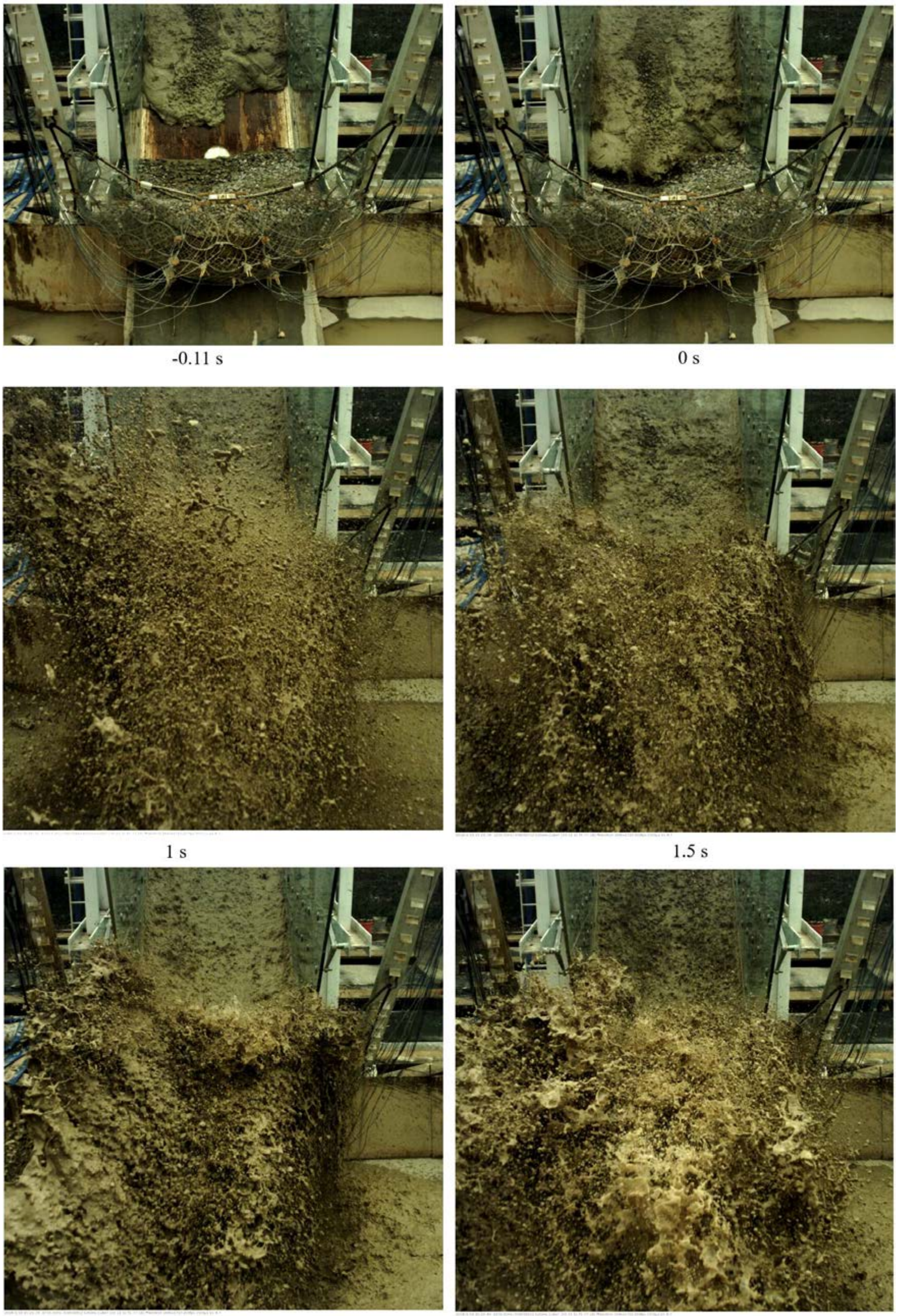

-0.11 s

0 s

1 s

1.5 s

2 s

2.5 s

Figure 6-9. Front-view photographs of the impact process in Debris Test 3 with IBR=0.78

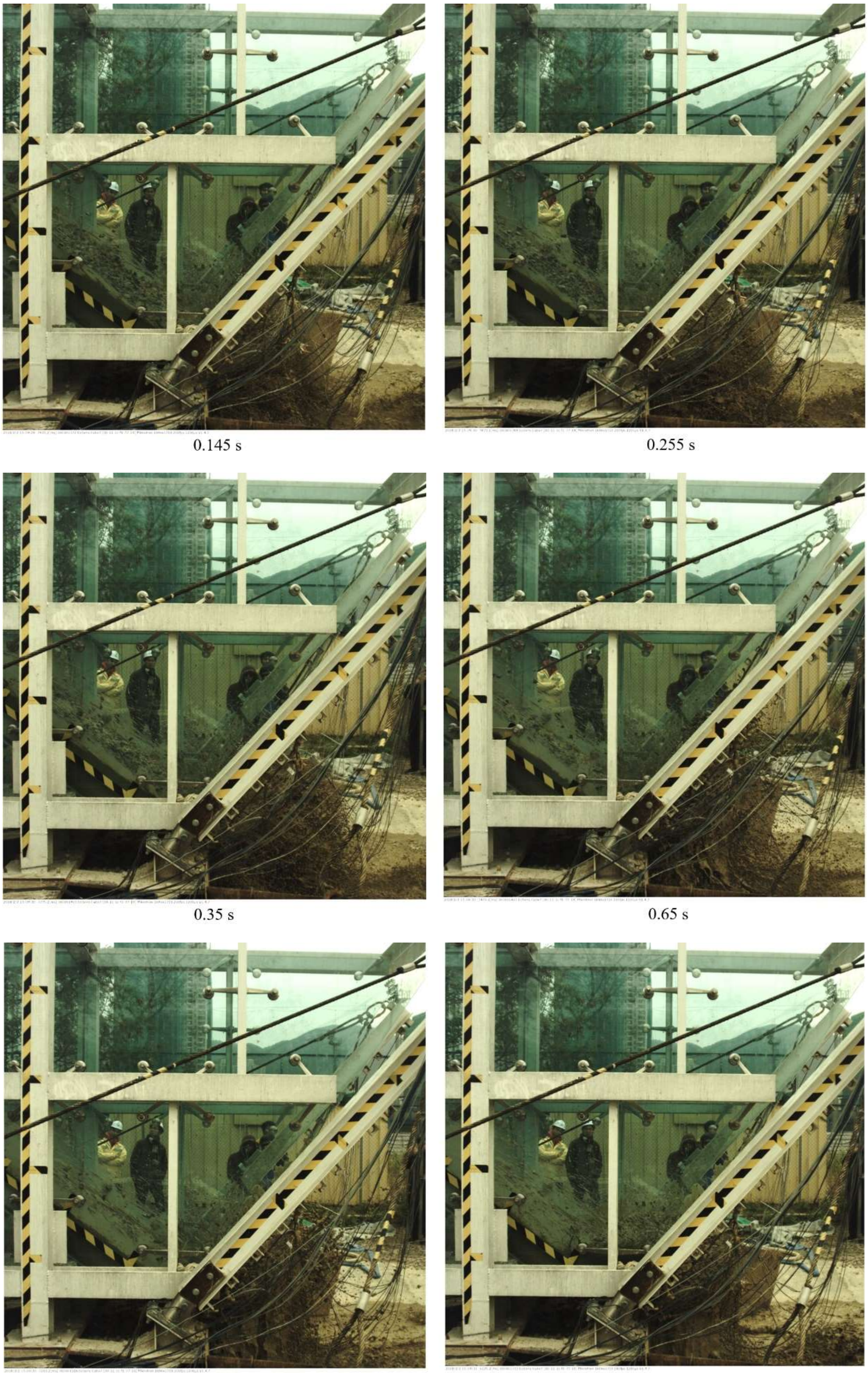

0.145 s

0.255 s

0.35 s

0.65 s

0.915 s

2 s

Figure 6-10. Side-view photographs of the impact process in Debris Test 4

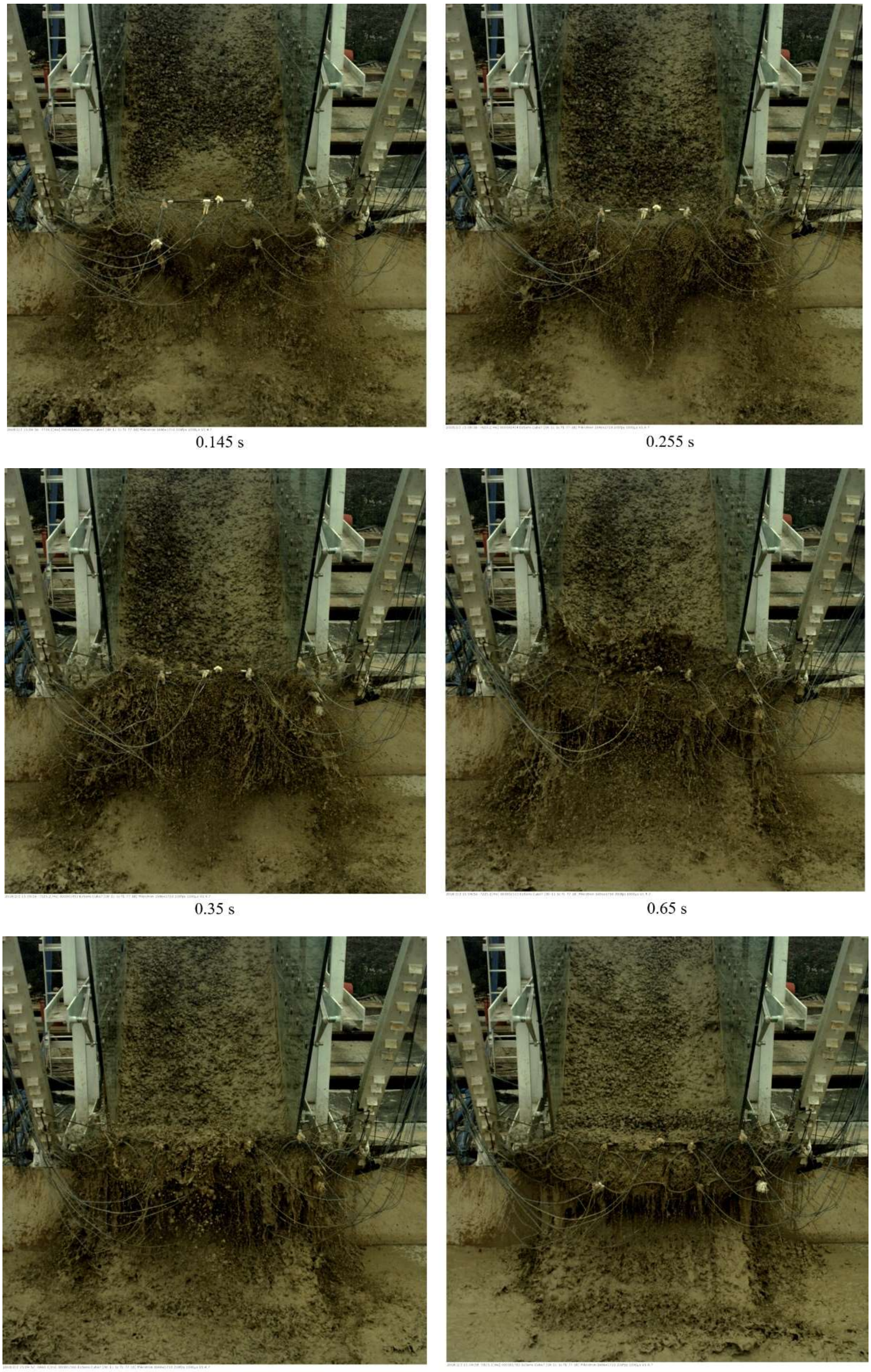

0.145 s

0.255 s

0.35 s

0.65 s

0.915 s

2 s

Figure 6-11. Front-view photographs of the impact process in Debris Test 4

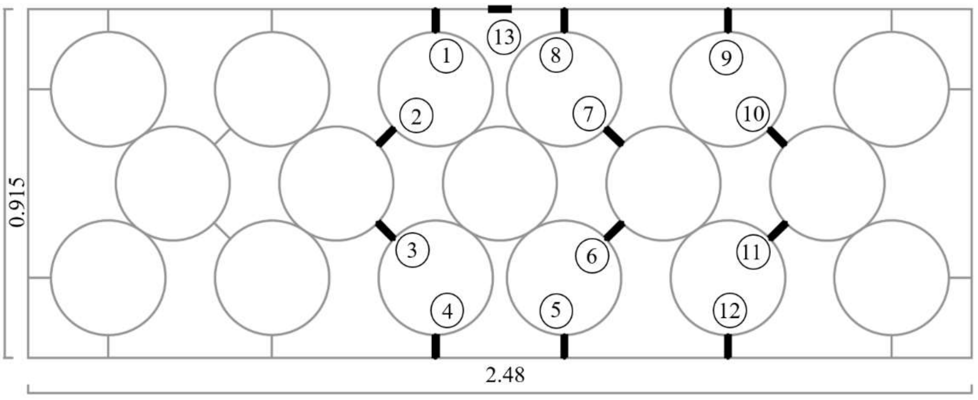
13
1
8
9
2
7
10
3
6
11
4
5
12
0.915
2.48

(a)

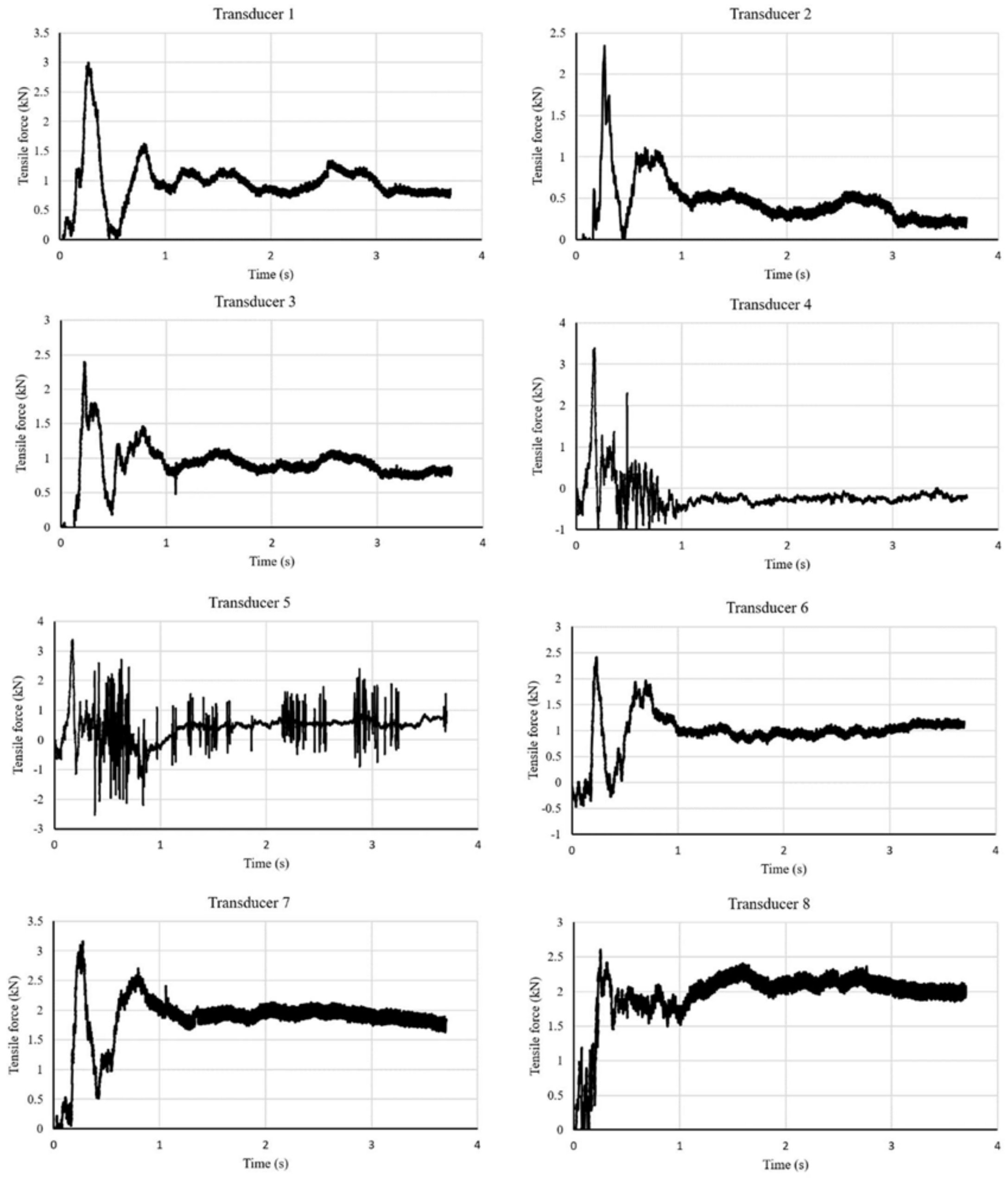
Transducer 1
Transducer 2
Transducer 3
Transducer 4
Transducer 5
Transducer 6
Transducer 7
Transducer 8
Tensile force (kN)
Time (s)
0
1
2
3
4
-3
-2
-1
0.5
1.5
2.5
3.5
-0.5

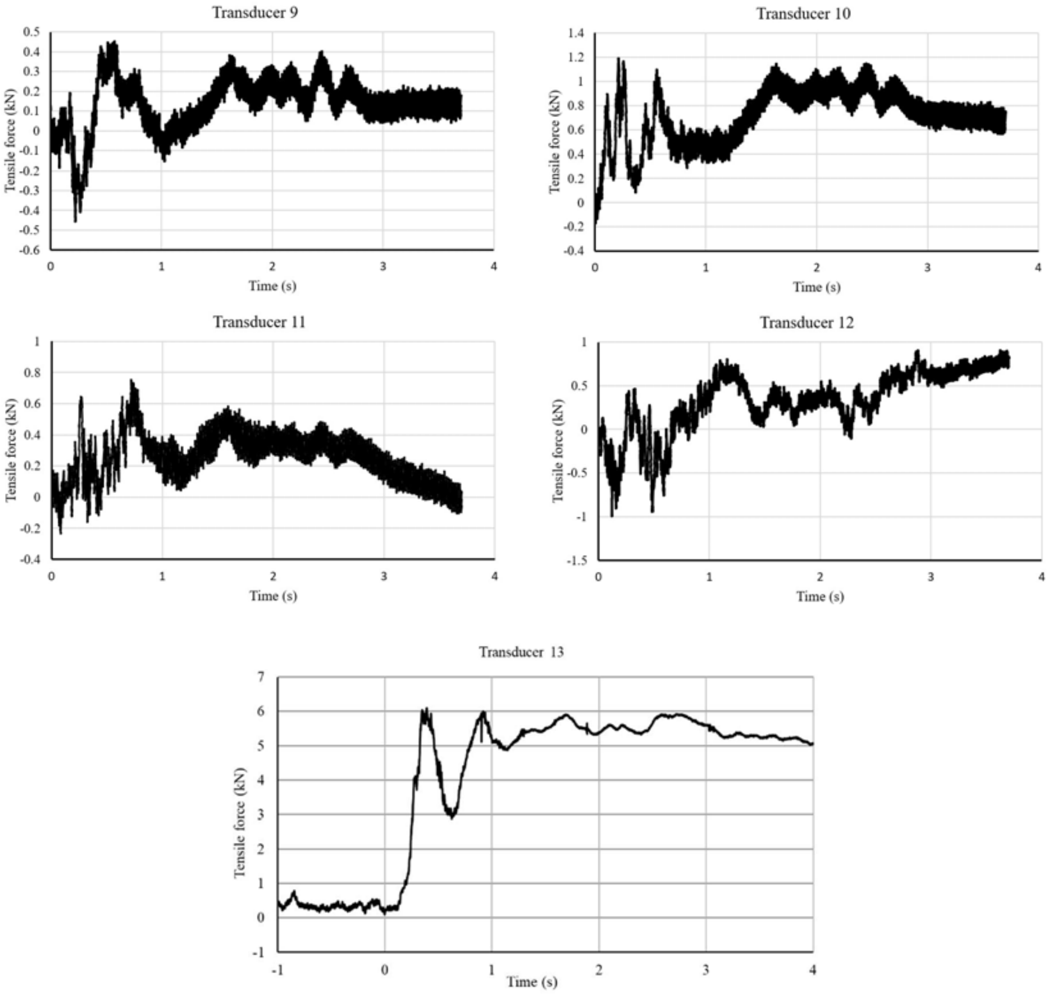

(b)

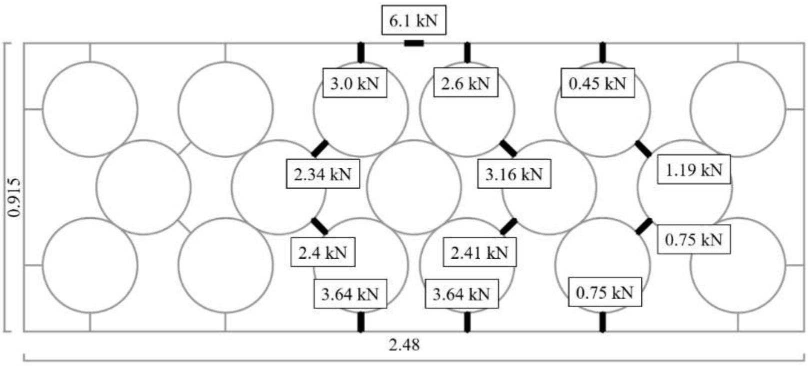

(c)

Figure 6-12. (a) Arrangement of the mini transducers on the flexible barrier in Debris Test 4 (unit: *m*), (b) Tensile force histories of the mini tension link transducers in Debris Test 4, and (c) peak tensile forces of all the mini tension link transducers on the flexible barrier

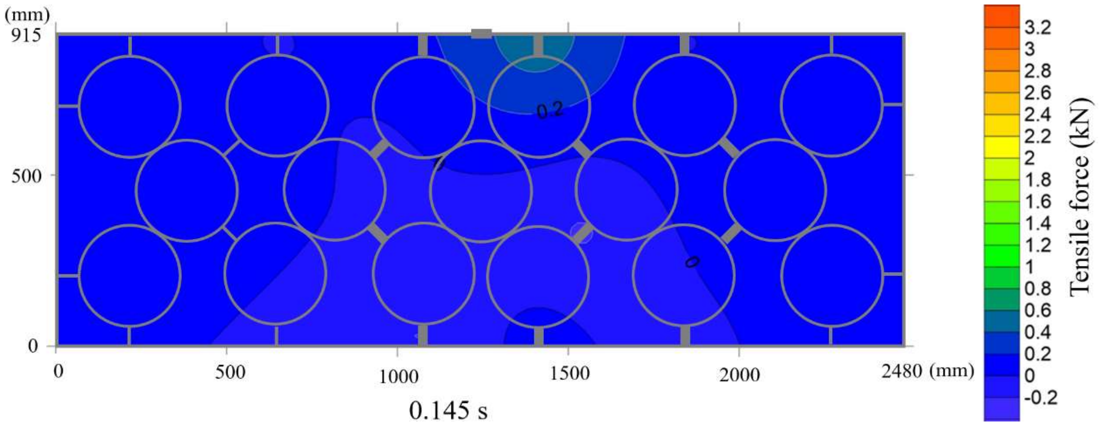

0.145 s

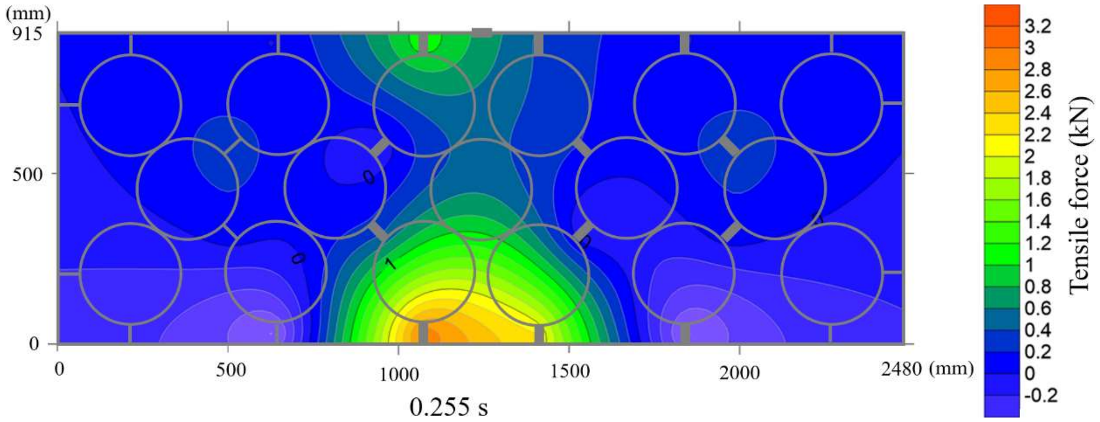

0.255 s

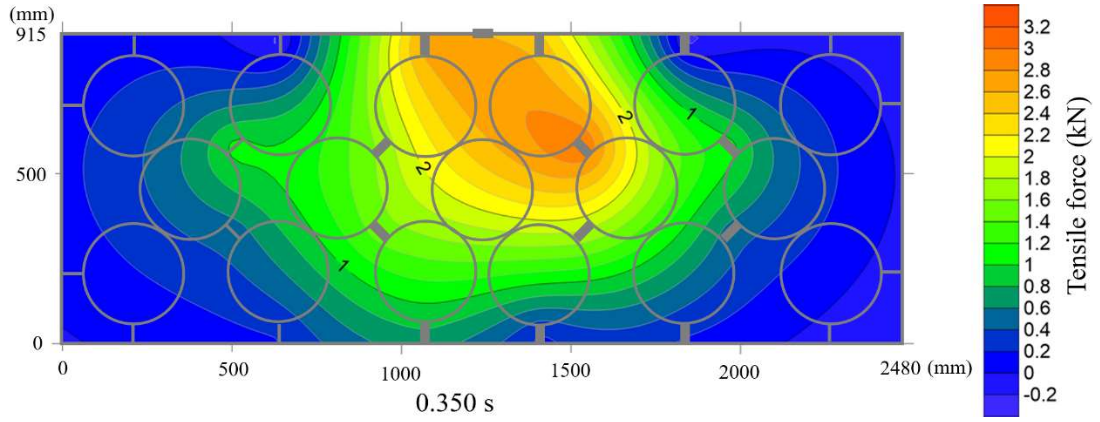

0.350 s

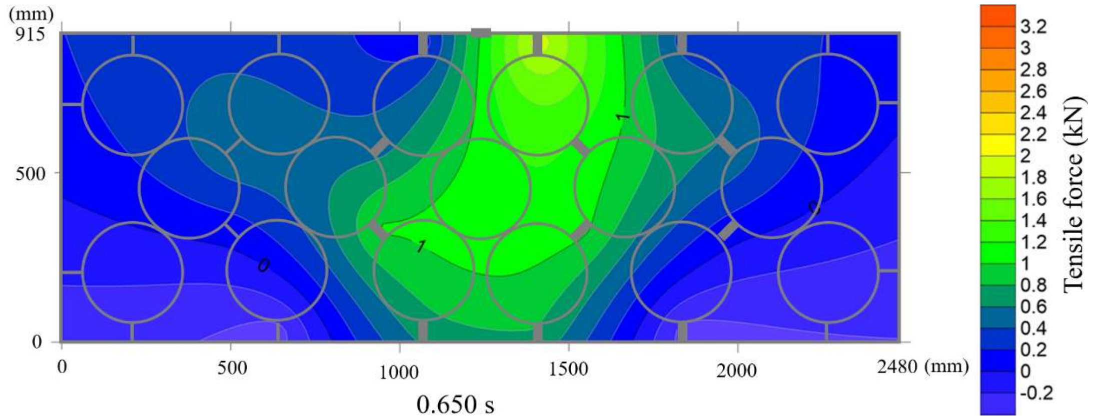

0.650 s

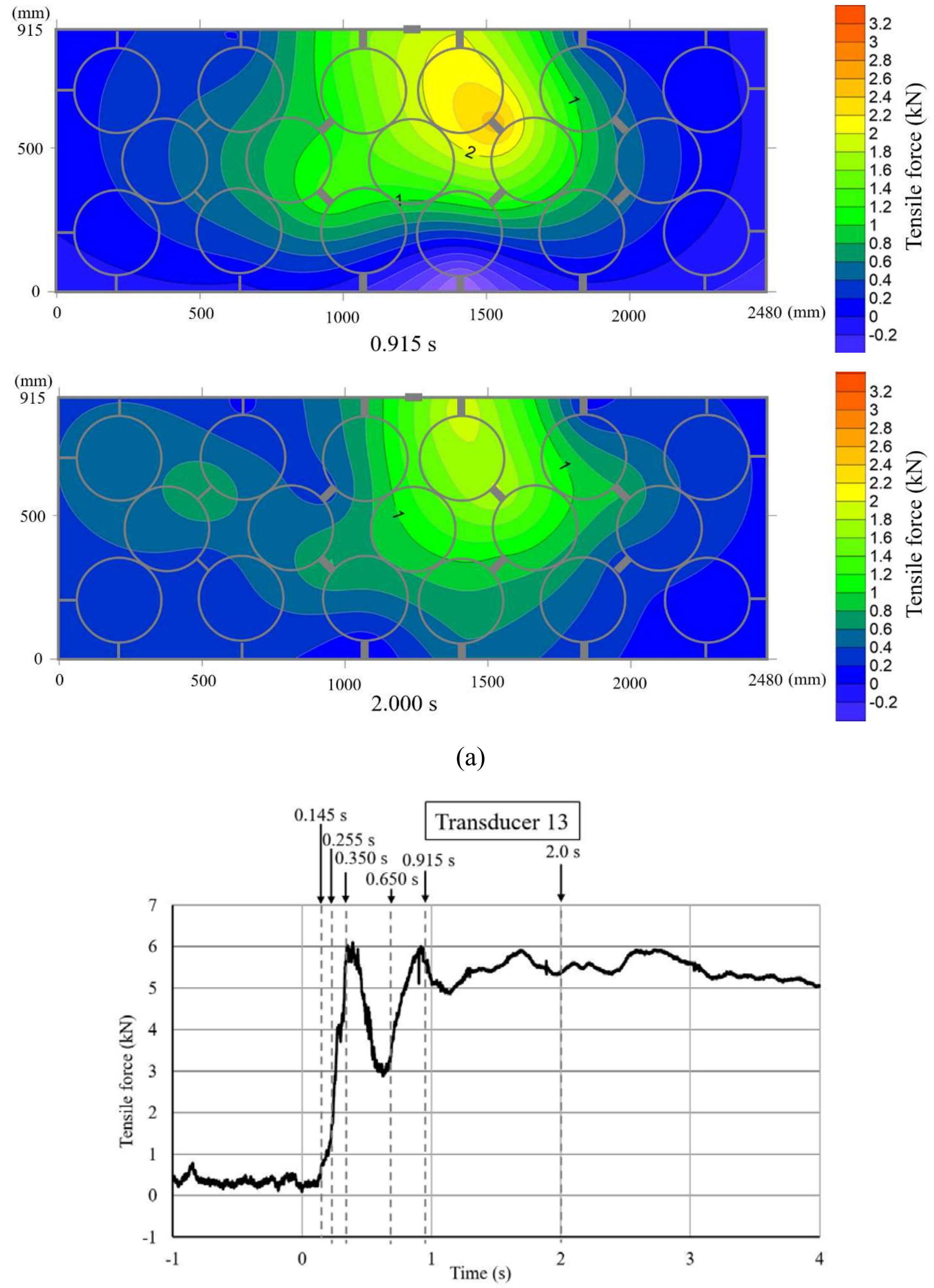

(a)

(b)

Figure 6-13. (a) Distributions of the tensile forces on the flexible barrier at typical time points and (b) the selected time points in the force history of Transducer 13

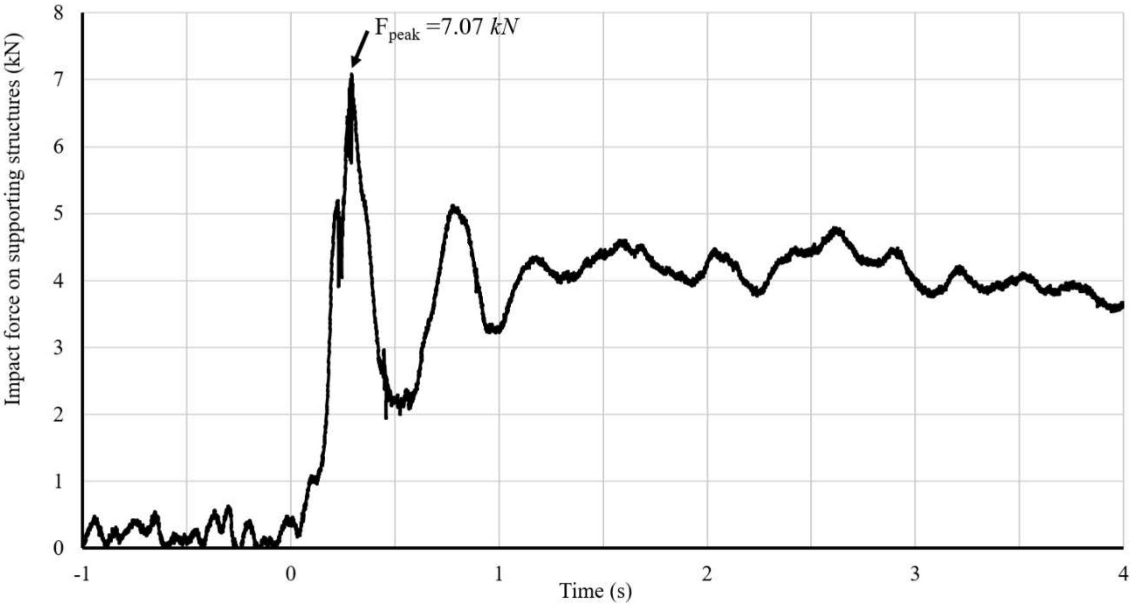

Figure 6-14. Impact force on the supporting structures in Debris Test 4

Table 6-1. Parameters and the measured values of debris flow tests (Debris Tests 1, 2, 3, and 4)

Test type	**Multiple debris flow impact tests with overflow**			**Single debris flow impact test with overflow**
Test Name	Debris Test 1	Debris Test 2	Debris Test 3	Debris Test 4
Designed barrier height (m)	1.48	1.48	1.48	0.92
Bulk density (kg/m^3)	1604	1811	1708	1739
Water content (%)	89.4	50.5	67	61.1
Total volume of debris flow mixture $V_{mixture}$ (m^3)	2.00	2.30	2.28	2.05
Retained volume of debris flow mixture V_d (m^3)	0.2	1.0	N/A (Overflowed)	0.64
the retaining rate (ϕ_d)	0.1	0.45	N/A	0.31
Initial Block Rate (IBR)	0	0.44	0.78	0
Velocity before impact v_0 (m/s)	6.7	6.5	6.1	5.8
Velocity after impact $v_{1,s}$ (m/s)	3.1	3.8	3.1	2.6
Velocity Loss Ratio, δ (%)	53.7	41.5	49.2	55.2
Flow depth h (m)	0.1	0.1	0.2	0.17
$Fr = \frac{v_0}{\sqrt{gh}}$	6.76	6.56	4.35	4.49
Equivalent maximum impact force on supporting structures (kN)	1.3	6.1	18.7	7.1

CHAPTER 7: A NEW SIMPLE METHOD FOR CALCULATING IMPACT FORCE ON FLEXIBLE BARRIER CONSIDERING PARTIAL DEBRIS FLOW PASSING-THROUGH

7.1 Introduction

Flexible barriers trap large particles and boulders in a debris flow but allow slurry and small particles to pass through. It is observed from field tests and real cases that a certain amount of slurry and small particles in a debris flow passes through a flexible barrier with residual velocities. In the design of flexible barriers for debris flow mitigation, accurate determination of the impact force is the key issue. Simple methods have been widely utilized by engineers because they can easily calculate the impact force on the mitigation structure with a few basic parameters and several assumptions. However, the assumptions in the simple methods may oversimplify the impact process and miss some significant interaction characteristics such as the passing-through of debris flow. Without considering the passing-through, the impact loading can be overestimated tremendously. Nevertheless, few of current simple methods have quantified the effect of passing-through on the impact force reduction. In this study, a new simple method considering the passing-through of slurry is proposed based on a two-phase flow model. This method is verified by the measured impact forces of two large-scale physical modeling tests. In the tests, debris flows with different water contents (89.4% and 61.1%) were initiated to impact a flexible barrier. The volume of the retained debris and the velocity loss of the passed slurry in the two tests are measured rigorously. This proposed simple method is further validated by the data from well-documented laboratory tests in the literature. From the comparisons and validations, it is concluded that the proposed simple method provides an accurate and creative way to predict the impact forces of debris flows on flexible barriers.

The passing-through of slurry has been observed in large-scale tests. Generally, a flexible barrier for debris flow mitigation normally consists of two layers of net: a high-strength primary net to sustain major impact loadings and intercept boulders similar to or larger than the mesh diameter (300 mm in our study) and a secondary wire mesh net to trap smaller particles and debris. The mesh net accelerates dewatering of the debris deposition and allows slurry and small particles in a debris flow to pass through (Volkwein 2014; Wendeler et al. 2018). DeNatale et al. (1999) observed a diffuse spray of debris material through the net in the first wave of the debris flow during impact, and some of the sprayed gravel travelled more than 3 m after passing the net. In the video records of field tests presented by Geobrugg AG (2012), it can also be observed that a certain amount of slurry and small particles can pass through the flexible barrier with residual velocities (see Figure 7-1). Wendeler and Volkwein (2015) conducted a series of laboratory tests to study the relationship between the mesh size of a flexible barrier and the retaining rate of debris material. In the tests, a certain volume percentage (40% ~ 50%) of small particles and slurry can pass through the net. Li and Zhao (2018) studied the interaction of a debris flow with a permeable flexible barrier with numerical simulations. In the numerical model, a debris flow was simulated using a mixture of particles modelled by the discrete element method (DEM) and fluid modelled by the computational fluid dynamics (CFD). A flexible mesh net was also simulated using bonded particles by DEM. The interactions among the particles, the fluid and the flexible net were achieved by a coupled CFD-DEM approach. In this model, the impact on the flexible barrier consists of the collision of the particles and the drag force of the passing fluid. This study investigated the relationship between the retained mass of the debris flow and the impact loading on the flexible barrier. The simulation results indicated that the impact loading on the flexible barrier increased with the increment of the retaining rate for debris flows with high water contents (solid fraction < 55%). However, the loading reduction due to fluid passing-through was not quantified in the literature, and the practical flexible protection system for debris flow mitigation was not simulated in the numerical model. Therefore, a deeper understanding of debris flow passing-through is required, and its influence on impact loading reduction should be quantified and integrated in the calculation of the impact force.

Considering the significance of debris flow passing-through in the impact with a flexible barrier, the passing-through effect should be quantified and integrated in the calculation of the impact force. Wendeler (2008) simply reduced the dynamic coefficient in the hydro-dynamic method for muddy debris flows with low densities (<1900 kg/m^3) considering the passing-through of small particles and water. However, the reduced constant empirical coefficient relying on calibration and cannot quantify the influence of various densities and different passing-through characteristics in different debris flow impact cases. Therefore, a developed simple method for impact force calculation is required to quantify the passing-through of slurry.

This chapter aims to clarify the impact and passing-through mechanism of a muddy debris flow on a flexible barrier and derive a new simple method to calculate the maximum impact force taking account of slurry passing-through. The passing-through of slurry and small particles has been investigated by two large-scale physical modeling tests with different water contents. Key parameters of passing-through: the retaining volume and velocity loss of the passed debris flow in the two tests are measured. The impact forces on the flexible ring nets in the two tests are directly measured and used to verify this method. Besides, the data from the laboratory tests presented in the literature are used to further validate this simple method.

7.2 A new simple method considering slurry passing-through

In this section, a new simple method for calculating the impact force of a debris flow on a flexible barrier is derived. Based on the grain size data of real cases, a debris flow can contain grains ranging from clay to boulders (King 2013; Iverson 1997). The single-phase flow model, which has been widely applied in debris flow research in the past few decades (Bagnold 1954; Chen 1988; O'Brien et al. 1993; Takahashi 2014), is not suitable to describe the interaction between particles and fluid and their interactions with the mitigation structure. Therefore, the two-phase flow model (Iverson 1997; Iverson and Denlinger 2001; Pudasaini et al. 2005) is introduced to study the different impact characteristics of particles and slurry in a debris flow during the interaction with a flexible barrier. Following the objective of this chapter, the two phases are classified based on the impact mechanisms of different phases on a permeable flexible barrier. Therefore, a debris flow is divided into a slurry phase which can pass through the flexible barrier and a debris phase which can be trapped by the flexible barrier. The composition of a debris flow in this two-phase model is schematically shown in Figure 7-2(a), where air entrained in the debris flow is neglected in this study.

7.2.1 General formulation

First of all, three assumptions are made to simplify the impact force calculation of a debris flow: (i) both the debris and the slurry phases are uniformly distributed in a debris flow travelling with the same velocity v_0; (ii) the cross-section area of the debris flow is a rectangle with the width of the channel w and the depth of the debris flow d; (iii) the "effective debris flow" is defined to describe the debris front which can exert pressure on the barrier. Thus, the total volume of the effective debris flow can be calculated as (Armanini 1997):

$$V_{mixture} = t_{impact} v_0 h w \tag{7-1}$$

where $V_{mixture}$ is the total volume of the debris flow; t_{impact} is the total impact time; v_0 is the impact velocity of the effective debris flow; h and w are the height of the effective debris flow and the width of the channel.

The retaining rate of the debris mass(ϕ_d) and the passing fraction of the slurry mass (ϕ_s) are expressed respectively as:

$$\phi_d = \frac{V_d}{V_{mixture}};\ \phi_s = \frac{V_s}{V_{mixture}} = \frac{V_{mixture} - V_d}{V_{mixture}} = 1 - \phi_d \tag{7-2}$$

where V_d is the volume of the debris phase retained by the net; and V_s is the volume of the slurry phase passing through the net.

The total mass of a debris flow ($m_{mixture}$) is quantified as:

$$m_d = \rho_d \phi_d V_{mixture};\ m_s = \rho_s \left(1 - \phi_d\right) V_{mixture} \tag{7-3}$$

$$m_{mixture} = m_d + m_s = \left[\phi_d \rho_d + \left(1 - \phi_d\right)\rho_s\right] V_{mixture} \tag{7-4}$$

Therefore, the relationship between the bulk density (ρ_{bulk}) of the debris flow mixture and the densities of the debris phase and the slurry phase can be given as:

$$\rho_{bulk} = \frac{m_{mixture}}{V_{mixture}} = \phi_d \rho_d + \left(1 - \phi_d\right)\rho_s \tag{7-5}$$

ρ_d is the density of the debris phase in a debris flow, here it is measured from the saturated aggregate; and ρ_s is the density of the slurry phase in a debris flow, which can be back calculated using Eq.(7-5).

7.2.2 Momentum conservation law

Based on the above definitions, the impact impulse on a flexible barrier is originated from the momentum change of the debris flow. During the impact process, the debris phase loses all its velocity, and the slurry phase only loses a part of its velocity by passing through the flexible barrier. Therefore, the impulse on the flexible barrier can be calculated by combining the momentum changes of the debris phase (Δp_d) and the slurry phase (Δp_s):

$$F_{impact} t_{impact} = \Delta p_d + \Delta p_s \tag{7-6}$$

The momentum changes of the debris phase and the slurry phase can be written as:

$$\Delta p_d = m_d \left(v_{0,d} - v_{1,d} \right) \tag{7-7}$$

$$\Delta p_s = m_s \left(v_{0,s} - v_{1,s} \right) \tag{7-8}$$

where $v_{0,d}$ and $v_{1,d}$ are the velocities of the debris phase before and after the impact; $v_{0,s}$ and $v_{1,s}$ are the velocities of the slurry phase before and after the impact. Substituting Eq.(7-7) and Eq.(7-8) into Eq.(7-6), the equation can be rewritten as:

$$F_{impact} = \frac{m_d \left(v_{0,d} - v_{1,d} \right)}{t_{impact}} + \frac{m_s \left(v_{0,s} - v_{1,s} \right)}{t_{impact}} \tag{7-9}$$

It is assumed that the debris phase and the slurry phase have the same velocity before impact:

$$v_0 = v_{0,d} = v_{0,\mathrm{s}} \tag{7-10}$$

In the simple method, the impact of a debris flow is regarded as a debris train impacting the mitigation structure (Hungr et al. 1984). Based on the assumption that the debris flow mixture is homogeneous before impact, the debris phase and the slurry phase are uniformly distributed in the debris flow.

Substituting Eq.(7-1), Eq.(7-3), and Eq.(7-10) into Eq.(7-9):

$$F_{impact}=\phi_d hwv_0\rho_d\left(v_0-v_{1,d}\right)+\left(1-\phi_d\right)hwv_0\rho_s\left(v_0-v_{1,s}\right) \qquad (7\text{-}11)$$

Based on the definitions of the debris phase and the slurry phase, the debris phase is trapped by the flexible barrier and loses all its velocity ($v_{1,d}$=0), and the slurry phase, on the other hand, passes the mesh net of the flexible barrier with a residual velocity ($v_{1,s}$>0). The different performances of the debris phase and the slurry phase during the interaction with a flexible barrier are illustrated in Figure 7-2(b). To quantify the velocity loss of the slurry phase during the passing-through process, a dimensionless parameter named Velocity Loss Ratio (VLR) is defined and expressed as follows:

$$VLR=\delta=\frac{v_0-v_{1,s}}{v_0} \qquad (7\text{-}12)$$

Thus, the simple method can be rewritten as:

$$F_{impact}=v_0^2\left[\phi_d\rho_d+\left(1-\phi_d\right)\delta\rho_s\right]hw \qquad (7\text{-}13)$$

Using this method, the dynamic impact force from a muddy debris flow on a flexible barrier can be calculated with the basic parameters of the impacting debris flow (ρ_d, ρ_s, v_0, h), the width of the flow channel (w), and two coefficients with specific physical meanings (δ, ϕ_d).

When both the debris mass and the slurry mass are fully trapped, δ=1, and Eq.(7-13) becomes:

$$F_{impact}=v_0^2\left[\phi_d\rho_d+\left(1-\phi_d\right)\rho_s\right]hw \qquad (7\text{-}14)$$

Substituting Eq.(7-5) into Eq.(7-14):

$$F_{impact} = v_0^2 \rho_{bulk} h w \tag{7-15}$$

The proposed equation becomes the hydro-dynamic method with the dynamic coefficient of 1.

The new method proposed in this study adopts the same theoretical basis as the hydro-dynamic method proposed by Armanini (1997). In the derivation of the hydro-dynamic method, Armanini (1997) identified two types of impact behaviors: the “jet-like” impact and the “reflected wave” impact, and he concluded that the hydro-dynamic method can only be utilized to calculate the impact force from a debris flow imposing a “jet-like” impact on a barrier by neglecting the time variation in the momentum balance (from Eq.(12) to Eq.(14)). For the “reflected wave” impact, the dynamic impact force is much larger because the debris flow will bounce back with a rebound velocity after impact.

Based on the observations from the debris flow impact tests in this study and in the literature (Song et al. 2018; Wendeler et al. 2018), a muddy debris flow impacts on a flexible barrier, decelerates gradually due to large deformation, and normally forms a “jet-like” impact. On the other hand, reflected waves can be generated in the impact of a granular debris flow on a flexible barrier (Wendeler 2016) or the impact of a debris flow on a rigid barrier (Canelli et al. 2012; Ng et al. 2016). Therefore, only the impact force from a muddy debris flow on a flexible barrier can be calculated using the simple method proposed in this study. For the calculation of the impact force from a granular debris flow or on a rigid barrier, this method needs to be adjusted by introducing an empirical coefficient larger than 1 corresponding to developing reflected waves.

7.3 Analysis of Results from impact tests using debris flows with different water contents

7.3.1 Experiment material and procedure

Here I use the test results from Debris Test 1 and Debris Test 4 to verify the proposed simple method. In both tests, debris materials with different water contents were prepared to study the impact and the passing-through mechanisms of debris flows with different water contents (89.4% for Debris Test 1 and 61.1% for Debris Test 4). The PSD (Particle Size Distribution) curves of the debris materials used in the tests are plotted in Figure 6-1. The basic parameters of Debris Test 1 and Debris Test 4 are listed in Table 7-1.

7.3.2 Experiment results

The debris flow in Debris Test 1 has a higher impact velocity (6.7 m/s) due to its higher water content compared to the impact velocity of 5.8 m/s in Debris Test 4. It can be observed from Figure 7-3 that a large percentage of slurry passed the flexible barrier and sprayed out, and only large debris was retained by the flexible barrier in both tests. With the continuous photographs taken in the impact period by the high-speed cameras, the velocities of particles at different locations are measured including one particle representing the debris flow velocity before the impact and several particles representing the velocities of the passed slurry at different locations (see Figure 7-4(a) and Figure 7-5(a)). To increase the accuracy of the measurement, the velocity of each particle is measured from 5 continuous photographs with the assistance of the reference lines attached to the flume. The average velocities and the standard deviations in the measurement of all particles are plotted in Figure 7-4(b) and Figure 7-5(b). The average velocity of all the passed particles is selected as the residual velocity of the slurry phase after the impact ($v_{1,s}$). By comparing the velocities of the slurry before and after the impact, the VLRs (Velocity Loss Ratio, δ) in both tests are obtained (53.7% in Debris Test 1 and 55.2% in Debris Test 4), which are similar regardless of the different water contents (89.4% in Debris Test 1 and 61.1% in Debris Test 4). The trapped debris material in Debris Test 1 and Debris Test 4 are plotted in Figure 7-6. The retaining volume of the debris phase was measured during the removal of the trapped debris after each test. The included angle and the maximum measured tensile forces in central area of the flexible barrier in the two tests are plotted in Figure 7-7 and Figure 7-8. From the force histories of mini tension link transducers installed on the flexible barrier, dynamic impact forces are dominant in the two tests, thus the impact forces on the flexible ring net are calculated using Eq.(3-2). All the parameters and the test results are listed in Table 7-1. It can be observed that even the debris materials used in the two tests have similar total volumes and particle size distribution curves, the retaining rate of debris in Debris Test 1 is much smaller than which of Debris Test 4.

7.4 Verification of the new simple method

7.4.1 Comparison of the results from large-scale tests and simple methods

The measured impact forces in the two tests are compared with the calculated impact forces using the simple method proposed in this chapter and several other representative simple methods in the literature. To quantify the accuracies of those methods, RC (Relative Change) is defined and given as:

$$RC = \frac{F_{impact} - F_{measured}}{F_{measured}} \times 100\% \tag{7-16}$$

The positive value of RC means an over-estimation of the calculated result compared with the measured value, and the negative value of RC represents an under-estimation of the calculated result. The calculated results and the Relative Changes of all the methods are listed in Table 7-2. The hydro-dynamic methods with $\alpha = 1.5$ and $\alpha = 2.0$ considerably over-estimate the impact loadings. This over-estimation is because these methods ignored the passing-through of slurry. The hydro-dynamic method was developed by Wendeler (2008) using a reduced dynamic coefficient of 0.7 to represent the lower impact loadings from debris flows with lower densities ($\rho_{bulk} < 1900$ kg/m^3) based on field data. This method can accurately predict the impact force from the debris flow in Debris Test 4 with the density of 1739 kg/m^3. However, for the debris flow with a higher water content of 89.4% and lower density of 1604 kg/m^3 in Debris Test 1, this method overestimates the impact force on the barrier. To improve this method, the dynamic coefficient (α) should be further reduced for debris flows with lower densities (*e.g.* $\alpha = 0.55$ for $\rho_{bulk} \leq 1600$ kg/m^3). The hydro-static method with $\kappa = 1.0$ obviously underestimates the impact loadings since dynamic loadings are dominant in the impacts of rapid debris flows. The empirical method introduced by Cui et al. (2015) much underestimates the impact forces in both tests. While the empirical method proposed by Hübl et al. (2009) has an acceptable performance in predicting the impact forces of both tests. However, those empirical methods heavily rely on empirical coefficients obtained from statistical data, which cannot be used for extrapolative purposes (Thakur 1991). An equation based on the new method but ignores the passing-through of slurry is also verified. $\delta=1$ is used in this equation to represent the case that both debris and slurry are fully trapped by an impermeable barrier. Predictably, this method tremendously overestimates the impact forces in both tests with the maximum deviation of 79%. The comparison result indicates that the passing-through of slurry can obviously reduce the impact loading to be undertaken by a flexible barrier. Among all the compared methods, the proposed simple method considering slurry passing-through has the best performance in impact force prediction with small deviations. Based on the comparison results, it can be concluded that the new simple method proposed in this chapter can accurately calculate the impact forces of debris flows with high water contents (higher than 60%). Besides, a good consistency between the measured impact forces and the calculated results using current simple methods also corroborates that the measuring method of impact forces used in this chapter is reliable.

7.4.2 Verification with the results from laboratory tests

Few of the large-scale tests in literature have taken efforts to study the passing-through of debris flows through a flexible barrier or measure the residual velocity of the passed slurry. Thus, the data of small-scale laboratory tests conducted by Wendeler and Volkwein (2015) are used to further verify this new simple method. In that literature, a 3.88 m long, 0.3 m wide and 50° inclined chute was used to generate debris flows. Granular material with d_{90} (90% of the sample's mass is comprised of particles with a diameter less than this value) equals to 30 mm was used in those tests, and the water contents ranged between 40% and 50%. The aim of those tests was to investigate the relationship between the mesh size of a flexible barrier and the retaining rate of debris material. From the conclusions drawn in that literature, the test (Test 43) using the net with the mesh size equals to d_{90} of the debris material has the best performance in retaining debris material. Thus, the result of Test 43 in that literature is used in the verification. Since the VLRs (Velocity Loss Ratio, δ) in those tests were not mentioned, the average value of Debris Test 1 and Debris Test 4 in the study was used as a reference, so do the density of debris phase. The density of the slurry phase (ρ_s) is back calculated by substituting ρ_{bulk}, ρ_d, and ϕ_d into Eq.(7-5). The parameters and the results are listed in Table 7-3. The calculated impact force using the new simple method is 393 N, which fits well with the measured impact force of 400 N. It can be concluded that the simple method has a good performance in predicting the impact force of a debris flow with a high retaining rate.

7.5 Discussions

Two key parameters are identified in the proposed new method to quantify the passing-through of slurry: the VLR (Velocity Loss Ratio, δ) and the retaining rate, ϕ_d. Reliable values of VLR and ϕ_d are required to guarantee the accuracy of this simple method. In the large-scale physical modeling tests presented in this paper, the VLR values are 53.7% and 55.2%, respectively. Considering the different water contents of debris flows in the two tests (89.4% and 61.1%), it can be preliminarily concluded that the VLR is insensitive to variation of water content. For design analysis, the value of VLR is conservatively recommended to be 55% for debris flow-resisting flexible barriers based on the findings in this study. From the test results, the retaining rate (ϕ_d), as the other key parameter in this simple method, has a close relationship with the water content of a debris flow. It can be preliminarily concluded that the retaining rate of a debris flow rises with the decrease of the water content, which fits well with the conclusions drawn by Li and Zhao (2018) from the results of numerical simulations. For the engineering application of the proposed simple method, the relationships of the VLR (Velocity Loss Ratio, δ) and the retaining rate (ϕ_d) with the basic parameters of the debris flow and the flexible barrier should be established. Wendeler and Volkwein (2015) concluded from laboratory tests and dimensional analysis that the retaining rate (ϕ_d) can be affected by two dimensionless numbers, which are $\Pi_7 = h_b' / h_{fl}$ and $\Pi_8 = M / d_{90}$, where h_b' is the distance between the slope and the flexible barrier bottom cable; h_{fl} is the flow depth; M is the mesh size of the flexible net; and d_{90} is the diameter where 90% of the debris material has a smaller particle size. In this research, the relationships between the water content and the two coefficients (δ, ϕ_d) have been preliminarily investigated. From the results of the large-scale tests, it is found that the VLR is not sensitive to the change of water contents, and the retaining rate decreases with the increase of water contents. However, the number of tests in this study is difficult to establish quantitative relationships. More large-scale experiments are necessary to study the influencing factors on VLR and ϕ_d. For example, the ratio of the typical particle diameter to the mesh size, the water content, and the impact time will be investigated in the future study. If reliable relationships can be drawn, the VLR and the retaining rate in a design project can be determined by a detailed engineering geological investigation in the protected area. The dynamic impact load for design can therefore be calculated simply and accurately with the proposed simple method.

Due to the assumptions and simplifications in the derivation process, the proposed simple method has some limitations in the application:

a) The impulse impacts from large boulders entrained in a debris flow has not been considered.
b) For the impact of a debris flow with a small flow depth and a low velocity, the static earth pressure can be dominant, thus the calculated impact force cannot accurately represent the maximum loading on the flexible barrier.
c) This method can only be used to calculate the impact force from a muddy debris flow on a flexible barrier which performs a “jet-like” impact. If reflected waves are generated in the impact process, the theoretical basis of this simple method is no longer applicable.

Nevertheless, this simple method provides a simple way to calculate the impact force of a muddy debris flow on a permeable flexible barrier considering the force reduction due to partial debris flow passing-through, which can be utilized in the design of debris flow-resisting flexible barriers.

7.6 Summary

A new simple method has been proposed in this study to calculate the impact force of a debris flow on a flexible barrier considering the slurry passing-through. In this method, the debris flow is regarded as a two-phase flow: debris phase that can be retained by the flexible barrier and slurry phase that can pass through the flexible barrier. The impact force is calculated from the momentum changes of both phases in a debris flow during the impact. The results from two large-scale physical modeling tests are presented, analyzed, and applied to evaluate the performance of this new simple method. The data of the laboratory tests in the literature (Wendeler and Volkwein 2015) are used to further verify this simple method. From the comparisons and verifications, key findings and conclusions are summarized and presented as below:

(a) The passing-through of slurry can be observed in the large-scale physical modeling tests performed in this paper. By measuring the velocities of the passing slurry and the retaining volumes of the debris materials in the large-scale tests, more than 70% of slurry and small particles passed through the flexible barrier with the velocity loss of approximately 55% in this study.

(b) From the test results of debris flows with different water contents, it can be preliminarily concluded that the velocity loss ratio of the passing-through slurry is insensitive to the water content, and the retaining rate of the debris material rises with the decrease of the water content.

(c) The hydro-static method cannot accurately predict the impact forces of the debris flows in this study because the dynamic impact loadings are dominant in both tests. The hydro-dynamic method with a reduced dynamic coefficient of 0.7 (Wendeler 2016) has a feasible performance in predicting the impact force in Test 1, but it obviously overestimates the impact force of the debris flow with a lower density in Test 2, which indicates that the hydro-dynamic method with a constant coefficient cannot predict debris flows with various densities and different passing-through characteristics.

(d) The empirical method proposed by Hübl et al. (2009) has a feasible performance in the comparison. However, empirical methods heavily rely on existing experiment data, and the coefficients of empirical methods normally have limited physical meanings (Thakur 1991).

(e) The modified equation was originated from the new simple method without considering the passing-through of slurry extremely overestimates the impact forces in both tests, which corroborates that the slurry passing-through can significantly reduce the dynamic impact loading on a flexible barrier.

(f) The new simple method proposed in this study has the best performance in the comparison. It can be concluded that this new simple method can accurately predict the impact force of a muddy debris flow with a high water content on a flexible barrier. The comparison with the results of the laboratory test in the literature further validates the reliability of this new simple method in the case of high retaining rates.

Two coefficients with specific physical meanings have been defined in this paper: Velocity Loss Ratio (VLR, δ) of the passing slurry and the retaining rate of the trapped debris (ϕ_d). The coefficients are the key parameters in the new simple method to represent the interaction characteristics of a muddy debris flow with a flexible barrier. Further research should focus on establishing reliable relationships of the coefficients with the parameters of the impacting debris flow and the flexible barrier.

(a)

(b)

Figure 7-1. Passing-through of slurry in (a) the real debris flow and (b) a field-scale test (Geoburgg AG 2012)

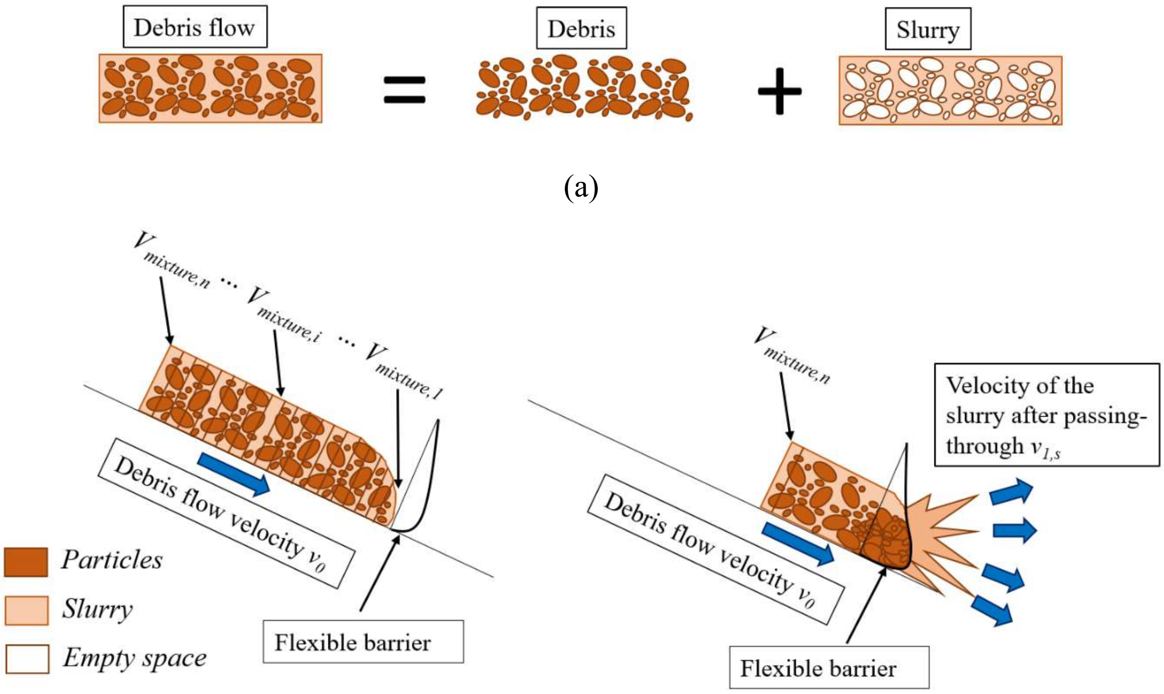

(a)

(b)

Figure 7-2. A schematic presentation of (a) debris and slurry phases in a debris flow and (b) different interaction mechanisms of the two phases with a flexible barrier

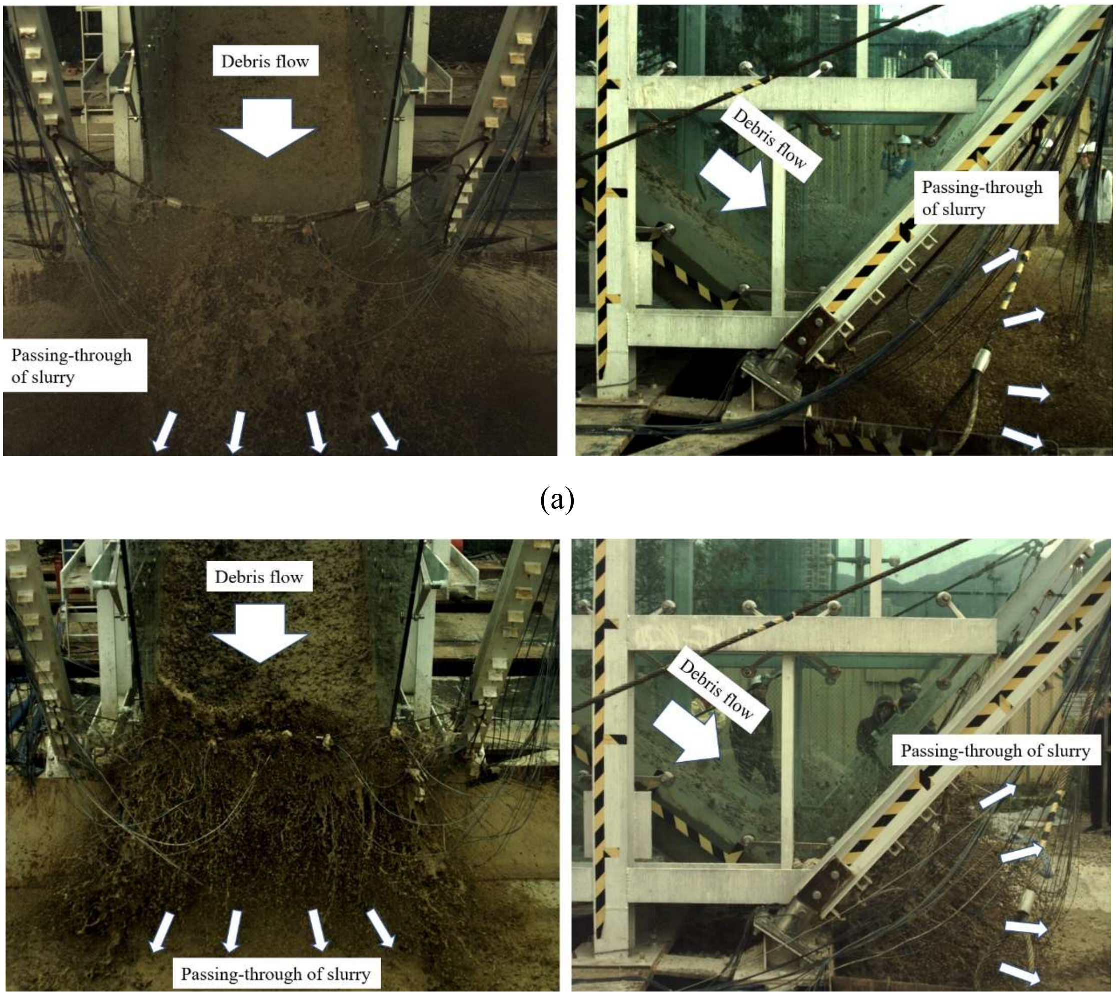

(a)

(b)

Figure 7-3. Photographs showing the phenomenon of slurry passing-through in (a) Debris Test 1 and (b) Debris Test 4

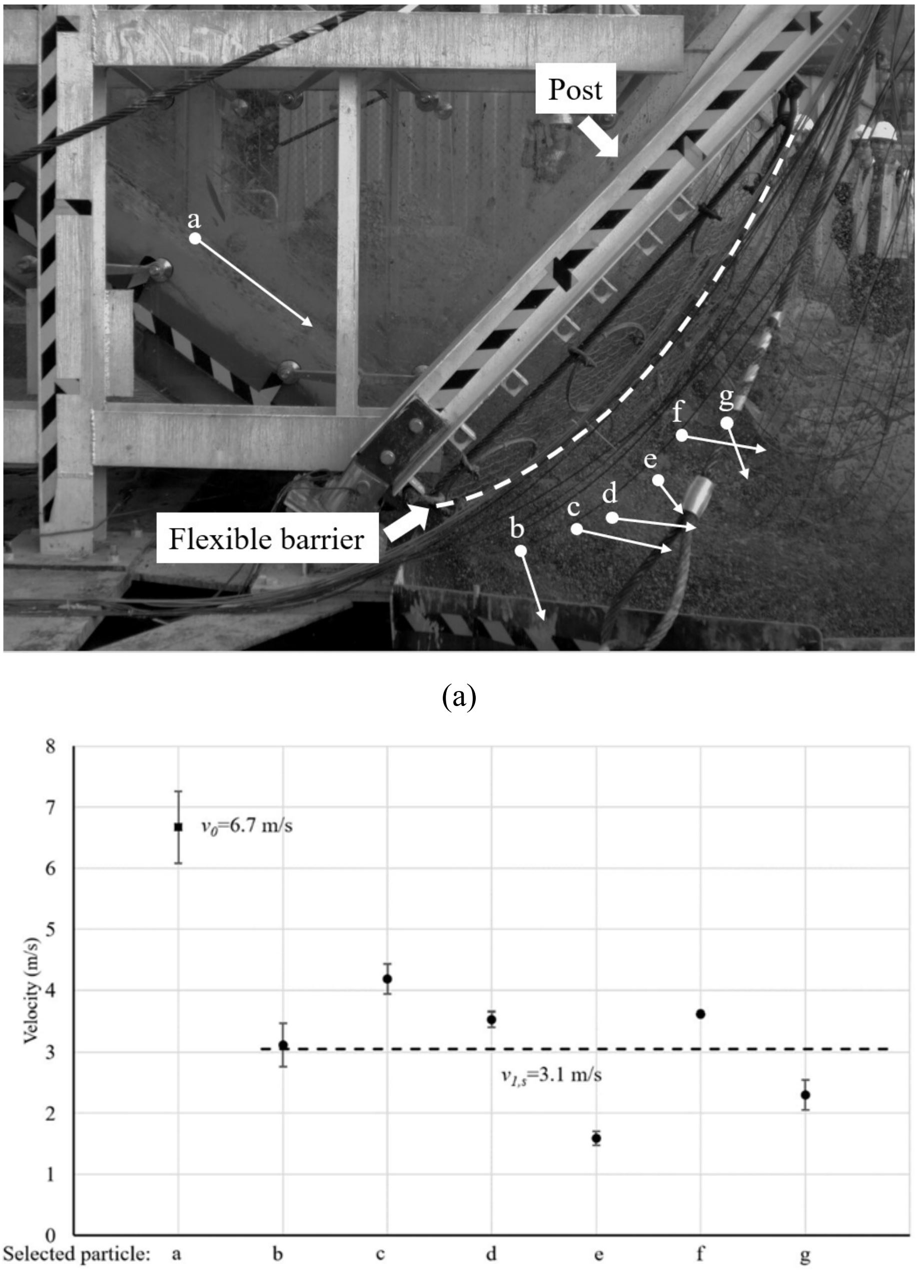

(a)

(b)

Figure 7-4. (a) Selected particles representing the velocities of the debris flow before and after passing through the flexible barrier and (b) the measured velocities in Debris Test 1

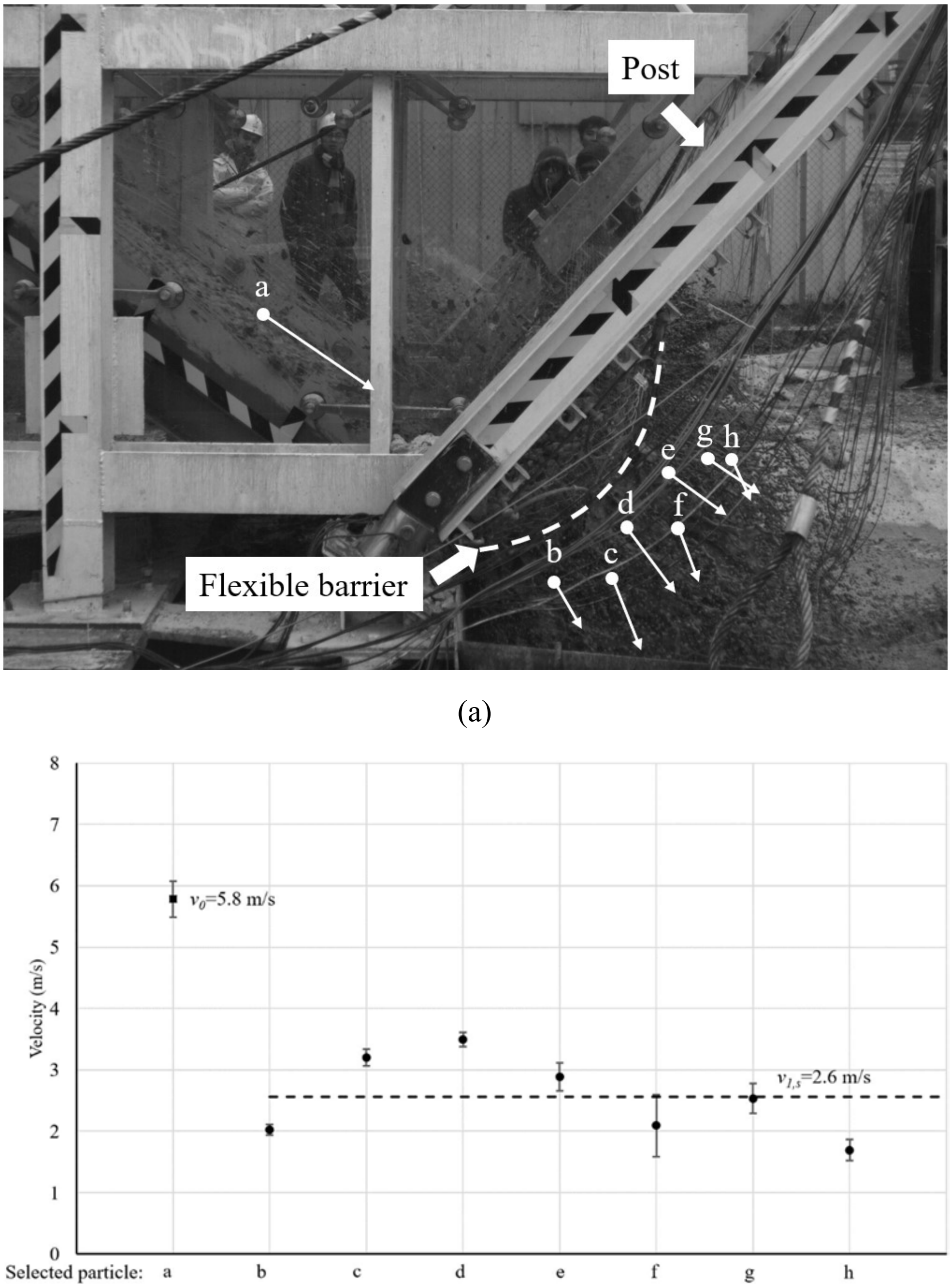

(a)

(b)

Figure 7-5. (a) Selected particles representing the velocities of the debris flow before and after passing through the flexible barrier and (b) the measured velocities in Debris Test 4

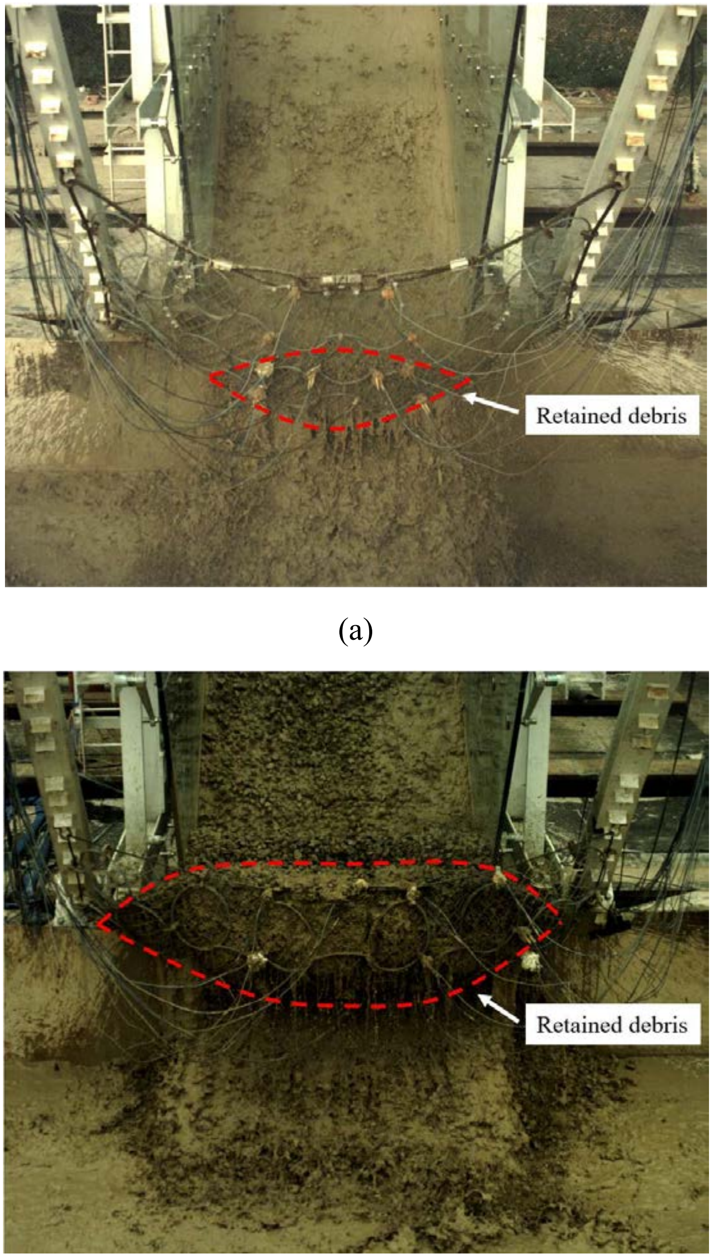

(a)

(b)

Figure 7-6. Retainment of debris in (a) Debris Test 1 and (b) Debris Test 4

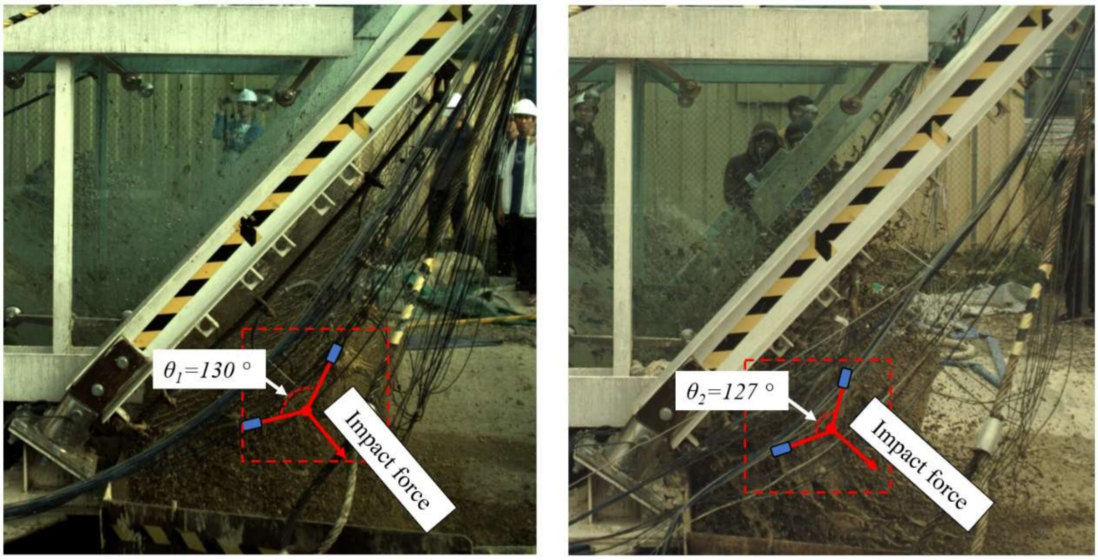

(a) (b)

Figure 7-7. Photographs taken by the side-view high-speed camera at the maximum deflection in (a) Debris Test 1 and (b) Debris Test 4

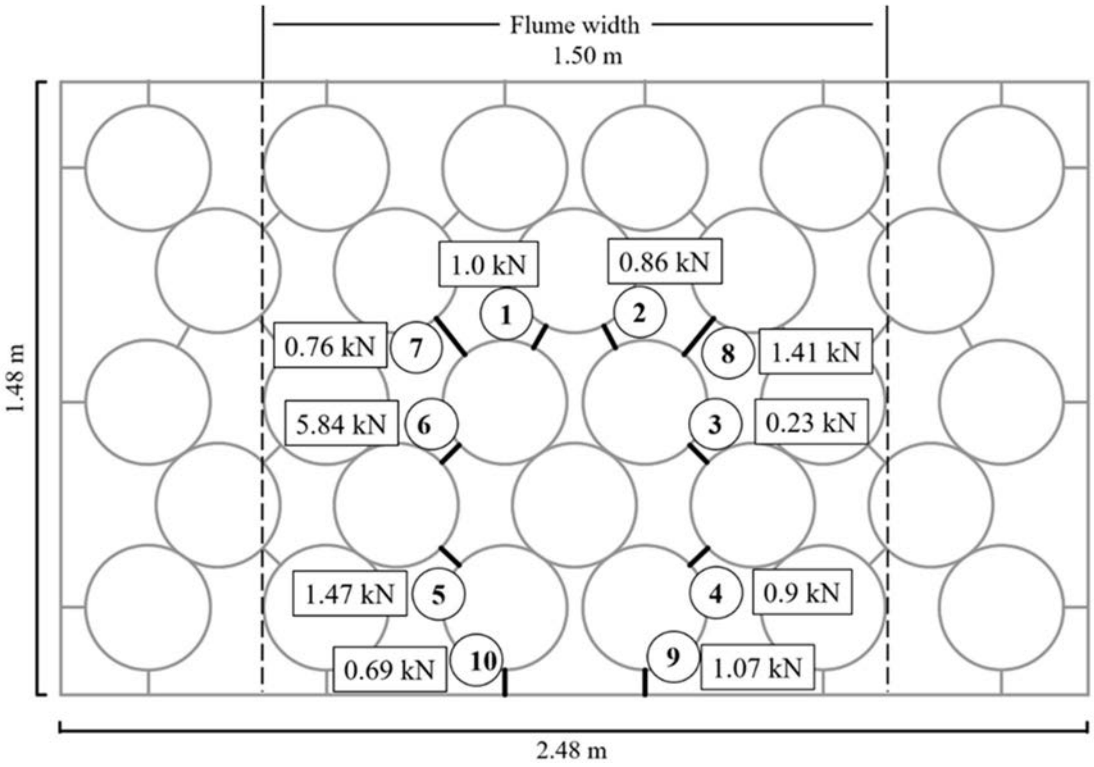

(a)

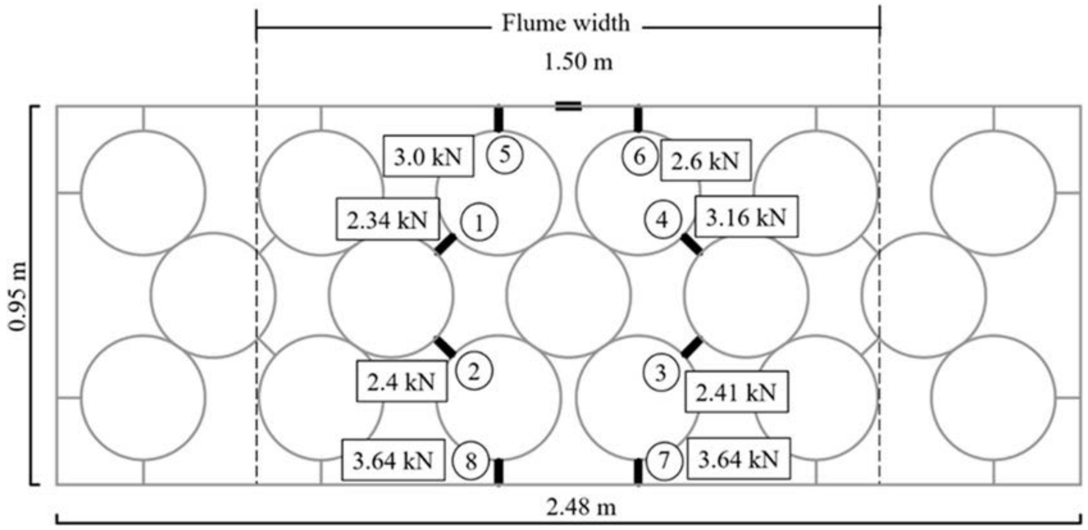

(b)

Figure 7-8. The maximum measured tensile forces of mini tension link transducers in (a) Debris Test 1 and (b) Debris Test 4

Table 7-1. Values of parameters of Debris Test 1 and Debris Test 4 for verification of the simple approach

Parameters	**Debris Test 1**	**Debris Test 4**
ρd (kg/m3)	2075	2075
ρs (kg/m3)	1552	1655
Bulk density of the debris flow ρbulk (kg/m3)	1604	1739
Water content (%)	89.4	61.1
Total volume of debris flow mixture Vmixture (m3)	2	2.05
Retaining volume of debris materials Vd (m3)	0.20	0.64
Φd	0.1	0.31
v0 **(m/s)**	6.7	5.8
v1,s **(m/s)**	3.1	2.6
$Fr = \frac{v_0}{\sqrt{gh}}$	6.76	4.49
δ (%)	53.7	55.2
h (m)	0.10	0.17
Total deposited height of the debris flow $h_{deposit}$ ***(m)***	0.2	0.4
Width of the flume w (m)	1.5	1.5
θ (°)	130	127
$F_{measured}$ **(kN)**	6.01	10.35

Table 7-2. Comparisons of the measured impact forces in Debris Test 1 and Debris Test 4 with the calculated results of several simple methods

Simple methods for impact force estimation	***Impact force in Debris Test 1* (kN)**	***RC (%)***	***Impact force in Debris Test 4* (kN)**	***RC (%)***
$F_{measured}$	6.01		10.35	
$F_{impact} = \alpha\rho_{bulk}{v_0}^2hw$ **(*α=1.5*)** **(Hungr et al. 1984)**	16.20	169.39	22.38	116.25
$F_{impact} = \alpha\rho_{bulk}{v_0}^2hw$ **(*α=2*)** **(Kwan and Cheung 2012)**	21.60	259.19	29.83	188.34
$F_{impact} = \alpha\rho_{bulk}{v_0}^2hw$ **(*α=0.7*)** **(for bulk density lower than 1900 *kg/m³*) (Wendeler 2008)**	7.56	25.72	10.44	0.92
$F_{impact} = \kappa\rho_{bulk}g{h_{deposit}}^2w$ **(*κ=1*)** **(Kwan and Cheung 2012)**	0.94	-84.30	4.09	-60.43
$F_{impact} = 5.3Fr^{-1.5}\rho_{bulk}v_0^2hw$ **(Cui et al. 2015)**	3.25	-45.90	8.31	-19.72
$F_{impact} = 5\rho_{bulk}v_0^{0.8}\left(gh\right)^{0.6}hw$ **(Hübl et al. 2009)**	5.45	-9.43	12.30	18.85
$F_{impact} = v_0^2\left[\phi_d\rho_d + \left(1-\phi_d\right)\rho_s\right]hw$ **(the new method neglecting the passing-through of slurry)**	10.80	79.59	15.32	48.07
$F_{impact} = v_0^2\left[\phi_d\rho_d + \left(1-\phi_d\right)\delta\rho_s\right]hw$ **(the method proposed in this paper)**	**6.45**	7.25	**10.94**	5.77

Table 7-3. Parameters and measured impact forces of the laboratory tests in the literature compared with the calculated impact force using the proposed simple method

Parameters	***Typical values***
v_0 **(m/s)**	3.48
h (m)	0.071
w (m)	0.3
ρ_{bulk} ***(kg/m³)***	1753
ρ_d ***(kg/m³)***	2075
ρ_s ***(kg/m³)***	1269
δ ***(%)***	54.5
ϕ_d	0.6
Water content (%)	45
$F_{measured}$ ***from laboratory tests (*Wendeler and Volkwein 2015*) (N)***	400
F_{impact} ***calculated using the new simple method (N)***	393

CHAPTER 8: AN IMPROVED DESIGN APPROACH FOR DEBRIS FLOW-RESISTANT FLEXIBLE BARRIER BASED ON IMPACT FORCE

Multiple flexible barriers can be installed in a risky natural gully to mitigate small-scale debris flows in the triggering stage before they grow to larger and more disastrous scales (Volkwein 2014). For multiple flexible barriers, overflow is allowed for the upstream flexible barriers. In this chapter, an improved design approach for flexible barriers is proposed. The design approach can be divided into two steps:

a) To determine the retaining capacity and the dimensions of the designed flexible barrier based on the required retaining volume of the potential debris flow;
b) To calculate the design impact loadings on different components (*e.g.* flexible ring net, supporting posts, supporting cables and foundations).

8.1. Retaining capacity determination of the flexible barrier

For a flexible barrier designed to mitigate channelized debris flows, the retaining capacity is an important design parameter. The retaining capacity can be used to determine the dimensions of the flexible barrier and the number of flexible barriers in a protection area. If the estimated retaining capacity of the designed flexible barrier is smaller than the active volume of possible debris flows, multiple flexible barriers should be considered to increase the retaining capacity. In this section, a simple method is proposed to estimate the retaining capacity. The dimensions of the designed flexible barrier can be determined by the required retaining capacity for potential debris flows. From the results of the large-scale debris flow impact tests presented and analysed in Chapters 6 and 7, the passing-through of the debris flow and the height reduction of the flexible barrier were observed in the impact process. Therefore, two parameters are integrated into the calculation of the retaining capacity:

retaining rate of the debris material and height reduction of the flexible barrier.

In the study, the retaining rate (ϕ_d) is measured from the retaining volume in the flexible barrier. Based on the conclusions drawn in Chapter 6, the retaining rate has a close relationship with the IBR (Initial Block Rate) of the flexible barrier. For a designed flexible barrier with the IBR=0, the retaining rate of 0.31 in Debris Test 4 is preliminary selected in the calculation of the retaining capacity. More tests are needed to establish a clear relationship between the IBR and the retaining rate.

The height reduction of the flexible barrier due to the large deformation during the impact has been observed and quantified in the literature (Volkwein et al. 2011b; Kwan and Cheung 2012; Wendeler et al. 2018). Here a coefficient named $c_{reduced}$ is identified to represent the ratio of the reduced height under impact to the design height of the flexible barrier. From the results of the large-scale experiments in this study, it has been measured that the deformed barrier height is 0.6 time of the design height (h_{design}). Wendeler et al. (2018) concluded from field experiments that the filled height of the flexible barrier is 0.75 time of the original height before the event. Due to the initial slack of the flexible ring net by its self-weight (see Figure 8-1), the height of the installed flexible barrier normally is shorter than the design height on the drawings. Thus, both $c_{reduced} = 0.6$ (for design height) proposed in this study and $c_{reduced} = 0.75$ (for installed height) estimated by Wendeler et al. (2018) are reasonable. In the calculation of the retaining capacity, the reduction rate $c_{reduced} = 0.6$ is selected because this value can be easily used to guide the design of the flexible barrier without considering the initial slack. Thus, the retaining capacity of a flexible barrier can be calculated by:

$$V_{retention} = 0.5 w \phi_d \left(c_{reduced} \cdot h_{design} \right)^2 \cot \varepsilon \tag{8-1}$$

where ϕ_d is the retaining rate. Here a value of 0.31 is proposed for empty flexible barriers from the measurement of the large-scale debris flow impact tests in this study. $c_{reduced}$ is the reduction ratio of the deformed height to the design height of the flexible barrier. Here a value of 0.6 is selected based on the test results in this study. Another important parameter ε is the deposition angle. Determination of this parameter will be discussed in the following section.

8.2. Design load determination of the flexible barrier

With the dimensions of the designed flexible barrier, the design loading of the flexible barrier can be determined. The maximum impact loading on the flexible barrier has been widely accepted as a design criterion of debris flow-resistant flexible barriers (Bungion et al. 2012; Kwan and Cheung 2012; Volkwein et al. 2015; Wendeler et al. 2018). From the experiment study, it can be found that the impact force on the flexible ring net are larger than the force on the supporting structures due to the large deformation of the flexible ring net, thus the loadings on them should be estimated separately. By applying the IRR (Impact Reduction Rate) and suitable impact loading estimation methods, the impact forces on the flexible ring net and on the supporting structures can be estimated individually. Thus, the design of a flexible barrier can be optimized by dimensioning and designing different components with different design loadings, which provides a safer and more economical design approach. The simple method for debris flow impact force calculation proposed in Chapter 7 and the results from multiple debris flow tests in Chapter 6 are utilized in this design approach.

8.2.1 Design load determination on the flexible ring net

The impact of a debris flow normally includes the dynamic loading from debris front impact and the static earth pressure from debris deposition. A load approach is proposed in this section to calculate the force on the flexible barrier during the impact process based on the debris flow impact mechanisms observed in Chapter 6, which divides the impact process into three stages (see Figure 8-2):

a) *First thrust*: the first debris front impacts the ring net barrier;

b) *Debris filling stage:* the subsequent debris flow impacts and fills the flexible barrier;

c) *Overflow stage:* the following debris flow overtops and exerts pressure on the flexible barrier after it is filled.

The impact forces on the flexible ring net in the three stages are calculated respectively based on the conclusions and findings drawn in this study:

First thrust

In this stage (see Figure 8-2(a)), only the dynamic loading from the first debris front is imposed on the flexible barrier. The dynamic impact force on a permeable flexible barrier has been calculated in Chapter 7 by a simple method considering the passing-through of partial debris flow using Eq.(7-13).

Debris filling stage

In this stage (see Figure 8-2(b)), the dynamic loading and the static loading act on the flexible barrier simultaneously. Thus, the force situation of the flexible barrier during the deposition process can be calculated by:

$$F_{impact} = F_{dyanmic} + F_{static} \tag{8-2}$$

The dynamic loading can be calculated using Eq.(7-13), and the static loading can be calculated using the hydro-static method in Eq.(2-7), which has been verified by the granular flow impact tests presented in Chapter 5. Thus, Eq.(8-2) can be specified into:

$$F_{impact} = v_0^{2}\left[\phi_d \rho_d + \left(1-\phi_d\right)\delta\rho_s\right]hw + 0.5\kappa\rho_d g h_{deposited}^{2} w \tag{8-3}$$

It should be noted in Eq.(8-3) that the bulk density used in the original hydro-static method is replaced by the density of trapped debris (ρ_d) obtained in Chapter 7. Based on the assumptions arisen in Chapter 7, the dynamic loading in the impact process is constant. Therefore, the loading combination in this stage increases with the deposition of debris material. In the filling stage, the maximum deposition height $h_{deposited}$ can be calculated:

$$h_{deposited} = h_{barrier} - h \tag{8-4}$$

where $h_{barrier}$ used here should be the reduced flexible barrier height after being filled $h_{barrier} = c_{reduced} \cdot h_{design}$; h is the height of the debris flow.

Therefore, by substituting Eq.(8-4) into Eq.(8-3):

$$F_{impact} = v_0^{2}\left[\phi_d \rho_d + \left(1-\phi_d\right)\delta\rho_s\right]hw + 0.5\kappa\rho_d g\left(c_{reduced} \cdot h_{design} - h\right)^{2} w \tag{8-5}$$

Overflow stage

The overflow stage is presented in Figure 8-2(c). In this stage, the load on the flexible barrier has been divided into three force components based on the findings in Chapter 6. The loading combination in the overflow stage consists of the static earth pressure from the debris deposition, the drag force from the overtopping debris flow, and the instant peak loading due to the debris flow direction change, which can be presented using the following equation:

$$F_{impact} = F_{static} + F_{peak} + F_{drag} \tag{8-6}$$

In the above equation, the static force (F_{static}) can be calculated with Eq.(2-7) using the density of trapped debris (ρ_d); and the drag force (F_{drag}) can be estimated using the Voellmy model:

$$\tau = h\rho_{bulk}g\left(\tan\varphi + \frac{v^2}{h\xi}\right) \tag{8-7}$$

where φ and ξ are the friction angle and the turbulence coefficient of the debris flow, Hungr (1998) suggested to use φ=11° and ζ=500m/s^2 for channelized debris flows based on the back analysis of real cases using numerical simulations; v, h and ρ_{bulk} are the velocity, the height, and the density of the debris flow, and g is the gravity acceleration.

The effective area for the drag force can be simply estimated by multiplying the top length of the deposition wedge with the width of the channel (Kwan and Cheung 2012). Thus, the drag force can be calculated using the following equation:

$$F_{drag} = h\rho_{bulk}g\left[\tan\varphi + \frac{v^2}{h\xi}\right]\cdot\frac{c_{reduced}\cdot h_{design}\cdot w}{\sin\varepsilon} \tag{8-8}$$

In this equation, the deposition angle (ε) is an important parameter. From the sketch of the overflow stage plotted in Figure 8-2(c), the deposition angle is the combination of the slope inclination (ε_{slope}) in the retention area and the sedimentation angle (ε_{sed}) of the debris deposition, which can be written as:

$$\varepsilon = \varepsilon_{slope} + \varepsilon_{sed} \tag{8-9}$$

In this study, the deposition angle (ε) is measured with a value of 40° from the photographs by the side-view camera in the overflow stage of Debris Test 3. The flume inclination of the large-scale physical modelling facility in the PolyU is 35°, thus the sedimentation angle in the overflow experiment is 5°. Volkwein et al. (2011) suggested to use 2/3 of the slope inclination (θ) to estimate the sedimentation angle, but the estimated value of 23° does not fit with the measurement in the large-scale tests. As a comparison, the value of 10° suggested by Kwan and Cheung (2012) based on back-analysis is much closer to the measured value in this study. Considering the different sedimentation angles of various debris materials, a conservative value of 10° is selected in this study for flexible barrier design.

In Chapter 6, it is found that the instant peak loading (F_{peak}) is the largest in the overflow status from the direction change of the debris flow. Based on the impulse-momentum theorem, a simple method is derived to calculate this peak loading. First, several assumptions are made to simplify the calculation:

(a) The debris flow is a homogeneous mass travelling with a uniform velocity v_0 and a uniform cross-sectional area, which is a rectangle with the width of the channel w and the height of the debris flow h;

(b) The speed and the height of the debris flow before and after the direction change is assumed constant (Armanini 1997). Thus, the mass of the debris flow can be calculated as:

$$m = t_{peak} v_0 h w \rho_{bulk} \tag{8-10}$$

where m is the total mass of the debris flow; t_{peak} is the duration of the peak loading; v_0 is the impact velocity of the debris flow; h and w are the height of the debris flow and the width of the channel; and ρ_{bulk} is the bulk density of the debris flow.

Based on the impulse-momentum theorem and the direction change during the impact:

$$F_{peak} t_{peak} = m v_0 - m v_0 \cdot \cos \varepsilon + m v_0 \cdot \sin \varepsilon \tag{8-11}$$

Substituting Eq.(8-10) into Eq.(8-11), t_{peak} in both sides of the equation are eliminated, thus:

$$F_{peak} = v_0^2 h w \rho_{bulk} (1 - \cos\varepsilon + \sin\varepsilon) \tag{8-12}$$

Substituting Eq.(2-7), Eq.(8-8), and Eq.(8-12) into Eq.(8-6), the impact force in the overflow stage can be written as:

$$F_{impact} = 0.5\kappa\rho_d g \left(0.6h_{design}\right)^2 w + v_0^2 h w \rho_{bulk} (1 - \cos\varepsilon + \sin\varepsilon) + h\rho_{bulk} g \left[\tan\varphi + \frac{v_0^2}{h\xi}\right] \cdot \frac{c_{reduced} \cdot h_{design} \cdot w}{\sin\varepsilon} \tag{8-13}$$

Debris fronts reaching the flexible barrier at different times may have different combinations of debris depths, velocities, and densities (Kwan and Cheung 2012, Wendeler et al. 2018). To be reasonably conservative in the design, the maximum values of those parameters should be used in impact force calculation.

8.2.2 Design load determination on supporting structures

A conclusion can be drawn from the test results in this study that the flexibility of the flexible ring net can obviously reduce the impact loading transferred to the supporting structures. In the single boulder (Chapter 4) and the granular flow (Chapter 5) impact tests, only 70% of the impact force from the impacting mass can be transferred to the supporting structures. Therefore, the design impact loading on the supporting structures should be reduced correspondingly from the design impact loading on the flexible ring net by introducing the IRR value (β). The impact loading on the supporting structures (including supporting posts, supporting strand cables and foundations) at different impact stages can be estimated using the following equations:

First thrust

$$F_{dyanmic,s}=\left(1-\beta\right)v_0^{\ 2}\left[\phi_d\rho_d+\left(1-\phi_d\right)\delta\rho_s\right]hw \tag{8-14}$$

Debris filling stage

$$\begin{aligned}F_{impact,f,s}&=F_{dynamic,s}+F_{static,s}\\&=\left(1-\beta\right)v_0^{\ 2}\left[\phi_d\rho_d+\left(1-\phi_d\right)\delta\rho_s\right]hw+0.5\left(1-\beta\right)\kappa\rho_d g\left(c_{reduced}\cdot h_{design}-h\right)^2 w\end{aligned} \tag{8-15}$$

Overflow stage

$$\begin{aligned}F_{impact,o,s}&=F_{static,s}+F_{peak,s}+F_{drag,s}=0.5\left(1-\beta\right)\kappa\rho_d g\left(c_{reduced}\cdot h_{design}\right)^2 w\\&+\left(1-\beta\right)v_0^2hw\rho_{bulk}(1-\cos\varepsilon+\sin\varepsilon)+\left(1-\beta\right)h\rho_{bulk}g\left[\tan\varphi+\frac{v_0^2}{h\xi}\right]\cdot\frac{c_{reduced}\cdot h_{design}\cdot w}{\sin\varepsilon}\end{aligned} \tag{8-16}$$

From the force history of the supporting structures in the multiple debris flow impact tests (see Figure 6-4), the maximum impact loading occurs in the overflow stage. Therefore, the measured force history in the overflow stage is used to verify the Eq.(8-16) in the proposed load approach. The force components, $F_{static,s}$, $F_{drag,s}$, and $F_{peak,s}$ in Eq.(8-16) are calculated separately using the parameters in Debris Test 3 and listed in Figure 8-3(a). The comparison between the impact force history on the supporting structures in Debris Test 3 and the calculation results of Eq.(8-16) is plotted in Figure 8-3(b). From this figure, the impact peak at the time of 19 s fits well with the combination of the three force components $\left(F_{static,s}+F_{peak,s}+F_{drag,s}\right)$. After the impact peak, the impact thrust lasting nearly 1.5 s is acceptably underestimated by the force combination of $\left(F_{static,s}+F_{drag,s}\right)$. After the dynamic impact, the static earth pressure from the debris deposition $F_{static,s}$ is accurately estimated by the hydro-static method using the density of the debris deposition (ρ_d). From the comparison results, the calculation results have a feasible performance in predicting the impact force history in the overflow stage. This proposed load approach can be practically applied to determine the design impact loading on different components of a flexible barrier for debris flow mitigation.

8.3 Summary

In this chapter, a load-based design approach is proposed for flexible barriers in debris flow mitigation. This design approach consists of two steps: determining the retaining capacity of the flexible barrier and determining the design impact loading on the flexible barrier. Considering the loading reduction due to the large deformation of the flexible ring net under impact, the design impact loadings on the flexible ring net and on the supporting structures are calculated separately with the utilization of the Impact Reduction Rate (IRR), which has been calculated in the single boulder impact tests and the granular flow impact tests. Key parameters in this approach are calibrated by the results from the large-scale physical modelling tests presented in this study. In the calculation of the design impact loading, the impact process is divided into three stages: *first thrust*, *debris filling stage* and *overflow stage*. Relevant equations are derived to calculate the impact force combinations at different stages. This proposed approach has been verified by the force history of the supporting structures in the multiple debris flow impact tests plotted in Figure 6-4. With the application of this design approach, the flexible barriers for debris flow mitigation can be designed using basic parameters and active volumes of potential debris flows in the protection area.

Figure 8-1. Initial slack of the supporting cables due to the self-weight of the flexible ring net (Wendeler et al. 2018)

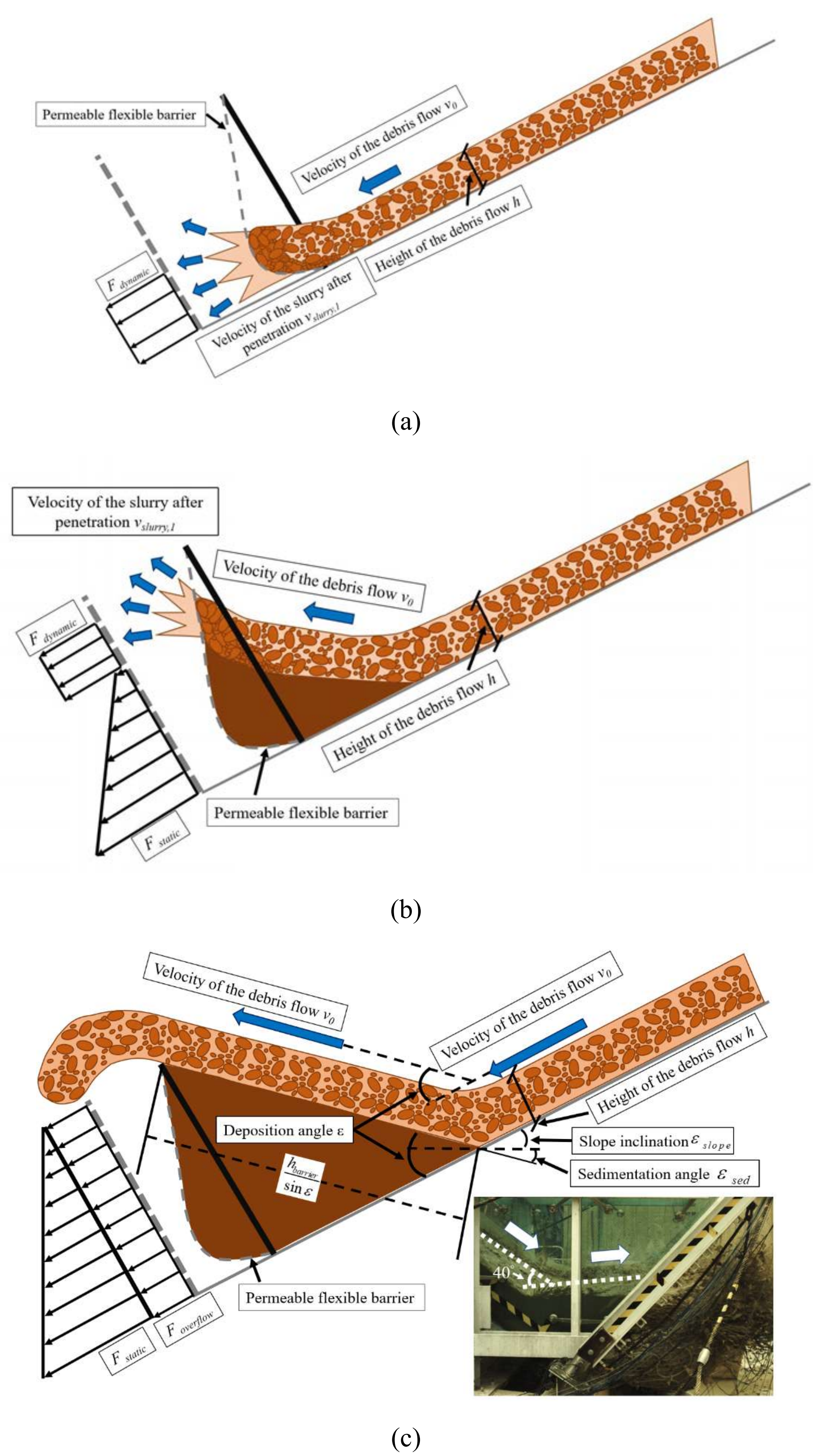

Figure 8-2. Sketches of different stages: (a) first thrust, (b) debris deposition stage, and (c) overflow stage in the interaction between a debris flow and a flexible barrier

g (m/s^2)	$h_{barrier}$ (m)	w (m)	κ	ρ_{bulk} (kg/m^3)	ρ_d (kg/m^3)	v (m/s)	h (m)	ε (°)	φ (°)	ξ (m/s^2)
9.81	0.89	1.5	1	1708	2075	6.1	0.2	40	11	500

$$F_{impact}=\overbrace{0.5(1-\beta)\kappa\rho_d g\left(0.6h_{design}\right)^2 w}^{F_{static}=8.4\ \mathrm{kN}}+\overbrace{(1-\beta)v_0^2 hw\rho_{bulk}(1-\cos\varepsilon+\sin\varepsilon)}^{F_{peak}=11.7\ \mathrm{kN}}+\overbrace{(1-\beta)h\rho_{bulk}g\left[\tan\varphi+\frac{v_0^2}{h\xi}\right]\cdot\frac{0.6wh_{design}}{\sin\varepsilon}}^{F_{drag}=2.8\ \mathrm{kN}}$$

(a)

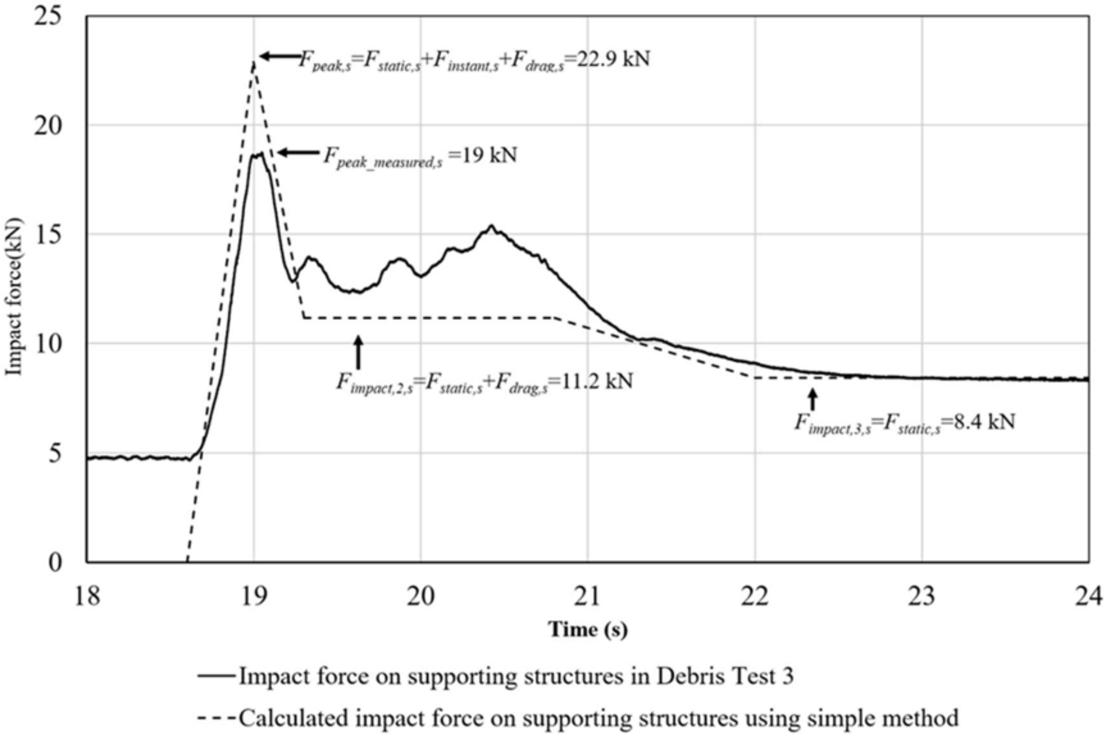

(b)

Figure 8-3. (a) Parameters and calculation results of Eq.8-16 and (b) the comparison of the impact loading history on the supporting structures in Debris Test 3 with the calculated impact forces on the supporting structures using the load approach

CHAPTER 9: CONCLUSIONS AND SUGGESTIONS FOR FUTURE RESEARCH

9.1 General summary

Natural hazards such as rockfalls and debris flows can cause destructive damages to infrastructures and human lives if no protection systems are adopted. There is a great significance to take appropriate mitigation countermeasures in risky areas. Among those measures, flexible barriers have been increasingly utilized in rockfall and debris flow mitigation. In this research, the interactions between different impact masses and a flexible barrier have been studied. By conducting large-scale physical modelling experiments, the impact mechanisms of single rock boulders, dry granular flows, and saturated debris flows on a flexible barrier have been investigated. The loading reduction capabilities of flexibility and permeability of a flexible barrier are quantitatively studied. Based on those findings and conclusions from the large-scale experiments, a load-based design approach of flexible barriers for debris flow mitigation is finally proposed. This approach has been validated by the results of the large-scale physical modelling tests in this study.

9.2 Major conclusions

9.2.1 A new large-scale physical modelling facility

Large-scale physical modelling is the main methodology of this study. A large-scale physical modelling facility with a prototype flexible barrier is established to replicate the interaction of rockfalls and debris flows with a flexible barrier. To better perform experiments, several developments have been made in the large-scale physical model:

- A novel fast door-opening device is designed and utilized to avoid the interference with the impact mass in the initiation process. With the application of this method, the door can be opened in less than 0.5 s without interfering with the generated rockfall or debris flow.
- On the prototype flexible barrier, mini tension link transducers are installed on the flexible ring net to measure the tensile forces between rings. The maximum tensile forces on the ring net can be utilized to directly measure the impact force on the flexible ring net using Eq.(3-2) or Eq.(3-3).
- Tension link transducers are installed on the supporting cables to measure the equivalent impact force on the supporting structures using Eq.(3-9).
- Two high-speed cameras are utilized to capture the motions and the interaction behaviours of the impact masses with the flexible barrier. The arrangement of the cameras is plotted in Figure 3-9.

With this developed large-scale physical model, two rock boulder impact tests, two dry granular flow impact tests, and four debris flow impact tests were successfully performed to study the interaction mechanisms between different impact masses and a flexible barrier.

9.2.2 The impact mechanisms of different impact masses on a flexible barrier

Single boulder

Multiple dynamic impacts were observed in the boulder impact tests. From the trajectory tracking of the impacting boulder, the boulder was decelerated and bounced back by the large elastic deformation of the flexible barrier. The kinetic energy of the boulder was dissipated by the recoverable large deformation of the flexible barrier. The measured impact forces on the flexible ring net and on the supporting structures are compared in the two rockfall impact tests using boulders with different diameters. In the 400-mm-diameter boulder impact test, 32% of the dynamic impact force was attenuated by the large deformation of the flexible ring net. While in the 600-mm-diameter boulder impact test, the impact loading reduction rate was 27%.

Dry granular flow

In the dry granular flow impact tests, the granular flow impacted on the flexible barrier directly, deposited behind the barrier layer by layer, and formed a deposition wedge which can attenuate the impact force of the later reached granular flow. In the impact process, the static loading from the debris deposition and the dynamic loading from the moving debris front co-existed, and the static loading was dominant due to the poor fluidity of dry granular flows. In this test, the maximum impact loadings on the flexible ring net and on the supporting structures were 10.96 kN and 7.89 kN, respectively. The measured impact loadings on different components are used to verify the hydro-dynamic method and the hydro-static method. From the verification, the hydro-dynamic method fits well with the impact loading on the flexible ring net with the relative error of 5.8%, and the hydro-static method performs perfectly in predicting the impact loading on the supporting structures with the relative error of 0.38%.

Saturated debris flows

Three continuous debris flow impact tests were conducted to explore the deposition and impact behaviours of multiple debris flows on a flexible barrier with different initial conditions. For the deposition behaviour, the retaining rate of the debris material increased with the increment of the Initial Block Rate (IBR) of the flexible ring net. In Debris Test 1 with the IBR=0, only 1/10 of the debris material was trapped. In Debris Test 2 with the

BR=0.44, the retaining rate increased to 0.45, and the flexible ring net was almost filled by the debris deposition. From the force histories of the large-scale tests, IBR values can also affect the impact behaviours. For Debris Test 1 with IBR=0, there was only a small dynamic impact force because of the debris flow passing-through with an impact peak of 1.3 kN. For Debris Test 2 with IBR=0.44, the impact force was mainly from the incremented earth pressure of the debris deposition with a peak loading of 6.1 kN. For Debris Test 3, the debris flow overflowed the flexible barrier via the deposition wedge. The impact force from the overflowing debris flow consists of three components: the static earth pressure from the debris deposition, the drag force from the overtopping debris flow and the dynamic impact loading from the direction change of the debris flow. The impact loading in the overflow stage is the largest among three tests with a peak loading of 19 kN. The impact mechanism of a debris flow filling and overflowing a flexible barrier in a short period is studied in Debris Test 4. The impact loading distributions on the flexible ring net at typical times are plotted and analysed. The impact force on the central area was much larger than that on the side areas, and the main impact area moved up gradually with the deposition of debris material.

9.2.3 Influence of flexibility and permeability on impact loading reduction

Flexibility and permeability, as two main characteristics of flexible barriers in impact force attenuation, have been identified and quantified in this research.

Flexibility

It has been concluded from this study that flexibility of a flexible barrier plays a significant role in reducing the impact force from impact masses. By tracing the interaction of a boulder with a flexible barrier, the impact from the boulder was attenuated by the large recoverable deformation of the flexible barrier. Recovery of the large deformation decomposed the large impact into several smaller impacts. By comparing the impact forces on the flexible ring net and on the supporting structures, around 30% of the impact force from the boulder was reduced by flexibility of the flexible barrier. In the granular flow impact tests, almost all the particles were trapped by the flexible ring net. Thus, the loading attenuation by the ring net should also be attributed to flexibility of the flexible ring net. Based on the test result, 28% of the impact force was attenuated by the flexible net in the granular flow impact test. In conclusion, flexibility of a flexible barrier can efficiently attenuate the impact forces from a rockfall and a debris flow.

Permeability

From the experimental study, the mesh net of a flexible barrier allows partial debris flow pass through the flexible barrier, which can reduce the impact force of the debris flow. From the results of the debris flow impact tests, a large percentage of slurry and small particles passed through the flexible barrier with a residual velocity. By analysing the impact processes of debris flows with different water contents, the passing rate of a debris flow through a flexible barrier has a close relationship with the water content of the debris flow. Even with similar impact velocities and similar bulk densities, the debris flow with a higher water content (89.4%) has a lower trapping rate (10%) and a smaller maximum impact force of 6.10 kN compared to the debris flow (Debris Test 4) with a lower water content of 61.1%, a higher trapping rate of 31% and a larger maximum impact force of 10.35 kN.

9.2.4 Simple methods for estimating impact forces on a flexible barrier

Rockfall

An empirical simple method in Eq.(4-5) is proposed to estimate the impact force from a single boulder on a flexible barrier. In this method, a coefficient S representing the stiffness of the flexible barrier and a coefficient D representing the impact area of the boulder are defined and implemented in the equation. This simple method only needs the diameter and the velocity of the potential rockfall to calculate the impact force on a flexible barrier with a calibrated stiffness coefficient S for a given type of flexible barriers. For the flexible barrier used in this study, the stiffness coefficient $S=2.76$ is calibrated using the result of Boulder Test 1. Using the calibrated coefficient, this method is verified by the result of Boulder Test 2 with a small relative error of 6.5%.

Debris flow

For the debris flow impact, a simple method considering the passing-through of partial debris flow is derived in this study. In this method, a debris flow is regarded as a two-phase flow which contains the debris phase that can be retained and the slurry phase that can pass through the flexible ring net, and the impact force is calculated from the momentum changes of the two phases during the interaction. This simple method is validated by the measured impact forces in the large-scale tests in this study and the data of the well-documented laboratory tests in the literature with a maximum relative error of 7.25%.

9.2.5 Design approach of debris flow-resistant flexible barriers

From the conclusions and findings from the experimental study, a developed design approach for flexible barriers in debris flow mitigation is proposed. In this approach, the retaining capacity and the design loading of a flexible barrier are determined step by step.

Determination of the retaining capacity of a flexible barrier

The retaining capacity of a flexible barrier should be determiend first according to the maximum active volume of potential debris flows in the protection area. An equation is proposed to estimate the retaining capacity of the flexible barrier installed in a channel. In this equation, the height reduction of the flexible barrier filled by debris material is represented by the reduction coefficient ($c_{reduced}$). Besides, the passing-through of debris flow is taken into account by integrating the retaining rate (ϕ_d) in the calculation. Both coefficients have been obtained from the results of the large-scale tests in this study. With the required retaining capacity to mitigate potential debris flows, the dimensions of the designed flexible barrier can be determined correspondingly.

Determination of the design impact loading of a flexible barrier

With the dimensions of the designed flexible barrier, the design loading of the flexible barrier can be calculated using the findings in this study. In the calculation of the design impact loading, the impact process is divided into three stages: *first thrust*, *debris filling stage* and *overflow stage*. Relevant equations are proposed based on the impact mechanisms of a debris flow at different stages. This approach is verified by the impact force history of the large-scale physical modelling tests in this study.

9.3 Suggestions for future work

9.3.1 Determination of VLR and ϕ_d

For the engineering application of the proposed simple method in Chapter 7, the relationships of the VLR (Velocity Loss Ratio, δ) and the retaining rate (ϕ_d) with basic parameters of the debris flow and the flexible barrier should be established. In this research, the relationships between the water content and the two coefficients (δ, ϕ_d) have been preliminarily investigated. From the results of the large-scale tests, it is found that the VLR is not sensitive to the change of water contents, and the retaining rate decreases with the increase of water contents. However, the number of tests in this study is not enough to establish clear relationships. In the future, more large-scale experiments should be performed to build reliable relationships of the mesh size of the flexible barrier, the particle size distribution and the water content of the debris flow with the two coefficients (δ, ϕ_d). If the relationships can be drawn, the VLR and the retaining rate in a design case can be determined by the data of engineering geological investigations and raining records in the protection area. Therefore, the flexible barrier can be designed based on the calculated retaining capacity and the design impact load using the design approach proposed in Chapter 8.

9.3.2 Relationship between precipitation and the impact mechanism of debris flow

The relationship between the probability of landslide occurrence and rainfall has been established based on global database (Finlay et al. 1997; Guzzetti et al. 2008; Caine 1980). Case studies have been performed to investigate the relationship between raining intensity-duration and the triggering of debris flows (Bacchini and Zannoni 2003, Chien et al. 2005). Empirical correlations of numbers, scar areas, and the volumes of landslides or channelized debris flows with maximum rainfall intensities have been established in Hong Kong based on the landslide records (Gao et al. 2018). However, further research is required to investigate the relationship between the precipitation and the impact mechanism of the triggered debris flow on protection structures. A heavy rainfall in the protection area can initiate debris flows with large magnitudes and high impact velocities, which could lead to large impact loadings. On the other side, the debris flows initiated by heavy rainfalls may have high water contents and low densities, which decreases their ability to carry large boulders and reduce the impact load on debris-resisting structures (Song et al. 2018b). Based on the findings in this study, debris flows with high water contents also have low retaining rates and small impact forces due to the high passing-through rate of slurry and debris material. Therefore, how the precipitation in a protection area can affect the flowing characteristics and the impact mechanisms of debris flows on a flexible barrier is worthy to be further studied.

9.3.3 Relationship between debris drainage and the static loading of debris deposition behind a barrier

The dynamic loading from the debris flow impact and the static loading from the debris deposition behind the barrier are two major force components in the impact process. Based on the findings in Chapter 8, the dynamic impact in the filling process is almost constant, and the static loading can be dominant in the design of mitigation structures with high retaining capacities and large dimensions. However, current calculation methods of static loading are based on the static earth pressure with a given earth pressure coefficient (Armanini 1997). Song et al. (2017) concluded from centrifuge modelling tests that the debris deposition can transform from the static state to the active state due to the large deformation of the flexible barrier , which reduces the earth pressure. Wendeler et al. (2018) raised the opinion that the increased density of the debris deposition due to dewatering could lead to an increase of the earth pressure, but the stabilised debris deposition and the increased soil parameters: c (cohesion intercept) and φ (angle of shear resistance) due to drainage, on the other hand, could reduce the earth pressure on the flexible barrier. Therefore, a suitable theoretical model to describe the behaviour of the debris deposition behind the barrier under drainage condition and a practical approach to accurately calculate the static loading on a permeable or an impermeable barrier are of great necessity. In the future, current constitutive models of soils can be developed to describe the soil behaviour of the debris deposition transforming from the fluid phase (fluidized soil) to the solid phase (consolidated soil).

REFERENCES

Agliardi, F., and Crosta, G. B. (2003). High resolution three-dimensional numerical modelling of rockfalls. *International Journal of Rock Mechanics and Mining Sciences*, 40(4), 455-471

Ancey, C. (2007). Plasticity and geophysical flows: A review. *Journal of Non-Newtonian Fluid Mechanics*, 142(1-3), 4-35.

Arattano, M., and Marchi, L. (2005). Measurements of debris flow velocity through cross-correlation of instrumentation data. *Natural Hazards and Earth System Sciences*, 5(1), 137-142.

Armanini, A. (1997). On the dynamic impact of debris flows. In *Recent developments on debris flows.* Springer, Berlin, Heidelberg, 208-226.

Ashwood, W., and Hungr, O. (2016). Estimating total resisting force in flexible barrier impacted by a granular avalanche using physical and numerical modeling. *Canadian Geotechnical Journal*, 53(10), 1700-1717.

ASTM: ASTM C29/C29M-17. (2017) Standard Test Method for Bulk Density (Unit Weight) and Voids in Aggregate, ASTM International, West Conshohocken, PA, available at: www.astm.org (last access: 26 September 2018).

Ayotte, D., Evans, N., and Hungr, O. (1999). Runout analysis of debris flows and avalanches in Hong Kong. In Proceedings, Slope Stability and Landslides, *Vancouver Geotechnical Society Symposium*, 39-46.

Azzoni, A., Rossi, P. P., Drigo, E., Giani, G. P., and Zaninetti, A. (1992). In situ observation of rockfall analysis parameters. *In Sixth International Symposium of Landslides,* 307-314.

Bacchini, M., and Zannoni, A. (2003). Relations between rainfall and triggering of debris-flow: case study of Cancia (Dolomites, Northeastern Italy). *Natural Hazards and Earth System Sciences*, 3(1/2), 71-79.

Badger, T. C., and Lowell, S. M. (1992). Rockfall control in Washington state. *Transportation Research Record,* 1343, 14-19.

Bagnold, R. A. (1954). Experiments on a gravity-free dispersion of large solid spheres in a Newtonian fluid under shear. *Proceedings of the Royal Society of London A*, 225(1160), 49-63.

Berti, M., Genevois, R., Simoni, A., and Tecca, P. R. (1999). Field observations of a debris flow event in the Dolomites. *Geomorphology*, 29(3-4), 265-274.

Bertolo, P., and Wieczorek, G. F. (2005). Calibration of numerical models for small debris flows in Yosemite Valley, California, USA. *Natural Hazards and Earth System Sciences*, 5(6), 993-1001.

Bowman, E. T., Laue, J., Imre, B., and Springman, S. M. (2010). Experimental modelling of debris flow behaviour using a geotechnical centrifuge. *Canadian Geotechnical Journal*, 47(7), 742-762.

Brighenti, R., Ferrero, A. M., Segalini, A., and Umili, G. (2015). Study on the Mechanical Behaviour of Flexible Barriers by in situ Testing and Modelling. In *Engineering Geology for Society and Territory-Volume 2*. Springer, Cham, 1651-1655.

Bugnion, L. (2008). Full-scale experiments on shallow landslides in combination with flexible protection barriers. In *Proceedings of the first world landslide forum, parallel session, Tokyo*, 99-102.

Bugnion, L., McArdell, B. W., Bartelt, P., and Wendeler, C. (2012). Measurements of hillslope debris flow impact pressure on obstacles. *Landslides*, 9(2), 179-187.

Bunce, C. M., Cruden, D. M., and Morgenstern, N. R. (1997). Assessment of the hazard from rock fall on a highway. *Canadian Geotechnical Journal,* 34(3), 344-356.

Buzzi, O., Leonarduzzi, E., Krummenacher, B., Volkwein, A., and Giacomini, A. (2015). Performance of high strength rock fall meshes: effect of block size and mesh geometry. *Rock Mechanics and Rock Engineering*, 48(3), 1221-1231.

Caine, N. (1980). The rainfall intensity-duration control of shallow landslides and debris flows. *Geografiska Annaler: series A, Physical Geography,* 62(1-2), 23-27.

Canelli, L., Ferrero, A. M., Migliazza, M., and Segalini, A. (2012). Debris flow risk mitigation by the means of rigid and flexible barriers-experimental tests and impact analysis. *Natural Hazards and Earth System Sciences*, 12, 1693-1699.

Castro-Fresno, D., del Coz Diaz, J. J., López, L. A., and Nieto, P. G. (2008). Evaluation of the resistant capacity of cable nets using the finite element method and experimental validation. *Engineering Geology*, 100(1-2), 1-10.

CEDD (2013). When Hillsides Collapse - A Century of Landslides in Hong Kong - Be Prepared for Danger in Times of Peace. Hong Kong SAR. (in Chinese).

Chau, K. T., Wong, R. H. C., and Wu, J. J. (2002). Coefficient of restitution and rotational motions of rockfall impacts. *International Journal of Rock Mechanics and Mining Sciences*, *39*(1), 69-77.

Chau, K. T., Wong, R. H. C., Liu, J., and Lee, C. F. (2003). Rockfall hazard analysis for Hong Kong based on rockfall inventory. *Rock Mechanics and Rock Engineering,* 36(5), 383-408.

Chen, C. L. (1988). Generalized viscoplastic modeling of debris flow. *Journal of Hydraulic Engineering*, 114(3), 237-258.

Chen, H. X., Zhang, L. M., Gao, L., Yuan, Q., Lu, T., Xiang, B., and Zhuang, W. L. (2017). Simulation of interactions among multiple debris flows. *Landslides,* 14(2), 595-615.

Chien-Yuan, C., Tien-Chien, C., Fan-Chieh, Y., Wen-Hui, Y., and Chun-Chieh, T. (2005). Rainfall duration and debris-flow initiated studies for real-time monitoring. *Environmental Geology*, 47(5), 715-724.

Chikatamarla, R., Laue, J., and Springman, S. M. (2006). Centrifuge scaling laws for guided free fall events including rockfalls. *International Journal of Physical Modelling in Geotechnics*, 6(2), 15-26.

Choi, C. E., Ng, C. W. W., Song, D., Kwan, J. H. S., Shiu, H. Y. K., Ho, K. K. S., and Koo, R. C. H. (2014). Flume investigation of landslide debris–resisting baffles. *Canadian Geotechnical Journal*, 51(5), 540-553.

Costa, J. E. (1984). Physical geomorphology of debris flows. In *Developments and applications of geomorphology*. Springer, Berlin, Heidelberg, 268-317.

Coussot, P., Laigle, D., Arattano, M., Deganutti, A., and Marchi, L. (1998). Direct determination of rheological characteristics of debris flow. *Journal of Hydraulic Engineering*, 124(8), 865-868.

Cui, P., Zeng, C., and Lei, Y. (2015). Experimental analysis on the impact force of viscous debris flow. *Earth Surface Processes and Landforms*, 40(12), 1644-1655.

Davies, T. R. H. (1986). Large debris flows: a macro-viscous phenomenon. *Acta Mechanica*, 63(1-4), 161-178.

DeNatale, J. S., Iverson, R. M., Major, J. J., LaHusen, R. G., Fiegel, G. L., and Duffy, J. D. (1999). *Experimental testing of flexible barriers for containment of debris flows*. US Department of the Interior, US Geological Survey, 39p.

Dhakal, S., Bhandary, N. P., Yatabe, R., and Kinoshita, N. (2011). Experimental, numerical and analytical modelling of a newly developed rockfall protective cable-net structure. *Natural Hazards and Earth System Sciences*, 11(12), 3197-3212.

Dilley, M., Chen, R. S., Deichmann, U., Lerner-Lam, A. L., and Arnold, M. (2005). *Natural disaster hotspots: a global risk analysis*. The World Bank.

Dorren, L. K. (2003). A review of rockfall mechanics and modelling approaches. *Progress in Physical Geography*, 27(1), 69-87.

Duffy, J. D., and Smith D. D. (1990). *Field tests and evaluation of rockfall restraining nets.* No. CA/TL-90/05, Final Report. California Department of Transportation, San Luis Obispo, 182p.

EOTA (2013) Guideline for European technical approval of falling rock protection kits. *ETAG 027*, Brussels.

Finlay PJ, Fell R, and Maguire PK (1997). The relationship between the probability of landslide occurrence and rainfall. *Canadian Geotechnical Journal,* 34(6):811–824.

Gao, L., Zhang, L. M., and Cheung, R. W. M. (2018). Relationships between natural terrain landslide magnitudes and triggering rainfall based on a large landslide inventory in Hong Kong. *Landslides*, 15(4), 727-740.

GEO (2014). Guidelines on Empirical Design of Flexible Barriers for Mitigating Natural Terrain Open Hillslope Landslide Hazards (GEO Technical Guidance Note No. 37). Geotechnical Engineering Office, HKSAR, 18p.

GEO (2016). Natural Terrain Landslide Hazards in Hong Kong. Geotechnical Engineering Office, Hong Kong, 21p.

Geobrugg AG, (2012). Geobrugg: Protection systems for rockfall, debris flow, slope instability, mining, avalanche, 6 June 2012, YouTube. Available from: https://www.youtube.com/watch?v=LUUeBRZ-lOg.

Gerber, W. (2001). *Guideline for the approval of rockfall protection kits*. SAEFL, Swiss, 39p.

Gerrard, J. (1990). *Mountain environments: an examination of the physical geography of mountains*. MIT Press, USA.

Giani, G. P. (1992). *Rock slope stability analysis*. CRC Press.

Gottardi, G., and Govoni, L. (2010). Full-scale modelling of falling rock protection barriers. *Rock Mechanics and Rock Engineering*, *43*(3), 261-274.

Grassl, H., Bartelt, P. A., Volkwein, A., and Wartmann, S. (2003). Experimental and numerical modeling of highly flexible rockfall protection barriers. In *Proceedings of 12th Panamerican Conference on Soil Mechanics and Geotechnical Engineering, Cambridge, Massachusetts, USA*, 2589-2594.

Guzzetti, F., Peruccacci, S., Rossi, M., and Stark, C. P. (2008). The rainfall intensity–duration control of shallow landslides and debris flows: an update. *Landslides*, *5*(1), 3-17.

Halcrow China Limited. (2011). *Study on methods and supervision of rock breaking operations and provision of temporary protective barriers and associated measures. GEO Report 260*, Geotechnical Engineering Office, HKSAR, 250p.

Hambleton, J. P., Buzzi, O., Giacomini, A., Spadari, M., and Sloan, S. W. (2013). Perforation of flexible rockfall barriers by normal block impact. *Rock Mechanics and Rock Engineering*, 46(3), 515-526.

Hearn, G., Barrett, R. K., and Henson, H. H. (1995). Testing and modeling of two rockfall barriers. *Transportation Research Record*, 1504, 1-11.

Herschel, W.H.; Bulkley, R. (1926). Konsistenzmessungen von Gummi-Benzollösungen, *Kolloid Zeitschrift*, 39: 291–300, doi:10.1007/BF01432034.

Hewitt, K. (2004). Geomorphic hazards in mountain environments in *Mountain geomorphology* (pp. 187-218). Arnold Publishers: London.

Hu, K., Wei, F., and Li, Y. (2011). Real-time measurement and preliminary analysis of debris-flow impact force at Jiangjia Ravine, China. *Earth Surface Processes and Landforms*, *36*(9), 1268-1278.

Hu, K., Wei, F., Hong, Y., and Li, X. (2006). Field measurement of impact force of debris flow. *Yanshilixue Yu Gongcheng Xuebao/Chinese Journal of Rock Mechanics and Engineering*, *25*, 2813-2819.

Hübl, J., Suda, J., Proske, D., Kaitna, R., and Scheidl, C. (2009). Debris flow impact estimation. In *Proceedings of the 11th international symposium on water management and hydraulic engineering, Ohrid, Macedonia,* 1-5.

Huebl, J., and Fiebiger, G. (2005). Debris-flow mitigation measures. In *Debris-flow hazards and related phenomena.* Springer, Berlin, Heidelberg, 445-487.

Huebl, J., Ganahl, E., Gruber, H., Holub, M., Holzinger, G., Moser, M., and Pichler, A. (2004). Grundlagenerhebung für das Schutzkonzept Lattenbach (Catchrisk). *Grundlagen fuer eine Murenprognose und darauf aufbauend die Entwicklung eines Warn-und Alarmsystems*.

Huebl, J., and Steinwendtner, H. (2000). Debris flow hazard assessment and risk mitigation. *Felsbau–Rock and Soil Engineering*, *1*, 17-23.

Hungr, O. (1995). A model for the runout analysis of rapid flow slides, debris flows, and avalanches. *Canadian Geotechnical Journal*, *32*(4), 610-623.

Hungr, O. (1998). Mobility of Landslide Debris in Hong Kong: Pilot Back Analyses using a Numerical Model. Report prepared for the Geotechnical Engineering Office, Hong Kong, 50p.

Hungr, O., Evans, S. G., and Hutchinson, I. (2001). A Review of the Classification of Landslides of the Flow Type. *Environmental and Engineering Geoscience*, *7*(3), 221-238.

Hungr, O., Morgan, G. C., and Kellerhals, R. (1984). Quantitative analysis of debris torrent hazards for design of remedial measures. *Canadian Geotechnical Journal*, *21*(4), 663-677.

Hussin, H. Y., Quan, L. B., Van Westen, C. J., Christen, M., Malet, J. P., and van Asch, T. W. (2012). Parameterization of a numerical 2-D debris flow model with entrainment: a case study of the Faucon catchment, Southern French Alps. *Natural Hazards and Earth System Sciences*, 12, 3075-3090, https://doi.org/10.5194/nhess-12-3075-2012.

Hutter, K., and Koch, T. (1991). Motion of a granular avalanche in an exponentially curved chute: experiments and theoretical predictions. *Philosophical Transactions of the Royal Society of London A*, 334(1633), 93-138.

Hutter, K., Svendsen, B., and Rickenmann, D. (1995). Debris flow modeling: A review. *Continuum Mechanics and Thermodynamics*, 8(1), 1-35.

Ishikawa, N., Inoue, R., Hayashi, K., Hasegawa, Y., and Mizuyama, T. (2008). Experimental approach on measurement of impulsive fluid force using debris flow model. *INTERPRAEVENT 2008- Conference Proceedings, Dornbirn, Austria,* 343–354.

Iverson, R. M. (1997). The physics of debris flows. *Reviews of Geophysics*, 35(3), 245-296.

Iverson, R. M. (2014). Debris flows: behaviour and hazard assessment. *Geology Today*, 30(1), 15-20.

Iverson, R. M. (2015). Scaling and design of landslide and debris-flow experiments. *Geomorphology*, 244, 9-20.

Iverson, R. M., Costa, J. E., and LaHusen, R. G. (1992). *Debris-flow flume at HJ Andrews experimental forest, Oregon*. US Geological Survey, Dept. of the Interior.

Iverson, R. M., and Denlinger, R. P. (2001). Flow of variably fluidized granular masses across three-dimensional terrain: 1. Coulomb mixture theory. *Journal of Geophysical Research: Solid Earth*, 106(B1), 537-552.

Iverson, R. M., Logan, M., LaHusen, R. G., and Berti, M. (2010). The perfect debris flow? Aggregated results from 28 large-scale experiments. *Journal of Geophysical Research*, 115, F03005.

Iverson, R. M., and Vallance, J. W. (2001). New views of granular mass flows. *Geology*, 29(2), 115-118.

Jakob, M., Hungr, O., and Jakob, D. M. (2005). *Debris-flow hazards and related phenomena (Vol. 739).* Berlin: Springer.

Jeong, S. W. (2014). The effect of grain size on the viscosity and yield stress of fine-grained sediments. *Journal of Mountain Science*, *11*(1), 31-40.

Johnson, K. L., and Johnson, K. L. (1987). *Contact mechanics*. Cambridge University Press, UK.

Kane, W. F., Fletcher, D. Q., and Duffy, J. D. (1993). Low-impact rock net testing, performance, and foundation design. In *Transportation Facilities Through Difficult Terrain. Proceedings of a Conference, Held August 8-12, 1993, Aspen-Snowmass, Colorado, USA*.

Kawahara, S., and Muro, T. (2006). Effects of dry density and thickness of sandy soil on impact response due to rockfall. *Journal of Terramechanics*, 43(3), 329-340.

King, J. P. (2013). *Tsing Shan debris flow and debris flood (GEO Report 281*). Geotechnical Engineering Office, HKSAR, 268p.

Koo, R. C., Kwan, J. S., Lam, C., Ng, C. W., Yiu, J., Choi, C. E., and Pun, W. K. (2017). Dynamic response of flexible rockfall barriers under different loading geometries. *Landslides*, 14(3), 905-916.

Kwan, J. S. H. (2012). *Supplementary technical guidance on design of rigid debris-resisting barriers (GEO Report 270)*. Geotechnical Engineering Office, HKSAR, 270p.

Kwan, J. S. H., and Cheung, R. W. M. (2012). *Suggestion on design approaches for flexible debris-resisting barriers (Discussion Note DN1/2012).* The Government of Hong Kong Standards and Testing Division, HKSAR, 90p.

Kwan, J. S., Chan, S. L., Cheuk, J. C., and Koo, R. C. H. (2014). A case study on an open hillside landslide impacting on a flexible rockfall barrier at Jordan Valley, Hong Kong. *Landslides,* 11(6), 1037-1050.

Labiouse, V., Descoeudres, F., and Montani, S. (1996). Experimental study of rock sheds impacted by rock blocks. *Structural Engineering International*, 6(3), 171-176.

Leonardi, A., Wittel, F.K., Mendoza, M., Vetter, R. and Herrmann, H.J., (2016). Particle–fluid–structure interaction for debris flow impact on flexible barriers. *Computer-Aided Civil and Infrastructure Engineering,* 31(5), 323-333.

Li, X., and Zhao, J. (2018). A unified CFD-DEM approach for modeling of debris flow impacts on flexible barriers. *International Journal for Numerical and Analytical Methods in Geomechanics*, 42(14), 1643-1670.

Lichtenan, C. (1973). Die Berechnung von Sperren in Beton und Eisenbeton, Kolloquium on Torrent Dams ODC 384.3. *Mitteilungen der Forstlichen Bundes-Versuchsanstalt, Wien*, 91-127 (in German).

Lo, D. O. K. (2000). *Review of natural terrain landslide debris-resisting barrier design*. Geotechnical Engineering Office, HKSAR.

Locat, J., and Demers, D. (1988). Viscosity, yield stress, remolded strength, and liquidity index relationships for sensitive clays. *Canadian Geotechnical Journal*, 25(4), 799-806.

Margreth, S., and Roth, A. (2008). Interaction of flexible rockfall barriers with avalanches and snow pressure. *Cold Regions Science and Technology*, 51(2-3), 168-177.

Matsukura, Y. (2001). Rockfall at Toyohama Tunnel, Japan, in 1996: effect of notch growth on instability of a coastal cliff. *Bulletin of Engineering Geology and the Environment*, 60(4), 285-289.

Mavrouli, O., Giannopoulos, P. G., Carbonell, J. M., and Syrmakezis, C. (2017). Damage analysis of masonry structures subjected to rockfalls. *Landslides*, 14(3), 891-904.

Milne, F. D., Brown, M. J., Knappett, J. A., and Davies, M. C. R. (2012). Centrifuge modelling of hillslope debris flow initiation. *Catena*, 92, 162-171.

Miura, K., Maeda, K., and Toki, S. (1997). Method of measurement for the angle of repose of sands. *Soils and Foundations*, 37(2), 89-96.

Mullenbach, J. (2018). *Experimental Studies of the Influence of the Properties of the Matrix of a Debris Flow on Its Erosional Behavior* (master's thesis). University of Minnesota, Minneapolis, U.S.

Muraishi, H., Samizo, M., and Sugiyama, T. (2005). Development of a flexible low-energy rockfall protection fence. *Quarterly Report of RTRI*, 46(3), 161-166.

Naef, D., Rickenmann, D., Rutschmann, P., and McArdell, B. W. (2006). Comparison of flow resistance relations for debris flows using a one-dimensional finite element simulation model. *Natural Hazards and Earth System Sciences*, 6(1), 155-165.

Nakano, T., Kadomura, H., Mizutani, T., Okuda, M., and Sekiguchi, T. (1974). Natural hazards: report from Japan. *Natural hazards: local, regional, global. Oxford University Press, Oxford*, 231-243.

Neri, M. (1986). Barriere paramassi deformabili ad elevato assorbimento di energia. *Quarry and Constructions, PEI, Padova (in Italian).*

Ng, C. W. W., Song, D., Choi, C. E., Koo, R. C. H., and Kwan, J. S. H. (2016a). A novel flexible barrier for landslide impact in centrifuge. *Géotechnique Letters*, 6(3), 221-225.

Ng, C. W. W., Song, D., Choi, C. E., Liu, L. H. D., Kwan, J. S. H., Koo, R. C. H., and Pun, W. K. (2016b). Impact mechanisms of granular and viscous flows on rigid and flexible barriers. *Canadian Geotechnical Journal*, 54(2), 188-206.

Ng, K. C., Parry, S., King, J. P., Franks, C. A. M., and Shaw, R. (2003). *Guidelines for natural terrain hazard studies*. GEO Report, Geotechnical Engineering Office, HKSAR, 138p.

Nicot, F., Cambou, B., and Mazzoleni, G. (2001). From a constitutive modelling of metallic rings to the design of rockfall restraining nets. *International Journal for Numerical and Analytical Methods in Geomechanics*, 25(1), 49-70.

O'Brien, J. S., Julien, P. Y., and Fullerton, W. T. (1993). Two-dimensional water flood and mudflow simulation. *Journal of Hydraulic Engineering*, 119(2), 244-261.

Paik, J., Son, S., Kim, T., and Kim, S. (2012). A real-scale field experiment of debris flow for investigating its deposition and entrainment. In *AGU Fall Meeting Abstracts*.

Peila, D., Pelizza, S., and Sassudelli, F. (1998). Evaluation of behaviour of rockfall restraining nets by full scale tests. *Rock Mechanics and Rock Engineering*, 31(1), 1-24.

Petley, D. (2012). Global patterns of loss of life from landslides. *Geology*, 40(10), 927-930.

Prochaska, A. B., Santi, P. M., Higgins, J. D., and Cannon, S. H. (2008). A study of methods to estimate debris flow velocity. *Landslides*, *5*(4), 431-444.

Proske, D., Suda, J., and Hübl, J. (2011). Debris flow impact estimation for breakers. *Georisk*, 5(2), 143-155.

Pudasaini, S. P., Wang, Y., and Hutter, K. (2005). Modelling debris flows down general channels. *Natural Hazards and Earth System Sciences, 5*(6), 799-819.

Rankine, W. M. (1857). On the Stability of Loose Earth. *Proceedings of the Royal Society of London*, 147, 9-27.

Rickenmann, D., and Koch, T. (1997). Comparison of debris flow modelling approaches. In *Debris-flow hazards mitigation: mechanics, prediction, and assessment,* 576-585.

Rickenmann, D., Laigle, D. M. B. W., McArdell, B. W., and Hübl, J. (2006). Comparison of 2D debris-flow simulation models with field events. *Computational Geosciences*, 10(2), 241-264.

Ritchie, A. M. (1963). Evaluation of rockfall and its control. *Highway Research Record*, National Academy of Sciences-National Research Council. Washington, DC, 17, 13-28.

Santi, P. M., Hewitt, K., VanDine, D. F., and Cruz, E. B. (2011). Debris-flow impact, vulnerability, and response. *Natural Hazards*, *56*(1), 371-402.

Scheidl, C., Chiari, M., Kaitna, R., Müllegger, M., Krawtschuk, A., Zimmermann, T., and Proske, D. (2013). Analysing debris-flow impact models, based on a small scale modelling approach. *Surveys in Geophysics*, *34*(1), 121-140.

Schofield, A. N. (1981). Dynamic and earthquake geotechnical centrifuge modelling. *International Conferences on Recent Advances in Geotechnical Earthquake Engineering and Soil Dynamics,* 5, 1081-1100.

Schuster, R. L., Salcedo, D. A., and Valenzuela, L. (2002). Overview of catastrophic landslides of South America in the twentieth century. *Catastrophic Landslides: Effects, Occurrence, and Mechanisms*, 15, 1-33.

Scotto di Santolo, A., Pellegrino, A. M., and Evangelista, A. (2010). Experimental study on the rheological behaviour of debris flow. *Natural Hazards and Earth System Sciences*, 10(12), 2507-2514.

Scotton, P., and Trivellato, F. (1995). Dynamic pressure on check-dam due to debris flow collision. In *Proceedings of Twelfth Australasian Fluid Mechanics Conference,* 15.

Song, D. (2016). *Mechanisms of debris flow impact on rigid and flexible barriers* (Doctoral dissertation). The Hong Kong Universtiy of Science and Technology, Hong Kong.

Song, D., Choi, C. E., Ng, C. W. W., and Zhou, G. G. D. (2018a). Geophysical flows impacting a flexible barrier: effects of solid-fluid interaction. *Landslides*, 15(1), 99-110.

Song, D., Choi, C. E., Zhou, G. G. D., Kwan, J. S. H., and Sze, H. Y. (2018b). Impulse Load Characteristics of Bouldery Debris Flow Impact. *Géotechnique Letters*, 8(2), 111-117.

Song, D., Ng, C. W. W., Choi, C. E., Zhou, G. G., Kwan, J. S., Koo, R. C. H. (2017). Influence of debris flow solid fraction on rigid barrier impact. *Canadian Geotechnical Journal,* 54(10), 1421-1434.

Spadari, M., (2013) *Experimental and numerical investigations on barriers for rockfall hazard mitigation* (Doctoral dissertation). The University of Newcastle, Callaghan, 2308, Australia.

Spadari, M., Giacomini, A., Buzzi, O. and Hambleton, J.P., (2012) Prediction of the bullet effect for rockfall barriers: a scaling approach. *Rock Mechanics and Rock Engineering,* 45(2), 131-144.

Speerli, J., Hersperger, R., Wendeler, C., and Roth, A. (2010). Physical modeling of debris flows over flexible ring-net barriers. In *Proceedings of the 7th International Conference on Physical Modelling in Geotechnics*, 28, 1285-1290.

Su, L. J., Xu, X. Q., Geng, X. Y., and Liang, S. Q. (2017). An integrated geophysical approach for investigating hydro-geological characteristics of a debris landslide in the Wenchuan earthquake area. *Engineering Geology*, 219, 52-63.

Sun, H. W., Lam, T. T. M., and Tsui, H. M. (2005). *Design basis for standardised modules of landslide debris-resisting barriers*. Geotechnical Engineering Office, HKSAR, 161p.

Sun, H. W., and Law, R. P. H. (2012). *A preliminary study on impact of landslide debris on flexible barriers*. Technical Note, The Government of Hong Kong Standards and Testing Division, HKSAR, p 47.

Takahashi, T. (2014). *Debris flow: mechanics, prediction and countermeasures*. CRC press.

Tan, D. Y., Yin, J. H., Feng, W. Q., Qin, J. Q., and Zhu, Z. H. (2018a). Large-scale physical modelling study of a flexible barrier under the impact of granular flows. *Natural Hazards and Earth System Sciences,* 18, 2625-2640, https://doi.org/10.5194/nhess-18-2625-2018.

Tan, D. Y., Yin, J. H., Qin, J. Q., Zhu, Z. H., and Feng, W. Q. (2018b). Large-scale physical modeling study on the interaction between rockfall and flexible barrier. *Landslides*, 15(12), 2487-2497, https://doi.org/10.1007/s10346-018-1058-1.

Thakur, A. K. (1991). Model: mechanistic *v.s.* empirical. *In: New trends in pharmacokinetics*, 41-51. Springer, Boston.

Tiberghien, D., Laigle, D., Naaim, M., Thibert, E., and Ousset, F. (2007). Experimental investigations of interaction between mudflow and an obstacle. *Debris-flow hazards mitigation: mechanics, prediction and assessment, Millpress, Rotterdam*.

Timpong, S., Itoh, K., and Toyosawa, Y. (2007). Geotechnical centrifuge modelling of slope failure induced by ground water table change. *Landslides and Climate Change. London: Taylor and Francis Group*, 107-112.

Vagnon, F., and Segalini, A. (2016). Debris flow impact estimation on a rigid barrier. *Natural Hazards and Earth System Sciences*, 16(7), 1691-1697.

Varnes, D. J. (1958). Landslide types and processes. *Landslides and Engineering Practice*, 29(3), 20-45.

Voellmy, A. (1955). Uber die Zerstorungskraft von Lawinen. *Schweizerische Bauzeitung, Jahrg.*, 73, 159-162.

Volkwein, A. (2005). Numerical simulation of flexible rockfall protection systems. In *Computing in Civil Engineering,* 1-11.

Volkwein, A. (2014). Flexible debris flow barriers. Design and application. WSL Berichte. Issue 18, 29.

Volkwein, A., Baumann, R., Rickli, C., and Wendeler, C. (2015). Standardization for flexible debris retention barriers. In *Engineering Geology for Society and Territory-Volume 2*, 193-196. Springer, Cham.

Volkwein, A., Melis, L., Haller, B., and Pfeifer, R. (2005). Protection from landslides and high speed rockfall events: reconstruction of Chapman's Peak Drive. In *IABSE Symposium Report*. International Association for Bridge and Structural Engineering 90(6): 47-54.

Volkwein, A., Roth, A., Gerber, W., and Vogel, A. (2009). Flexible rockfall barriers subjected to extreme loads. *Structural Engineering International*, 19(3), 327-332.

Volkwein, A., Schellenberg, K., Labiouse, V., Agliardi, F., Berger, F., Bourrier, F., and Jaboyedoff, M. (2011a). Rockfall characterisation and structural protection-a review. *Natural Hazards and Earth System Sciences*, 11, 2617-2651.

Volkwein, A., Wendeler, C., and Guasti, G. (2011b). Design of flexible debris flow barriers. In *5th International Conference debris-flow hazard mitigation. Mechanics, prediction and assessment. Padua, Italy,* 1093-1100.

Wang, B., and Cavers, D. S. (2008). A simplified approach for rockfall ground penetration and impact stress calculations. *Landslides*, *5*(3), 305.

Wartmann, S., and Salzmann, H. (2002) Debris flow and floating tree impacts on flexible barriers. *In Proceedings of the Conference on Natural Terrain—a constraint to development*, Hong Kong: 125-131.

Wendeler, C. (2016). Debris-flow protection systems for mountain torrents: basics principles for planning and calculation of flexible barriers. WSL Berichte. 44, 281.

Wendeler, C. (2008). *Murgangrückhalt in Wildbächen: Grundlagen zu Planung und Berechnung von flexiblen Barrieren* (Doctoral dissertation), ETH, Zurich.

Wendeler, C., and Volkwein, A. (2015). Laboratory tests for the optimization of mesh size for flexible debris-flow barriers. *Natural Hazards and Earth System Sciences,* 15, 2597-2604.

Wendeler, C., McArdell, B. W., Rickenmann, D., Volkwein, A., Roth, A., and Denk, M. (2006). Field testing and numerical modeling of flexible debris flow barriers. In *Proceedings of the International Conference on Physical Modelling in Geotechnics, Hong Kong, China*, 4-6.

Wendeler, C., McArdell, B., Volkwein, A., Denk, M., and Gröner, E. (2008). Debris flow mitigation with flexible ring net barriers—field tests and case studies. *WIT Transactions on Engineering Sciences*, 60, 23-31.

Wendeler, C., Volkwein, A., McArdell, B. W., and Bartelt, P. (2018). Load model for designing flexible steel barriers for debris flow mitigation. *Canadian Geotechnical Journal*, 99 1-39.

Wendeler, C., Volkwein, A., Roth, A., Denk, M., and Wartmann, S. (2007). Field measurements and numerical modelling of flexible debris flow barriers. *Debris-Flow Hazards Mitig. Mech. Predict. Assess. Millpress, Rotterdam*, 681-687.

Won, S., Lee, S. W., Paik, J., Yune, C. Y., and Kim, G. (2016). Analysis of Erosion in Debris Flow Experiment Using Terrestrial LiDAR. *Journal of the Korean Society of Surveying, Geodesy, Photogrammetry and Cartography*, 34(3), 309-317.

Xu, Q., Zhang, S., Li, W. L., and Van Asch, T. W. (2012). The 13 August 2010 catastrophic debris flows after the 2008 Wenchuan earthquake, China. *Natural Hazards and Earth System Sciences*, 12, 201-216.

Yagi, H., Sato, G., Higaki, D., Yamamoto, M., and Yamasaki, T. (2009). Distribution and characteristics of landslides induced by the Iwate–Miyagi Nairiku Earthquake in 2008 in Tohoku District, Northeast Japan. *Landslides,* 6(4), 335-344.

Yifru, A. L. (2014). *Assessment of rheological models for run-out distance modeling of sensitive clay slides, focusing on Voellmy rheology* (master's thesis). Norwegian University of Science and Technology, Trondheim, Norway.

Yu, B., Yi, W., and Zhao, H. (2018a). Experimental study on the maximum impact force by rock fall. *Landslides*, 15(2), 233-242.

Yu, Z. X., Qiao, Y. K., Zhao, L., Xu, H., Zhao, S. C., and Liu, Y. P. (2018b). A simple analytical method for evaluation of flexible rockfall barrier part 2: Application and full-scale test. *Advanced Steel Construction*, 14, 142-165.

Zakeri, A. (2009). Submarine debris flow impact on suspended (free-span) pipelines: Normal and longitudinal drag forces. *Ocean Engineering*, 36(6-7), 489-499.

Zanuttigh, B., and Lamberti, A. (2006). Experimental analysis of the impact of dry avalanches on structures and implication for debris flows. *Journal of Hydraulic Research*, 44(4), 522-534.

Zeng, C., Cui, P., Su, Z., Lei, Y., and Chen, R. (2015). Failure modes of reinforced concrete columns of buildings under debris flow impact. *Landslides*, 12(3), 561-571.

Zhang, S. (1993). A comprehensive approach to the observation and prevention of debris flows in China. *Natural Hazards*, 7(1), 1-23.

Zhang, S. L., Yang, X. G., and Zhou, J. W. (2018). A theoretical model for the estimation of maximum impact force from a rockfall based on contact theory. *Journal of Mountain Science*, 15(2), 430-443.

Zhao, H., Yao, L., You, Y., Wang, B., and Zhang, C. (2018). Experimental Study of the Debris Flow Slurry Impact and Distribution. *Shock and Vibration*.

Zhou, G. G., Ng, C. W., and Sun, Q. C. (2014). A new theoretical method for analyzing confined dry granular flows. *Landslides*, 11(3), 369-384.

Zhu, H., and Randolph, M. F. (2009). Large deformation finite-element analysis of submarine landslide interaction with embedded pipelines. *International Journal of Geomechanics*, 10(4), 145-152.

Zollinger, F. (1985). Debris detention basins in the European Alps. In *Proc. Int. Symp. Erosion, debris flow and disaster prevention, Tsukuba, Japan,* 1, 433-438.